

EXPERIMENTAL AND NUMERICAL ASSESSMENT OF
PRESSUREMETER TESTING

A THESIS SUBMITTED TO
THE GRADUATE SCHOOL OF NATURAL AND APPLIED SCIENCES
OF
MIDDLE EAST TECHNICAL UNIVERSITY

BY

NIHAT SİNAN IŞIK

IN PARTIAL FULFILLMENT OF THE REQUIREMENTS
FOR
THE DEGREE OF DOCTOR OF PHILOSOPHY
IN
GEOLOGICAL ENGINEERING

JANUARY 2006

Approval of the Graduate School of Natural and Applied Sciences

Prof. Dr. Canan ÖZGEN
Director

I certify that this thesis satisfies all the requirements as a thesis for the degree of Doctor of Philosophy.

Prof. Dr. Vedat DOYURAN
Head of Department

This is to certify that we have read this thesis and that in our opinion it is fully adequate, in scope and quality, as a thesis for the degree of Doctor of Philosophy.

Prof. Dr. Reşat ULUSAY
Co-Supervisor

Prof. Dr. Vedat DOYURAN
Supervisor

Examining Committee Members

Assoc. Prof. Dr. Tamer TOPAL (METU,GEOE) _____

Prof. Dr. Vedat DOYURAN (METU,GEOE) _____

Prof. Dr. Reşat ULUSAY (Hacettepe Unv., GEOE) _____

Assoc. Prof. Dr. Önder ÇETİN (METU,CE) _____

Assoc. Prof. Dr. Mehmet ORHAN (Gazi Unv., CONST.) _____

I hereby declare that all information in this document has been obtained and presented in accordance with academic rules and ethical conduct. I also declare that, as required by these rules and conduct, I have fully cited and referenced all material and results that are not original to this work.

Name, Last name : Nihat Sinan IŞIK

Signature :

ABSTRACT

EXPERIMENTAL AND NUMERICAL ASSESSMENT OF PRESSUREMETER TESTING

Işık, Nihat Sinan

Ph.D., Department of Geological Engineering

Supervisor : Prof. Dr. Vedat Doyuran

Co-Supervisor: Prof. Dr. Reşat Ulusay

January 2006, 228 pages

The purposes of this study are to investigate the possible effects of variables like testing depth, length to diameter ratio of the probe, presence of disturbed annulus around the borehole etc. on the derived parameters from the pressuremeter test, and to develop possible alternative methods for the determination of undrained shear strength of cohesive soils, and cohesion and internal friction angle of intermediate geomaterials. For this purpose numerical simulations of pressuremeter test were performed. In the study, it is also aimed to investigate the effect of rock quality designation (RQD) or some other rock mass parameters such as geological strength index (GSI) and rock mass rating (RMR) and intact rock strength on the deformation modulus determined from the pressuremeter test. To accomplish this task, Dikmen greywackes, weathered andesites and mudrocks exposed around Ankara - Sincan region were selected for field and laboratory studies. Empirical relationships using GSI, RMR, RQD were

developed for the estimation of deformation modulus of greywackes and mudrocks cropping out around Ankara. Numerical simulations revealed the presence of disturbed annulus around the borehole causes underestimation of deformation modulus and overestimation of undrained shear strength. Test depth has no effect on the deformation modulus and undrained shear strength; the effect of length to diameter ratio of the probe on the deformation modulus is minor where as it causes overestimations of undrained shear strength. Pore pressure dissipation in low permeability soils around the pressuremeter was studied using numerical simulations. These analyses suggest that for permeabilities lower than 10^{-10} m/sec there is no pore pressure dissipation around the pressuremeter probe. It was determined that the inverse analysis yielded successful results for the determination of shear strength parameters of intermediate geomaterials.

Keywords: Pressuremeter, Undrained Shear Strength, Rock Mass, Numerical Analysis, Inverse Analysis, Geological Strength Index (GSI)

ÖZ

PRESİYOMETRE DENEYİNİN DENEYSEL VE SAYISAL İNCELENMESİ

Işık, Nihat Sinan

Doktora, Jeoloji Mühendisliği Bölümü

Tez Yöneticisi : Prof. Dr. Vedat Doyuran

Ortak Tez Yöneticisi: Prof. Dr. Reşat Ulusay

Ocak 2006, 228 sayfa

Bu çalışmanın amaçları, deney derinliği, presiyometre başlığının boy / çap oranı, sondaj deliği etrafında örselenmiş bir bölgenin varlığı gibi faktörlerin, ve presiyometre deneyinden elde edilen zemin – kaya parametreleri üzerindeki etkisinin araştırılması; kohezyonlu zeminlerin drenajsız makaslama dayanımı; hem kohezyon hem de sürtünme açısı olan zemin – kaya malzemelerin makaslama dayanımı parametrelerinin belirlenmesi için alternatif yöntemlerin geliştirilmesine çalışmaktır. Bu amaçla, presiyometre deneyinin sayısal analizleri yapılmıştır. Bu çalışmanın diğer bir amacı da, kaya kalite göstergesi (RQD), ya da jeolojik dayanım indeksi (GSI), kaya kütlesi sınıflama puanı (RMR) gibi kaya kütlesi parametrelerinin ve sağlam kayacın dayanımının, presiyometreden elde edilen deformasyon modülü üzerindeki etkilerinin araştırılmasıdır. Bu amaçla; Dikmen grovıkları, ayrılmış andezitler, ve Ankara – Sincan bölgesinde yüzeylenen çamurtaşları seçilmiştir. Arazi ve laboratuvar çalışmaları sonucunda,

grovaklar ve amur tařlarının kaya kütlesi deformasyon modülünü tahmin edebilmek amacıyla, GSI, RMR ve RQD parametrelerini esas alan görgül eşitlikler, geliştirilmiştir. Presiyometre deneyinin sayısal analizleri, sondaj deliğinin eperlerindeki örselenmiş bölgenin varlığının, presiyometreden elde edilen deformasyon modülünü azalttığını, drenajsız makaslama dayanımını ise arttırdığını göstermiştir. Deney derinliğinin deformasyon modülü ve drenajsız makaslama dayanımı üzerinde etkili olmadığı görülmüştür. Presiyometre başlığının boy / ap oranı ise, drenajsız makaslama dayanımının olduğundan büyük belirlenmesine sebep olmakla birlikte, deformasyon modülü üzerinde önemsiz bir etkiye sahiptir. Düşük geçirimliliğe sahip zeminlerde, presiyometre deneyi sırasında, aşırı boşluk suyu basıncının drenaj miktarını belirlemek için sayısal analizler yapılmış olup bu analizler, geçirimliliği 10^{-10} m/sn den düşük zeminlerde drenajın gerçekleşmediğini göstermiştir. Ters analiz tekniğinin, hem kohezyon hem de sürtünme açısına sahip zemin ve kayaların makaslama dayanımının belirlenmesinde başarılı sonuçlar verdiği görülmüştür.

Anahtar kelimeler: Presiyometre, Drenajsız Makaslama Dayanımı, Kaya Kütlesi, Sayısal Analiz, Ters Analiz, Jeolojik Dayanım İndeksi (GSI)

To My Family

ACKNOWLEDGEMENTS

I express sincere appreciation to Prof. Dr. Vedat Doyuran and Prof. Dr. Reşat Ulusay for their guidance and kind restless supervision throughout this thesis and since the beginning of my Ph.D program. I also extend my sincere thanks to Assoc. Prof. Dr. Tamer Topal and Assoc. Prof. Dr. K. Önder Çetin for their positive attitude and helpful feedback. I would further like to thank Assoc. Prof. Dr. K. Önder Çetin for helping me to understand soil behavior and concepts of numerical modeling. I would like to thank Assoc. Prof. Dr. Mehmet Orhan and Dr. Mustafa Özer for their support during field and laboratory studies. I extend my thanks to Mr. Fatih Adil, without whose efforts, drilling operations would not have been so effective. I cordially would to like to thank my family and my wife Gökçen Işık for their encouragements, patience and support during my Ph.D program. Finally I would like to express my sincere thanks to the faculty members at Gazi University Construction Department.

TABLE OF CONTENTS

PLAGIARISM	iii
ABSTRACT	iv
ÖZ	vi
DEDICATION	viii
ACKNOWLEDGEMENTS	ix
TABLE OF CONTENTS	x
LIST OF FIGURES	xiv
LIST OF TABLES	xxiii
CHAPTER	
1. INTRODUCTION	1
2. PREVIOUS STUDIES	3
2.1 Studies on Determination of Deformation Modulus by Pressuremeter	3
2.2 Determination of Undrained Shear Strength of Saturated Clays.....	11
2.3 Inverse Analysis of Pressuremeter Test	16
2.4 Studies on the Materials Selected for the Thesis	18
2.4.1 Engineering geological studies on Dikmen greywackes..	18
2.4.2 Engineering geological studies on Ankara andesites	19
2.4.3 Soil mechanics studies on the Eymir Lake clay	19

3. DESCRIPTION OF THE SELECTED LITHOLOGICAL UNITS	20
3.1 Selected Lithological Units and Sites	20
3.2 Geology of the Ankara Region	21
3.3 Lithological Characteristics of the Test Sites	25
4. GEOTECHNICAL SITE INVESTIGATIONS	37
4.1 Rock Mass Characterisation	37
4.1.1 Dikmen greywackes	38
4.1.2 Weathered andesites	48
4.1.3 Mudrocks	49
4.2 Pressuremeter Tests	51
4.2.1 Types of pressuremeters	51
4.2.1.1 Ménard type pressuremeters	52
4.2.1.2 Self boring pressuremeters	56
4.2.1.3 Cone – pressuremeter	57
4.2.1.4 The push – in pressuremeter (PIP)	58
4.2.1.5 The oymeter	59
4.2.1.6 Definition of limit pressure	60
4.2.2 Pressuremeter test results	61
4.2.2.1 Pressuremeter tests in Dikmen greywackes	61
4.2.2.2 Pressuremeter tests in the weathered andesites .	70
4.2.2.3 Pressuremeter tests in mudrocks	74
4.2.2.4 Pressuremeter tests in the Eymir Lake clays	77
4.3 Seismic Refraction Surveys	79
4.3.1 Seismic refraction surveys in Dikmen greywackes	81
4.3.2 Seismic refraction studies in the weathered andesites	84

4.3.3 Seismic refraction studies in the mudrocks	85
4.4 Cone Penetration Tests	86
4.5 Field Vane Tests	88
4.6 Schmidt Hammer Tests	90
5. LABORATORY GEOMECHANICAL TESTS	94
5.1 Block Punch Strength Index Tests	94
5.2 Uniaxial Compressive Strength Tests	99
5.3 Soil Mechanics Index Tests	106
5.4 Laboratory Vane Shear Tests	108
5.5 Consolidation Tests	110
5.6 Triaxial Tests	112
5.7 Direct Shear Box Tests	115
6. EVALUATION OF THE PRESSUREMETER TEST RESULTS	118
6.1 Determination of Deformation Modulus	118
6.1.1 Numerical simulation of the pressuremeter tests for determination of deformation modulus	124
6.1.1.1 One-dimensional simulation of the pressuremeter test	124
6.1.1.2 Two-dimensional simulation of the pressuremeter test	130
6.1.1.3 Effect of disturbance on shear modulus	134
6.1.1.4 Determination of the volume of the material tested by a pressuremeter test	136
6.1.1.5 Discrete element modeling of pressuremeter test	139
6.1.2 Determination of deformation modulus from pressuremeter tests	141
6.1.2.1 Eymir Lake clays	141
6.1.2.2 Weathered andesites	144

6.1.2.3	Dikmen greywackes	147
6.1.2.4	Pressuremeter tests in the mudrocks	161
6.1.3	Relationship between seismic velocities and shear modulus	162
6.2	Determination of Undrained Shear Strength	164
6.2.1	One-dimensional simulation of the pressuremeter test in clays	174
6.2.1.1	Effect of disturbance on the undrained shear strength derived from pressuremeter	176
6.2.1.2	Effect of unloading on the derived undrained shear strength	181
6.2.1.3	Pore pressure dissipation during pressuremeter test	184
6.2.2	Two-dimensional simulation of the pressuremeter test in clays	186
6.2.3	Undrained shear strength of the Eymir Lake clays	190
6.2.3.1	Cone penetration tests in the Eymir Lake clays ..	190
6.3	Inverse Analysis Technique	200
7.	CONCLUSIONS AND RECOMMENDATIONS	204
	REFERENCES	208
	VITA	227

LIST OF FIGURES

Figure 2.1	Typical curve obtained from a Ménard pressuremeter (modified from Mair and Wood, 1987)	4
Figure 2.2	Rock mass model containing three orthogonal discontinuity sets (Kulhawy, 1978)	9
Figure 2.3	Joint set aligned perpendicular with respect to vertical borehole axis	9
Figure 2.4	Graphical representation of the Palmer's solution	14
Figure 2.5	The curve matching procedure (Cambou et al., 1990) ...	17
Figure 2.6	Determination of shear strength parameters of the c , ϕ soils (Cambou et al., 1990)	17
Figure 3.1	Location map of the selected sites which are shown by flags	22
Figure 3.2	Generalized stratigraphic column of Ankara and its vicinity (arranged from Chaput, 1931; Leuchs, 1944; Erol, 1954, 1961, 1968; Dağer et al., 1963; Norman, 1972, 1973; DSI, 1976; Çalgın et al., 1973; Çapan and Buket, 1975 by Kasapoğlu, 1980)	23
Figure 3.3	(a) Geological map of Beytepe campus and its vicinity (Özilcan, 2004), (b) distribution of greywacke outcrops in Ankara (Nurlu, 1996), (c) distribution of the Miocene volcanics	24
Figure 3.4	A close up view of the greywacke rock mass at the Beytepe campus site of Hacettepe University	26
Figure 3.5	Photograph of the greywacke with carbonate matrix	26
Figure 3.6	Thin-section photograph of the greywacke with carbonate matrix (cross nicols)	27

Figure 3.7	Thin-section photograph of the greywacke with clay matrix (cross nicols).....	27
Figure 3.8	Thin section photograph of greywacke sample taken from the site near to Beyaz Ev (cross nicols).....	28
Figure 3.9	A view from the greywacke rock mass at Dikmen	29
Figure 3.10	Intact core sample of greywacke from Dikmen	30
Figure 3.11	The thin section view of the sample taken from Dikmen site (cross nicols)	30
Figure 3.12	General profile of the highly weathered andesites in Ankara and a shallow slope failure occurred within the intensely weathered rock mass	32
Figure 3.13	The XRD diffractogram of the andesite sample taken from Solfasol district	32
Figure 3.14	(a) Rock material, (b) rock mass of the weathered andesite.....	34
Figure 3.15	The thin section of the andesite sample (cross nicols).....	34
Figure 3.16	XRD diffractogram of one of the andesite samples taken from Pursaklar district	35
Figure 4.1	Panoramic view of the greywacke from an old foundation cut near the boreholes at Beytepe area (workshop site)	40
Figure 4.2	The range of GSI values based on the classification sheet of Hoek (1999) for the greywackes	41
Figure 4.3	The range of GSI values based on the classification sheet of Sönmez and Ulusay (2002) for the greywackes.....	42
Figure 4.4	General view of the rock mass from an old foundation cut near one of the boreholes at Beytepe Campus (Beyaz Ev)	44
Figure 4.5	General view of the greywacke rock mass from a foundation cut near the boreholes 1 and 2 at CAKS	46
Figure 4.6	Photograph of a typical discontinuity surface from the CAKS	47

Figure 4.7	Histogram of the RQD values for the mudrocks	50
Figure 4.8	Ménard Pressuremeter (type GC) and its probe used in this study	54
Figure 4.9	Inside of the Ménard pressuremeter probe	54
Figure 4.10	Three possible cases related to the pressures of gas and water in pressuremeter probe (Apageo Segelm, 1997).....	55
Figure 4.11	Self boring pressuremeter kit, probe and control parts (Cambridge In-situ, 2005)	57
Figure 4.12	Cone pressuremeter (modified from, Yu et al., 1996)	58
Figure 4.13	The assembled Elastometer and testing equipment (Oyo – Corporation, 2005)	60
Figure 4.14	Summary of the method of calculation of shear modulus (G)	62
Figure 4.15	A view from drilling near the workshop	64
Figure 4.16	Borehole locations and seismic survey lines at the workshop area	64
Figure 4.17	The corrected pressuremeter graph performed at a depth of 2.5 m in BH 2	65
Figure 4.18	The borehole locations and seismic survey lines at the Beyaz Ev area	66
Figure 4.19	The corrected pressuremeter graph obtained from a depth of 3.7 m in BH 4	67
Figure 4.20	Borehole locations and seismic survey lines for the CAKS site on a plan view	68
Figure 4.21	The histogram of the deformation modulus obtained from all pressuremeter tests performed at Dikmen greywackes	70
Figure 4.22	The histogram of deformation modulus values of the weathered andesites.	73
Figure 4.23	Sample PMT graph obtained from the depth of 7.7 m in BH 15	73

Figure 4.24	Histogram of the deformation modulus for mudrocks	74
Figure 4.25	A sample PMT graph obtained at a depth of 2 m in BH 21	77
Figure 4.26	A sample PMT graph obtained from the depth of 2 m in Eymir Lake clays	78
Figure 4.27	The seismometer used during the seismic refraction surveys	80
Figure 4.28	Field layout of the refraction survey at Beytepe campus of Hacettepe University, Beyaz Ev location	82
Figure 4.29	(a) The depth model and (b) time distance graphs of the seismic refraction survey performed in greywackes at workshop location of Beytepe Campus (section A)	83
Figure 4.30	(a) The CPT data logging system and (b) the cone used in the study	86
Figure 4.31	The tip resistance, sleeve friction, excess pore pressure measurements and soil behavior type determined from the CPT tests in the Eymir Lake clays	87
Figure 4.32	Field vane used in the study	89
Figure 4.33	Histogram of the uniaxial compressive strength values of the greywackes at workshop site.....	91
Figure 4.34	The histogram of the uniaxial compressive strength of the greywackes at Beyaz Ev site.....	92
Figure 4.35	Histogram of the uniaxial compressive strength of the greywackes at CAKS	93
Figure 5.1	Disk shearing channel and its dimensions (Ulusay et al., 2001)	95
Figure 5.2	Uniformly failed BPI specimen (Ulusay et al., 2001)	95
Figure 5.3	The histogram and descriptive statistics of the BPI results	98
Figure 5.4	The axial stress versus axial strain graph of the greywacke sample taken from Beyaz Ev location at Beytepe Campus of Hacettepe University	100

Figure 5.5	Axial stress versus axial strain graph of the andesite sample from Ovacık taken from a depth of 6 m	101
Figure 5.6	Axial stress versus axial strain plot of the weathered andesite sample from Pursaklar taken from a depth of 15 m in BH 2	102
Figure 5.7	The histogram and descriptive statistics of the UCS values of the weathered andesites	103
Figure 5.8	Histogram of the UCS values of the mudrock samples ..	104
Figure 5.9	Laser diffraction instrument, employed in the study	107
Figure 5.10	(a) The laboratory vane test apparatus, (b) and its parts.	109
Figure 5.11	(a) Void ratio versus logarithm pressure plot, and (b) settlement versus square root of time of the Eymir Lake sample taken from a depth of 8.2 m	111
Figure 5.12	The soil sample with vertical filter paper strip wrapped around, prior to test	114
Figure 5.13	Mohr – Coulomb failure envelopes of the samples taken from (a) a depth of 1 m at Solfasol district, (b) a depth of 3.2 m at Pursaklar district	116
Figure 5.14	(a) The shear stress versus horizontal displacement and (b) vertical displacement versus horizontal displacement graphs obtained from direct shear box tests performed on Eymir Lake clay	117
Figure 6.1	A typical deviatoric stress versus axial strain graph and the modulus definitions	119
Figure 6.2	Stress paths followed during pressuremeter tests, laboratory compression tests and plate loading tests up to the failure	121
Figure 6.3	Simplified mesh and boundary conditions of the one-dimensional model (y-dimension of the grid is exaggerated for presentation purposes)	127
Figure 6.4	Pressure versus cavity strain graphs of one-dimensional pressuremeter simulation in a linearly elastic material for a shear modulus of 3846.2 kPa	127

Figure 6.5	One-dimensional pressuremeter simulations using a shear modulus of 3846.2 kPa and two different bulk modulus values, K (8333.3 and 15000 kPa)	129
Figure 6.6	The UDEC model for the one-dimensional pressuremeter simulations	129
Figure 6.7	Mesh (grid) for a pressuremeter simulation at a depth of 3 m	131
Figure 6.8	The boundary conditions at the membrane soil contact..	132
Figure 6.9	The relationship of the ratio of the thickness of the disturbed zone (T_d) to the probe diameter (D_p) with the ratio of the calculated shear modulus to the undisturbed shear modulus	135
Figure 6.10	Stress distributions around the pressuremeter	138
Figure 6.11	Stress distributions around the plate during plate load test	138
Figure 6.12	Comparison of volumes of the material tested by (a) plate load and (b) pressuremeter tests	139
Figure 6.13	The discontinuity model used in UDEC	140
Figure 6.14	The variation of the deformation modulus with depth obtained from pressuremeter tests and from UU triaxial tests	143
Figure 6.15	The relationship between the values of deformation modulus obtained from the pressuremeter tests (PMT) and uniaxial compression (UCST) tests	145
Figure 6.16	Hoek – Brown failure envelope for the greywackes exposed around Beyaz Ev site	148
Figure 6.17	The failure surface of slope 1 at Beyaz Ev	149
Figure 6.18	The failure surface of slope 2 at Beyaz Ev	149
Figure 6.19	The Hoek – Brown failure envelope and the corresponding Mohr – Coulomb failure line within the 0 to 500 kPa normal stress range	151
Figure 6.20	The finite element mesh and boundary conditions for slope 1	151

Figure 6.21	The incremental shear strain contours for slope 1	152
Figure 6.22	The incremental shear strain contours for slope 2	152
Figure 6.23	Variation of the deformation modulus with GSI estimated from Hoek (1999)	154
Figure 6.24	Variation of the deformation modulus with GSI estimated from Sönmez and Ulusay (2002)	154
Figure 6.25	Variation of the deformation modulus with RMR estimated from Bieniawski (1989)	155
Figure 6.26	Variation of UCS with the rock mass deformation modulus	155
Figure 6.27	Variation of the ratio of rock mass modulus to intact rock modulus (E_m/E_i), with RQD for the mudrocks in Sincan	162
Figure 6.28	Relationship between shear wave velocity and shear modulus	163
Figure 6.29	Relationship between primary wave velocity and shear modulus	163
Figure 6.30	Total and effective stress paths of an undrained triaxial test in clay (ESP: effective stress path; TSP: total stress path; OC: overconsolidated; NC: normally consolidated).....	164
Figure 6.31	Simulated pressuremeter curves in a linearly elastic perfectly plastic soil, having same undrained shear strength and different shear modulus values	165
Figure 6.32	The effective stress path of a normally consolidated clay during direct simple shear test	169
Figure 6.33	The state of the Mohr circle at the start and at the failure for a vane test	170
Figure 6.34	Graphical representation of the equations proposed by Wroth (1984)	172
Figure 6.35	The pressure versus $\ln(dV/V)$ plot of the one-dimensional pressuremeter simulation for $I_r = 100$	175

Figure 6.36	Shear stress versus cavity strain plots of undisturbed and completely disturbed soil, and apparent cases for various disturbed zone thicknesses	177
Figure 6.37	Shear stress versus cavity strain, plots of undisturbed soil, and apparent cases for various disturbed zone thicknesses which are determined with one-dimensional Flac (2002) simulations performed for case “a”	179
Figure 6.38	The pressure versus LN (dV/V), plots of undisturbed soil and apparent case for t/r_0 equal to 1 determined with one-dimensional Flac (2002) simulations performed for case “a”	179
Figure 6.39	The overestimation ratio versus normalized thickness of the disturbed zone	180
Figure 6.40	(a) Uncorrected LN(dV/V) versus pressure plot of the simulation with $I_r = 100$, $\sigma_{vt} = 100$ kPa and $K_0 = 1.0$ case, (b) after correction	183
Figure 6.41	One-dimensional model, used for the simulation of pore pressure dissipation	186
Figure 6.42	Relationship between permeability and dissipation of excess pore pressures at the selected points	186
Figure 6.43	Comparison of the undrained shear strength values obtained from L/D ratio of 5.3 and 11 for $I_r = 25$, $S_u = 50$ kPa conditions	188
Figure 6.44	Cone factors determined from various solutions	191
Figure 6.45	Plasticity index versus cone factors (Lunne and Kleven, 1981)	191
Figure 6.46	The finite difference grid and the boundary conditions used during the study	193
Figure 6.47	Tip resistance versus tip displacement for small and large strain simulations	194
Figure 6.48	Plastic zones during cone penetration for a rigidity index of 50	194
Figure 6.49	Plastic zones during cone penetration for a rigidity index of 200	195

Figure 6.50	Tip resistance versus cone displacement for various K_0 values	195
Figure 6.51	Vertical stress distribution due to second stage of the cone penetration simulation	197
Figure 6.52	The pressure versus $\text{LN}(dV/V)$ plot for the pressuremeter test performed at a depth of 2 m (a) for uncorrected, and (b) datum corrected cases	198
Figure 6.53	Variation of undrained shear strength of the Eymir Lake clay determined by various tests	199
Figure 6.54	Curve matching procedure and obtained geotechnical parameters for the highly weathered andesite from Solfasol district at a depth of 1.5 m	201
Figure 6.55	Curve matching procedure and obtained shear strength parameters for the highly weathered andesite in Pursaklar district at a depth of 3.2 m	202

LIST OF TABLES

Table 2.1	Some examples of the theoretical interpretation of a pressuremeter tests in saturated clays. (Modified from Clarke, 1995)	14
Table 4.1	The rock mass parameters and RMR values of the greywacke at the workshop location	43
Table 4.2	Various rock mass parameters and RMR values for the Beyaz Ev site	44
Table 4.3	Various rock mass parameters and RMR values at the CAKS site	47
Table 4.4	Probe dimensions (Centre D'Etudes Ménard, 1975)	54
Table 4.5	Shear modulus, deformation modulus and Ménard limit pressure of the rock mass determined at the workshop area	65
Table 4.6	Shear modulus, deformation modulus and Ménard limit pressure of the rock mass determined at Beyaz Ev area	67
Table 4.7	Shear modulus and deformation modulus of the rock mass observed at CASK	69
Table 4.8	Summary of pressuremeter tests performed in Solfasol district	71
Table 4.9	Summary of pressuremeter tests performed in Ovacık district	71
Table 4.10	Summary of pressuremeter tests performed in Pursaklar district	72
Table 4.11	Shear modulus, deformation modulus and Ménard limit pressure from PMT	75

Table 4.12	Shear modulus, deformation modulus and Ménard limit pressure of the Eymir Lake clays	78
Table 4.13	Summary of the results obtained from the seismic refraction surveys performed at Beytepe campus of Hacettepe University, Workshop location	81
Table 4.14	Summary of the results obtained from the seismic refraction surveys performed at Beytepe campus of Hacettepe University, Beyaz Ev location	81
Table 4.15	Summary of the results obtained from the seismic refraction surveys performed at Dikmen CAKS location.....	82
Table 4.16	The summary of the results obtained from the seismic refraction surveys performed at Solfasol district	84
Table 4.17	The summary of the results obtained from the seismic refraction surveys performed at Ovacık district	84
Table 4.18	The summary of the results obtained from the seismic refraction surveys performed at Pursaklar district	84
Table 4.19	The summary of the results obtained from the seismic refraction surveys performed at mudrocks	85
Table 4.20	The values of undrained shear strength determined from the field vane tests	89
Table 5.1	Block punch index test results of Dikmen greywackes ..	97
Table 5.2	Summary of the uniaxial compressive strength test results, from greywacke samples	100
Table 5.3	Results of the UCS tests performed on the weathered andesites taken from Ovacık	102
Table 5.4	The results of the UCS tests performed on the Pursaklar samples	103
Table 5.5	Summary of the UCS test results from mudrocks	105
Table 5.6	The summary of the index test results of studied cohesive soils	107
Table 5.7	The undrained shear strength values of the samples ...	109
Table 5.8	Summary of the consolidation test results	112

Table 5.9	Undrained shear strength values of the Eymir Lake clay samples determined from UU tests	113
Table 5.10	Undrained shear strength values of the Eymir Lake clay samples determined from the CU tests	114
Table 6.1	The L/D ratio versus G_{calc}/G_{true} relationship, determined from two-dimensional linearly elastic pressuremeter simulations	132
Table 6.2	The Hoek and Brown failure parameters used in the analyses	148
Table 6.3	The results of the analyses for slopes 1 and 2	148
Table 6.4	Empirical methods used for the estimation of the deformation modulus	157
Table 6.5	The input parameters used in the empirical equations, for the greywackes	158
Table 6.6	The rock mass deformation modulus values (MPa) for the greywackes determined by various empirical equations.....	159
Table 6.7	The results of one-dimensional simulations for the determination of the effect of unloading on S_u	182
Table 6.8	Results of the numerical simulations performed in 3 meter depth	188
Table 6.9	Correction factors for varying L/D ratios	189
Table 6.10	S_u determined from pressuremeter tests	197

CHAPTER 1

INTRODUCTION

The pressuremeter test, first developed by Ménard (1956), is a widely used in-situ test, which can provide stress and deformation relationship of a particular ground in-situ. In spite of the apparently considerable potential of this device, inconsistencies in results are common (Bowles, 1996).

During a pressuremeter test shear modulus and limit pressure (P_l) are directly measured. From the measured limit pressure (P_l), undrained shear strength and friction angle of the soils can be estimated by utilizing previously established empirical methods. In the literature, there are also more robust theoretical methods for the estimation of shear strength parameters of soils from the pressuremeter tests which are based on the infinitely long cylindrical cavity expansion theory. Therefore, these methods do not account for the effects of limited length of the probe which may probably affect the results.

The purpose of this thesis is to investigate the possible effects of some variables like testing depth, length to diameter ratio of the probe, in-situ lateral stress, presence of disturbed annulus around the borehole etc. on the derived parameters from the pressuremeter test, and to develop possible alternative methods for the determination of undrained shear strength of cohesive soils, and cohesion and internal friction angle of intermediate geomaterials. In this study, it is also aimed to investigate the effect of RQD, (or some other rock mass parameters such as GSI and

RMR) and intact rock strength on the deformation modulus determined from the pressuremeter test. For this purpose, Dikmen greywackes, weathered andesites and mudrocks exposed around Ankara - Sincan region were selected.

The undrained shear strength determined from the pressuremeter test is generally higher than those from other field or laboratory tests (Bowles, 1996; Houlsby and Carter, 1993). In the literature, differences in strain rate, mode of failure, partial consolidation, and length to diameter ratio are attributed to this overestimation. However, partial consolidation, strain rate and different mode of failure alone could not cause this large difference (Houlsby and Carter, 1993). In this study, numerical methods are used to determine the effects of test depth, length to diameter ratio of the pressuremeter probe, disturbance on the pressuremeter determined deformation modulus and undrained shear strength and possible correction factors depending on length to diameter ratio, are established. The applicability of these correction factors is tested by performing pressuremeter tests, field vane tests, cone penetration tests and laboratory tests on normally to slightly overconsolidated clays from the Eymir Lake.

There is no widely accepted direct solution for the determination of the cohesion and internal friction angle of intermediate geomaterials from the pressuremeter test. The inverse analysis technique, which is a type of back-analysis, for the determination of constitutive parameters of the ground by matching the observed pressuremeter curve with the numerically determined curve (e.g. Cambou et al. 1990, Zentar et al. 2001), may be used to estimate both cohesion and internal friction angle. In this study, the applicability of the inverse analysis is checked using the direct shear box and pressuremeter tests in the weathered andesites.

CHAPTER 2

PREVIOUS STUDIES

This study is focused on the pressuremeter. In this section literature review related to pressuremeter is presented and the main findings of the previous studies are discussed. For pressuremeter testing, weak rocks (weathered Ankara andesites, dikmen greywackes and mudrocks exposing around Sincan) and saturated clay deposits (Eymir Lake clays) were selected. Therefore, the previous studies performed on these materials will also be reviewed under separate subheadings.

2.1 Studies on Determination of Deformation Modulus by Pressuremeter

For a linearly elastic soil, the shear modulus can be theoretically determined from the slope of the pressure – expansion curve of the pressuremeter. This method is based on the infinitely long cylindrical cavity expansion theory. Lamé (1852) first formulated the equation for the radial expansion of a cylindrical cavity in an infinite elastic medium. Ménard (1961) proposed the use of theory of expansion of infinitely long cylindrical cavity for the calculation of the shear modulus.

During an in-situ loading test (plate load test, borehole extension test, etc.) both loading and unloading modulus values can be determined. Loading modulus includes both plastic (permanent) and elastic deformations, and unloading modulus includes elastic displacements only. However, the term “modulus of deformation” (or deformation modulus, E) signifies that the value of E is calculated from the data of the loading portion of the load/deformation curve using both elastic and permanent deformation (Goodman, 1989). The pressuremeter modulus is often presumed to be roughly equivalent to Young’s modulus (Kulhawy and Mayne, 1990).

By using analysis of elastic expansion of cylindrical cavities, the well-known relationship given below is obtained. In this relationship, “ μ ” is the Poisson’s ratio, “V” is the sum of the initial volume of the measuring cell and the mean additional volume injected to the measurement probe.

$$E = (1 + \mu) \cdot 2V \cdot (\Delta P / \Delta V) \quad (2.1)$$

Therefore, using the slope of the linear part of the pressure expansion curve of the pressuremeter test graph (Figure 2.1) the deformation modulus of the soil is obtained.

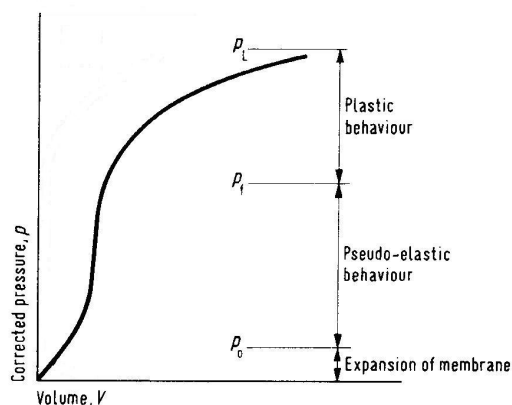


Figure 2.1 Typical curve obtained from a Ménard pressuremeter (modified from Mair and Wood, 1987).

Although the deformation modulus is determined from the theoretical solution of the infinitely long cavity expansion, the analysis based on theory of expansion of infinitely long cavity suffers from plane strain assumption, i.e, the length of the pressuremeter is assumed as infinite. In this analysis, the deformation occurring around the cavity is assumed to be radial only, i.e, no vertical deformation is considered.

Deformation and the strength properties of the rock mass are influenced from the mechanical properties of the rock material and the discontinuities. Discontinuities usually have negligible tensile and shear strength that are significantly smaller than that of the surrounding rock material under most circumstances. Therefore, it is reasonable to assume that the discontinuities will have a marked weakening effect on the rock masses, and the degree of weakening will depend on the orientation, frequency, size and the shear strength of the discontinuities. To obtain the strength and the deformation parameters of the rock mass, one should be able to test the adequate amount of rock mass which includes representative amount of discontinuities. To overcome this difficulty, large sized laboratory samples should be taken or alternatively a proper in-situ test should be performed. These two approaches may not be economical for the small projects or at the pre-design stage. The empirical methods can be used to estimate the strength and deformability of the rock masses. These methods depend on rock mass classification systems. For example, one can estimate the shear strength of the rock mass by using the Hoek – Brown nonlinear failure criterion (Hoek and Brown, 1997) or modulus of elasticity can be estimated using Rock Mass Rating (RMR) and Geological Strength Index (GSI).

Bieniawski (1973) and Serafim and Pereira (1983), developed empirical relationships for the estimation of deformation modulus from RMR only. Equations 2.2 and 2.3 present the relationship of Bieniawski (1978) and Serafim and Pereira (1983), respectively.

$$E_M = 2.RMR - 100 \quad (\text{for } RMR > 50) \quad (2.2)$$

$$E_M = 10^{(RMR-10)/40} \quad (\text{for } RMR \leq 50) \quad (2.3)$$

It was indicated by Ulusay (1991) that the methods of Serafim and Pereira (1983) and Bieniawski (1978) estimated a higher rock mass modulus of deformability than that of the rock material.

Nicholson and Bieniawski (1990) and Mitri et al. (1994) developed empirical relationships using both intact rock modulus and RMR. Equation 2.4 and 2.5 are the relationships, suggested by Nicholson and Bieniawski (1990) and Mitri et al. (1994), respectively.

$$E_M = E_i \cdot [0.0028.RMR^2 + 0.9 \exp(RMR / 22.82)] \quad (2.4)$$

$$E_M = E_i \cdot [0.5 \cdot (1 - (\cos(\pi.RMR / 100)))] \quad (2.5)$$

Where E_i is the intact rock modulus.

Hoek and Brown (1997) developed the following equation for the estimation of deformation modulus of the rock masses using GSI and uniaxial compressive strength (UCS), of the intact rock.

$$E_M = \sqrt{\frac{UCS}{100}} \cdot 10^{(GSI-10)/40} \quad (\text{for } UCS \leq 100 \text{ MPa}) \quad (2.6)$$

Barton (2002) utilized the rock mass classification system called “Q system” (Barton et al., 1974) for the development of an empirical relationship (Equation 2.7) considering the uniaxial compressive strength of the intact rock.

$$E_M = Q \cdot \frac{UCS}{100} \quad (2.7)$$

Kayabaşı et al. (2003), Gökçeoğlu et al. (2003), and Sönmez et al. (2004) used the data from 60 plate load and 55 dilatometer tests from two dam sites in Turkey called Deriner and Ermenek dams and developed empirical relationships for the estimation of deformation modulus of rock masses (Equations 2.8 - 2.10).

$$E_M = 0.135 \cdot \left[\frac{E_i (1 + RQD/100)}{WD} \right]^{1.1811} \quad (\text{Kayabaşı et al., 2003}) \quad (2.8)$$

$$E_M = 0.001 \cdot \left[\frac{(E_i / UCS) \cdot (1 + RQD/100)}{WD} \right]^{1.5528} \quad (\text{Gökçeoğlu et al., 2003}) \quad (2.9)$$

$$E_M = E_i \cdot (s^a)^{0.4} \quad (\text{Sönmez et al., 2004}) \quad (2.10)$$

Where, E_i is the intact rock modulus, WD is the degree of weathering based on ISRM (1981), “ s ” and “ a ” are the Hoek - Brown constants (Sönmez and Ulusay, 2002).

Zhang and Einstein (2004) proposed equations 2.11 to 2.13 for the estimation of rock mass modulus using the intact rock modulus and RQD.

$$E_M = E_i \cdot 0.2 \cdot 10^{0.0186RQD - 1.91} \quad (\text{lower bound}) \quad (2.11)$$

$$E_M = E_i \cdot 10^{0.0186RQD - 1.91} \quad (\text{mean}) \quad (2.12)$$

$$E_M = E_i \cdot 1.8 \cdot 10^{0.0186RQD - 1.91} \quad (\text{upper bound}) \quad (2.13)$$

Gökçeoğlu et al. (2004) developed a neuro – fuzzy model for the prediction of rock mass deformation modulus by using the data mentioned above.

Goodman and Duncan (1971), and Kulhawy (1978) suggested equivalent continuum models for a rock mass containing three orthogonal discontinuity sets. Figure 2.2 shows the model that was used by Kulhawy (1978). Equations 2.14 and 2.15 can be used for the estimation of the rock mass deformation modulus which is generated by using the model of Kulhawy (1978).

$$E_{i(\text{mass})} = \left(\frac{1}{E_{\text{rock}}} + \frac{1}{S_i \cdot K_{ni}} \right)^{-1} \quad (i = 1,2,3) \quad (2.14)$$

$$\frac{E_{\text{mass}}}{E_{\text{rock}}} = \alpha_E = \left(1 + \frac{E_{\text{rock}}}{S_i \cdot K_{ni}} \right)^{-1} \quad (2.15)$$

Where, E_{rock} is the intact rock modulus, S_i is the spacing of the i^{th} discontinuity set, K_{ni} is the normal stiffness of the i^{th} discontinuity set and E_{mass} is the rock mass deformation modulus.

For transversely isotropic rock masses (including one major joint set), such as slate or schist, the rock mass can be assumed as isotropic if the joint set aligned perpendicular with respect to vertical borehole axis (Wittke, 1990) as illustrated in Figure 2.3. For a transversely isotropic rock mass with one major joint set parallel to vertical borehole axis, a solution for elastic constants (E_1 , E_2 , G_2) is available for the borehole expansion tests capable of measuring displacements in different directions. The details of this solution is given by Wittke (1990).

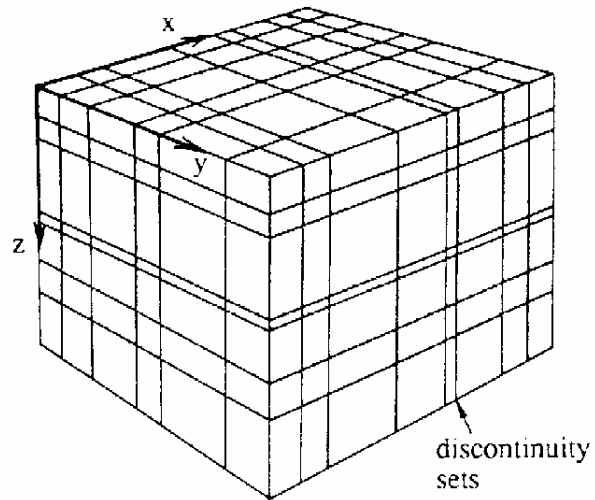


Figure 2.2 Rock mass model containing three orthogonal discontinuity sets (Kulhawy, 1978).

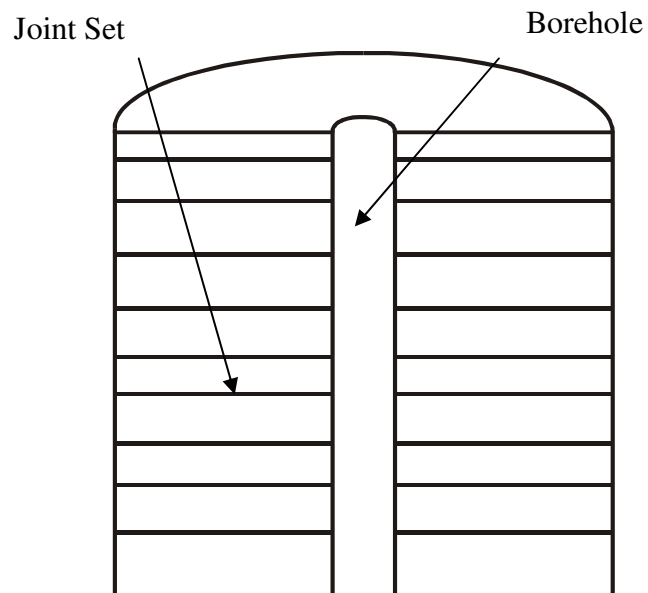


Figure 2.3 Joint set aligned perpendicular with respect to vertical borehole axis.

Greenland (1964) found close agreement between deformation modulus values determined from the plate load and pre-bored pressuremeter tests.

Baguelin et al. (1973) stated that the initial modulus determined from the self boring pressuremeter is significantly higher than that determined from Ménard probe, although Amar et al. (1975) reported similar values of deformation modulus on a dense sand.

Shields and Bauer (1975) found that the values of deformation modulus determined from the pressuremeter are similar to those determined from unconsolidated triaxial tests. However, 1/3 to 1/2 smaller than those determined from plate load tests.

Windle and Wroth (1977 a) suggested that the values of initial shear modulus from the self boring pressuremeter test agree well with the results from the large plate tests in London clay.

Tan and Kaya (1988) indicated that the values of deformation modulus obtained from dilatometer are similar to those determined from plate load tests, although there are some different results too, which are probably due to the volume of the rock tested by dilatometer is not representative of the rock mass.

Powell (1990) found out that the unloading-reloading modulus values obtained from self boring pressuremeters, pre-bored pressuremeters and push-in-pressuremeters were similar.

Wilson and Corke (1990) also indicated that the initial loading values of shear modulus from high pressure dilatometer and from plate load test having 865 mm diameter in sandstone rock mass were very similar.

Based on field and laboratory studies in breccias having carbonate, gypsum, limestone or dolomite matrix, Mahmoud et al. (1990) stated that the laboratory compression tests yielded considerably higher values of secant deformation modulus, and values of deformation modulus from eight of the plate load tests were very close to those from the pressuremeter values. However, 5 of the plate load tests were close to the results of the unconfined compression tests.

2.2 Determination of Undrained Shear Strength of Saturated Clays

Komornik and Frydman (1969) proposed various correlations between the pressuremeter, cone penetration test (CPT), standard penetration test (SPT) and vane shear test. They suggested the following equation for the estimation of undrained shear strength of saturated clays from pressuremeter limit pressure.

$$P_1 - P_0 = 4.S_u \quad (2.16)$$

Where, P_1 is the Ménard limit pressure, P_0 is the pressure at the start of the pseudo – elastic phase of pressuremeter test and S_u is the undrained shear strength.

Amar and Jezequel (1972), and Marsland and Randolph (1977) also suggested the following empirical equations, respectively for the estimation of undrained shear strength from Ménard limit pressure.

$$S_u = \left(\frac{P_1}{10} \right) + 25 \text{ (kPa)} \quad (2.17)$$

$$S_u = \frac{(P_1 - P_0)}{6.18} \text{ (kPa)} \quad (2.18)$$

Gibson and Anderson (1961) developed a method of analysis of pressuremeter test based on undrained expansion of infinitely long cylindrical cavity in a linearly elastic-perfectly plastic soil. Therefore, their analysis is applicable to saturated clays based on the total stress concept.

$$P_{lt} = S_u \left(1 + \ln \frac{G}{S_u} \right) \quad (2.19)$$

Similar analyses were presented by Palmer (1972), Ladanyi (1972), and Baguelin et al. (1972) for the derivation of stress–strain curves for saturated clays from pressuremeter test results. These analyses were also based on the assumption of undrained expansion of infinitely long cylindrical cavity. This method is known as Palmer’s method. The Palmer’s method utilizes P versus $\ln(dV/V)$ curve. The plastic part of the curve should be linear and slope of this portion should be equal to S_u according to theoretical solution (Figure 2.4).

In literature, there are numerous solutions for the interpretation of the pressuremeter test (e.g. Jefferies, 1988; Cao et al., 2001). These solutions are also based on the theory of expansion of infinitely long cavities. Table 2.1 summarizes the examples of the theoretical interpretations of a pressuremeter test.

Houlsby and Carter (1993) proposed correction factors for undrained shear strength determined from the conventional interpretation of the pressuremeter. Their work is based on two-dimensional small strain finite element analyses. Their correction factor depends on the rigidity index (i.e. G/S_u). However, the Houlsby and Carter’s (1993) finite element analyses are based on a mesh consisting of 182 eight – noded quadrilateral elements. For length over diameter ratio equal to infinity case (i.e. plain

strain) they could not obtain the same undrained shear strength input to the model with the one obtained from the interpretation of the simulated pressuremeter curve.

Jefferies (1995; after Houlsby and Carter, 1995), suggested that the correction factor for the determination of undrained shear strength should be lower than that suggested by Houlsby and Carter (1993). He stated that there were some errors with the finite element analyses of Houlsby and Carter (1993).

Shuttle (1995; after Houlsby and Carter, 1995) indicated that further work on the effect of finite pressuremeter length on the undrained shear strength, are needed.

Yeung and Carter (1990) also studied the effect of finite pressuremeter length on the undrained shear strength by finite element method. They suggested increasing correction factors with increasing rigidity values, in contrast Houlsby and Carter (1993) suggested decreasing correction factors with increasing rigidity values.

Collins and Yu (1996) developed analytical solutions for undrained expansion of cavities in both normally and overconsolidated clays using critical state soil models.

Silvestri (1998) showed that the exact solutions of Baguelin et al. (1972), Ladanyi (1972), and Palmer (1972) could also be derived from the expansion of a thick hollow cylinder for which the solution was obtained by Nadai (1950).

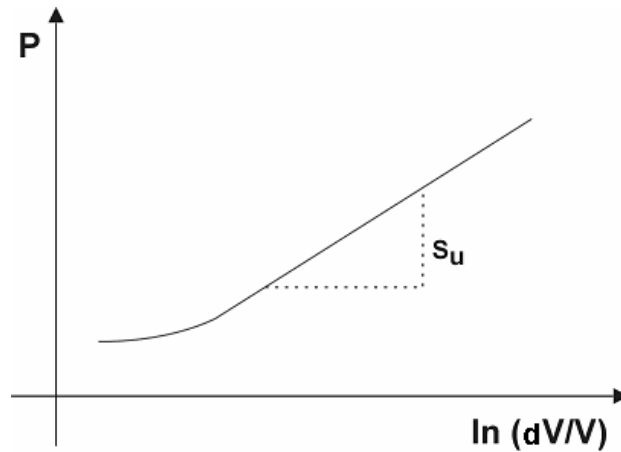


Figure 2.4 Graphical representation of the Palmer's solution.

Table 2.1 Some examples of the theoretical interpretation of a pressuremeter tests in saturated clays (Modified from Clarke, 1995).

Author	Property
Gibson and Anderson (1961)	Linear elastic perfectly plastic material with no volume changes
Windle and Wroth (1977, b)	
Jefferies (1988)	
Houlsby and Withers (1988)	
Denby (1978)	Non-linear elastic perfectly plastic material with no volume changes
Ferreira and Robertson (1992)	
Prévost and Hoeg (1975)	Elastic-plastic with strain hardening or softening with no volume changes
Collins and Yu (1996)	Critical state soil models
Cao et al. (2001)	Modified cam clay model

Most of these analyses are based on small strain theory, however, pressuremeter tests can cause strains of up to 50 % at the pocket wall (Clarke, 1995). Several investigators (e.g. Hughes et al., 1977; Robertson and Hughes, 1986) investigated the expansion of cavities in compressible and dilatant material by taking into account the large strains involved. They found that the solution for incompressible materials (undrained tests for clays) is similar to those for small and large strain theories.

Although the cylindrical cavity expansion theory should provide a sound basis for obtaining the undrained shear strength of clays from pressuremeter tests, the interpreted strengths are often inconsistent with the data measured in high quality laboratory tests (Aubeny et al., 2000). In addition to Aubeny et al. (2000) numerous authors also indicated this phenomenon, for example according to Mair and Wood (1987), the undrained strength values obtained from the conventional interpretation of the pressuremeter are significantly higher than those obtained from other tests.

Lacasse et al. (1990) stated that the undrained shear strength of a clay depends on the mode of failure, anisotropy, strain rate, stress history and the degree of disturbance due to probe installation.

Penumadu et al. (1998) studied the effect of rate of the probe expansion in pressuremeter testing for cohesive soils. These investigators used a special device (flexible boundary cuboidal shear device) for the simulation of pressuremeter device. According to Penumadu et al. (1998), a log cycle increase in strain rate shows an increase in undrained shear strength of 14 %. Therefore, they concluded that strain rate alone cannot be the cause for significant discrepancy in measured undrained shear strength values by considering the strain rates often used for triaxial and self boring pressuremeter testing for clays.

Wroth (1984) has interpreted the effective stress paths of different laboratory and in-situ tests and presented comparisons of undrained shear strength ratios (S_u/σ'_v) for these tests as a function of the effective friction angle and overconsolidation ratio.

2.3 Inverse Analysis of Pressuremeter Test

Cambou et al. (1990) conducted research on the determination of constitutive parameters from pressuremeter tests. These investigators developed a simple one - dimensional (by using axial symmetry and plane strain conditions) finite element software called “PRESSIDENT” to match experimental results with the numerical simulation results. By using this curve matching procedure, one can determine the constitutive parameters of the soil tested. “PRESSIDENT” can use the non-linear elastic model developed by Duncan and Chang (1970), the elasto-plastic model developed by Lade and Oner (1984), the elasto-plastic model developed by Cambou and Lainer (1988). Figure 2.5 shows the curve matching procedure which was used in the study mentioned above.

Cambou et al. (1990) developed a procedure based on their curve matching technique to determine shear strength parameters (c, ϕ) of soils. But this procedure requires two different pressuremeter test curves for the same material from different test depths. This back-analysis procedure is depicted in Figure 2.6.

Zentar et al. (2001) used a one-dimensional finite element software to identify the modified Cam – Clay model parameters from a pressuremeter curve. They have called this curve matching procedure as “inverse analysis”.

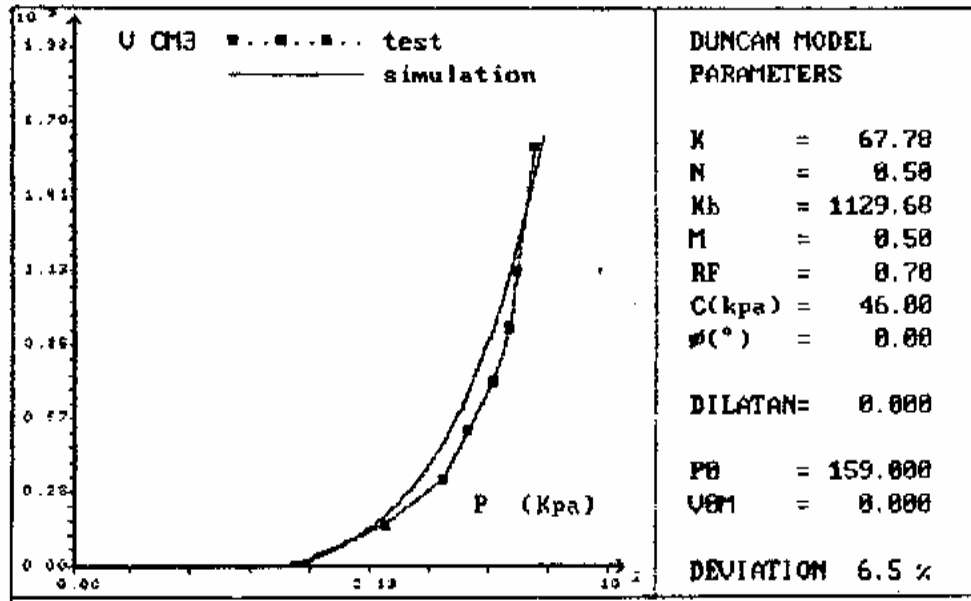


Figure 2.5 The curve matching procedure of (Cambou et al., 1990).

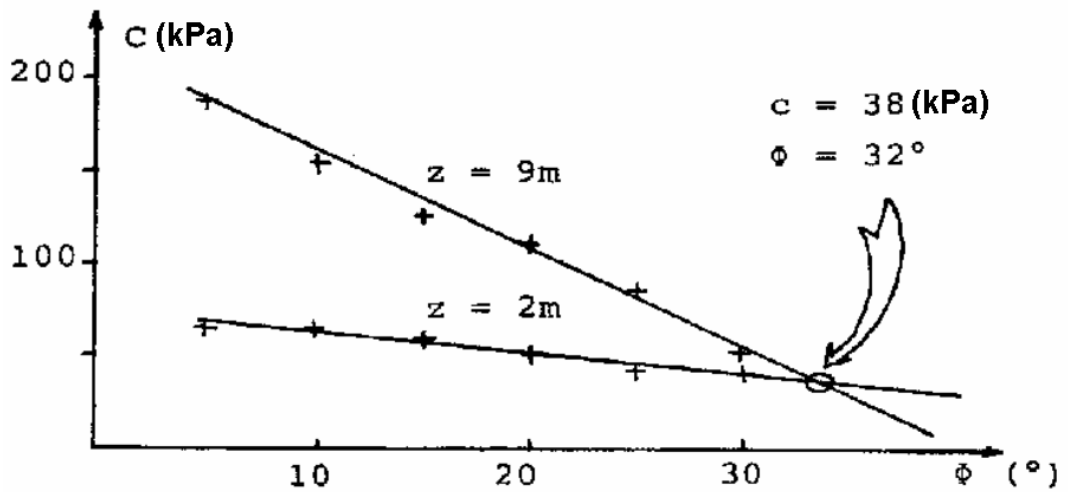


Figure 2.6 Determination of shear strength parameters of the c, ϕ soils (Cambou et al., 1990).

There are also some studies on the numerical interpretation of pressuremeter tests. Examples of such studies are those of Salgado and Byrne (1990), and Houlsby and Yu (1990).

2.4 Studies on the Materials Selected for the Thesis

Weak rocks (weathered Ankara andesites, dikmen greywackes and mudrocks exposing around Sincan) and saturated clay deposits (Eymir Lake clays) were selected for the pressuremeter test studies.

2.4.1 Engineering geological studies on Dikmen greywackes

First engineering geological study on Dikmen greywackes was performed by Kasapoğlu (1980). He determined the intact rock properties such as uniaxial compressive strength, modulus of elasticity and tensile strength of this rock unit.

Nurlu (1996) developed a weathering map of the Dikmen greywackes cropping out in Ankara city center.

Kumtepe (1996) determined the rock mass strength and deformability of the greywackes exposed at various parts of the Ankara metropolitan area using empirical methods of Serafim and Perreira (1983) and Nicholson and Bieniawski (1990).

Çevik (2000) applied the Hoek and Brown empirical failure criterion to the greywackes exposed at Beytepe Campus of Hacettepe University, and analyzed the failed slopes in this unit.

None of the previous studies on the Dikmen greywackes included the direct measurement of rock mass properties.

2.4.2 Engineering geological studies on Ankara andesites

Nathaneil (1972) determined some mechanical properties of the intact Ankara andesites by laboratory tests. Özdoğan (1973) determined dynamic elastic constants of the Ankara andesites with laboratory resonant frequency techniques.

Ulusay (1975) investigated the mechanical properties of the andesites cropping out at the northern part of the city of Ankara.

Karpuz (1982) studied the relationships between weathering degrees of Ankara andesites and its rock mechanical properties.

Karacan (1984) investigated the geomechanical properties of discontinuities of the Ankara andesites.

Ertürk (1997) investigated the engineering properties of the residual soils derived from andesites exposing around the north of Ankara (Solfasol mahallesi) and slope stability problems associated with this soil.

Arıkan (2002) proposed a weathering degree classification system including the Ankara andesites and dacites, based on a rating system.

As with Dikmen greywackes, there is no previous study in which rock mass deformability of the andesites is directly measured.

2.4.3 Soil mechanics studies on the Eymir Lake clay

Bakışkan (1978) studied the shear strength of the Eymir Lake clay taken from a depth of 2.5 m by unconsolidated - undrained, consolidated – undrained and consolidated – drained triaxial compression tests. This study suggested that the Eymir Lake clay is a lightly overconsolidated clay with isotropic undrained shear strength.

CHAPTER 3

DESCRIPTION OF THE SELECTED LITHOLOGICAL UNITS

The greywackes, weathered andesites, Eocene mudrocks exposed at and around Ankara metropolitan area and the saturated clays of Eymir Lake were selected as the materials of this study. Geological and engineering geological features of these lithological units are briefly given in the following sections.

3.1 Selected Lithological Units and Sites

The greywackes are widely distributed around Küçükesat, Büyükesat, Dikmen, and Beytepe districts of Ankara. Rock mass structure of the Dikmen greywackes varies between blocky, and highly fractured and sheared. The highly fractured and sheared greywackes are observed at Beytepe campus of Hacettepe University where two sites were selected for the pressuremeter testing. The site is about 20 km away from the city center (Figure 3.1). A typical site located on blocky greywackes in the Dikmen district, about 4 km away in the south west direction from the city center, was selected for the determination of the deformation modulus (Figure 3.1).

The weathered andesites are typically observed at the north of Ankara. Three sites, namely Ovacık, Solfasol District and Pursaklar, where exists highly to completely weathered andesites crop out, are shown in Figure 3.1.

For undrained shear strength determinations, soft to medium consistency clay deposits are needed. Young and saturated clays of Eymir Lake are considered to be suitable for this purpose. The Eymir Lake clays are exposed 100 m across the main entrance of the General Directorate of Turkish Electricity Authority (TEK) and this site is also accessible for drilling and cone penetration test equipment (Figure 3.1). In addition, mudrocks from a location near to Sincan, north of Ankara, were also employed in the study.

3.2 Geology of the Ankara Region

The oldest rock units cropping out around Ankara are the Paleozoic epimetamorphic schists (Erol, 1961 and 1968). These oldest units are overlain by the Triassic series composed of basaltic blocks and greywackes. Conglomerate, sandstone, siltstone and fossiliferous calcarenites (Lower Jurassic) overlie Triassic rocks and are overlain by the limestone series of Middle and Upper Jurassic. Cretaceous period is represented by ophiolitic melange and flysch series, which are widely distributed around Kırıkkale and Yahşihan. The Paleogene series are widely distributed around the northern part of Ankara, particularly in Karyağdı Mountains and Orhaniye village. These series are composed of conglomerate, sandstone, siltstone, marl and limestone units. Miocene is characterised by lacustrine limestone, marl, claystone, conglomerate, andesite, basalt, agglomerates and tuffs. These units unconformably overlie the Oligocene rocks. Andesites, agglomerates and tuffs, which are the products of Miocene volcanism, crop out around Karşıyaka, Keçiören, Hasköy, Altındağ, Ankara Castle and Mamak. The Pliocene deposits unconformably overly the volcanics. Especially Upper Pliocene series are commonly observed in Ankara and have been formed by the deposition of weathering products of volcanic rocks into the lakes (Erol 1954). The

Quaternary deposits are represented by alluviums and talus. The generalized stratigraphic column of Ankara and geological maps of the test sites are given in Figures 3.2 and 3.3, respectively.

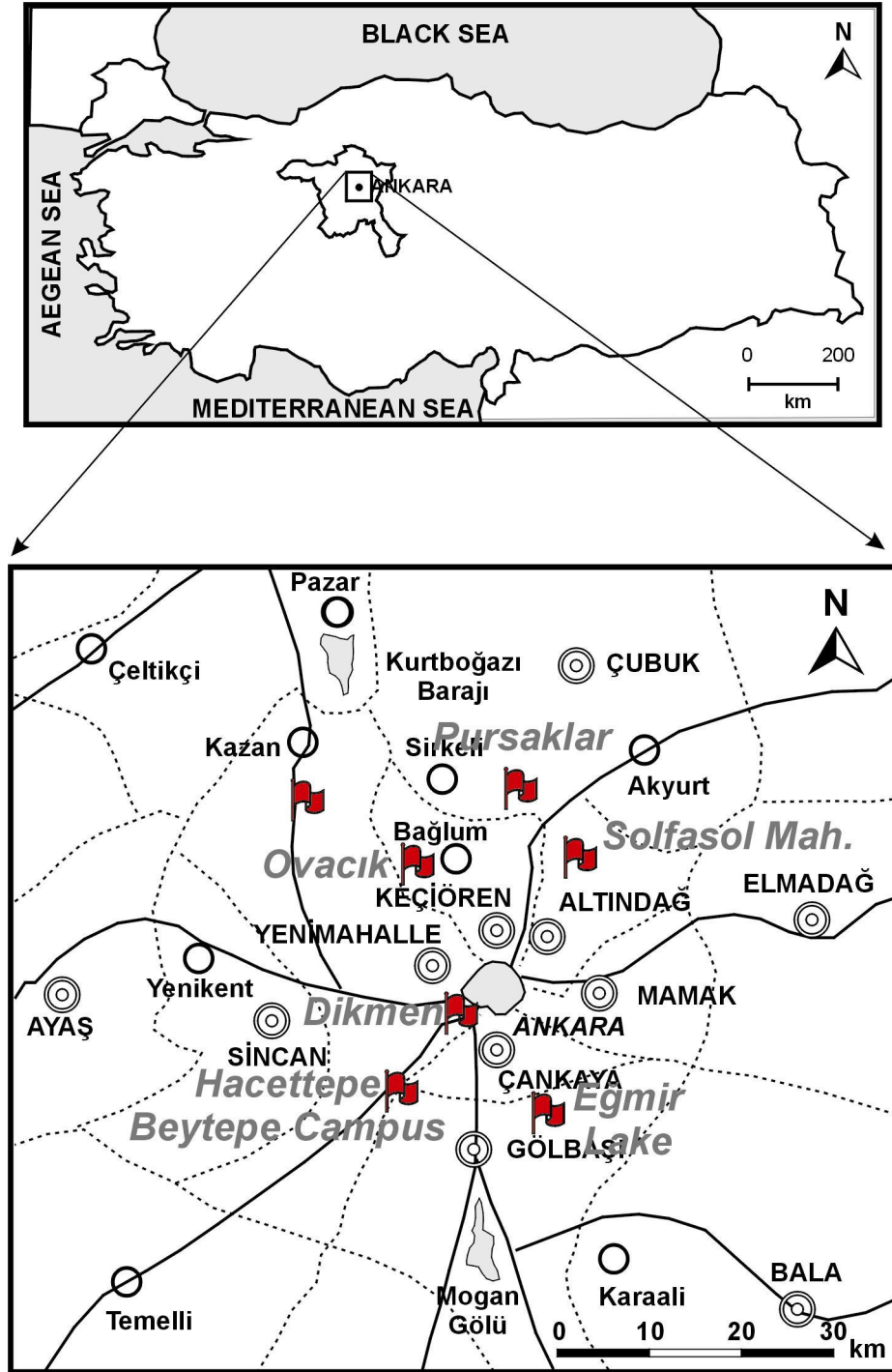


Figure 3.1 Location map of the selected sites which are shown by flags.

Era	Period	Epoch	LITHOLOGICAL SYMBOL	EXPLANATIONS		
CENOZOIC	Quaternary			Alluvium (gravel, sand, silt, clay)		
	Tertiary	Neogene	Pliocene	Upper		Weakly cemented conglomerates red sandy, silty clay, red clays with carbonate concretions
			Pliocene	Lower		Lava blocks mixed with pink marls and tuffs
		Miocene		Lacustrine limestones with chert, clay, marl, claystone, conglomerate andesite, basalt, agglomerates and tuffs		
		Paleogene	Oligocene		Conglomerate, sandstone, marl gypsum	
			Eocene		Fossiliferous sandy limestones and sandstones	
			Paleocene		Flysch sequence (conglomerate, sandstone, siltstone, marl, limestone)	
	MESOZOIC	Cretaceous	Upper		Flysch sequence (conglomerate, sandstone, siltstone, marl, olistostrome)	
			Lower		Ophiolitic melange (serpentinite, radiolarite, spillite, basalt, diabase, limestone, mudstone, marl, flintstone, gabbro and olistostromes)	
		Jurassic	Upper	Malm		Ammonitic limestone, cherty limestone, sandstone, mudstone and limestones
Middle			Dogger		Basaltic conglomerate, sandstone, siltstone and fossiliferous calcarenites	
Lower			Lias		Blocky series: Pillow spillite-basalt blocks, greywackes including Permo - Carboniferous and Triassic limestone blocks	
Triassic				Blocky series: Pillow spillite-basalt blocks, greywackes including Permo - Carboniferous and Triassic limestone blocks		
	Permo - Carboniferous			Epimetamorphic schists (phyllite, graphitic schist, micaschist, chlorite schist, quartzite)		

Not - to - scale

Figure 3.2 Generalized stratigraphic column of Ankara and its vicinity (arranged from Chaput, 1931; Leuchs, 1944; Erol, 1954, 1961, 1968; Dağer et al., 1963; Norman, 1972, 1973; DSİ, 1976; Çalgın et al., 1973; Çapan and Buket, 1975 by Kasapoğlu, 1980).

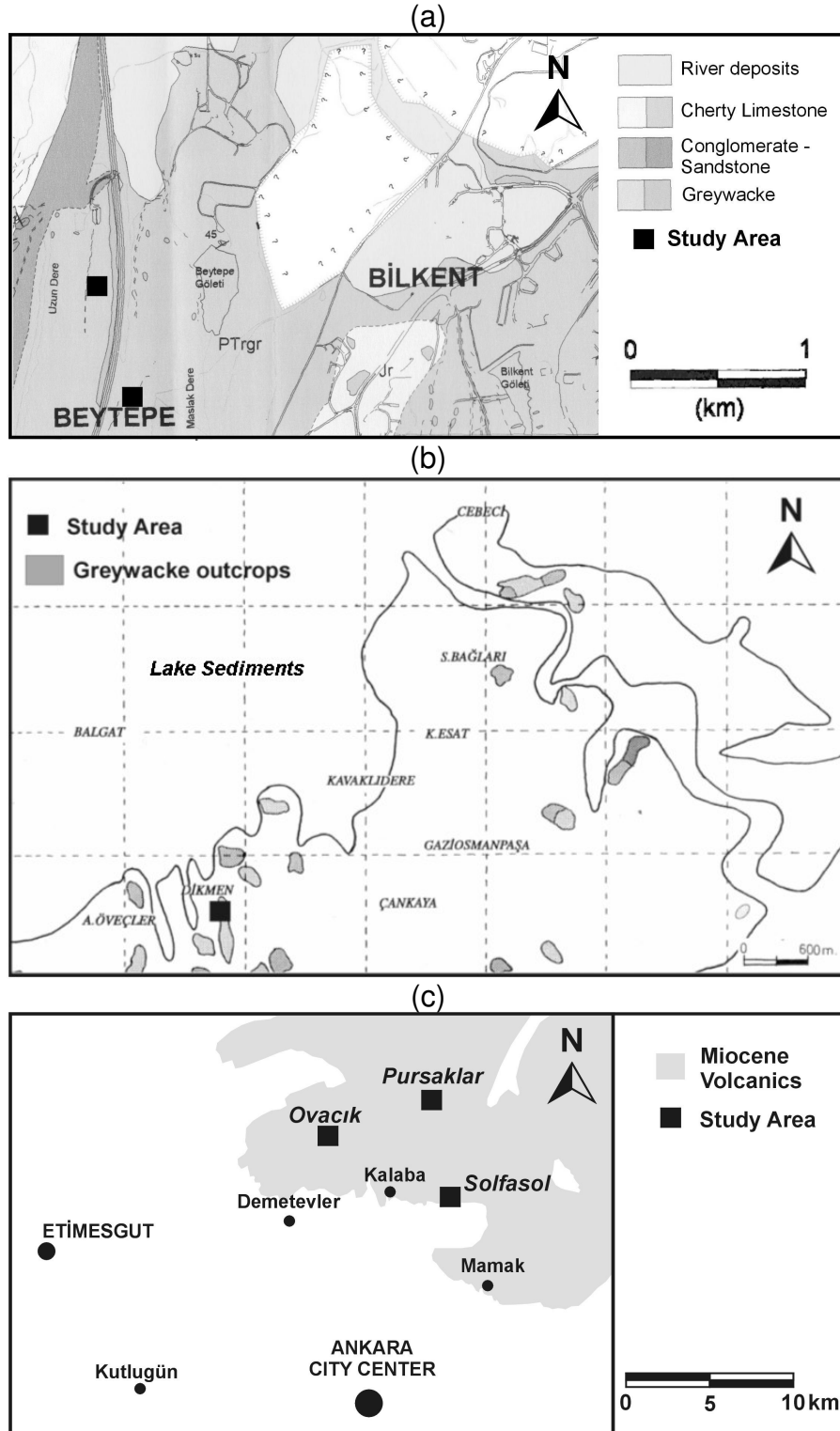


Figure 3.3 (a) Geological map of Beytepe campus and its vicinity (Özilcan, 2004), (b) distribution of greywacke outcrops in Ankara (Nurlu, 1996), (c) distribution of the Miocene volcanics.

3.3 Lithological Characteristics of the Test Sites

(a) Beytepe Campus site of Hacettepe University:

Highly fractured and sheared greywackes crop out at the Beytepe Campus area of Hacettepe University. Two distinct locations with different rock mass characteristics were selected for field studies. These areas are located near a workshop and at the University Club called Beyaz Ev. The greywackes constitute brown to yellow intensively sheared and very weak rock masses. A close-up view of the greywacke rock mass in the Beytepe campus area is shown in Figure 3.4.

Two types of greywackes are distinguished at the Beytepe campus. These are greywackes with clay and carbonate matrix, which are intensively sheared both in micro - and macro – scale. Figures 3.5 and 3.6 display a photograph and thin section view of the greywacke with carbonate matrix taken from near the workshop at the study site, respectively.

The greywackes with carbonate matrix involve strained angular quartz and feldspar grains, chlorite, biotite flakes, rock fragments (rhyolite) and chert fragments. There are many fractures with calcite and iron oxide infillings. Fractures suggest at least two brittle deformation stages. Due to the absence of new mineralization and brittle deformations, it can be assumed that the metamorphism was at very low grade (Göncüoğlu, 2005).

The greywackes contain high amount of clayey matrix and randomly oriented iron oxide stained fractures. The grains are composed of quartz, rock fragments and some feldspar (Figure 3.7).



Figure 3.4 A close up view from the greywacke rock mass at the Beytepe campus site of Hacettepe University.



Figure 3.5 Photograph of the greywacke with carbonate matrix.

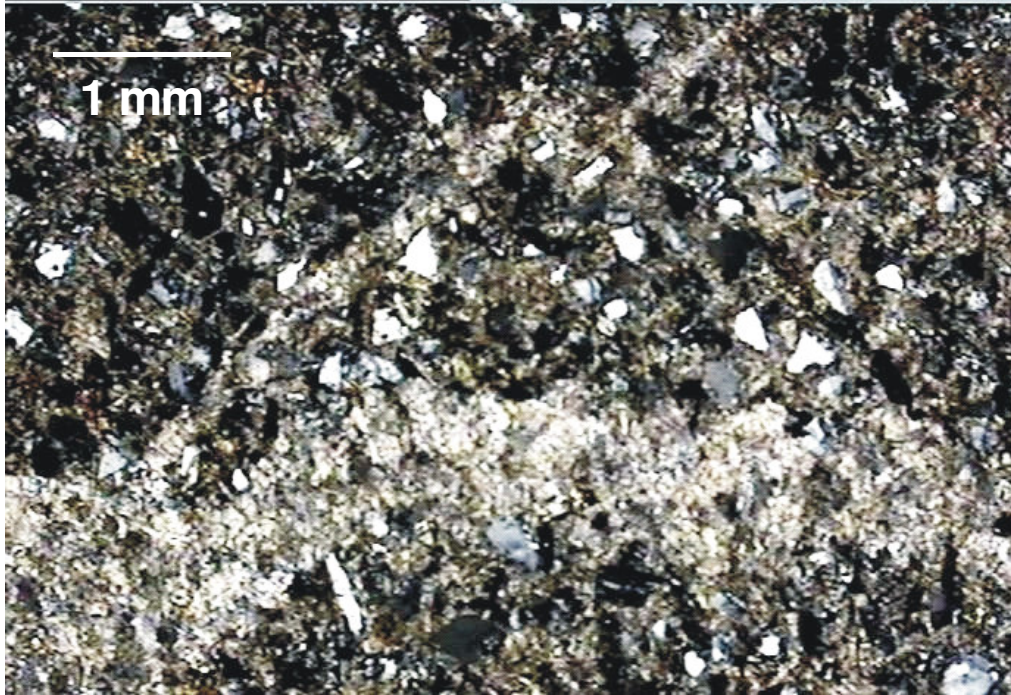


Figure 3.6 Thin-section photograph of the greywacke with carbonate matrix (cross nicols).

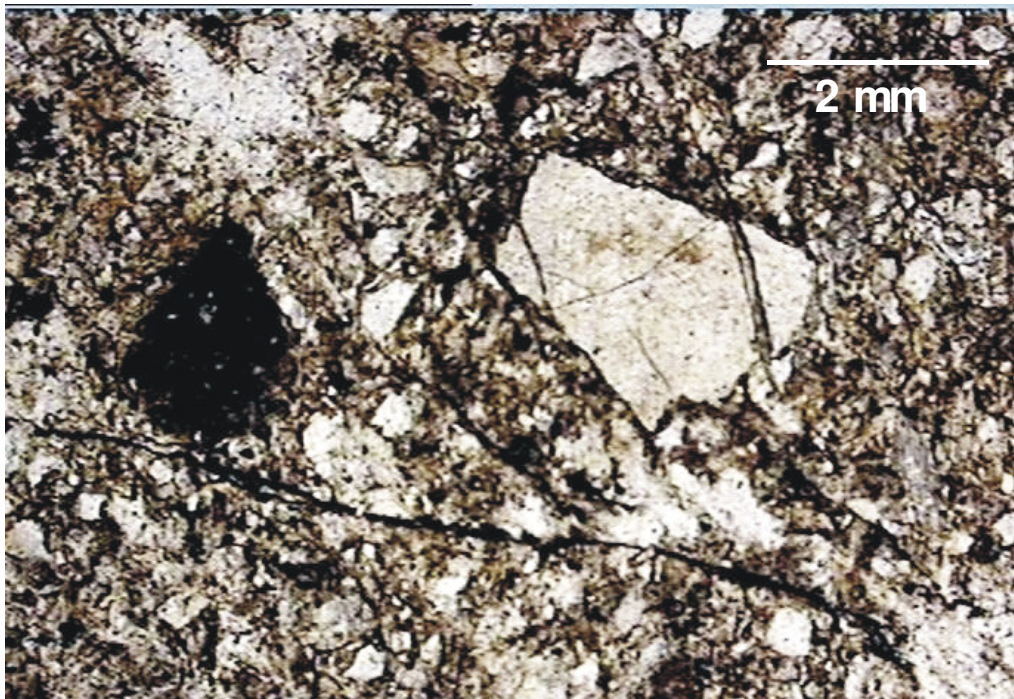


Figure 3.7 Thin-section photograph of the greywacke with clay matrix (cross nicols).

Some of the samples taken from the location near Beyaz Ev include randomly oriented cracks and show some degree of foliation. Fractures are stained by iron oxide and some of them are also filled by calcite. Quartz grains are dominant and to a lesser amount rock fragments, feldspar and biotite are present. This sample has grain-supported structure with very fine grained clayey matrix (Figure 3.8).

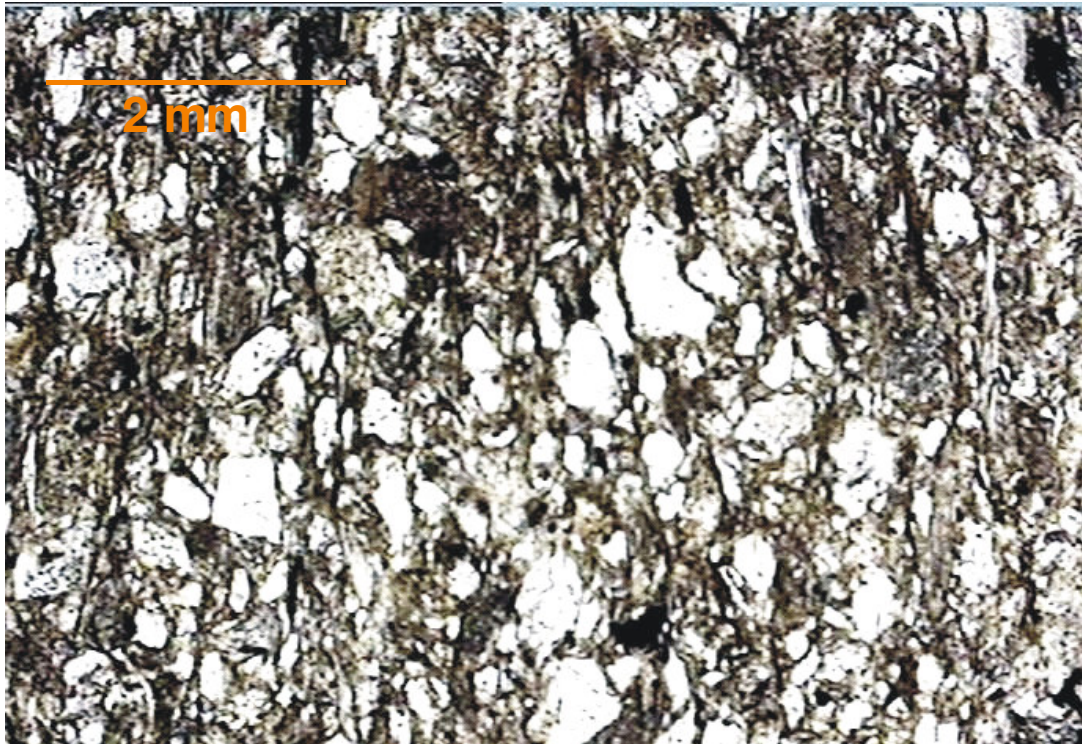


Figure 3.8 Thin section photograph of greywacke sample taken from the site near to Beyaz Ev (cross nicols).

(b) *Dikmen site:*

This site is located on the Ceyhun Atif Kansu Street (CAKS) in Dikmen district. Blocky greywackes are common in Dikmen district (Figure 3.9). The greywackes cropping out around Dikmen are coarser grained than those observed at Beytepe. This unit also includes macro and micro fractures (Figure 3.10).

The sample shows medium-to-coarse angular grains and the fractures intersect and displace each other (Figure 3.11). The grains are mainly consisting of quartz with volcanic rock fragments (rhyolite), chert fragments and plagioclase. Matrix is clayey. Metamorphism is brittle with at least three deformation stages (repeated periods of fracturing) (Göncüoğlu, 2005).

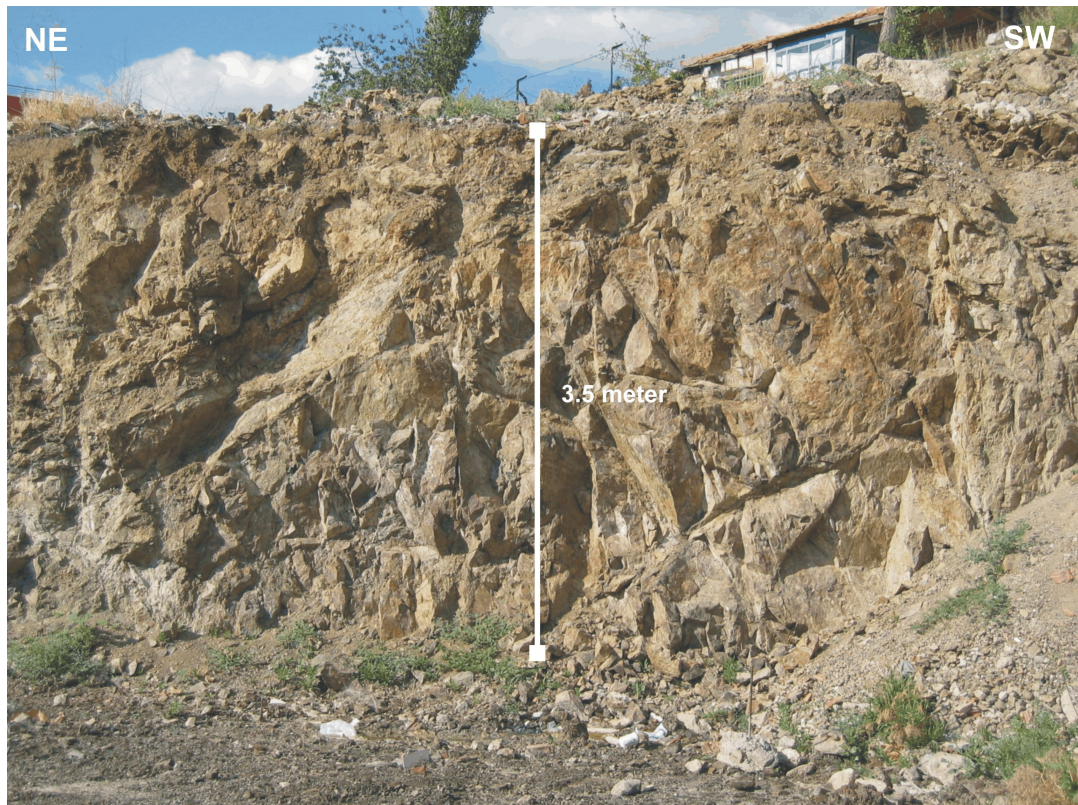


Figure 3.9 A view from the greywacke rock mass at Dikmen.

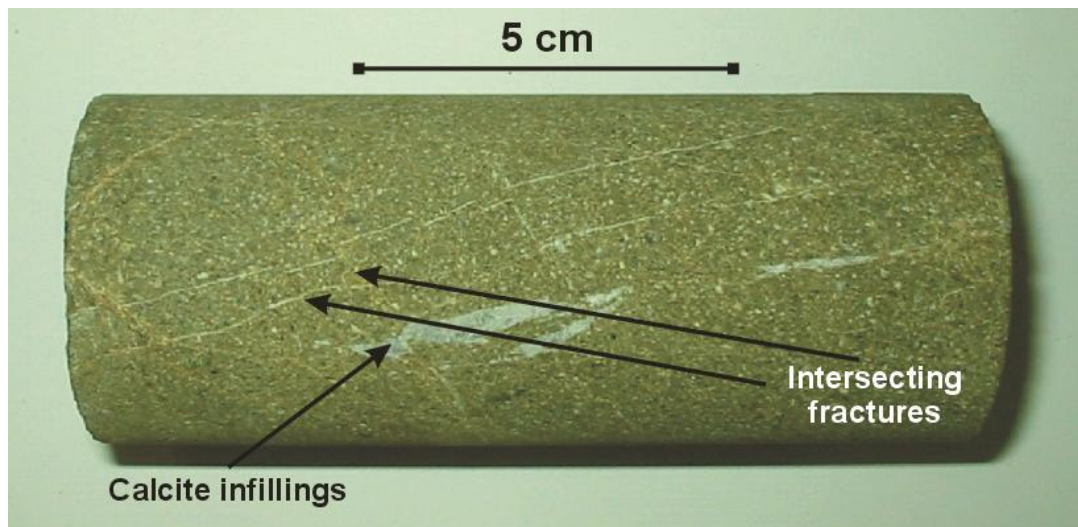


Figure 3.10 Intact core sample of greywacke from Dikmen.

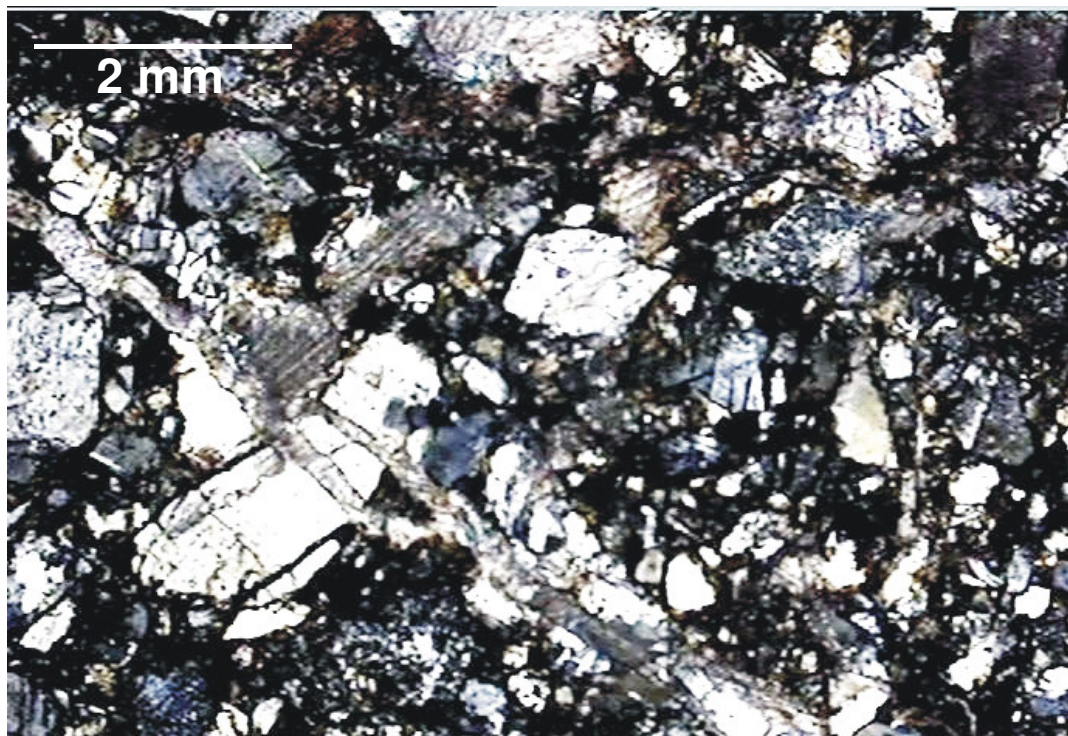


Figure 3.11 The thin section view of the sample taken from Dikmen site (cross nicols).

(c) Solfasol district:

Completely weathered yellowish andesites are observed at this site. The original rock structure has almost been destroyed; thus the rock unit can be classified as completely weathered (grade V) to residual soil (grade VI) according to the weathering classification system suggested by ISRM (1981). Figure 3.12 shows a general view from the highly weathered andesites and a shallow slope failure within intensely weathered rock mass. Discontinuities cannot be identified within the rock mass due to the transformation of the rock into soil - like material due to weathering.

The mineralogical composition of the andesite samples was determined with the aid of X – Ray Diffraction (XRD) technique using Cu K α radiation in the laboratories of General Directorate of Mineral Research and Exploration. Based on the XRD diffractograms, minerals present in the sample are feldspar, smectite, mica, quartz, amorphous silica and amphibolite in the order of decreasing abundance. Figure 3.13 shows the XRD diffractogram of the sample taken from Solfasol district. The XRD result indicates the effect of chemical weathering.



Figure 3.12 General profile of the highly weathered andesites in Ankara and a shallow slope failure occurred within the intensely weathered rock mass.

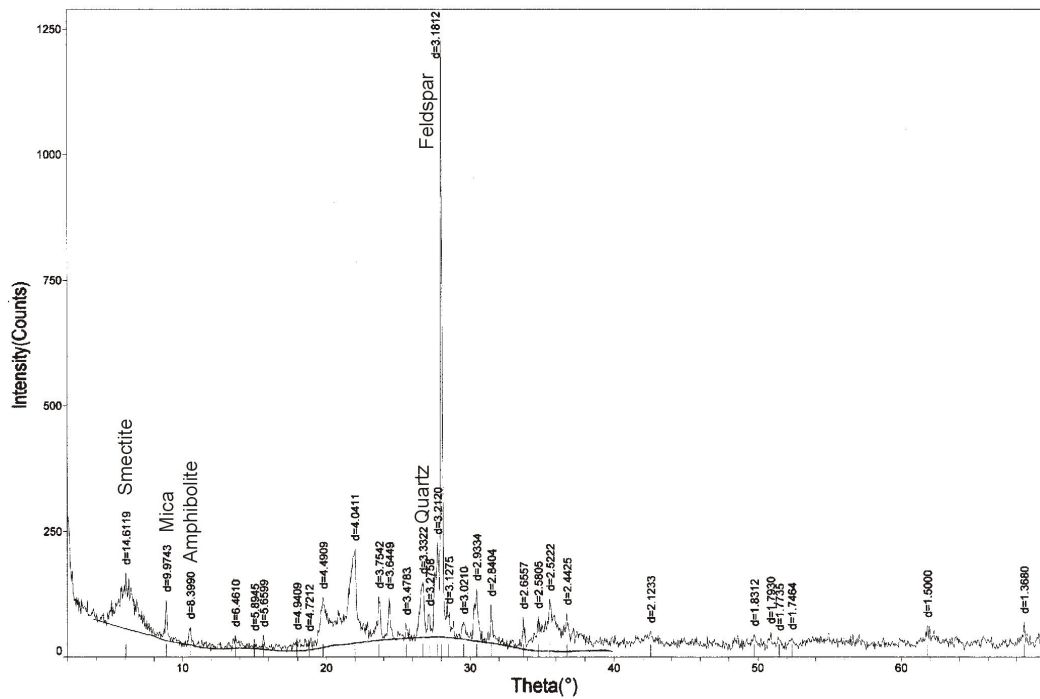


Figure 3.13 The XRD diffractogram of the andesite sample taken from Solfasol district.

(d) Pursaklar and Ovacık districts:

At this site, highly weathered and pink andesites are observed. Although the original structure of the intact rock can be distinguished, the rock material has completely lost its strength (Figure 3.14 a). Less weathered core stones are also seen within the rock mass (Figure 3.14 b). Therefore, these units can be classified as highly (grade IV) to completely weathered (grade V) according to ISRM (1981)'s classification. Due to intensive weathering, discontinuities cannot be distinguished within the rock mass. Thin section view of the andesite sample collected from this site is shown in Figure 3.15.

The andesite sample contains plagioclase minerals, as phenocrysts and amphiboles within a sericitized microlite matrix. The accessory minerals are biotite (< 5 %), quartz (< 5 %) and chert (< 5 %). The iron oxide stained fractures are rarely observed within the matrix; however, all large plagioclase crystals contain fractures.

The XRD analyses were performed on the bulk samples taken from various depths and suggested the presence of smectite, feldspar, mica, cristobalite, quartz and amphibole minerals. Figure 3.16 shows the XRD diffractogram of one of the samples taken from 2 – 3 meter depth at Pursaklar district. The XRD results indicate the presence of chemical weathering products.

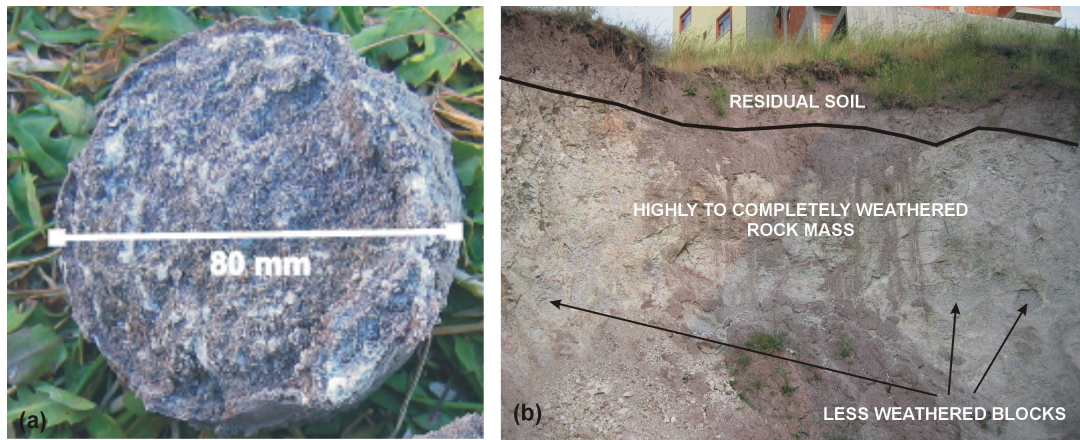


Figure 3.14 (a) Rock material, (b) rock mass of the weathered andesite.

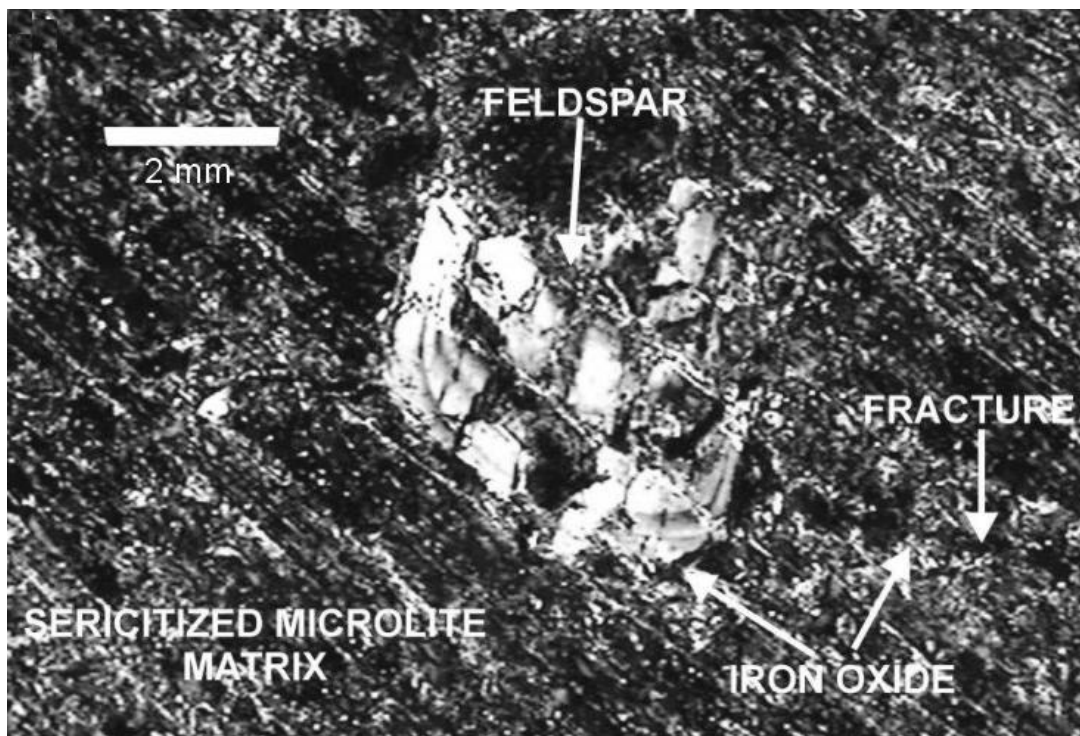


Figure 3.15 The thin section of the andesite sample (cross nicols).

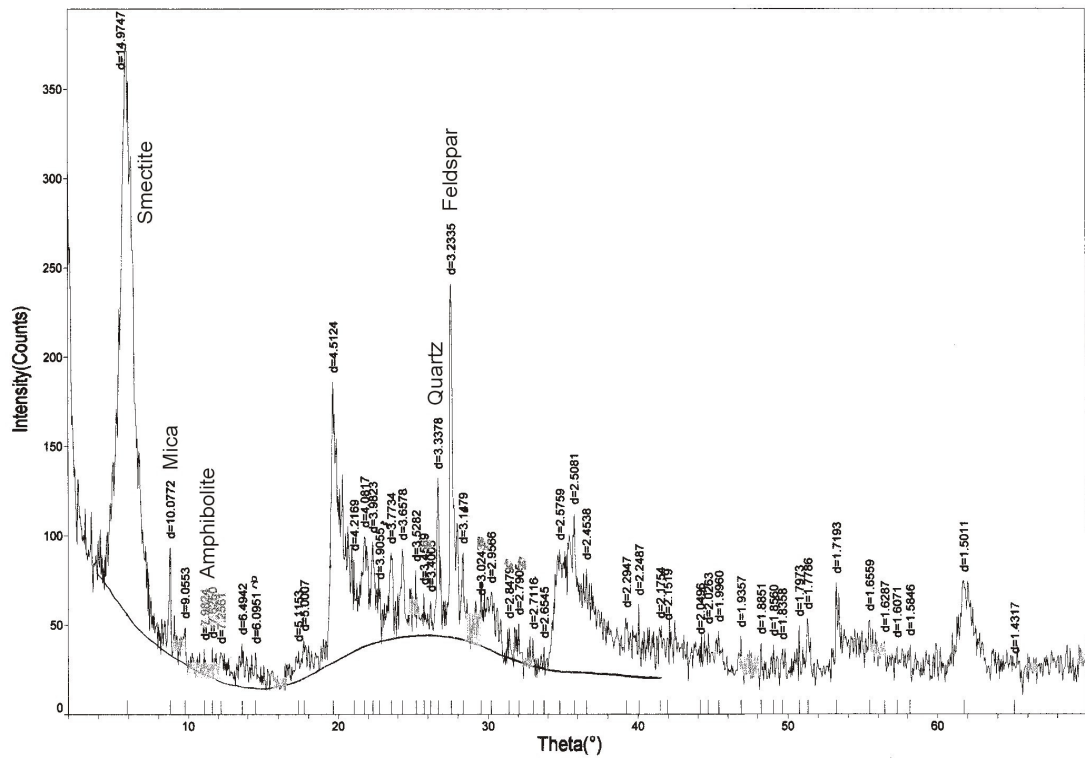


Figure 3.16 XRD diffractogram of one of the andesite samples taken from Pursaklar district.

(e) *Eymir Lake site:*

Soft to medium consistency, saturated and young clay deposits are observed around Eymir Lake. The color of the clay is grayish green. Clay has generally high plasticity. One location with high water table, which is easily accessible for borehole operations and cone penetration testing, was selected as a test site.

(f) Mudrocks exposing around Sincan:

The Eocene and Upper Neogene mudrocks of this locality can be classified as weak rock masses. The rock material is weak to strong and brittle. The amount of carbonate varies within the rock mass. Color changes from yellowish brown to grayish green depending on the composition of the rock.

CHAPTER 4

GEOTECHNICAL SITE INVESTIGATIONS

The purpose of the geotechnical investigations is to assess the engineering characteristics of the rocks and soils at the selected sites. For this purpose, rock mass characterization surveys, pressuremeter tests, seismic investigations, Schmidt hammer tests and sampling were performed on rock units. For soil units, in addition to pressuremeter tests and sampling, field vane shear and cone penetration tests were also carried out on the saturated Eymir Lake clays.

4.1 Rock Mass Characterisation

As it was previously explained, it is also aimed to investigate the effect of Rock quality designation (RQD), (or some other rock mass parameters such as GSI, RMR) and intact rock strength on the deformation modulus determined from pressuremeter test. For this purpose, the Dikmen greywackes, weathered andesites and mudrocks exposed around Sincan were selected. For the Dikmen greywackes and weathered andesites rock mass characterization studies were performed along rock-cut surfaces. Scan-line surveys could not be carried out at mudrocks around Sincan due to the lack of exposed rock-cut surfaces. For the highly weathered – sheared Dikmen greywackes methodology given by ISRM (1981) could not be applicable, because this unit is divided by intensive discontinuities without distinct orientations. Therefore, instead of describing the properties

of discontinuities, the general rock mass characterization study on the exposed greywacke surfaces is preferred by using GSI (Hoek, 1999), system. In order to apply this system, information on blockiness of the rock mass and the surface quality of the discontinuities are needed.

Sönmez and Ulusay (1999) developed a quantitative GSI chart to provide a numerical basis for evaluating the GSI and then these investigators modified it (Sönmez and Ulusay, 2002). In this system, the discontinuity conditions are evaluated using the surface condition rating SCR, which is represented by three variables called properties roughness rating (R_r), weathering rating (R_w) and infilling rating (R_f). The blockiness of the rock mass is numerically evaluated using the structure rating SR which is calculated from volumetric joint count (J_v). This quantitative GSI chart does not include the laminated-sheared structure in contrast to Hoek (1999).

4.1.1 Dikmen greywackes

Physical and mechanical characteristics of the greywackes cropping out around Ankara region are required for the settlement and bearing capacity calculations of the foundations of high-rise buildings, design of deep excavations and for future underground projects. Determination of the geomechanical properties of the Dikmen greywackes is a very difficult task due to their heterogeneous nature and difficulties associated with undisturbed sampling of the rock mass. In order to obtain geomechanical properties of the greywackes, indirect empirical methods and field tests such as plate loading and pressuremeter (and dilatometer) test could be used. Although direct measurement of geomechanical properties is a better choice, the budget for these field tests is often incompatible with the economy of the small projects. Determination of the deformation modulus of Dikmen greywackes by using pressuremeter tests, and comparison of the modulus of deformability values obtained from field tests with those determined by empirical methods are performed. For this purpose, a total of

27 pressuremeter tests were performed in Dikmen greywackes showing different characteristics. To determine the rock mass characteristics of the greywackes, rock mass characterization surveys were performed.

(a) Beytepe campus of Hacettepe University:

Two locations with different rock mass characteristics were selected for field studies of the greywackes in Beytepe Campus of Hacettepe University. These areas are located near a workshop and University club called Beyaz Ev. Figure 4.1 presents a panoramic view of the rock mass from an old foundation cut near borehole locations. Both of the rock masses include distinct shear zones. No groundwater is observed in the workshop and Beyaz Ev sites. The rock mass structure can be classified as disintegrated to laminated – sheared according to GSI system (Hoek, 1999). The rock mass exposed around Beyaz Ev site is weaker than that of exposed around the workshop site.

The field observations suggest that R_r ranges between 3 (slightly rough) to 1 (slickensided), R_w ranges between 1 (highly weathered) to 0 (decomposed) and R_f is between 2 (hard infilling > 5 mm) to 0 (soft infilling > 5 mm) for the site near workshop. Therefore, the overall surface condition rating ranges between 6 to 1. This corresponds to poor to very poor surface condition in the GSI system (Hoek, 1999).

The structure rating of the rock mass is calculated using equation 4.1 (Sönmez and Ulusay, 2002) by using a value of 6 for D_n .

$$J_v = D_n \frac{1}{S} \quad (4.1)$$

The resulted range of GSI values are displayed in Figures 4.2 (Hoek, 1999) and 4.3 (Sönmez and Ulusay, 2002) by shaded areas.



Figure 4.1 Panoramic view of the greywacke from an old foundation cut near the boreholes at Beytepe area (workshop site).

		SURFACE CONDITIONS				
		VERY GOOD	GOOD	FAIR	POOR	VERY POOR
STRUCTURE		DECREASING SURFACE QUALITY →				
	INTACT OR MASSIVE - intact rock specimens or massive in situ rock with few widely spaced discontinuities	90	80	70	N/A	N/A
	BLOCKY - well interlocked undisturbed rock mass consisting of cubical blocks formed by three intersecting discontinuity sets	80	70	60	50	40
	VERY BLOCKY- interlocked, partially disturbed mass with multi-faceted angular blocks formed by 4 or more joint sets	70	60	50	40	30
	BLOCKY/DISTURBED/SEAMY - folded with angular blocks formed by many intersecting discontinuity sets. Persistence of bedding planes or schistosity	60	50	40	30	20
	DISINTEGRATED - poorly interlocked, heavily broken rock mass with mixture of angular and rounded rock pieces	50	40	30	20	10
	LAMINATED/SHEARED - Lack of blockiness due to close spacing of weak schistosity or shear planes	N/A	N/A	10	5	0

↑ DECREASING INTERLOCKING OF ROCK PIECES ↓

Dikmen C.A.K.S

Workshop

Beyaz Ev

Figure 4.2 The range of GSI values based on the classification sheet of Hoek (1999) for the greywackes.

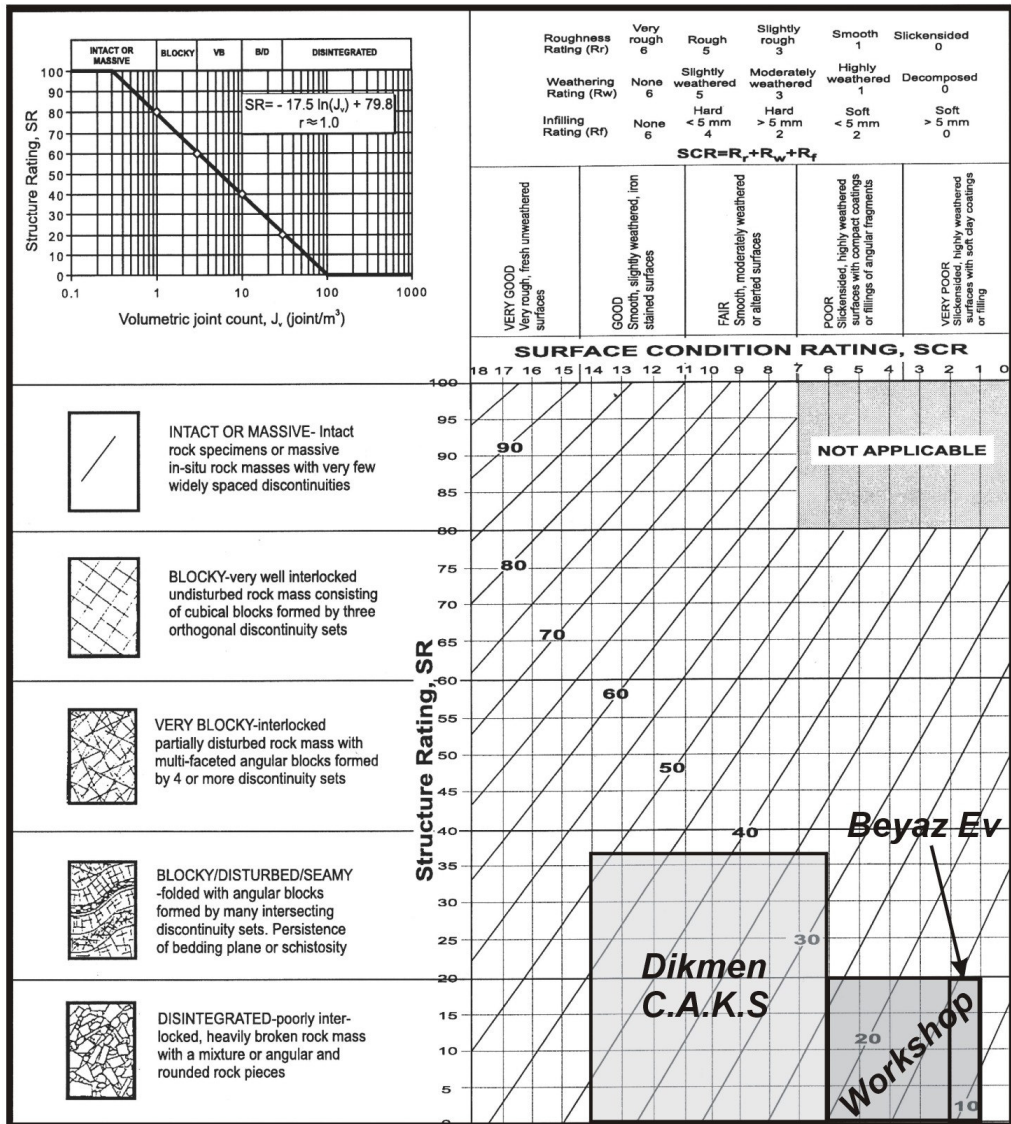


Figure 4.3 The range of GSI values based on the classification sheet of Sönmez and Ulusay (2002) for the greywackes.

The differences between GSI values determined by Hoek (1999) and Sönmez and Ulusay (2002) systems can be explained by the fact that quantitative GSI chart of Sönmez and Ulusay (2002) does not include the laminated-sheared structure in contrast to Hoek (1999).

The rock mass is also characterized by using the RMR system (Bieniawski, 1989), and the rock mass parameters and RMR values are given in Table 4.1. Based on the RMR value of the greywackes cropping out at the workshop site, the rock mass is classified as weak rock (grade IV).

Table 4.1 The rock mass parameters and RMR values of the greywacke at the workshop location.

	UCS (MPa)	RQD (%)	Discontinuity spacing (mm)	Condition of discontinuity surfaces	GW. cond.	RMR _{TOT}
Minimum	0.8	0	20	Slickensided	Dry	34
Average	12	0	80	Slickensided	Dry	36
Maximum	22.9	0	200	Slickensided	Dry	39

General view of the rock mass cropping out at the site near Beyaz Ev from an old foundation cut near one of the boreholes is shown in Figure 4.4.

The block dimensions range from one centimeter to 20 centimeters. Based on the field observations, R_r is estimated as 1 (slickensided); R_w ranges between 1 (highly weathered) and 0 (decomposed), and R_f is 0 (soft infilling > 5 mm). As a result overall surface condition, rating varies between 1 and 2 which corresponds to very poor surface condition in the GSI system (Hoek, 1999). The resulted range of the GSI values are depicted in Figures 4.2 (Hoek, 1999) and 4.3 (Sönmez and Ulusay, 2002) by shaded areas.

Table 4.2 displays the various rock mass parameters and RMR (Bieniawski, 1989) values for the Beyaz Ev site. Based on the RMR value of the greywackes exposing at the Beyaz Ev site, the rock mass is classified as weak rock (grade IV).



Figure 4.4 General view of the rock mass from an old foundation cut near one of the boreholes at Beytepe Campus (Beyaz Ev).

Table 4.2 Various rock mass parameters and RMR values for the Beyaz Ev site.

	UCS (MPa)	RQD (%)	Discontinuity spacing (mm)	Condition of discontinuity Surfaces	GW. cond.	RMR _{TOT}
Minimum	4.30	0	10	Soft fault infilling	Dry	24
Average	22	0	80	Soft fault infilling	Dry	28
Maximum	51.00	0	200	Soft fault infilling	Dry	30

(b) Dikmen Ceyhun Atif Kansu Street (CAKS):

Dikmen is a densely populated district of Ankara and founded entirely on the greywackes. At the upper part of Dikmen, generally blocky greywackes are exposed. These are more massive when compared to those exposed around Beytepe, Ayrancı and Oran. In order to determine their geomechanical properties a location, which is near to Ceyhun Atif Kansu Street (CAKS), was selected. This site is characterized by blocky greywackes. Figure 4.5 shows a general view of the rock mass from a foundation cut near the boreholes 1 and 2.

The rock mass includes occasional shear zones and blocks of various sizes. Groundwater was not observed in the rock mass. The dimensions of the blocks range from 5 to 50 cm. The field observations suggest that rock mass structure can be classified as disintegrated according to GSI system (Hoek, 1999). The field observations indicated that R_r values range between 1 and 5 (smooth to rough); R_w values between 3 and 5 (moderately to slightly weathered) and R_f values 2 to 4 (hard infilling > 5 mm and < 5 mm). Therefore, the overall surface condition rating ranges between 6 and 14. A typical discontinuity surface from CAKS is shown in Figure 4.6. The surface condition corresponds to fair to good based on the GSI system. The resulted range of GSI values are depicted in Figures 4.2 (Hoek, 1999) and 4.3 (Sönmez and Ulusay, 2002) by shaded areas.

Although the attempts for obtaining core samples from the boreholes using a double tube core barrel is unsuccessful (only small pieces could be obtained, RQD = 0), it was determined that the RQD has to be measured from the rock mass surface. Various rock mass parameters and RMR values at CAKS are tabulated in Table 4.3. The RMR values of the greywackes exposing at CAKS are classified as weak to good rock (grade II - III).



Figure 4.5 General view of the greywacke rock mass from a foundation cut near the boreholes 1 and 2 at CAKS.

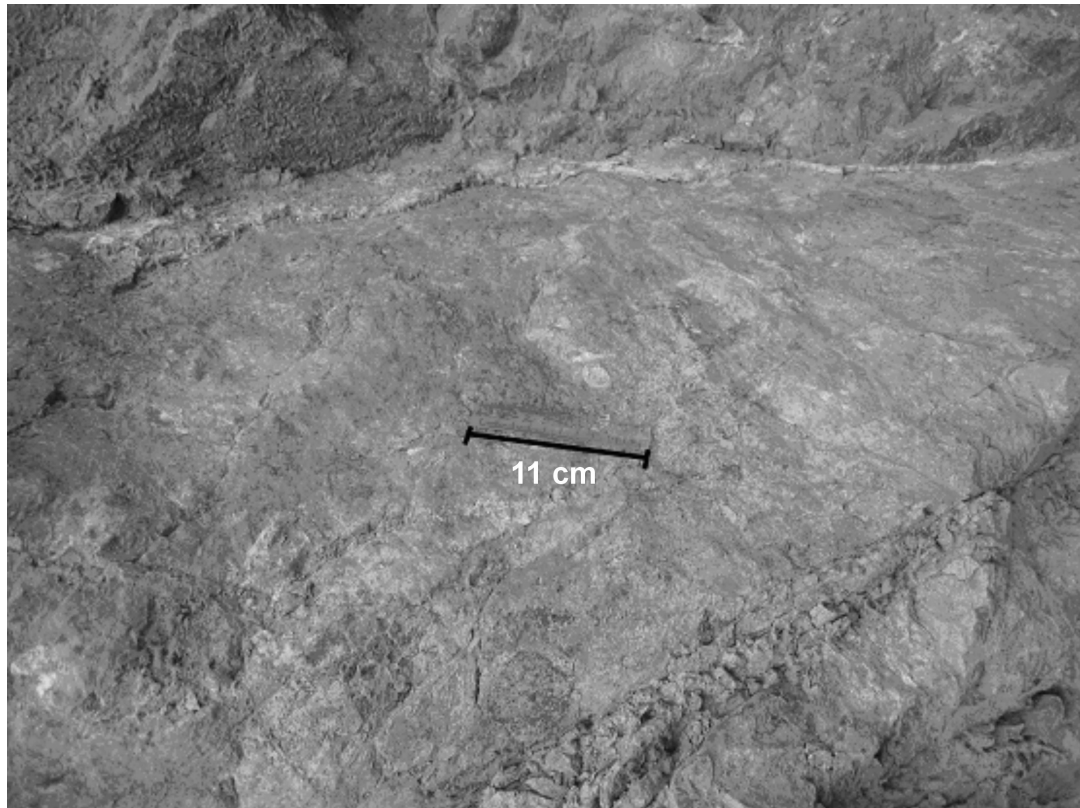


Figure 4.6 Photograph of a typical discontinuity surface from the CAKS.

Table 4.3 Various rock mass parameters and RMR values at the CAKS site

	UCS (MPa)	RQD (%)	Discontinuity spacing (mm)	Condition of discontinuity surfaces	GW. cond.	RMR _{TOT}
Minimum	0.80	27	50	Slickensided	Dry	38
Average	19	35	200	Slightly rough	Dry	53
Maximum	57.10	46	500	Slightly rough	Dry	61

4.1.2 Weathered andesites

Residual soils (ISRM, 1981, category VI) and completely weathered rocks (ISRM, 1981, category V) formed by the weathering – decomposition of the andesites are exposed at Solfasol, Pursaklar and some parts of Keçiören (especially Ovacık). These soils are classified as group “b” residual soils according to Wesley (1988) and are saprolitic. The rock mass characterization studies are performed at Solfasol district and Pursaklar. Because no rock-cut surface is not observed at the Ovacık region, rock mass characterization could not be carried out in this area.

(a) Solfasol district

At this site completely weathered yellowish andesites are observed. Because the original rock structure has almost been destroyed, the discontinuities could not be evidently observed within the rock mass. The RQD of the rock mass is 0 at this location.

(b) Pursaklar district

In this district, highly weathered pink andesites, and less weathered blocks are present within the rock mass. Therefore, these units are classified as highly (grade IV) to completely weathered (grade V) according to ISRM (1981). Due to intensive weathering, discontinuities cannot be observed within the rock mass. Approximately the first 5 meters of the rock mass from the surface had been extensively weathered (top soil – residual soil) and the degree of weathering decreases with depth. Therefore, during boring studies continuous flight auger and double tube core barrel were employed for the first 5 m and through greater depths, respectively. The total core recovery is % 100. In BH 1, RQD is about 75 % at depths

between 5 m and 15 m and % 90 between depths of 15 m and 25 m. In BH 3, RQD is about 60 % at depths between 5 m and 7 m depths, % 82 between 7 m and 15 m depths, and 93 % down to 25 m.

(c) Ovacık district:

A continuous flight auger was adopted for the first 4 meters, after this depth a double tube core barrel was utilized for coring. The total core recovery is determined as % 100. RQD is about 75 % at depths between 4 m and 15 m, and approximately % 90 down to 25 m.

The field observations and core examinations revealed that the weathered andesites cropping out at the Ovacık and Pursaklar sites can be classified as blocky, having very poor surface quality (Hoek, 1999). Therefore, GSI ranges between 25 and 44.

4.1.3 Mudrocks

In order to investigate the geotechnical characteristics of the Eocene and Upper Neogene mudrocks cropping out around Sincan region, eight boreholes with a total depth of 150 m were drilled. Each borehole was opened with continuous flight auger and double tube core barrel was used when the geomaterial was weak and stronger, respectively.

The claystones and marls are classified as weak rock masses because they have been divided by a number of discontinuities. RQD determinations were also performed on core samples.

The RQD calculations showed that the minimum and maximum RQD values were 0 % and 95 %, respectively, with an average of 50 % and

standard deviation of 25. There are two distinct peaks in the RQD histogram as shown in Figure 4.7, which indicates two distinct RQD distributions. In order to determine the average values of these two groups, a clustering analysis was performed. Based on the K – means clustering analysis, RQD values of 23 and 67 were obtained as the averages of the two groups. The discontinuity surfaces are slightly rough to slickensided with no infillings, and the rock mass is dry. Mudrocks can be classified as very blocky, with a surface quality of fair to poor, therefore, GSI ranges between 33 and 50.

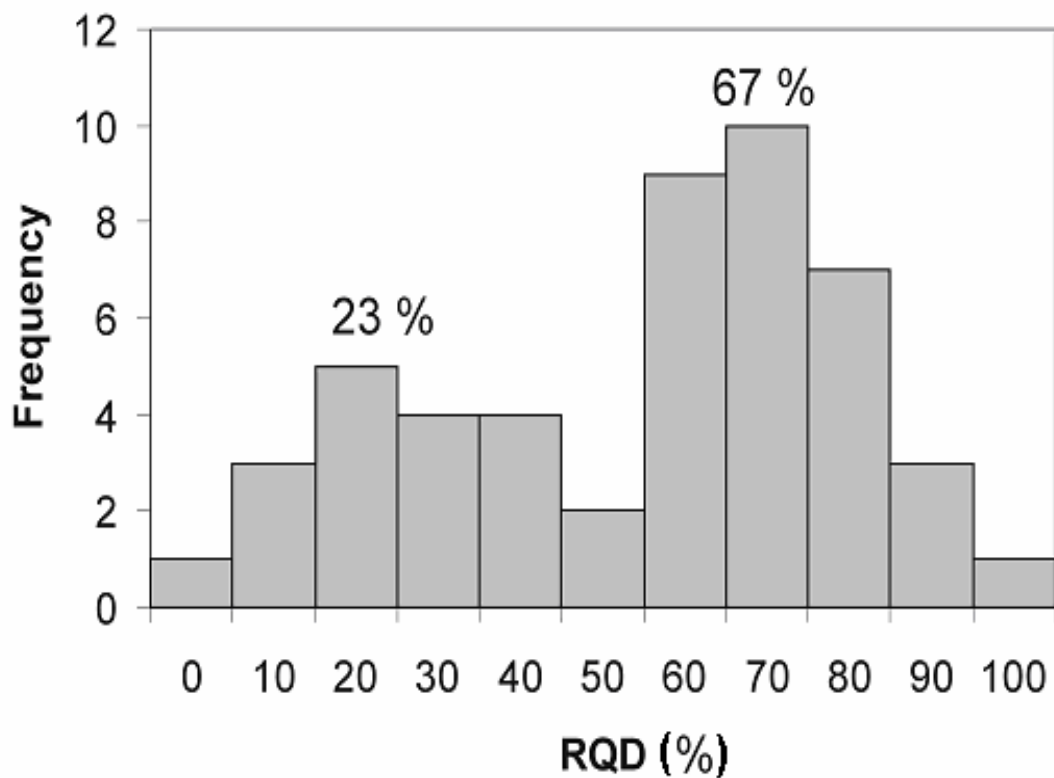


Figure 4.7 Histogram of the RQD values for the mudrocks.

4.2 Pressuremeter Tests

The pressuremeter tests were conducted in the Dikmen greywackes, highly weathered andesites, mudrocks cropping out around Sincan and normally consolidated Eymir Lake clays. A brief summary on the pressuremeter tests and the test results obtained from different geomaterials at various locations are given in the following sections.

4.2.1 Types of pressuremeters

The pressuremeter was first invented as an in-situ testing tool in the mid of 1950s by Louis Ménard (Ménard, 1956) who then went on to develop a semi-empirical design method for foundations based on pressuremeter test results. The testing equipment and the related design techniques have been continuously refined.

The pressuremeter test consists of applying a radial pressure to the soil by inflating a rubber membrane and measures the ensuing radial deformation under conditions of axial symmetry and plane strain. The rubber membrane is inflated by means of hydraulic or gas pressure and the radial displacement is measured with an indirect measuring system (volumetric measurements) or with strain gauges placed in the same plane about halfway along the membrane height. The casing of the borehole depends on the type of the soil tested and the depth at which test is undertaken. As a definition, a pressuremeter is a cylindrical probe that has an expandable flexible membrane designed to apply uniform pressure to the walls of a borehole (Clarke, 1995).

The pressuremeters are generally designed for use in most soils, having capacities between about 2.5 and 10 MN/m². The walls of pressuremeters are usually composed of a flexible membrane with some form of outer

protection. When used in coarse grained soils, most devices incorporate protective steel strips around the membrane known as the “Chinese Lantern”. The length of the flexible part of a pressuremeter, including any guard cells, should not be less than 6 diameters. All methods of interpretation of the pressuremeter test results assume that the expanding cavity is sufficiently long for the deformation to be considered as cylindrical. The shorter the expanding length, the more nearly the deformation approximates to an expanding sphere rather than an expanding cylinder (Mair and Wood, 1987).

4.2.1.1 Ménard type pressuremeters (MPM)

The MPM device is a type of pressuremeter designed for use in a preformed borehole. There are two main types of MPM device, differing in the means of applying the pressure to the membrane and in the method of measuring the response of the borehole to that pressure. The first type (type 1), based on the development by Ménard, comprises a central measurement cell filled with water to which pressure is applied by gas pressure controlled at the surface. An indirect measuring system is employed, whereby the change in radius of the borehole during expansion of the membrane is obtained by measuring the change in volume of the water-filled central cell. This central cell is located between an upper and lower guard cell, both of which are inflated with gas or water pressure. Ideally, the guard cell pressure ought to be maintained at the same pressure as the central cell. When inflated with water, this is the case, but when inflated with gas, the guard cells are often maintained at a slightly lower pressure than the central cell. The purpose of the guard cells is to prevent the central cell from expanding in any direction other than radially. In the second type (type 2), the membrane is expanded under gas or oil pressure and displacement of the borehole wall is more directly measured by feeler arms or displacement transducers inside the membrane.

The Ménard test is a true static soil loading test and must, therefore, yield the two characteristic parameters of the soil tested i.e. a deformation parameter and a failure parameter (Gambin, 1995). Furthermore, the pressuremeter test is the only in-situ test in which the boundary conditions are theoretically fully known, apart from the remoulding of the borehole walls caused by the drilling operation and the time elapsing between drilling and testing (Gambin, 1995).

The pressuremeter used in this study is a type-1 Ménard Pressuremeter (type GC according to Centre D'Etudes Ménard, 1975, ASTM D 4719 (ASTM, 2000); Figure 4.8). The pressure range of the device is up to 40 bars.

The Ménard pressuremeter has a series of probes which correspond to most usual borehole dimensions (Figure 4.9). Table 4.4 tabulates the probe dimensions. Three possible cases related to the pressures of gas and water are illustrated in Figure 4.10.

In order to obtain a valid test, the central cell has to be in contact with the soil (Case 1) over its full length. It can be concluded that in order to be in case 1, pressure in the guard cells should be slightly lower than the central cell.

In many cases, the Ménard Pressuremeter probe can be lowered into the boreholes pre – drilled with flight augers, roller bits or rock bits. The test should be carried out after each pass of the drill which itself must be limited to a length ranging between 3 to 30 m depending on the nature of the ground (Centre D'Etudes Ménard, 1975). The common test spacings range from 1 to 3 m (ASTM, 2000). In submerged granular soils (sand, sand and gravel below water table), the probe must be driven to the required elevation either by driving as in the “Standard Penetration Test” or by static pressure such as in the “Dutch Cone Soundings” or again by vibration in this case, the probe is protected by a casing with longitudinal slits which allow radial expansion (Centre D'Etudes Ménard, 1975). Very compact

deposits of sand and gravel require a mixed method of driving and drilling by using casing (Centre D'Etudes Ménard, 1975).



Figure 4.8 Ménard Pressuremeter (type GC) and its probe used in this study.

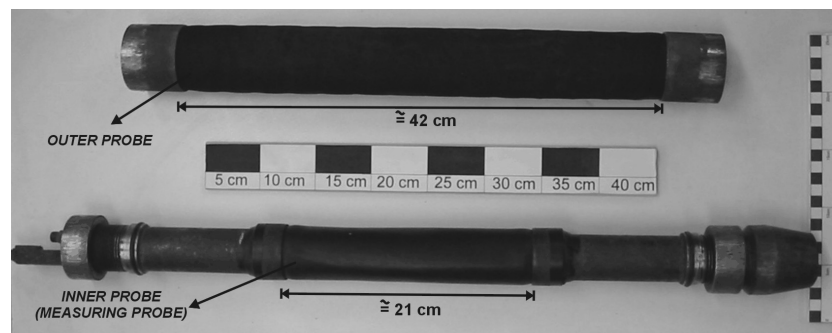


Figure 4.9 Inside of the Ménard pressuremeter probe.

Table 4.4 Probe dimensions (Centre D'Etudes Ménard, 1975).

Code	Probe diameter (mm)	Borehole Diameter (mm)	
		Minimum	Maximum
EX	32	34	38
AX	44	46	52
BX	58	60	66
NX	74	76	80

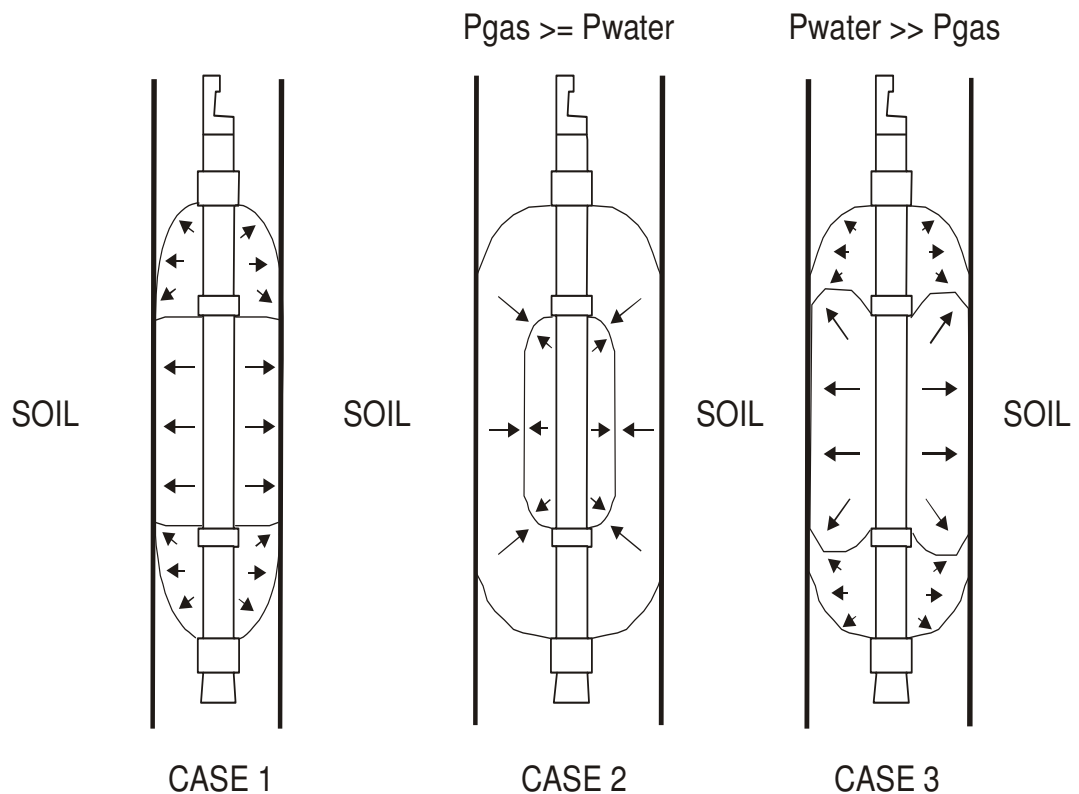


Figure 4.10 Three possible cases related to the pressures of gas and water in pressuremeter probe (Apageo Segelm, 1997).

The pressuremeter tests were performed according to ASTM (2000) and Centre D'Etudes Ménard (1975). The pressure losses occur due to the rigidity of the probe walls. The pressure readings obtained during the test on the readout device include the pressure required to expand the probe walls, this membrane resistance must be deduced to obtain actual pressure applied to the soil. Volume losses occur due to expansion of tubing and compressibility of any part of the testing equipment including the probe and the liquid. This calibration is made by pressurizing the equipment with the probe in heavy duty steel casing or pipe. In this study both of these calibrations were performed according to ASTM (2000).

4.2.1.2 Self boring pressuremeters

In order to reduce soil disturbance effects encountered in MPM test, self – boring pressuremeters have been developed both in UK (Wroth and Hughes, 1973) and France (Baguelin et al., 1972). The self boring pressuremeter kit probe and control parts are shown in Figure 4.11.

The self-boring pressuremeters are all similar in principle in that they are, in essence, miniature tunnelling machines which are steadily jacked into the ground. The soil displaced by the instrument enters the cutting head where it is broken into small pieces by a rotating cutter, then flushed to the surface (Mair and Wood, 1987). The device developed in UK is known as the Cambridge Pressuremeter (Camkometer), and the French instruments are known as the Pressiometre Autoforeur (PAF) or more recently, Pressiometre Autoforeur pour Sol Raide (PAFSOR).

The pressure and soil deformation measuring systems of the Camkometer are based on the MPM type-2 system. After installation, the membrane is inflated by gas pressure controlled from the surface, and its expansion is measured by three separate deformation-sensing feelers spaced at 120° around its mid plane. The gas pressure applied to expand the membrane and the pore pressure in the soil in contact with the membrane are also measured by electrical transducers mounted within the pressuremeter.

The PAF (and PAFSOR) devices differ from the Camkometer in three major respects. While the Camkometer displacement measuring system corresponds to the type-2 MPM device, the PAF system corresponds to a type-1 device (i.e. the volume of the expanding membrane is recorded as a change in level of liquid). The second major difference is that the PAF devices do not have a rigid wall inside the membrane to support it during installation and prior to expansion. The membrane is supported by the liquid inside it and may deform

during installation. The third major difference is in the method of driving the cutter. The Camkometer cutter is rotated by rods connected to the drilling machine, whereas the PAFSOR cutter is rotated by a hydraulic motor installed within the pressuremeter cutting shoe. Although the PAF and PAFSOR have been used fairly in France, all of the UK experience of SBP testing has been with the Camkometer.



Figure 4.11 Self boring pressuremeter kit probe and control parts (Cambridge In-situ, 2005).

4.2.1.3 Cone – pressuremeter

This type of pressuremeter is inserted in to the ground by soil displacement. The idea is to fix a pressuremeter probe above a penetrometer cone, by this way the device enables to simultaneously obtain the pressuremeter data and the cone penetration test data (Figure 4.12). In this type of pressuremeter, the pressuremeter probe has 44 mm nominal diameter, the

cone has an area of 15 cm^2 and the probe has a length over diameter ratio (L/D) of 10.

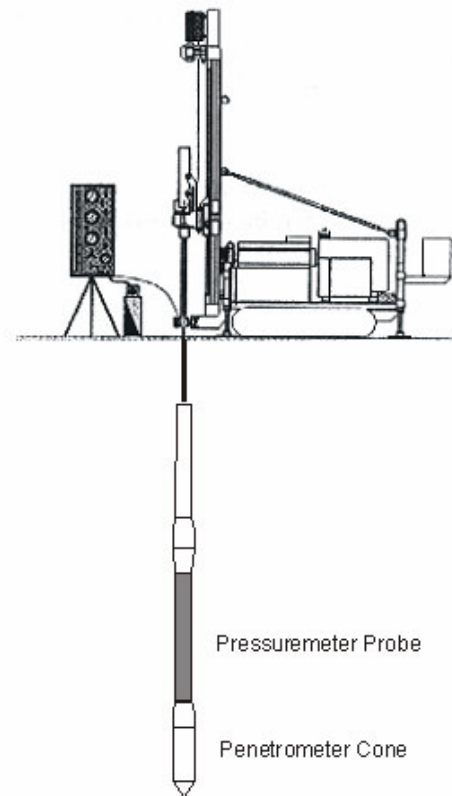


Figure 4.12 Cone pressuremeter (modified from Yu et al., 1996).

4.2.1.4 The push – in pressuremeter (PIP)

With the increasing interest in offshore design and the need to obtain good measurements of the in-situ properties of offshore clays, a pressuremeter is required. This resulted in the development in the UK (Henderson et al., 1979) of the PIP. This is normally inserted by pushing either into an undersize pre-cored hole or into the bottom of a borehole without any pre-coring. Most of the experience with it to date has been offshore, and this has been relatively limited in comparison with MPM and SBP testing onshore (Mair and Wood, 1987).

The principal differences between the three classes of pressuremeters lie in the stresses applied to the probe at the start of the test. Ménard pressuremeters start from a horizontal stress level close to zero. The self boring pressuremeters start the test at approximately the horizontal total stress level in the ground before insertion. Push in pressuremeters start with a horizontal total stress which can be expected to be much greater than that originally existed in the ground (Clayton et al., 1995).

4.2.1.5 The oyometer

The Oyometer is the general term for those instruments developed by the OYO Corporation, Japan. The three probes - the LLT, Elastometer 100 and Elastometer 200 - are monocell probes.

The Elastometer 100 and Elastometer 200 were the first commercial probes with displacement transducers (LVDT). Both elastometers are designed for testing rock and can operate up to pressures of 10 and 20 MPa, respectively (Clarke, 1995). The displacement transducers are used because of the problems of obtaining accurate information of the cavity expansion with remote volume-measuring systems. This is particularly important for tests in rock where displacements are likely to be small.

The probes can be either 62 or 72 mm in diameter. The membrane, which is the same as those used in packers, has L/D ratio of between 7.2 and 8.4. The membranes used vary in thickness and type depending on the ground to be tested. The membrane is prevented from expanding into the annulus between the probe and the pocket above and below the test section by its thickness, which can be up to 8 mm, and its stiffness. Figure 4.13 shows the assembled elastometer and testing equipment and the schematic view of the elastometer 100 probe, respectively.



Figure 4.13 The assembled Elastometer and testing equipment (Oyo – Corporation, 2005).

4.2.1.6 Definition of limit pressure

The theoretical limit pressure (P_{it}) is defined as the pressure at which pressuremeter cavity expands indefinitely i.e $dV/V = 1$. However, this pressure can never be attained in a real pressuremeter test because of the limited water volume capacity of the devices. Ménard defined a conventional limit pressure for $dV/V_0 = 1$ (P_{lm}) in which V_0 is the cavity volume for $p = 0$ (i.e cavity volume just at the start of the test) (Gambin, 1995).

Since the initial volume for a standard AX or BX probe is in the order of 600 cm^3 ($535 \text{ cm}^3 + \text{volume injected to contact the borehole walls}$) dV/V_0 may be assumed to occur for a reading of $V = 700 \text{ cm}^3$ (Centre D'Etudes Ménard, 1975).

The estimation of the asymptotical limit pressure, therefore, requires extrapolation from data at lower values of dV/V . $dV/V_0 = 1$ corresponds to $dV/V = 0.5$ and $\epsilon_c = 0.41$, where, ϵ_c is the cavity strain (Mair and Wood, 1987). This extrapolation can be made by eye on the pressuremeter P vs V plot or by

using P vs LN(dV/V) plot. The cavity strain (or circumferential strain) is formulated as below.

$$\varepsilon_c = (d - d_0)/d_0 = (r - r_0)/r_0 \quad (4.2)$$

Where, d is the diameter and r is the radius.

Volumetric strain (dV/V) can be obtained by using cavity strain,

$$dV/V = 1 - (1 + \varepsilon_c)^{-2} \quad (4.3)$$

as ε_c approaches infinity, dV/V approaches to 1.

4.2.2 Pressuremeter test results

The pressuremeter tests were carried out both in the weak rocks cropping out around Ankara (Dikmen greywackes, highly weathered andesites, mudrocks exposing around Sincan) and soils (Eymir lake clays) using a type-1 Ménard pressuremeter.

4.2.2.1 Pressuremeter Tests in Dikmen greywackes

A total of 27 pressuremeter (PMT) tests were performed in Dikmen greywackes showing different characteristics. The boreholes were drilled with continuous flight augers for the pressuremeter testing. Flight auger is the best method of drilling in the Dikmen greywackes because it causes minimum disturbance to the ground. While the rotary coring is not desirable in Dikmen greywackes, because it disintegrates easily under the action of the rockbit – core with water and results in the undesirable enlargement of the hole and extensive disturbance to the ground. The attempts to obtain core samples were unsuccessful at each location due to the very weak nature (weak rock material and closely spaced discontinuities) of the

greywackes. Although few PMT curves can reach to plastic part in greywacke tests, deformation modulus of the greywackes can be calculated from the PMT data.

In order to calculate the shear modulus (G) of the material tested, the slope of the linear portion of the corrected pressuremeter graph is considered. In the early stage of the elastic portion, loosened zone around the borehole yields lower values of G . However, when the applied pressure becomes higher, the loosened zone becomes compacted and the stress is transferred to the undisturbed portion of the ground, therefore, the effect of loosened zone becomes nil. Because of this reason, the slope of the uniform later portions of the elastic stage is utilized in the determination of the shear modulus of the ground (Figure 4.14). The values of deformation modulus were calculated from the shear modulus using a Poisson's ratio of 0.3.

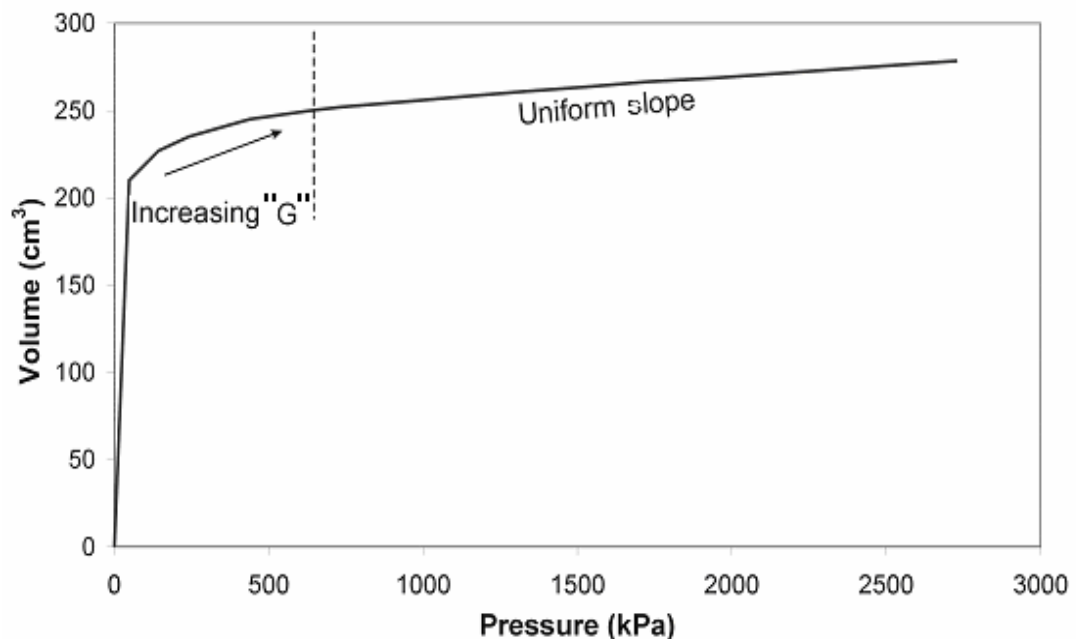


Figure 4.14 Summary of the method of calculation of shear modulus (G).

Hacettepe University Beytepe campus area:

(a) Workshop location

At the workshop location, three boreholes with 5.7, 6, and 6.5 m depths were drilled (Figure 4.15). The borehole locations and seismic survey lines are shown on a simplified sketch given in Figure 4.16.

From the slope of the linear part of the corrected pressuremeter curve, the shear modulus of the rock mass is determined by the following equation.

$$G = V_{ave}(\Delta P/\Delta V) \quad (4.4)$$

The deformation modulus of the rock mass can be estimated from the shear modulus using the following equation with an assumed Poisson's ratio value of 0.3, which is typical for most of the rock masses.

$$E = 2G(1+\mu) \quad (4.5)$$

Figure 4.17 displays the corrected pressuremeter graph performed at a depth of 2.5 m in BH 2. Table 4.5 tabulates the shear modulus, deformation modulus and Ménard limit pressure of the rock mass at the workshop area together with the testing depth.

In most of the tests, the volume of the probe could not reach 700 cm³ due to the limited pressure capacity of the pressuremeter. Therefore, most of the tests could not yield Ménard limit pressure. The normal distribution parameters of the deformation modulus are 102 MPa and 35.6 MPa for mean value and standard deviation, respectively.



Figure 4.15 A view from drilling near the workshop.

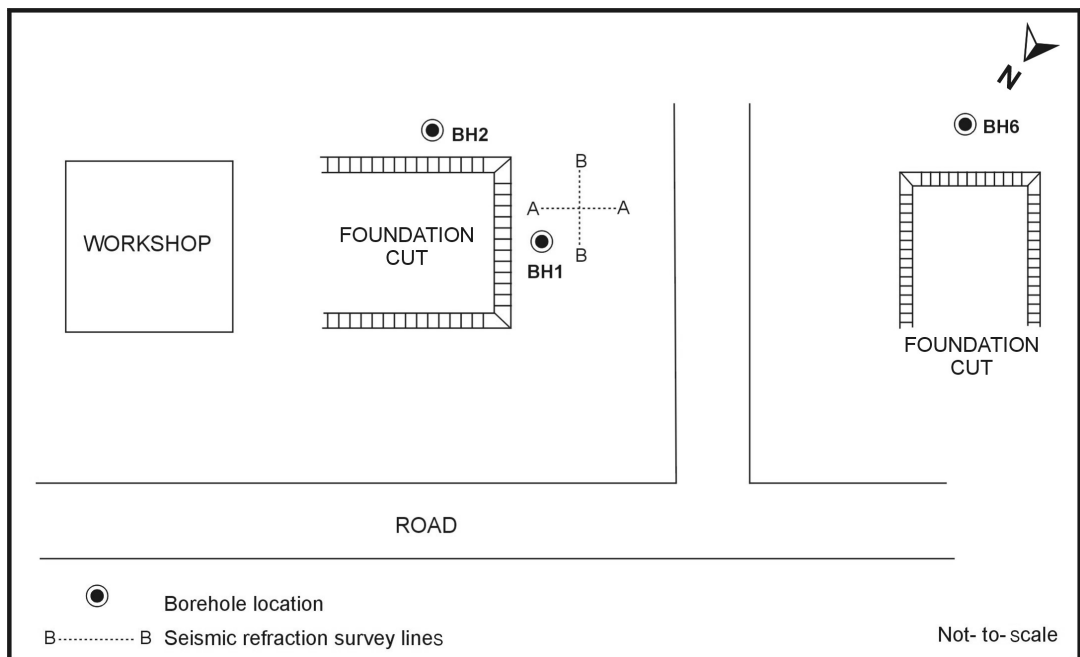


Figure 4.16 Borehole locations and seismic survey lines at the workshop area.

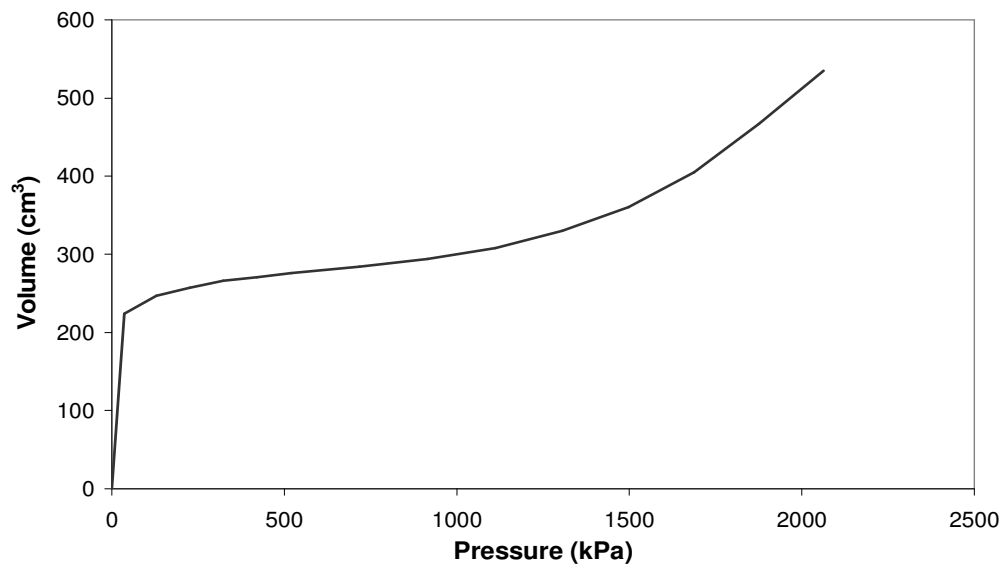


Figure 4.17 The corrected pressuremeter graph performed at a depth of 2.5 m in BH 2.

Table 4.5 Shear modulus, deformation modulus and Ménard limit pressure of the rock mass determined at the workshop area.

Borehole No.	Test depth (m)	Shear modulus, G (MPa)	Deformation modulus, E (MPa)	Ménard limit pressure (MPa)
BH 1	2.2	22.5	58.5	1.4
BH 1	3.5	37.0	96.1	-
BH 1	5.2	44.8	116.5	-
BH 1	6.0	65.1	169.3	-
BH 2	2.5	20.1	52.4	> 2.2
BH 2	3.65	39.4	102.4	-
BH 2	4.5	27.8	72.3	-
BH 2	5.5	42.3	110.0	-
BH 6	3.5	51.3	104.4	-
BH 6	5.5	54.0	138.4	-

- Indicates the tests at which Ménard limit pressure could not be obtained due to the limited pressure capacity of the pressuremeter.

> Indicates that plastic stage is obtained during the test. However, Ménard limit pressure could not be obtained due to the limited pressure capacity of the pressuremeter.

(b) *Beyaz Ev:*

Three boreholes 5, 5.5 and 7 m deep were drilled at this location. Through these boreholes, a total of 9 pressuremeter tests were performed. The borehole locations and seismic survey-lines are depicted on a simplified sketch given in Figure 4.18.

The shear modulus, deformation modulus and Ménard limit pressure of the rock mass determined by the pressuremeter test obtained from Beyaz Ev area together with testing depths are given in Table 4.6. The normal distribution parameters of the deformation modulus are 62.4 MPa for mean value and 30.6 MPa for the standard deviation, respectively. The corrected pressuremeter graph obtained from the depth of 3.7 m in BH 4 is depicted in Figure 4.19.

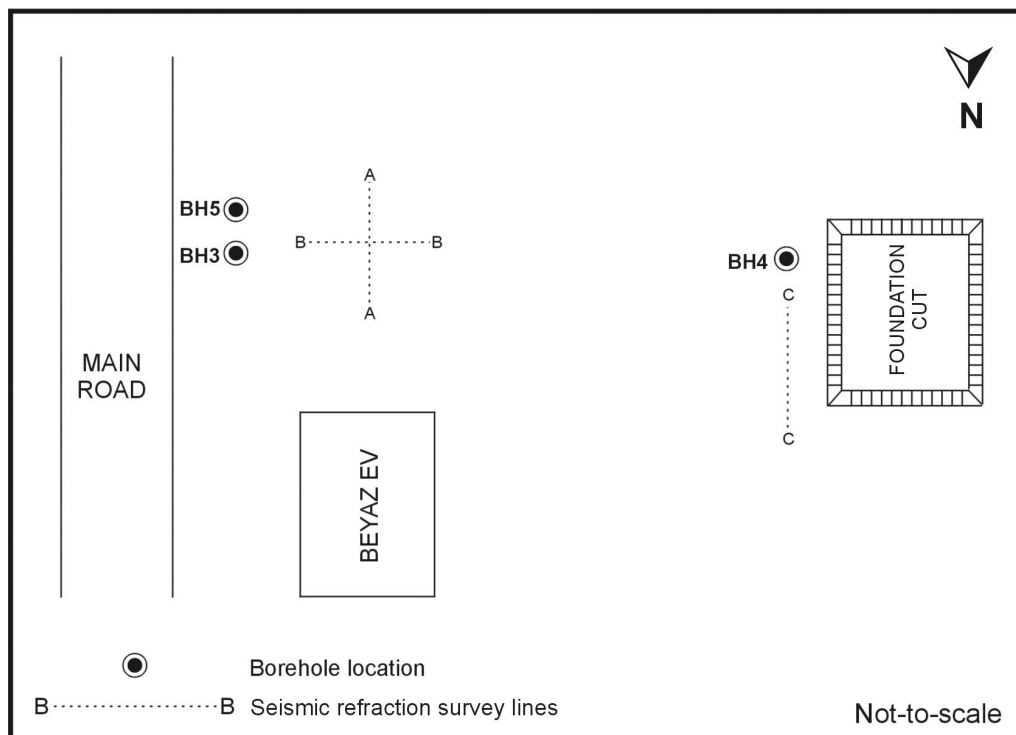


Figure 4.18 The borehole locations and seismic survey lines at the Beyaz Ev area.

Table 4.6 Shear modulus, deformation modulus and Ménard limit pressure of the rock mass determined at Beyaz Ev area.

Borehole no.	Test depth (m)	Shear modulus, G (MPa)	Deformation modulus, E (MPa)	Ménard limit pressure (MPa)
BH 3	4.0	18.0	46.8	-
BH 3	5.5	6.2	16.1	1.8
BH 3	6.5	17.1	44.5	-
BH 4	2.4	46.1	119.9	-
BH 4	3.7	36.5	94.9	-
BH 4	5.7	23.7	61.6	-
BH 5	2.5	22.1	57.5	2.0
BH 5	3.5	28.4	73.8	-
BH 5	4.5	17.9	46.5	-

- indicates the tests at which Ménard limit pressure could not be obtained due to the limited pressure capacity of the pressuremeter.

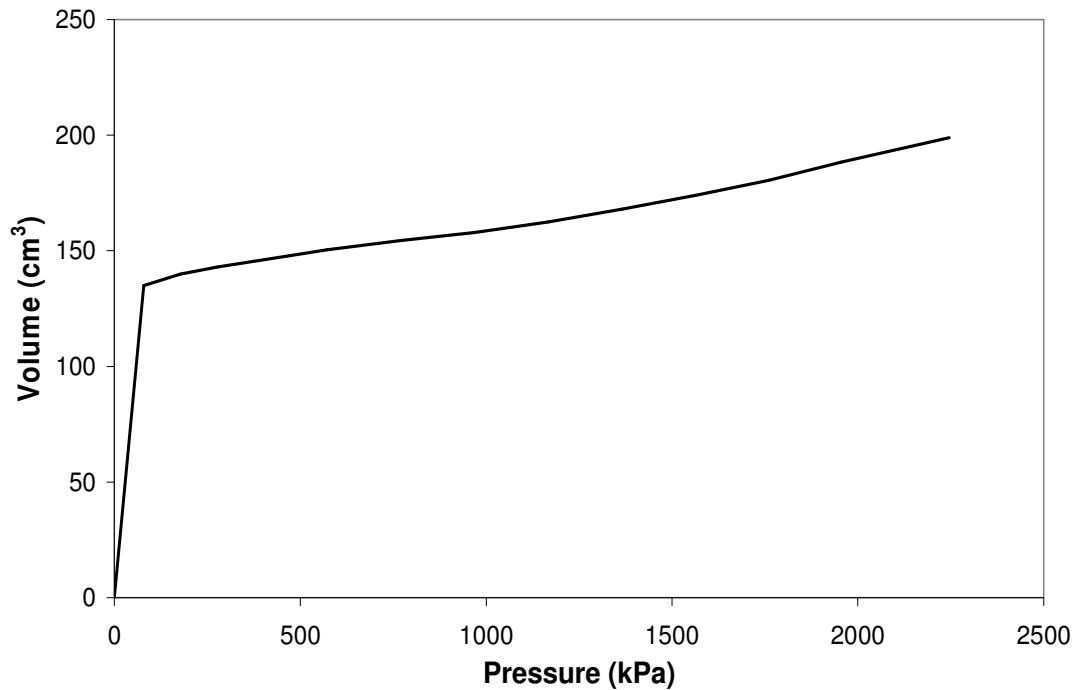


Figure 4.19 The corrected pressuremeter graph obtained from a depth of 3.7 m in BH 4.

(c) *Dikmen Ceyhun Atif Kansu Street (CAKS) location:*

At CAKS two boreholes 2.5 and 6.5 m deep next to each other were drilled. BH 1 was stopped at 2.5 meter from the surface due to the jamming of the continuous flight auger. A total of eight pressuremeter tests were performed. The plan view of the borehole locations and seismic survey line are shown in Figure 4.20. The limit pressure could not be reached in none of the pressuremeter tests performed at this location.

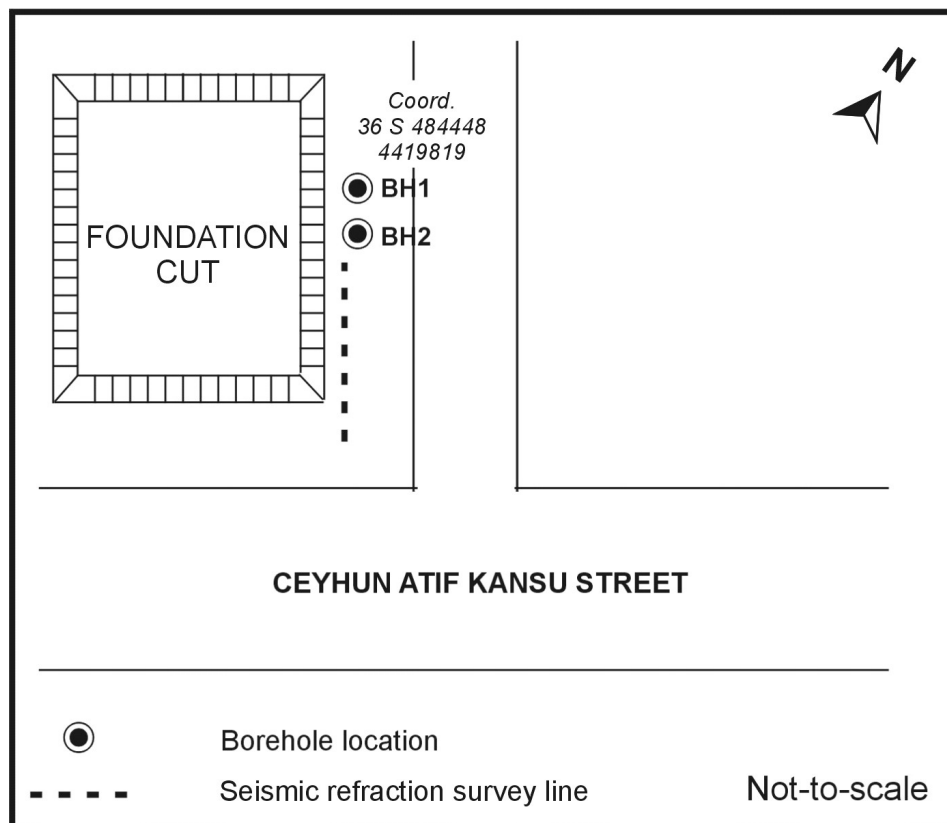


Figure 4.20 Borehole locations and seismic survey lines for the CAKS site on a plan view.

Table 4.7 shows the shear modulus and deformation modulus of the rock mass determined by the pressuremeter test at CASK site together with testing depths.

Table 4.7 Shear modulus and deformation modulus of the rock mass observed at CASK.

Borehole no.	Test depth (m)	Shear modulus, G (MPa)	Deformation modulus, E (MPa)
BH 7	1.0	52.3	136.0
BH 7	1.6	57.5	149.5
BH 7	2.3	63.3	164.6
BH 8	1.0	56.6	147.1
BH 8	2.5	104.7	272.2
BH 8	4.0	102.2	265.7
BH 8	5.0	73.5	191.1
BH 8	6.0	52.7	137.0

If all values of deformation modulus (total of 27) from the Dikmen greywackes determined by the pressuremeter testing are used to obtain normal distribution, the histogram given in Figure 4.21 is obtained. The normal distribution parameters of the overall values of the deformation modulus are 112.8 MPa for mean value and 63.3 MPa for standard deviation.

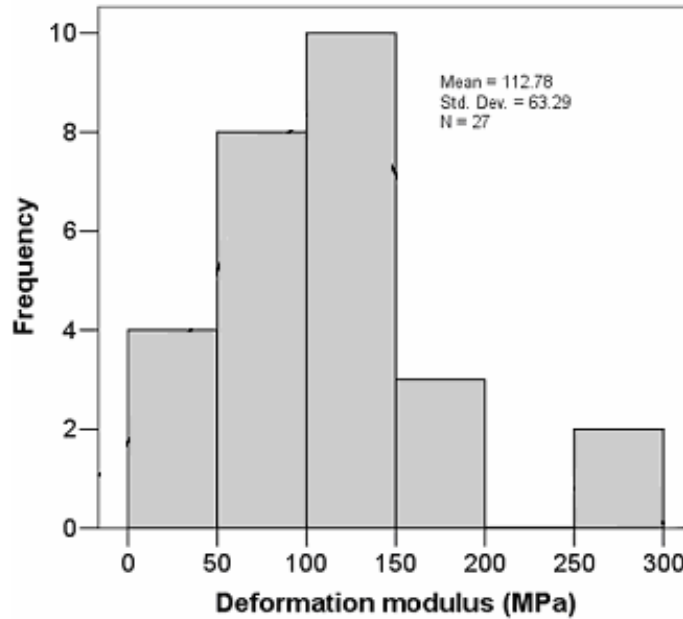


Figure 4.21 The histogram of the deformation modulus obtained from all pressuremeter tests performed at Dikmen greywackes.

4.2.2.2 Pressuremeter tests in the weathered andesites

A total of 9 boreholes were drilled in the weathered andesites. Four of them were utilized for pressuremeter testing and drilled using continuous flight auger. The others were drilled for sampling using a double tube core barrel and/or large diameter continuous flight auger depending on the ground conditions. The values of deformation modulus (E) were calculated from the shear modulus using a Poisson's ratio of 0.3. Summary of the results of the pressuremeter tests performed in Solfasal, Ovacık and Pursaklar districts are depicted in Tables 4.8, 4.9 and 4.10, respectively. Some of the tests could not yield limit pressure due to the capacity restrictions of the pressuremeter. The mean value of the deformation modulus of the weathered andesites is 34.8 MPa and standard deviation is 25.8 MPa (Figure 4.22). A sample PMT graph obtained from a depth of 7.7 m in BH 15 is given in Figure 4.23.

Table 4.8 Summary of pressuremeter tests performed in Solfasol district.

Test depth (m)	Shear modulus, G (MPa)	Deformation modulus, E (MPa)	Ménard limit pressure (MPa)
1.5	6.3	16.3	1.2
3.0	12.6	32.7	1.8
4.5	11.2	29.1	1.4
6.0	15.5	40.3	-
8.0	21.0	54.6	-
15.0	28.1	73.06	-

- Indicates the tests at which Ménard limit pressure could not be obtained due to the limited pressure capacity of the pressuremeter.

Table 4.9 Summary of pressuremeter tests performed in Ovacık district.

Test depth (m)	Shear modulus, G (MPa)	Deformation modulus, E (MPa)	Ménard limit pressure (kPa)
1.0	4.4	11.4	630.3
1.5	4.1	10.7	584.8
3.0	3.6	9.4	597.9
4.5	4.4	11.4	665.9
6.0	7.3	19.0	1148.7
7.5	8.6	22.4	1386.6
10.0	9.1	23.7	1477.5
13.0	7.5	19.5	1267.2
17.0	11.0	28.6	1382.6

Table 4.10 Summary of pressuremeter tests performed in Pursaklar district.

Borehole No.	Test depth (m)	Shear modulus, G (MPa)	Deformation modulus, E (MPa)	Ménard limit pressure (kPa)
BH 15	1.7	1.4	3.6	137.6
	3.2	2.0	5.2	359
	4.7	7.3	19.0	874
	6.2	10.8	28.1	1373
	7.7	16.3	42.4	-
	10	17.4	45.2	-
	15	23.3	60.6	-
BH 17	1.7	7.9	20.5	650
	3.2	15.0	39.0	-
	4.7	12.2	31.7	-
	6.2	13.7	35.6	-
	7.7	33.2	86.3	-
	10	34.4	89.4	-
	15	38.9	101.1	-

- Indicates the tests at which Ménard limit pressure could not be obtained due to the limited pressure capacity of the pressuremeter.

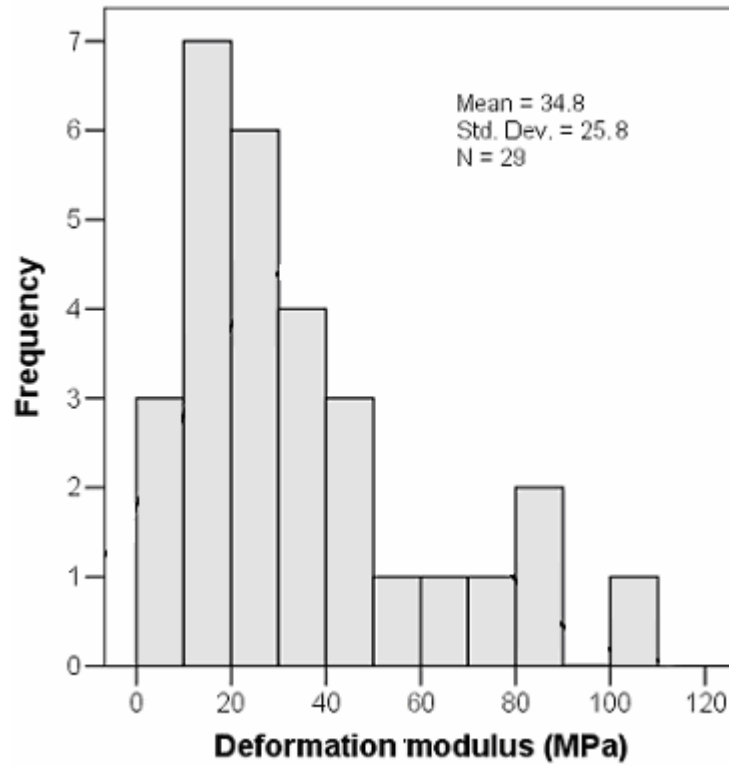


Figure 4.22 The histogram of deformation modulus values of the weathered andesites.

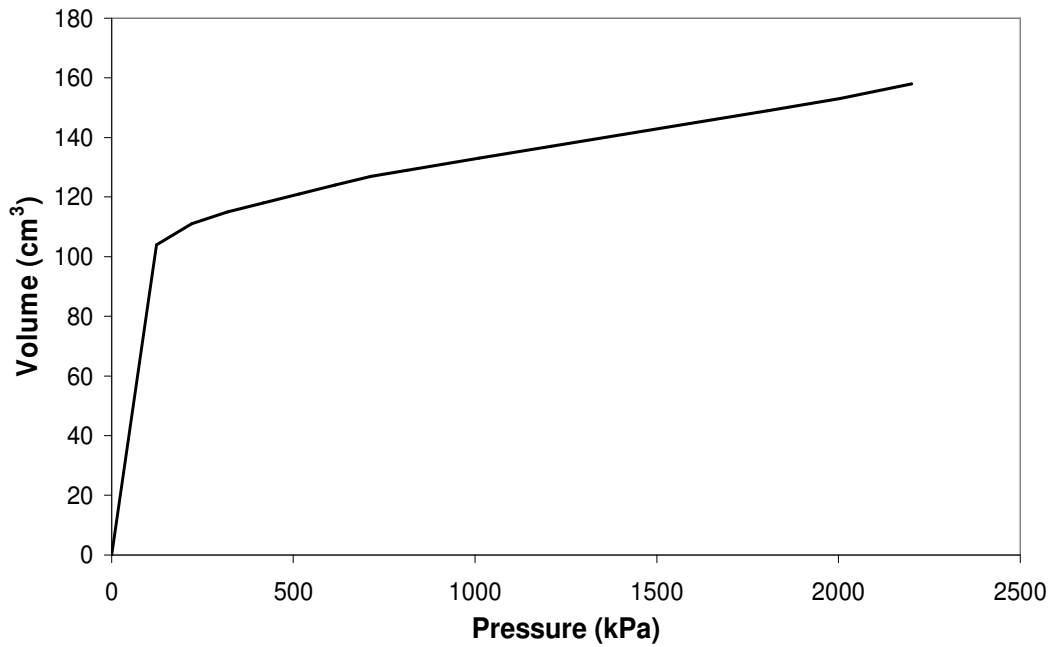


Figure 4.23 Sample PMT graph obtained from the depth of 7.7 m in BH 15.

4.2.2.3 Pressuremeter tests in mudrocks

For the purpose of obtaining strength and deformation behavior of the claystone and marl rock masses, a total of 50 PMT were performed in the boreholes at various depths. The values of shear modulus, deformation modulus and Ménard limit pressure are given in Table 4.11. The deformation modulus (E) values were calculated from the shear modulus Poisson's ratio of 0.3.

The mean of the deformation modulus of the mudrocks is 159.4 MPa and standard deviation is 81.9 MPa (Figure 4.24). A sample PMT graph obtained from the depth of 2 m in BH 21 is shown in Figure 4.25.

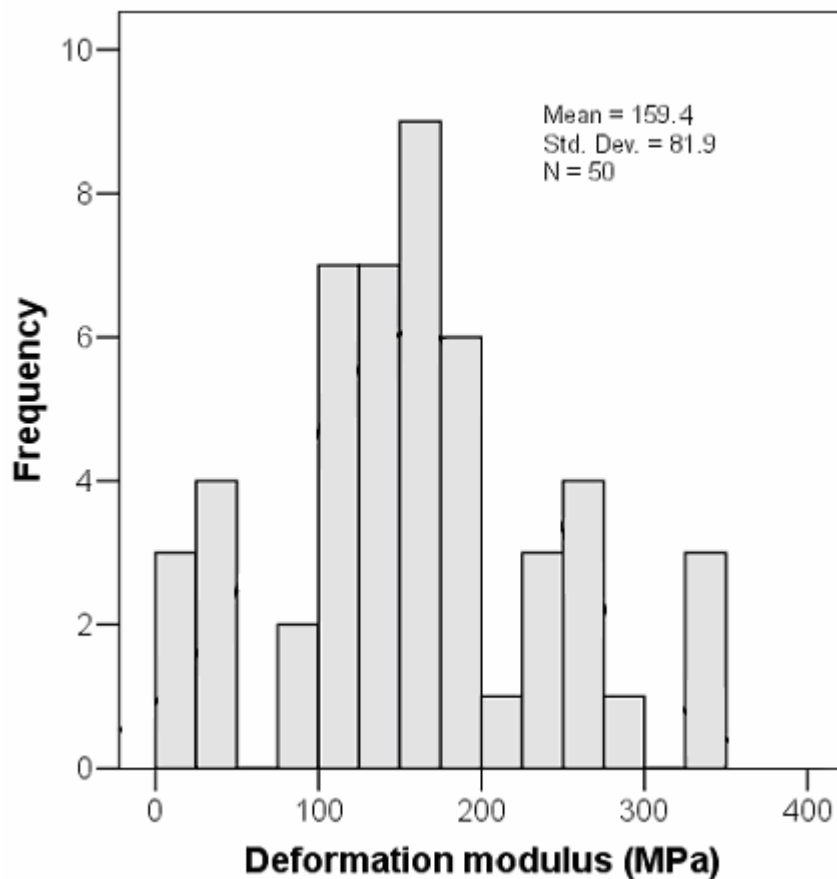


Figure 4.24 Histogram of the deformation modulus for mudrocks.

Table 4.11 Shear modulus, deformation modulus and Ménard limit pressure from PMT.

Borehole no.	Test depth (m)	Shear modulus, G (MPa)	Deformation modulus, E (MPa)	Ménard limit pressure (MPa)
BH 18	1.50	72.2	187.8	-
	2.50	49.2	128.0	-
	4.50	46.4	120.6	-
	7.00	75.1	195.2	-
	9.00	41.7	108.4	-
	11.00	14.5	37.8	-
	13.00	83.0	215.7	-
	15.00	72.2	187.8	-
BH 19	2.00	14.7	38.3	2.5
	4.00	43.4	112.8	-
	6.00	51.7	134.4	-
	8.00	71.7	186.3	-
	10.00	58.5	152.0	-
	12.00	98.5	256.0	-
	14.00	98.8	256.9	-
BH 20	2.00	14.3	37.3	0.9
	4.00	64.1	166.7	-
	6.00	61.7	160.3	-
	9.00	40.0	104.0	-
	13.00	34.3	89.2	-
	16.00	43.0	111.8	-
	20.00	53.4	138.8	-
	21.00	65.1	169.2	-
22.00	64.1	166.7	-	
BH 21	2.00	65.1	169.2	-
	4.00	52.4	136.3	-
	7.00	63.4	164.8	-
	9.00	66.0	171.6	-

Table 4.11 (continued)

Borehole no.	Testing depth (m)	Shear modulus, G (MPa)	Deformation modulus, E (MPa)	Ménard limit pressure (MPa)
BH 22	1.50	7.2	18.6	0.9
	3.50	7.5	19.6	1.7
	4.75	5.7	14.7	1.1
	6.25	36.2	94.1	-
	7.80	39.6	103.0	-
	11.00	71.7	186.3	--
	14.00	86.8	225.6	-
BH 23	6.50	89.6	232.9	-
	9.00	130.1	338.3	-
	11.00	130.1	338.3	-
	13.00	130.1	338.3	-
BH 24	2.00	54.7	142.2	-
	4.00	87.9	228.5	-
	6.50	101.8	264.8	-
	9.00	105.6	274.6	-
	12.00	107.7	280.0	-
BH 25	2.00	9.6	25.0	1.5
	4.00	57.2	148.8	-
	7.00	48.5	126.0	-
	9.00	46.8	121.6	-
	12.00	67.9	176.5	-
	15.00	64.5	167.7	-

- Indicates the tests at which Ménard limit pressure could not be obtained due to the limited pressure capacity of the pressuremeter.

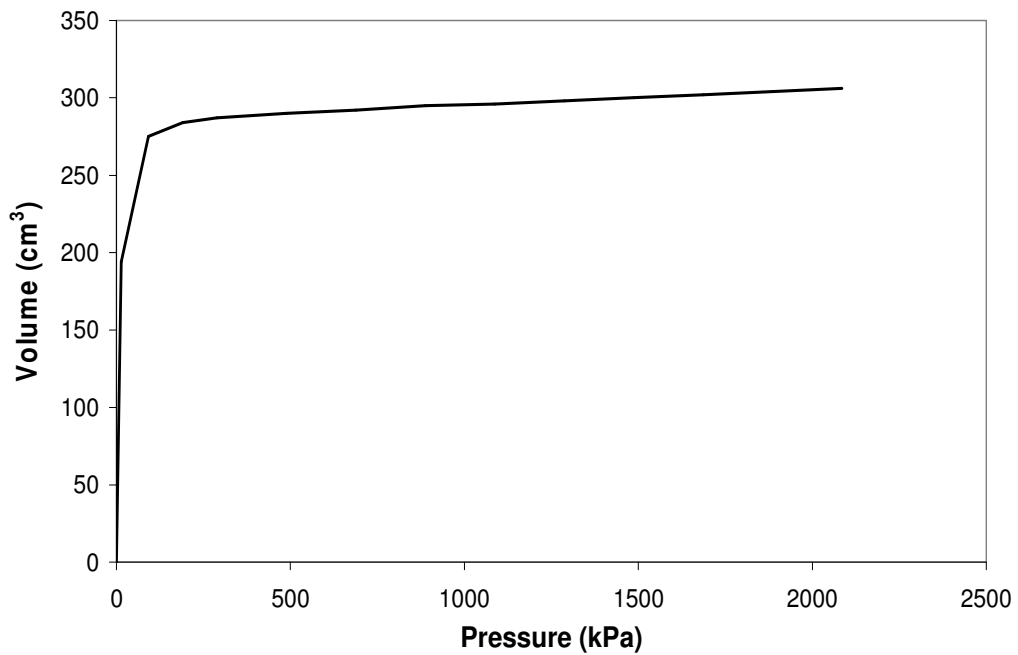


Figure 4.25 A sample PMT graph obtained at a depth of 2 m in BH 21.

4.2.2.4 Pressuremeter tests in the Eymir Lake clays

During the field study on the Eymir Lake clay, 3 boreholes were drilled next to each other. First borehole was drilled using continuous flight auger for the pressuremeter testing. Through this borehole 7 pressuremeter tests were performed at depths of 1, 2, 3, 4.2, 5.3, 6.8, 8 m. In the other borehole, 7 field vane tests at the same depths as the pressuremeter tests were performed. Undisturbed samples were taken from the last borehole. The values of deformation modulus were calculated from the shear modulus by using Poisson's ratio of 0.5. The values of the shear modulus, deformation modulus and Ménard limit pressure are given in Table 4.12. A sample PMT graph obtained at a depth of 2 m is shown in Figure 4.26.

Table 4.12 Shear modulus, deformation modulus and Ménard limit pressure of the Eymir Lake clays.

Test Depth (m)	Shear modulus, G (kPa)	Deformation modulus, E (kPa)	Ménard limit pressure (kPa)
1.0	660	1979	136
2.0	1375	4125	330
3.0	2042	6127	393
4.2	817	2452	290
5.3	823	2468	360
6.8	2327	6982	548
8.0	1722	5167	461

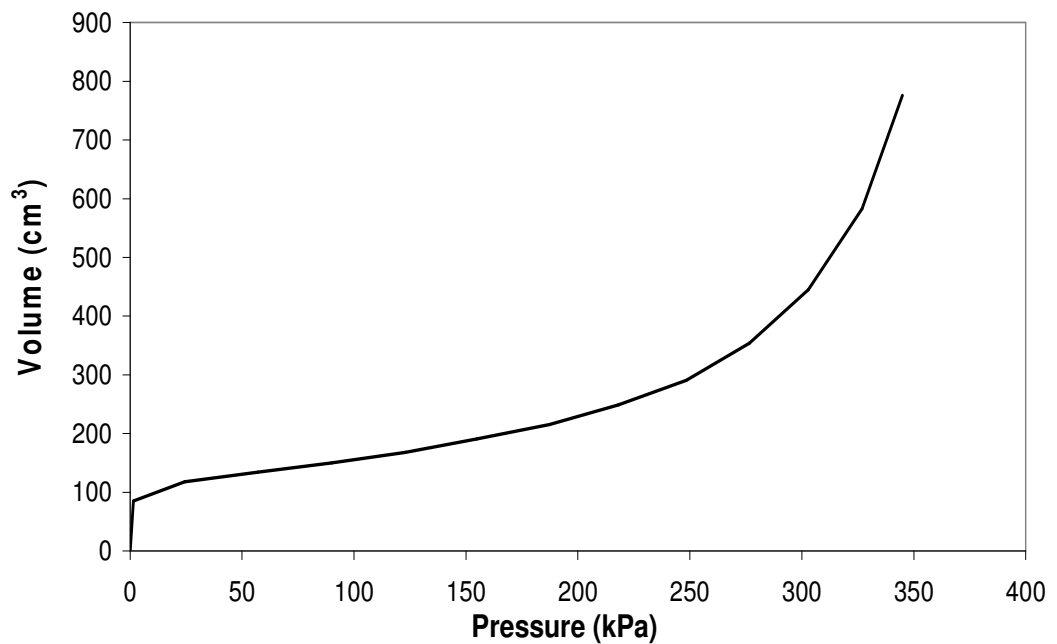


Figure 4.26 A sample PMT graph obtained from the depth of 2 m in Eymir Lake clays.

4.3 Seismic Refraction Surveys

The seismic refraction surveys involving both P and S wave measurements were conducted using a multi-channel seismograph to assess the dynamic parameters of the rock mass under consideration. The purpose of the tests is to use the shear wave velocities for a probable correlation with the modulus of deformation values obtained from the pressuremeter test. The seismometer includes a computer and a data acquisition system. The elastic deformability parameters can be directly obtained from the P and S waves utilizing the principles of theory of elasticity. However, these elastic parameters correspond to very small strain levels and cannot reflect the deformations under working load conditions. In spite of this limitation, the P and S wave velocities are valuable parameters for comparing the rock mass quality. Figure 4.27 shows the seismometer used in the seismic refraction surveys.

During the refraction surveys, 12 pressure (P) and 12 shear (S) wave recording geophones were utilized and the spacing between geophones was selected as 3 m. In order to create seismic waves required to perform refraction survey, impact of a sledge hammer was employed and two shot point locations were selected for each section.

All data from this survey were analyzed with SIP software by Rimrock Geophysics (1992) based on the USGS developed SIP routines. The interpretation program (SIPIN) uses the delay-time method (Hagedoorn, 1965) to obtain a first-approximation depth model, which is then modified by a series of ray-tracing and model adjustment iterations to minimize any discrepancies between the picked arrival times and corresponding times obtained from the depth model.



Figure 4.27 The seismometer used during the seismic refraction surveys.

By using the P and S wave velocities, the values of dynamic deformation modulus (E_{max}), shear modulus (G_{max}) and dynamic Poisson's ratio of the materials were calculated based on the theory of elasticity (Equations 4.6 and 4.7).

$$G = V_s^2 \cdot \delta \quad (4.6)$$

Where, V_s is the shear wave velocity, δ is the density of the material (unit weight/gravitational acceleration).

$$V_p/V_s = ((2^{0.5}) \cdot ((1-\mu)/(1-2\mu)))^{0.5} \quad (4.7)$$

Where, μ is the Poisson's ratio of the material.

4.3.1 Seismic refraction surveys in Dikmen greywackes

The seismic refraction surveys were performed in all greywacke locations (Figures 4.16, 4.18 and 4.20). Figure 4.28 shows the seismic refraction field layout at Beyaz Ev location in Beytepe campus of Hacettepe University. The depth model and time distance graphs of the seismic refraction survey performed in the greywackes at the Workshop area (section A) is depicted in Figure 4.29 as a selected example.

Summary of results obtained from the seismic refraction surveys performed in Workshop, Beyaz Ev and CAKS are given in Tables 4.13, 4.14 and 4.15.

Table 4.13 Summary of the results obtained from the seismic refraction surveys performed at Beytepe campus of Hacettepe University, Workshop location.

Survey line	Layer No.	Depth (m)	V_p (m/sec)	V_s (m/sec)	G_{max} (MPa)	E_{max} (MPa)	Dynamic Poisson's ratio
A	1	0.5 – 3	816	394	396	1067	0.348
	2	-	1366	576	846	2355	0.392
B	1	-	1384	720	1322	3475	0.315

V_p : Velocity of the pressure wave; V_s : Velocity of the shear wave; G_{max} : Maximum shear modulus, E_{max} : Maximum modulus of elasticity.

Table 4.14 Summary of the results obtained from the seismic refraction surveys performed at Beytepe campus of Hacettepe University, Beyaz Ev location.

Survey line	Layer No.	Depth (m)	V_p (m/sec)	V_s (m/sec)	G_{max} (MPa)	E_{max} (MPa)	Dynamic Poisson's ratio
A	1	-	1698	517	682	1975	0.449
B	1	-	1666	422	454	1331	0.466
C	1	-	1893	787	1579	4408	0.396

Table 4.15 Summary of the results obtained from the seismic refraction surveys performed at Dikmen CAKS location.

Survey line	Layer No.	Depth (m)	V_p (m/sec)	V_s (m/sec)	G_{max} (MPa)	E_{max} (MPa)	Dynamic Poisson's ratio
A	1	1 - 2	767	242	149	432	0.445
	2	-	2405	1365	4751	11996	0.263



Figure 4.28 Field layout of the refraction survey at Beytepe campus of Hacettepe University, Beyaz Ev location.

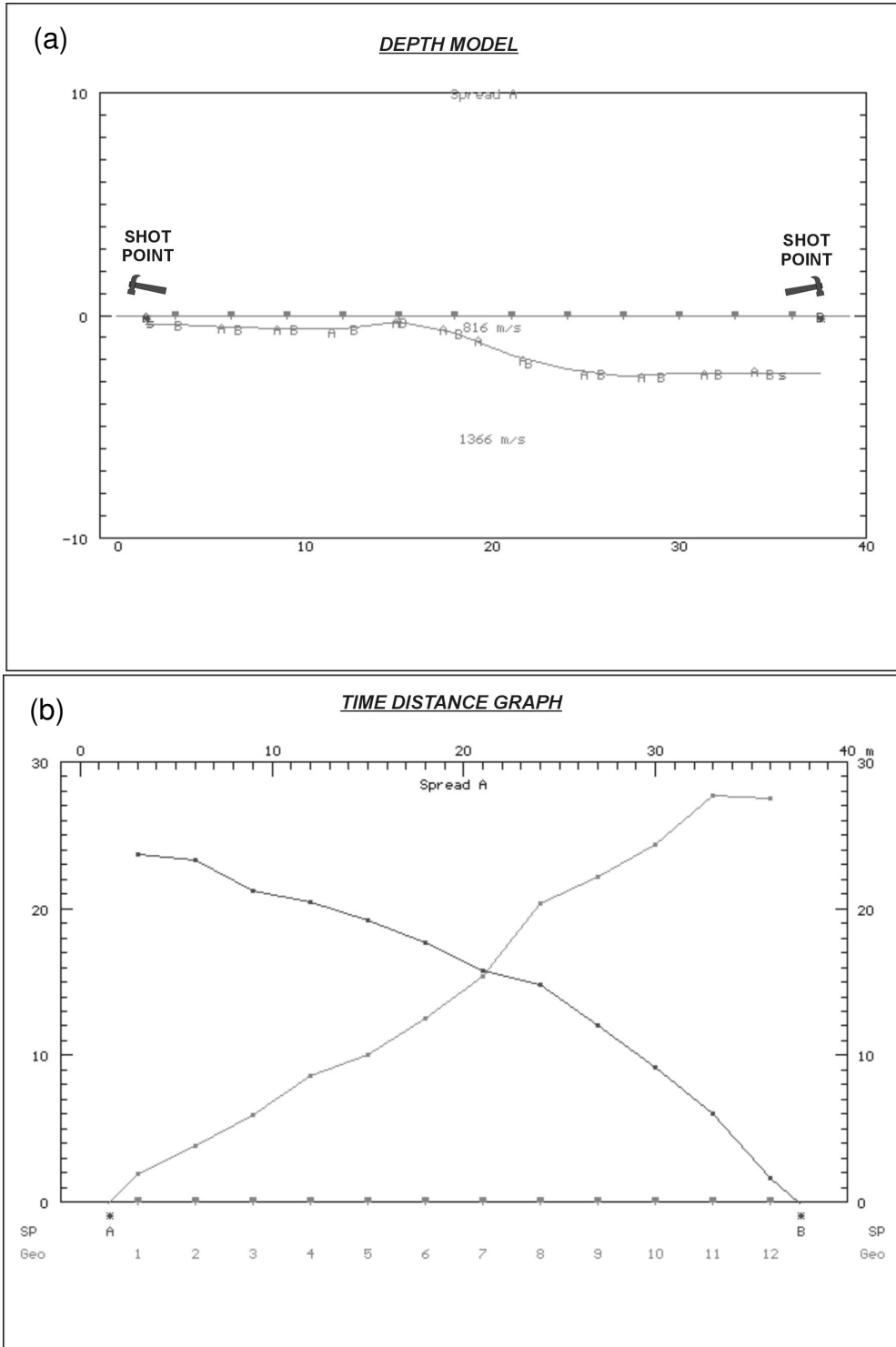


Figure 4.29 (a) The depth model and (b) time distance graphs of the seismic refraction survey performed in greywackes at workshop location of Beytepe Campus (section A).

4.3.2 Seismic refraction studies in the weathered andesites

The seismic refraction surveys were also performed in the weathered andesites for rock mass characterization. The results of the surveys are tabulated in Tables 4.16 through 4.18.

Table 4.16 The summary of the results obtained from the seismic refraction surveys performed at Solfasol district.

Layer No.	Depth (m)	V_p (m/sec)	V_s (m/sec)	G_{max} (MPa)	E_{max} (MPa)	Dynamic Poisson's ratio
1	7 - 8	368	108	23	67	0.453
2	-	2431	457	418	1224	0.482

Table 4.17 The summary of the results obtained from the seismic refraction surveys performed at Ovacık district.

Layer No.	Depth (m)	V_p (m/sec)	V_s (m/sec)	G_{max} (MPa)	E_{max} (MPa)	Dynamic Poisson's ratio
1	4 - 5	1125	280	157	460	0.467
2	-	2874	374	280	834	0.491

Table 4.18 The summary of the results obtained from the seismic refraction surveys performed at Pursaklar district.

Survey line	Layer No.	Depth (m)	V_p (m/sec)	V_s (m/sec)	G_{max} (MPa)	E_{max} (MPa)	Dynamic Poisson's ratio
A	1	4 - 6	507	31	1.9	5.8	0.498
	2	-	1683	231	107	318	0.490
B	1	2 - 5	760	58	6.8	20	0.497
	2	-	1245	339	229	671	0.460

4.3.3 Seismic refraction studies in the mudrocks

Within the mudrocks exposed around Sincan the surveys were performed along four sections which are very close to the borehole locations. Table 4.19 gives the summary of the results obtained from the seismic refraction surveys.

Table 4.19 The summary of the results obtained from the seismic refraction surveys performed at mudrocks.

Survey line	Layer No.	Depth (m)	V_p (m/sec)	V_s (m/sec)	G_{max} (MPa)	E_{max} (MPa)	Dynamic Poisson's ratio
A	1	2 - 3	257	154	55	135	0.220
	2	12 - 16	1645	315	232	688	0.481
	3	-	6364	580	787	2355	0.496
B	1	4 - 5	251	128	38	102	0.324
	2	-	2493	189	84	250	0.497
C	1	2	213	67	11	30	0.445
	2	5 - 7	1091	391	358	1021	0.426
	3	-	2899	947	2099	6045	0.440
D	1	2 - 3	332	92	20	58	0.458
	2	-	1703	665	1035	2918	0.410

4.4 Cone Penetration Tests

For the determination of soil profile and undrained shear strength of the Eymir Lake clay, Cone Penetration Tests (CPT) were performed close to the boreholes by using electronic piezocone with 10 cm² tip area. The CPT tests were performed by Zemar Zemin Araştırma Ltd. Şti.

During testing, the penetration rate was kept as 2 cm/sec. The tip resistance, sleeve friction and pore pressure measurements were taken using electronic transducers. The tests were performed according to ASTM (1994 a). Figure 4.30 shows the CPT data logging system and the cone used in the study.

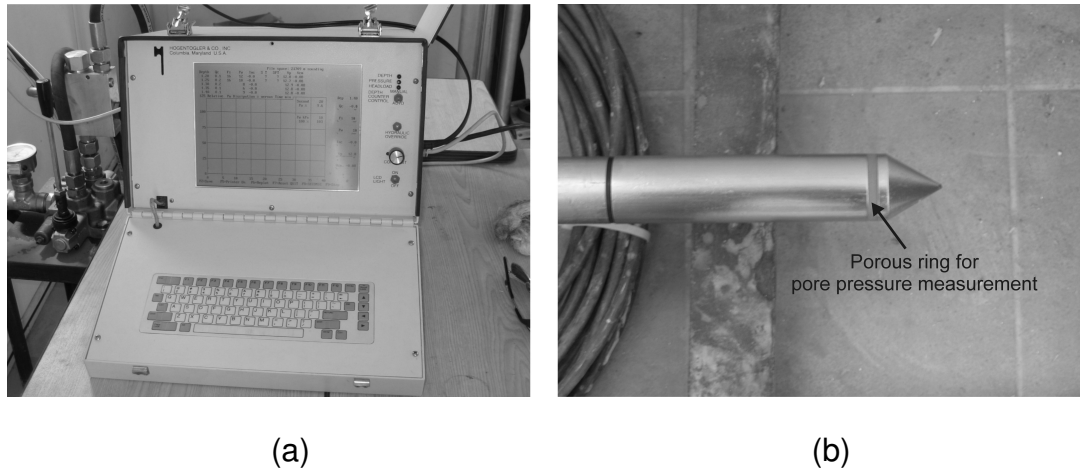


Figure 4.30 (a) The CPT data logging system and (b) the cone used in the study.

The tip resistance, sleeve friction, excess pore pressure measurements and soil behavior type determined from CPT in Eymir Lake clays are depicted in Figure 4.31.

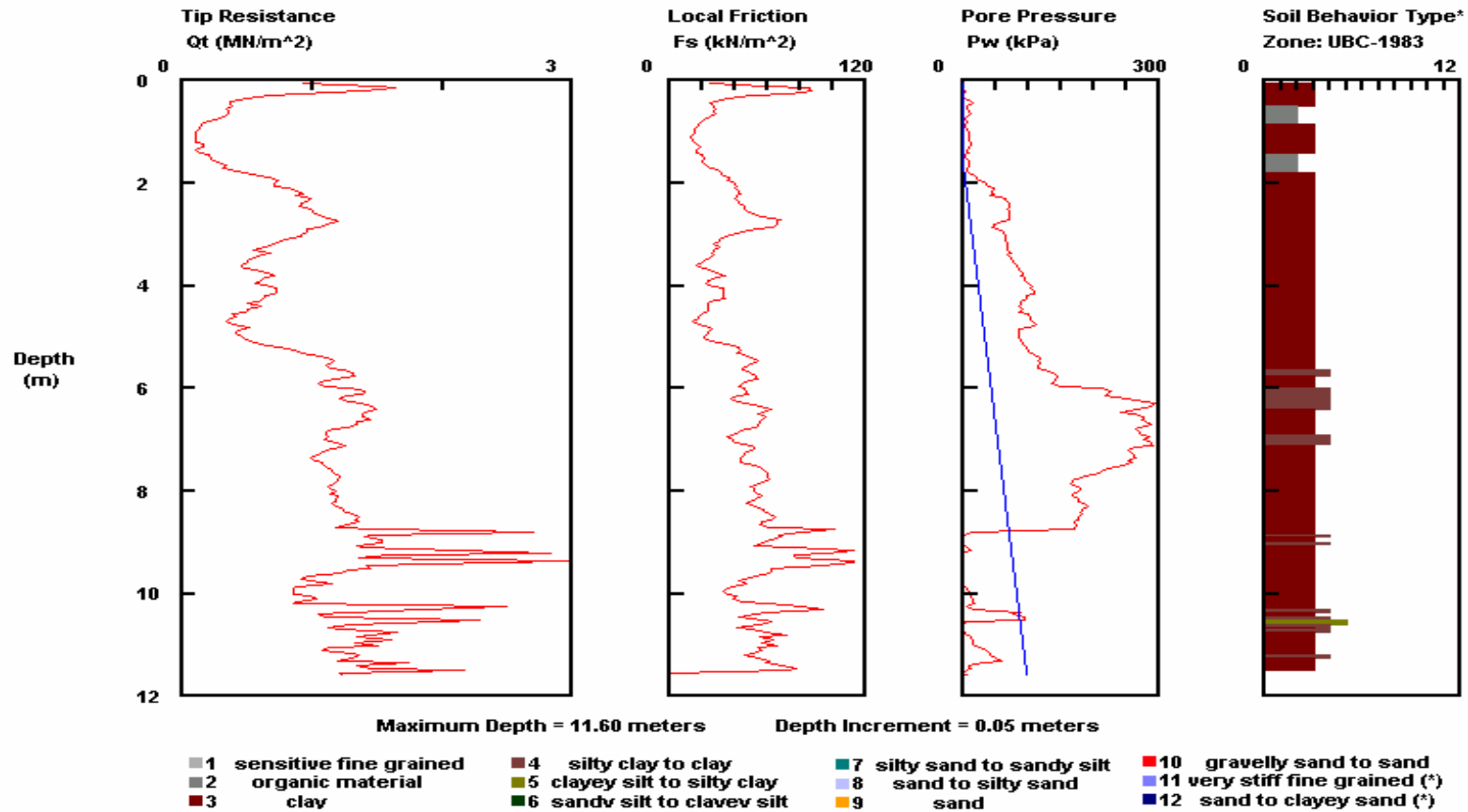


Figure 4.31 The tip resistance, sleeve friction, excess pore pressure measurements and soil behavior type determined from the CPT tests in the Eymir Lake clays.

4.5 Field Vane Tests

The field vane tests were performed in the Eymir Lake clays to determine undrained shear strength which will be compared with those determined from the pressuremeter tests. The field vane test system used in this study has two blades. The first blade is for relatively soft clays with undrained shear strength of between 0 and 80 kPa and its dimensions are 151.5 mm (height), 75.8 mm (diameter) and 1.5 mm (blade thickness). The second blade is for stiffer clays with undrained shear strength of between 0 and 160 kPa, and its dimensions are 120 mm, 60 mm, 1.5 mm respectively. The tip blades are sharpened using 45° cut. In this study, second blade (120 * 60 mm) was utilized (Figure 4.32). The system has a special anti-friction rod system which always ascertains the real friction between the rods and soil. The tests were performed according to ASTM (1994b). Instead of the torque, the undrained shear strength was directly measured from the dial gauge. The gauge displays the undrained shear strength according to the equation 4.8 (uniform shear stress distribution at top and bottom of the cylindrical shear surface assumed). Table 4.20 shows the undrained shear strengths obtained with field vane tests.

For a vane with $H = 2D$;

$$T = 3.667D^3 S_u \quad (4.8)$$

Where, T is the torque, D is the blade diameter (mm) and S_u is the undrained shear strength.



Figure 4.32 Field vane used in the study.

Table 4.20 The values of undrained shear strength determined from the field vane tests.

Depth (m)	Undrained shear strength, S_u (kPa)
1	36
2	84
3	83
4.2	81
5.3	131
6.8	127

4.6 Schmidt Hammer Tests

Because during the drilling operations no intact core samples could be taken from the Dikmen greywackes, L-type Schmidt hammer with 0.74 Nm impact energy was utilized for indirect determination of the intact rock strength in the greywackes. The tests were performed according to ISRM (1981) and the values of uniaxial compressive strength of the rock was estimated using Deere and Miller (1966)'s chart.

(a) Beytepe Campus of Hacettepe University, workshop site:

Figure 4.33 presents the histogram of the uniaxial compressive strength (greywackes at workshop site) indirectly obtained from the Schmidt hammer rebound values. The normal distribution parameters of the uniaxial compressive strength values are 12 MPa for mean value and 5.08 MPa for standard deviation. The minimum, mean and maximum values of the uniaxial compressive strength determined from the Schmidt hammer tests are given in Table 4.1 for the workshop location.

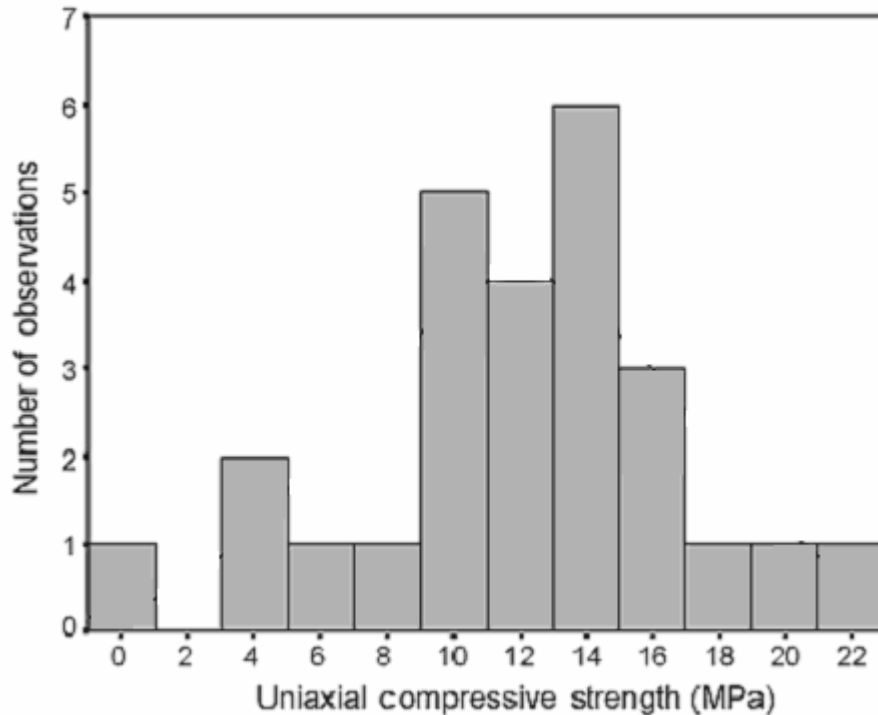


Figure 4.33 Histogram of the uniaxial compressive strength values of the greywackes at workshop site.

(b) *Beytepe Campus of Hacettepe University Beyaz Ev site:*

The histogram of the uniaxial compressive strength values of the greywackes at Beyaz Ev site obtained from the Schmidt hammer rebound values together with the fitted normal distribution curve is depicted in Figure 4.34. The normal distribution parameters of the uniaxial compressive strength are 22 MPa for mean value and 13.65 MPa for standard deviation. The minimum, mean and maximum values of the uniaxial compressive strength determined from the Schmidt hammer tests are given in Table 4.2 for Beyaz Ev location. The values of uniaxial compressive strength indirectly obtained from Schmidt hammer tests is surprising, because they are higher than those obtained from the workshop site. However, the rock mass seems to be weaker than that of workshop site. This is due to the fact that the rock mass exposed around Beyaz Ev site includes heavily

weathered – completely disintegrated soil matrix, and USC for this matrix is impossible to determine. However, when this matrix is excavated, less weathered portion will be exposed, and therefore, the USC given in Figure 4.35 is valid for the rock mass of Beyaz Ev site.

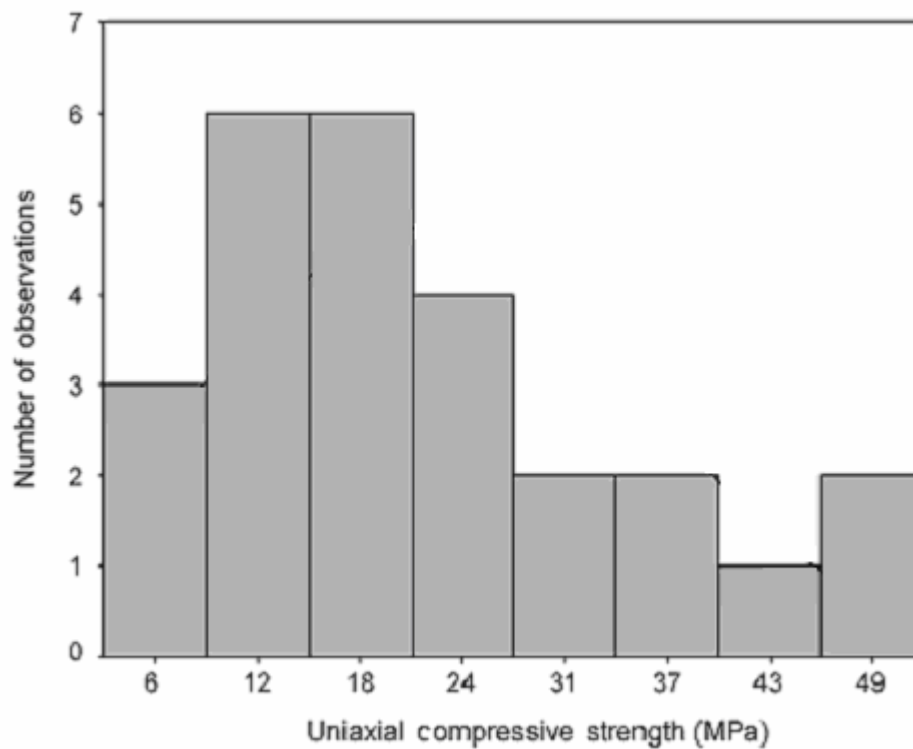


Figure 4.34 The histogram of the uniaxial compressive strength of the greywackes at Beyaz Ev site.

Kumtepe (1996) determined the USC as 36.7 MPa (one test on a core sample) of the greywackes around Beyaz Ev. This value will probably belong to an intact rock sample from the less weathered portion and does not reflect the overall intact rock strength of the greywackes at this site.

(c) *Dikmen Ceyhun Atif Kansu Street (CAKS):*

Figure 4.35 shows the histogram of the values of the uniaxial compressive strength indirectly obtained from the Schmidt hammer rebound values together with the fitted normal distribution curve. The normal distribution parameters of the uniaxial compressive strength values are 19 MPa for mean value and 11.58 MPa for standard deviation. The minimum, mean and maximum values of the uniaxial compressive strength determined from the Schmidt hammer tests are given in Table 4.3 for CAKS location. The values of the uniaxial compressive strength obtained from Schmidt hammer rebound values is again surprising, because they are nearly equal to those obtained from Beytepe Beyaz Ev site.

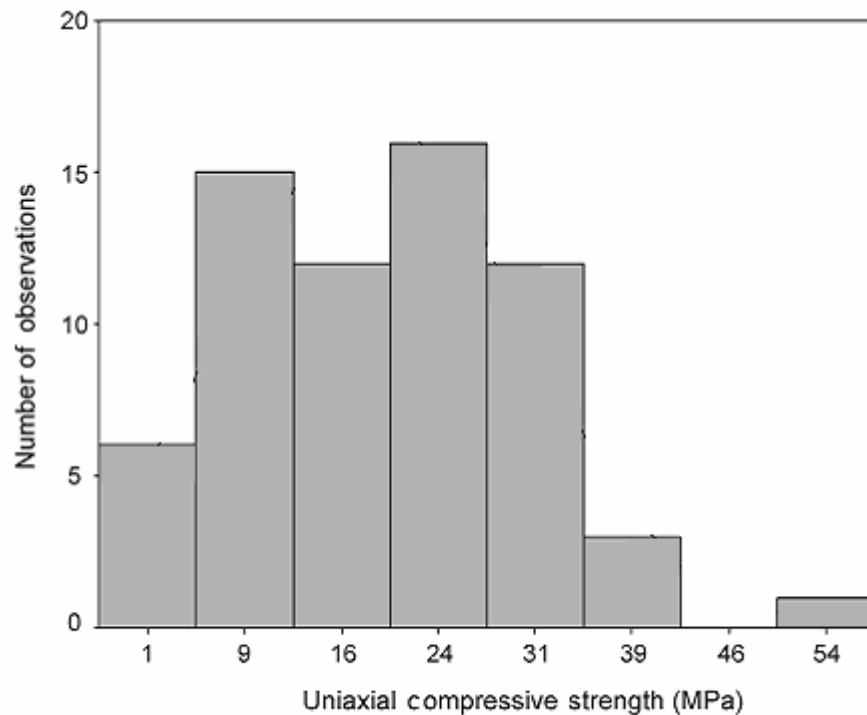


Figure 4.35 Histogram of the uniaxial compressive strength of the greywackes at CAKS.

CHAPTER 5

LABORATORY GEOMECHANICAL TESTS

In addition to the field test, laboratory geomechanical tests were also performed for the determination of soil and rock properties of the selected sites.

5.1 Block Punch Strength Index Tests

The Block Punch Strength Index (BPI) test is performed for indirectly estimation of the uniaxial compressive strength of intact rocks from which standard core specimens could not be prepared. The BPI test was specifically designed for rocks which are easily separated into slices such as slate etc. The test was improved by the studies of Ulusay and Gökçeoğlu (1997 and 1998), Gökçeoğlu (1997), Sülükçü and Ulusay (2001) who obtained satisfactory results for the estimation of uniaxial compressive strength. This method was accepted as a draft suggested ISRM method by ISRM in 2001 (Ulusay et al., 2001).

In BPI, disk specimens are prepared from the core samples having thicknesses ranging between 5 – 15 mm with parallel faces. The disk shaped specimens are placed to a disk shearing channel whose dimensions are given in Figure 5.1. The tests were carried out following the procedure described by Ulusay et al. (2001). For a valid test, the specimen has to be uniformly failed as shown in Figure 5.2.

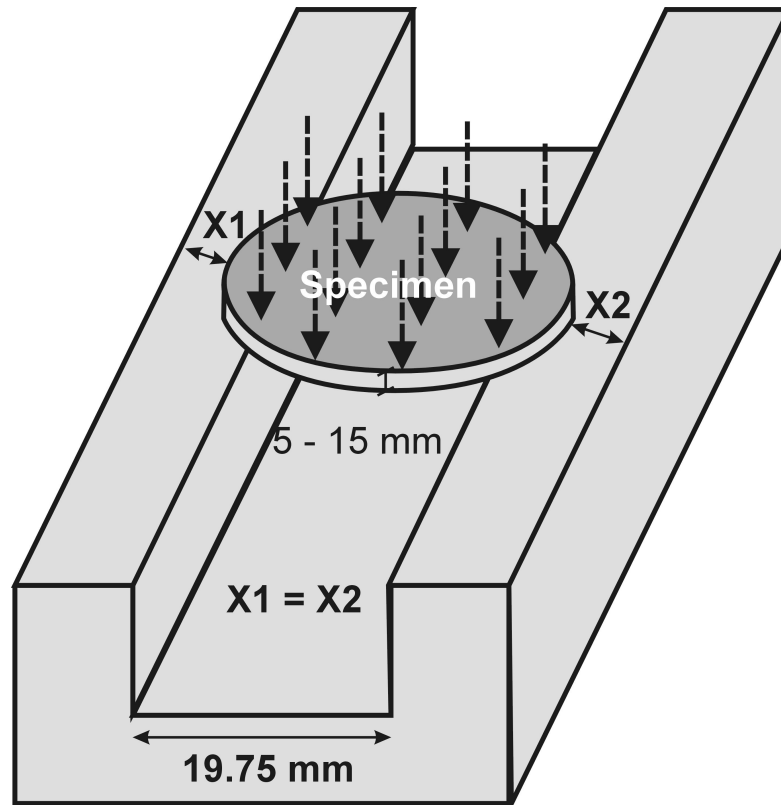


Figure 5.1 Disk shearing channel and its dimensions (Ulusay et al., 2001).

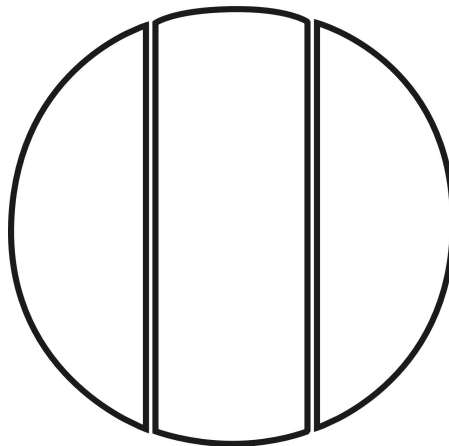


Figure 5.2 Uniformly failed BPI specimen (Ulusay et al., 2001).

In order to improve the Schmidt test results and to obtain uniaxial compressive strength of intact greywacke samples to be used in developing empirical equations for the deformation modulus of the greywackes, 29 BPI tests were performed on the greywacke samples extracted from greywacke blocks which were selected as being most compact and including less number of discontinuities. The tests were carried out at Hacettepe University, Geological Engineering Department Rock Mechanics Laboratory. Unfortunately no sample could be extracted from the blocks taken from Beyaz Ev site.

The values of the corrected BPI is calculated according to the equation 5.1.

$$BPI_c = 3499.D^{-1.3926}.t^{-1.1265}.F \quad (5.1)$$

Where, BPI_c is the corrected block punch strength index (MPa), D is the diameter of the specimen (mm), t is the thickness of the specimen (mm), and F is the failure load (kN).

From the corrected BPI, the uniaxial compressive strength of the rock can be estimated from the following equation.

$$UCS = 5.1.BPI \text{ (Ulusay et. al, 2001)} \quad (5.2)$$

However, based on the BPI tests carried on Dikmen greywackes by Gökçeoğlu and Zorlu (2004), the following equation was suggested specifically for the estimation of UCS of this rock unit.

$$UCS = 2.72.BPI_c + 13.7 \quad (5.3)$$

Table 5.1 presents the block punch index test results of Dikmen greywackes. The histogram and descriptive statistics of the BPI results are depicted in Figure 5.3.

Table 5.1 Block punch index test results of Dikmen greywackes.

Sample	D (mm)	T (mm)	F (kN)	BPI (MPa)	UCS	
					Ulusay et al. (2001) (MPa)	Gökçeoğlu & Zorlu. (2004) (MPa)
Workshop carbonate matrix	54.5	11.5	11.2	9.55	48.72	39.69
	54.5	10	12	11.98	61.11	46.29
	54.5	12.3	14	11.07	56.46	43.81
	54.5	11.7	7.2	6.02	30.72	30.08
	54.5	11.1	17.5	15.54	79.23	55.96
	54.5	12.6	11.5	8.85	45.14	37.77
	54.5	14.5	14.5	9.53	48.58	39.61
	54.5	11.3	13	11.31	57.68	44.47
	54.5	11.5	8.2	6.99	35.67	32.73
	54.5	13.2	20	14.61	74.49	53.43
	54.5	13.6	14	9.89	50.42	40.59
	54.5	13.6	14.9	10.52	53.66	42.32
	54.5	13.2	19.5	14.24	72.63	52.44
	54.5	14.3	28.5	19.02	97.00	65.43
	54.5	14.5	17	11.17	56.96	44.08
54.5	9.1	10	11.10	56.63	43.90	
54.5	14	14	9.57	48.80	39.73	
Workshop clay matrix	54.5	11.8	3.8	3.15	16.06	22.26
	54.5	10.6	2	1.87	9.54	18.79
	54.5	10.4	1.6	1.53	7.80	17.86
	41.5	12.2	6	7.00	35.69	32.74
	41.5	11.2	6	7.71	39.30	34.66
	41.5	11.8	3	3.63	18.53	23.58
	41.5	11.2	4.5	5.78	29.48	29.42
	41.5	10.5	4	5.53	28.18	28.73
CAKS	41.5	12.8	10	11.05	56.36	43.76
	54.5	14	9	6.15	31.37	30.43
	54.5	13.4	9.5	6.82	34.79	32.25
	54.5	13	12	8.92	45.47	37.95

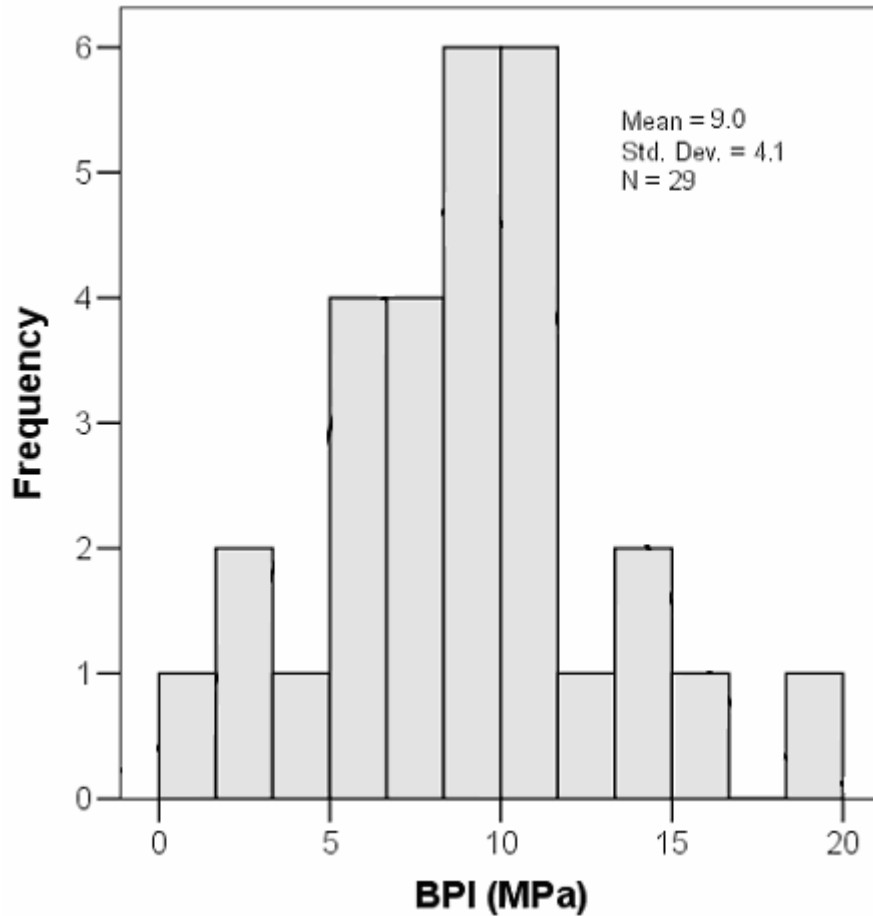


Figure 5.3 The histogram and descriptive statistics of the BPI results.

The mean value of the UCS of the greywackes extracted from the workshop site using the relationship proposed by Gökçeoğlu and Zorlu (2004) is 38.4 MPa with a standard deviation of 11.7 MPa. For CAKS site, mean value of UCS is 36.1 MPa and standard deviation is 6.03 MPa.

The values of UCS determined from the BPI tests are higher than those estimated from the Schmidt hammer rebound values. This is an expected result because the core samples extracted from the greywackes have higher strengths.

5.2 Uniaxial Compressive Strength Tests

Tests were performed on weathered andesites, mudrocks and greywackes to determine uniaxial compressive strength and deformation modulus of the intact rock samples. The tests were carried out at Gazi University Construction Edu. Department Concrete Laboratory. For the axial deformation measurements, two electronic displacement transducers with 0.0001 mm sensitivities were utilized. Two different compression machines with 3000 kN and 800 kN capacities were used for testing appropriate intact rock samples. All tests were performed according to ISRM (1981).

(a) Greywackes:

Because of the very weak nature of the Dikmen greywackes, only three UCS test samples could be extracted from the selected blocks. As for the case of BPI tests, these samples do not reflect the overall quality of the greywackes. Figure 5.4 shows the axial stress versus axial strain graph of the greywacke sample taken from Beyaz Ev location at Beytepe Campus of Hacettepe University. The summary of the uniaxial compression test results are given in Table 5.2.

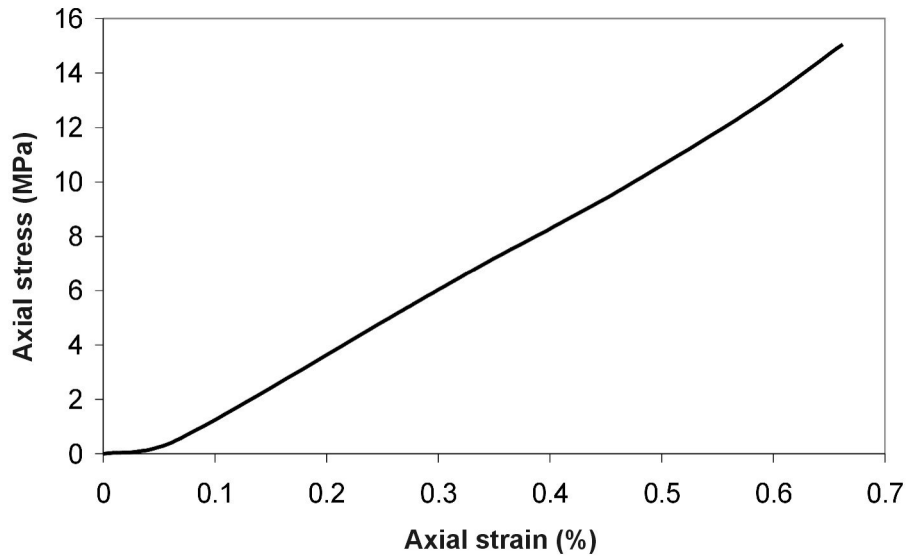


Figure 5.4 The axial stress versus axial strain graph of the greywacke sample taken from Beyaz Ev location at Beytepe Campus of Hacettepe University.

Table 5.2 Summary of the uniaxial compressive strength test results, from greywacke samples.

Sample	UCS (MPa)	E ₅₀ (MPa)
Dikmen – CAKS, A	20.8	4934
Dikmen – CAKS, B	13.3	2174
Beytepe Campus Beyaz Ev	15.1	2353

(b) *Weathered andesites:*

No core samples could be taken from Solfasol district thus the uniaxial compressive strength tests could not be performed. However, 10 and 18 uniaxial compressive strength tests were performed on samples taken from Ovacık and Pursaklar districts, respectively. Figure 5.5 depicts the axial stress versus axial strain graph of the Ovacık sample taken from a depth of 6 m.

Table 5.3 summarizes the results of the UCS tests performed on Ovacık samples. Figure 5.6 displays the axial stress versus axial strain plot of the Pursaklar sample taken from 15 m depth of BH 2.

Figure 5.7 depicts the histogram and descriptive statistics of the UCS values of the weathered andesites. The results of the UCS tests on the Pursaklar samples are given in Table 5.4. Figure 5.7 suggests that two distributions are super-imposed, left peak belongs to the UCS of Pursaklar site, whereas right distribution belongs to the Ovacık site.

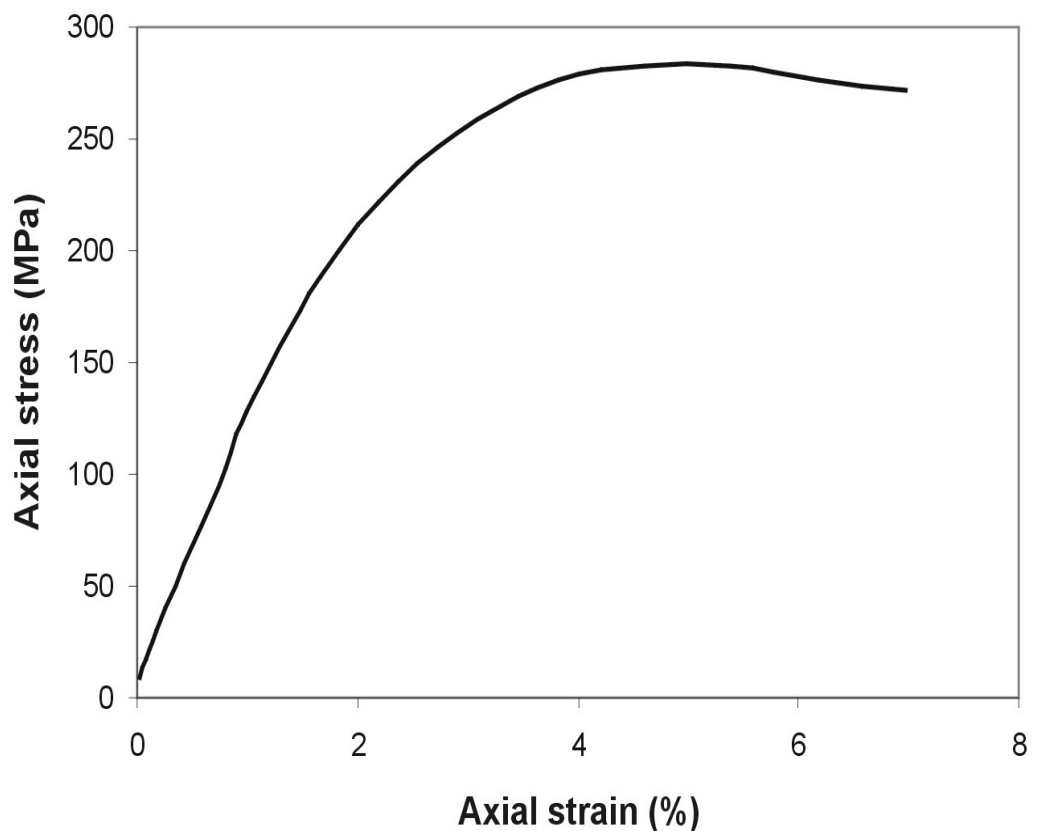


Figure 5.5 Axial stress versus axial strain graph of the Ovacık sample taken from a depth of 6 m.

Table 5.3 Results of the UCS tests performed on the weathered andesites taken from Ovacik.

Sampling depth (m)	UCS (kPa)	E ₅₀ (MPa)
4.0	283	12.4
4.5	248	14.0
5.0	385	17.5
6.0	347	23.5
7.5	344	23.7
10.0	415	28.4
13.0	471	18.5
15.0	428	20.1
16.0	518	25.4
18.0	468	32.7

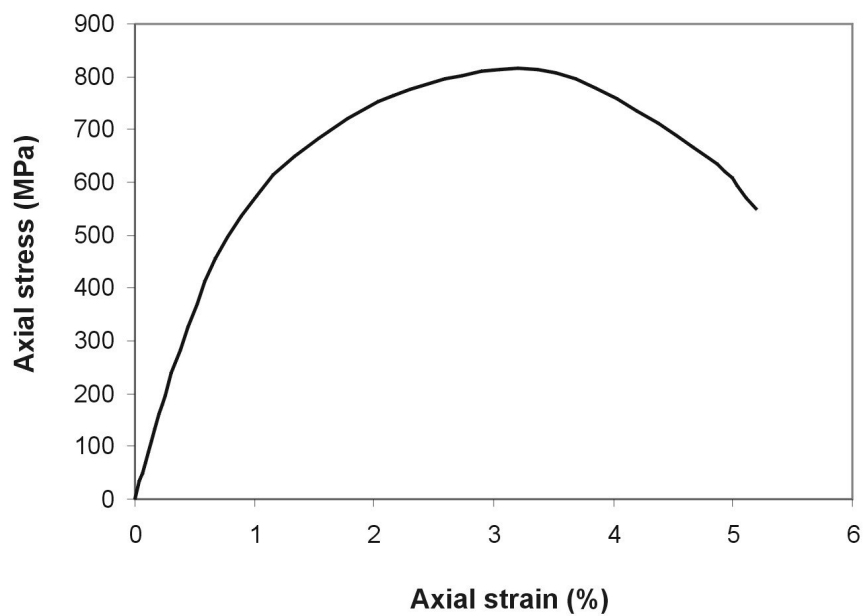


Figure 5.6 The axial stress versus axial strain plot of the weathered andesite from Pursaklar taken from a depth of 15 m in BH 2.

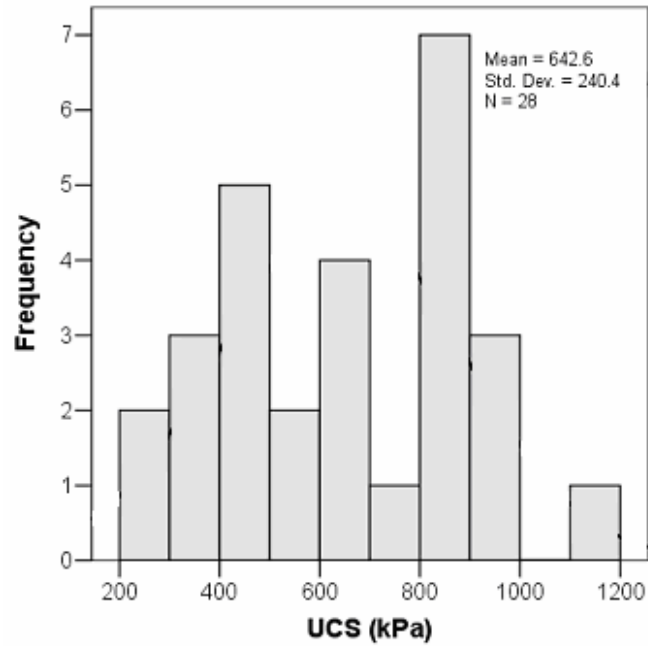


Figure 5.7 The histogram and descriptive statistics of the UCS values of the weathered andesites.

Table 5.4 The results of the UCS tests performed on the Pursaklar samples.

Borehole No.	Sampling depth (m)	UCS (kPa)	E ₅₀ (MPa)
BH 2	5.0	775	31.0
	6.0	604	32.3
	7.0	665	28.4
	8.0	816	54.9
	9.0	689	43.1
	10.0	615	46.8
	12.0	890	64.4
	15.0	808	69.5
18.0	856	76.3	
BH 4	5.0	513	37.1
	6.0	417	42.6
	7.0	839	89.4
	8.0	947	96.7
	10.0	818	124.7
	12.0	1112	109.1
	13.0	987	112.1
	15.0	836	92.2
18.0	900	135.8	

(c) Mudrocks cropping out around Sincan:

A total of 39 uniaxial compressive strength tests were performed on the intact mudrock core samples with deformation measurements (Table 5.5). The histogram of the UCS tests is depicted in Figure 5.8. There are two distinct peaks in the UCS histogram shown in Figure 5.8. In order to determine the average values of these two groups a clustering analysis was performed. Based on the K – means clustering analysis, the UCS values of 4.97 and 19.47 MPa UCS were obtained as the average values of these groups.

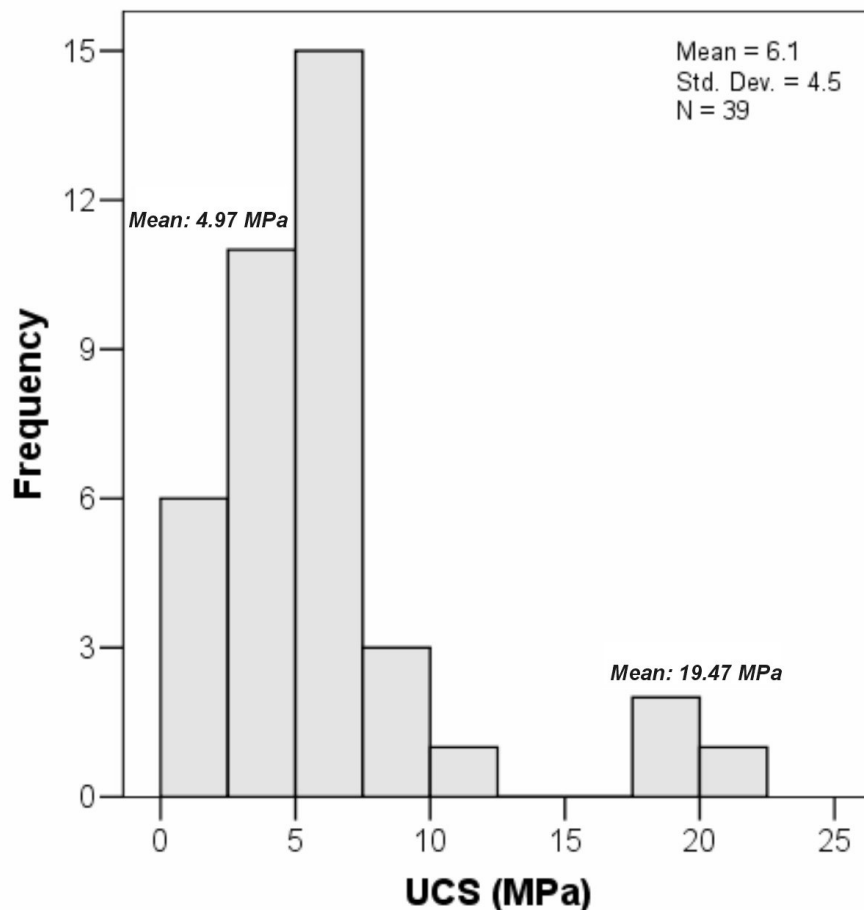


Figure 5.8 Histogram of the UCS values of the mudrock samples.

Table 5.5 Summary of the UCS test results from mudrocks.

Borehole No.	Depth (m)	Sample No.	USC (MPa)	E ₅₀ (MPa)
P 1	11 - 15	1	6.30	641.4
P 3	18 - 20	1	0.83	78.7
		2	2.96	507.2
	20 - 22	1	1.56	213.4
		2	1.27	136.9
	24 - 26	1	1.97	70.2
		2	2.40	171.4
	25 - 26	1	7.12	640.2
26 - 27	1	7.90	458.5	
P 5	10 - 12	1	5.80	522.7
		2	5.70	520.9
		3	6.80	688.0
		4	6.20	298.1
	12 - 14.5	1	6.76	2223.0
		2	6.76	4192.7
		3	6.60	7573.5
	14.5 - 15.5	1	2.91	2029.3
		2	3.74	354.3
	15.5 - 18	1	4.16	1481.2
		2	3.51	846.0
		3	8.06	11926.3
		4	3.95	407.5
18 - 20	1	2.34	205.5	
P 6	9.5 - 10.5	1	6.2	376.4
		2	4.5	419.2
	11 - 12.5	1	5.2	257.1
		2	3.5	1533.4
	12.5 - 15.5	1	9.9	1465.9
		2	6.5	1222.6
	14 - 15	1	18.6	799.7
		2	21.4	1717.5
	15 - 16	1	5.7	656.8
		2	6.6	893.9
P 8	8 - 12.5	1	18.4	7301.9
	12.5 - 16	1	3.6	242.1
		2	10.1	664.6
	16 - 30	1	2.5	105.1
		2	2.7	136.0
		3	6.3	495.5

5.3 Soil Mechanics Index Tests

In order to classify the soil according to Unified Soil Classification System (USCS), Atterberg limit determinations and grain size analyses including both sieve and laser particle sizing were performed for the Eymir Lake clays and the residual soils cropping out at Solfasol, Ovacik and Pursaklar districts. The tests were carried out at Gazi University Construction Edu. Department, Soil Mechanics Laboratory.

In the laser diffraction technique, laser beams are sent to the soil grains which are in suspension. Laser beams are diffracted from soil grains, and the diffracted beams are passed through a special lens (Fourier lens) and detected by a detector. There is an inverse relationship between the diffraction angle of the laser beam and grain size. Therefore, the densities of diffracted beams, which are diffracted with different angles, reflect the grain size distribution. By using the Mie theory (ISO, 1999), grain sizes, which are calculated by assuming sphere shaped grains and the volumetric amount grains, can be calculated. For this study, a laser diffraction device (Figure 6.9) which has a 2 mW He-Ne laser source producing laser beam with 0.633 μm wave length and 18 mm diameter, was used. The sedimentation techniques, such as hydrometer, use Stoke's law which assume settling particles as spheres. However, this assumption is not valid for clay minerals having flaky shapes. As a result of this assumption, hydrometer analysis determines the percentages of clay-sized particles higher than the actual amount. Because of this reason, laser diffraction method is superior to the sedimentation technique. The summary of the index test results of the studied cohesive soils is given in Table 5.6.

The calculated values of the clay fraction with the laser diffraction technique are lower than those determined from hydrometer. For example, clay

fraction of the Eymir Lake samples is about 50 - 60 %, whereas the laser diffraction technique yields about 20 - 25 %.

Table 5.6 The summary of the index test results of studied cohesive soils.

Name of location	Depth (m)	Soil type	Passing No 4 sieve (%)	Passing No 200 sieve (%)	LL (%)	PI (%)	Clay fraction %
Solfasol	0.5	CH	99.7	54.5	50.2	15.2	9.0
Ovacık	0.5	CH	99.7	83.4	83.9	51.6	35.7
	2.0	CH	100	93.9	80.6	36.8	26.0
Pursaklar	1.0	CH	97.3	57.4	76.3	45.6	15.0
	1.0	MH	96.7	57.9	66.5	32.5	13.0
Eymir Lake	1.0	CH	100	99.7	87	63	26.0
	2.0	CH	100	99.6	67	43	21.0
	3.0	CH	100	99.5	81	58	25.2
	4.5	CH	100	99.4	86	60	22.0
	6.0	CH	100	99.6	71	39	20.4
	8.0	CH	100	99.7	95	57	26.0

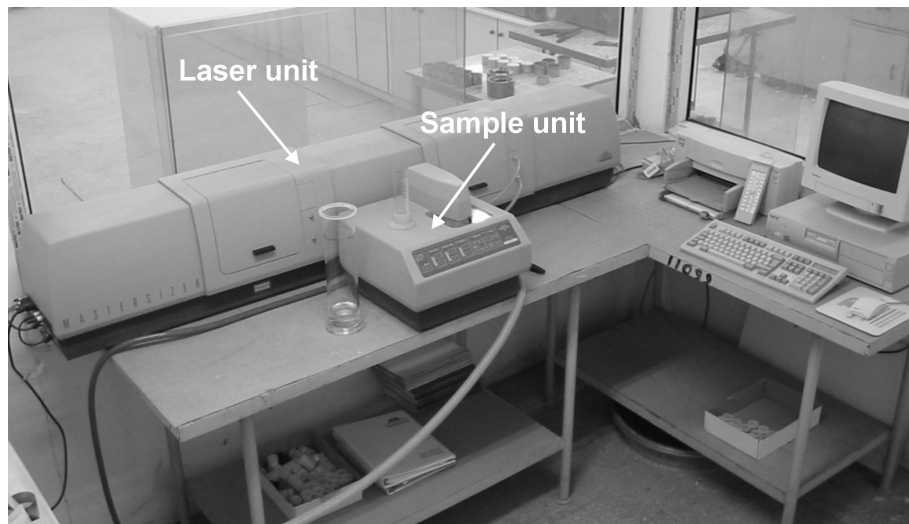


Figure 5.9 Laser diffraction instrument, employed in the study.

5.4 Laboratory Vane Shear Tests

The laboratory vane shear test is similar in principle which is used in the field, but on a smaller scale. The standard laboratory apparatus has a vane measuring 12.7 by 12.7 mm (Head, 1986). The test was carried out for the measurement of the undrained shear strength of the Eymir Lake clays in Gazi University Construction Edu. Department, Soil Mechanics Laboratory. The laboratory vane shear has a drive motor for the application of the torque. The equipment has four different springs each having different stiffness values. The tests were directly performed in the undisturbed sample tube to minimize disturbance effects. The vane is penetrated into the soil to obtain a minimum of 50 mm cover. Figure 5.10 shows the laboratory vane test apparatus and its parts. The maximum angular deflection of the spring is related to the undrained shear strength of the clay as given by equation 5.4.

$$S_u = \frac{K \cdot \theta_f}{4.29} \text{ (kPa)} \quad (5.4)$$

Where, K is the spring constant, and θ_f angular distortion of the spring at failure.

The tests were performed at five locations within the sample tube as recommended by Head (1986) and the test results were averaged for the calculation of the undrained shear strength. The undrained shear strength values (which will be used for the comparison with the values determined from pressuremeter) of the samples are given in Table 5.7.

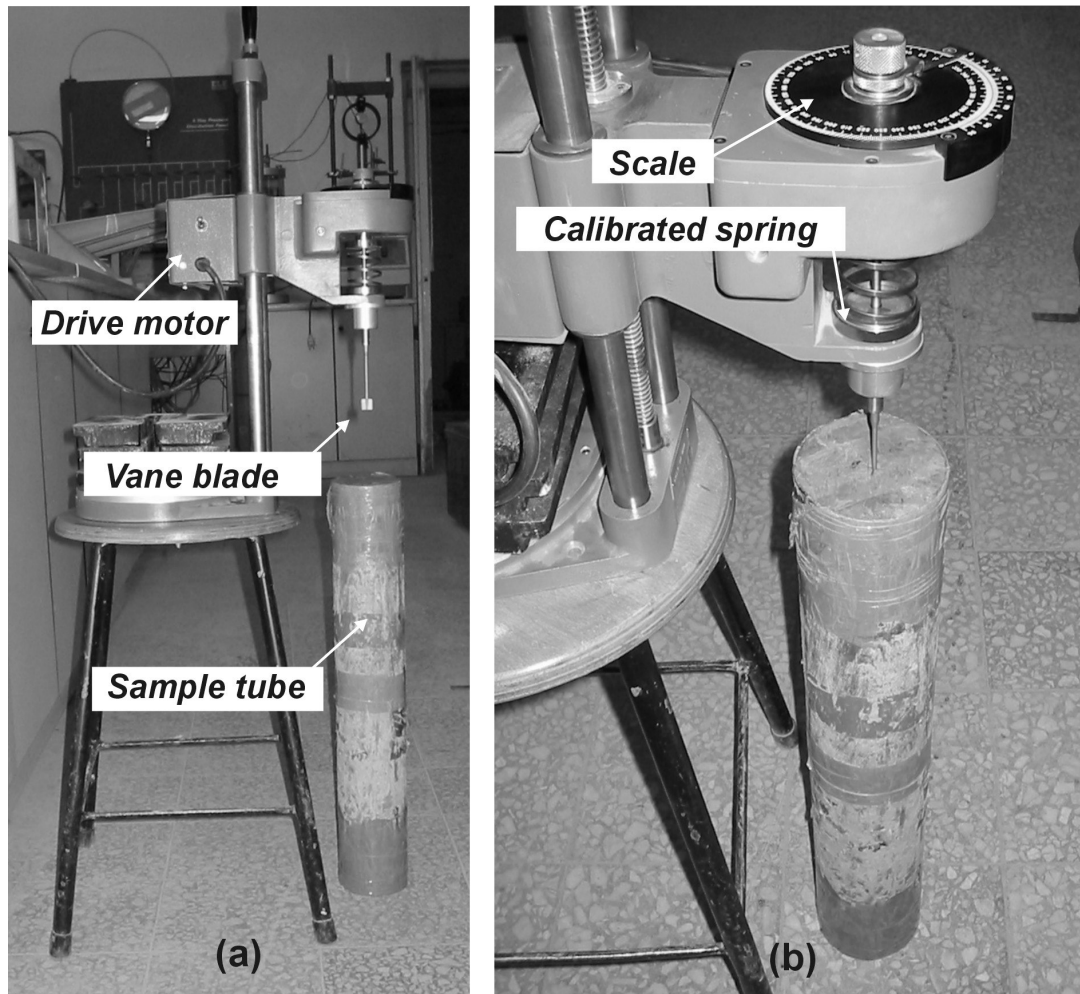


Figure 5.10 (a) The laboratory vane test apparatus, (b) and its parts.

Table 5.7 The undrained shear strength values of the samples.

Sampling depth (m)	Undrained shear strength, S_u (kPa)
1.0	25.3
2.0	69.5
3.0	71.0
4.2	65.1
6.2	111.0
8.2	147.1

5.5 Consolidation Tests

For the determination of the compressibility, overconsolidation ratio and permeability of the Eymir Lake clays, consolidation tests were performed on three samples using the oedometer apparatus in Gazi University Construction Edu. Department, Soil Mechanics Laboratory. The tests and associated calculations were performed according to ASTM D 2435 (ASTM, 2001). Pre-consolidation pressure (p_p) of the samples were calculated using the method recommended by ASTM D 2435 (ASTM, 2001) and the overconsolidation ratio of the samples were calculated by dividing the p_p to the present value of the effective stress. Figure 5.11 shows void ratio (e) versus logarithm of pressure plot, and settlement versus square root of time of the Eymir Lake sample taken from a depth of 8.2 m.

For the calculation of the permeability of the samples, both the coefficient of consolidation (c_v) and coefficient of the volume compressibility (m_v) are needed. Permeability of the soil is calculated using the following equation:

$$k = c_v \cdot m_w \cdot \gamma_w \quad (5.5)$$

Where, γ_w is the unit weight of water.

The values of coefficient of consolidation (c_v) of the soil for each loading increment were calculated by square-root-time method. Since c_v and m_v are both dependent on the load increment, the values of calculated permeability will also be dependent on the load increment. During consolidation, void ratio of the soil decreases so that the permeability decreases. Since permeability is dependent on the load increment, the average value of the permeability values were calculated by averaging the permeability values of

the load increments. However, the permeability values of the first and last load increments were discarded, because the permeability determined during the first load increment will be affected from the disturbance during field sampling and sample preparation. The last increment's permeability value will be too low compared to the field situation. For all tests, the calculated values of saturation ratios (S_r) are 100 %, in other words the samples are fully saturated. Table 5.8 summarizes the consolidation test results.

As it is clear from Table 5.10, the permeability of the Eymir Lake clay is very low. Craig (1992) suggests that the permeability values of the unfissured clays and clay silt mixtures (clay fraction > 20 % - by hydrometer) are greater than 10^{-7} m/sec. As it was previously mentioned, the clay sized fraction of the Eymir Lake clays is about 50 - 60 % (by hydrometer), therefore, the very low permeability values of the Eymir Lake clays are in agreement with their grain size distribution.

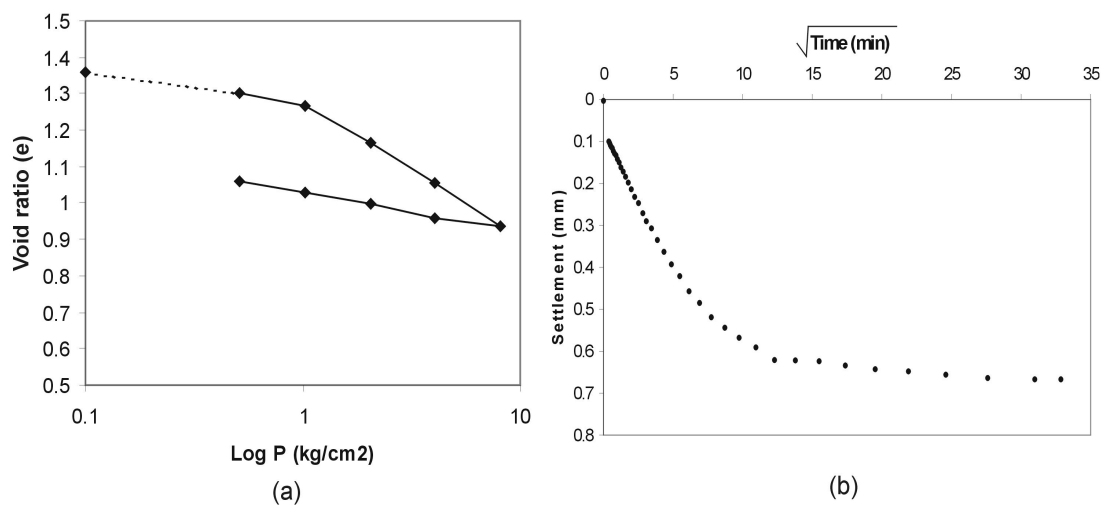


Figure 5.11 (a) Void ratio versus log pressure plot, and (b) settlement versus square root of time of the Eymir Lake sample taken from a depth of 8.2 m.

Table 5.8 Summary of the consolidation test results.

Sampling depth (m)	Compression index (C_c)	Swelling index (C_s)	Over-consolidation Ratio (OCR)	Average permeability (m/sec)
3.0	0.547	0.101	4	4×10^{-11}
6.2	0.175	0.052	2	2×10^{-11}
8.2	0.392	0.101	1.5	5×10^{-11}

5.6 Triaxial Tests

Unconsolidated undrained (UU) and consolidated undrained (CU) triaxial tests were performed on the samples of Eymir Lake clay for the determination of their undrained shear strength. The tests were carried out at Gazi University Construction Edu. Department, Soil Mechanics Laboratory.

(a) Unconsolidated undrained (UU) tests:

For the determination of the undrained shear strength, one specimen is extracted from each undisturbed sample tubes. Although the confining pressure (σ_3) does not have an effect on the undrained shear strength in unconsolidated undrained conditions, σ_3 were chosen as appropriate to the in-situ values. The tests were performed according to the ASTM D 2850 (ASTM, 1999). Saturation ratio of the specimens were determined from the values of water content, void ratio and specific gravity values, and for all samples saturation ratio is 100 %. The rate of loading was selected to

obtain 1 % strain per minute. Table 5.9 lists the undrained shear strength values of the Eymir Lake clay samples determined from UU tests.

Table 5.9 Undrained shear strength values of the Eymir Lake clay samples determined from UU tests.

Sampling depth (m)	Undrained shear strength (kPa)
1.0	28
2.0	73
3.0	63
4.2	80
6.2	131
8.2	148

(b) Consolidated undrained (CU) tests:

Consolidated undrained tests were performed for the estimation of the undrained shear strength and the increase of undrained shear strength with consolidation pressure. During the tests, the procedure recommended by ASTM D 4767 (ASTM, 1995) was followed. From each undisturbed sample tube taken from the field, two CU tests were performed. In order to minimize the effect of sampling disturbance the first test was carried out under an isotropic consolidation pressure that is 50 % higher than the in-situ effective stress. By performing at least two CU tests, apparent failure envelope of the soil can be determined for the estimation of the in-situ undrained shear strength. In order to accelerate the time required for consolidation, the vertical filter paper strips were wrapped around soil samples (Figure 5.12).

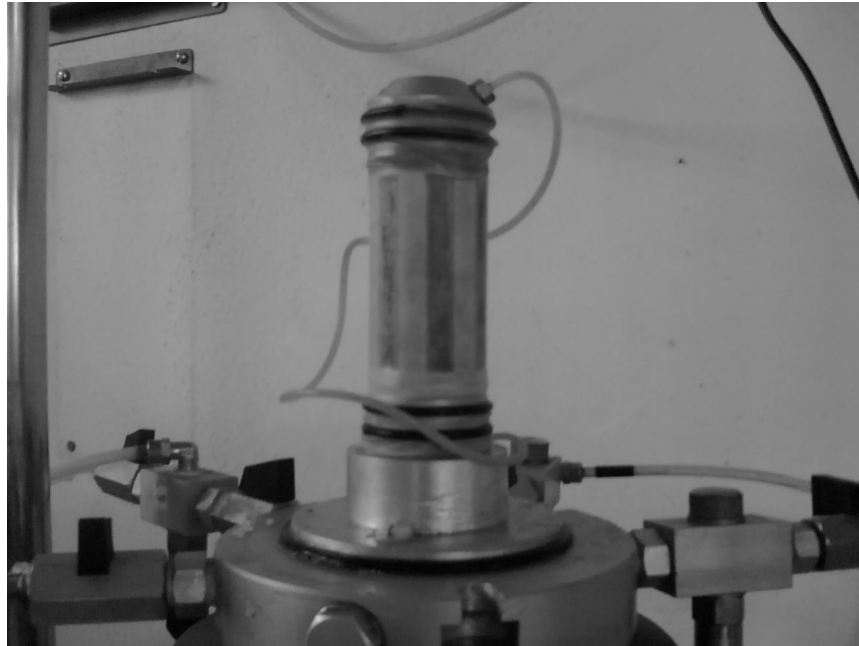


Figure 5.12 The soil sample with vertical filter paper strip wrapped around prior to test.

In order to ascertain fully saturated condition, each sample was saturated against back pressure, the degree of the saturation was controlled with “B” parameter and the consolidation stage was started after the achievement of at least a B value of 0.95 as recommended by ASTM D 4767 (ASTM, 1995). The results of the CU tests are given in Table 5.10.

Table 5.10 Undrained shear strength values of the Eymir Lake clay samples determined from the CU tests.

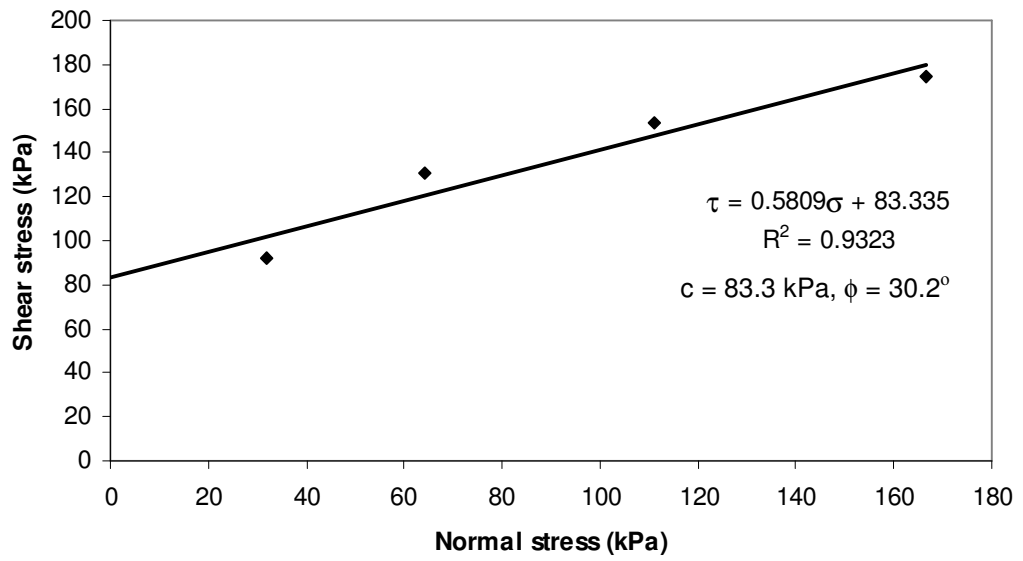
Sampling depth (m)	Undrained shear strength (kPa)
1.0	31
2.0	83
3.0	68
4.2	76
6.2	160
8.2	165

5.7 Direct Shear Box Tests

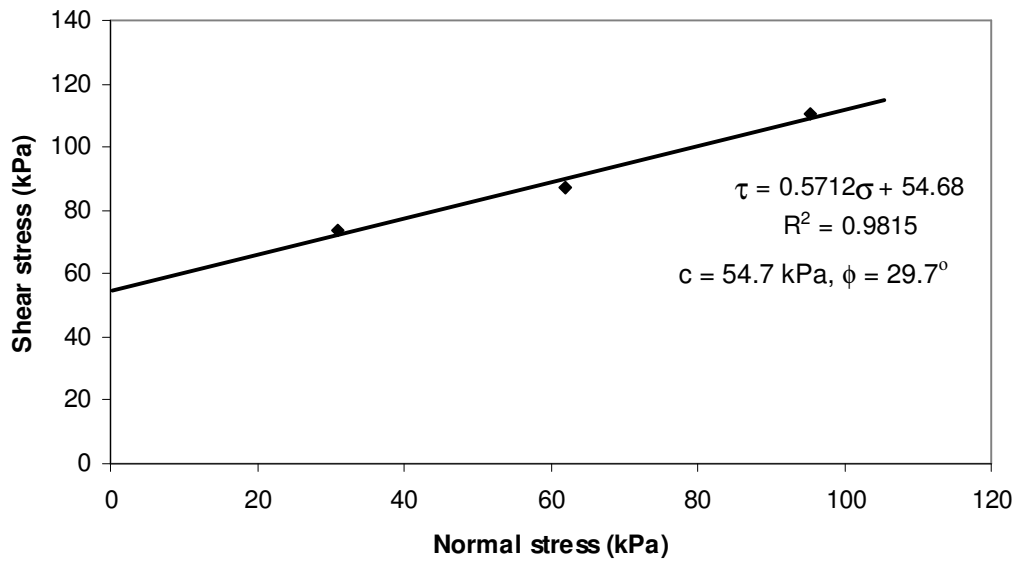
Unconsolidated undrained direct shear box tests were performed on two undisturbed samples taken from the weathered andesites, the results of which will be used for the comparison of the shear strength values deduced from the inverse analysis of the pressuremeter tests. The tests were carried out at Gazi University Construction Edu. Department, Soil Mechanics Laboratory. Consolidated drained direct shear box tests were performed on Eymir Lake clays, for the determination of effective shear strength parameters. Effective friction angle will be utilized in Chapter 6.2, in the comparison of undrained shear strength ratios of various tests using the methodology proposed by Wroth (1984). The tests were performed according to ASTM D 3080 (ASTM, 1998).

(a) Direct shear box tests on the weathered andesites:

In order to determine the undrained shear strength parameters of the weathered andesites, two direct shear box tests were performed on the undisturbed samples taken from a depth of 1 m at Solfasol district and from a depth of 3.2 m at Pursaklar district. The Mohr – Coulomb failure envelopes of these samples are given in Figure 5.13.



(a)



(b)

Figure 5.13 Mohr – Coulomb failure envelopes of the samples taken from (a) a depth of 1 m at Solfasol district, (b) a depth of 3.2 m at Pursaklar district.

(b) Direct shear box tests on Eymir Lake clays:

For the determination of the effective shear strength parameters of the Eymir Lake clay, one consolidated - drained shear box test was performed on the sample taken from a depth of 6.2 m. Figure 5.14 shows the shear stress versus horizontal displacement, and vertical displacement versus horizontal displacement graphs obtained from direct shear box tests performed on the Eymir Lake clay. The test results suggest that the effective shear strength parameters of the clay were $c^l = 6 \text{ kPa}$ and $\phi^l = 21.9^\circ$.

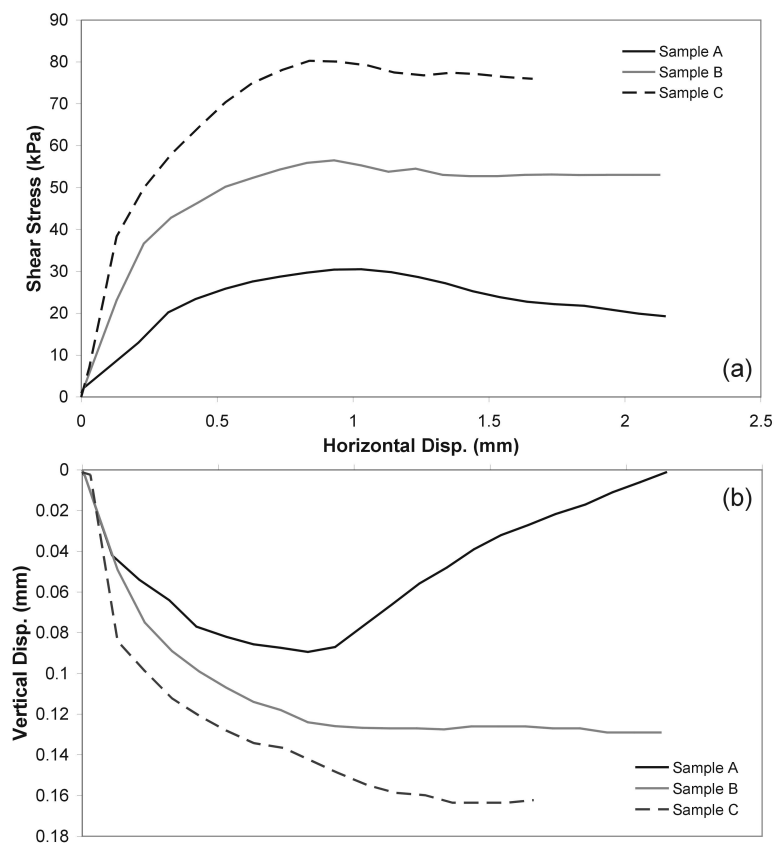


Figure 5.14 (a) The shear stress versus horizontal displacement and (b) vertical displacement versus horizontal displacement graphs obtained from direct shear box tests performed on Eymir Lake clay.

CHAPTER 6

EVALUATION OF THE PRESSUREMETER TEST RESULTS

Since pressuremeter test is a static test, it directly measures stress deformation relation of a particular ground. From the measured stress deformation relation, basic deformability and strength properties of the ground can be determined using the solutions of infinitely long cylindrical cavity in elastic or elastic perfectly plastic medium. In this section, the effect of pressuremeter geometry, testing depth and the discontinuities present in the ground on the measured geomechanical properties are presented.

6.1 Determination of Deformation Modulus

In order to evaluate the initial, time independent movement of foundations, slopes, tunnels etc., a knowledge of the so-called elastic behavior of ground is necessary. The deformability of a purely elastic material under uniaxial loading conditions is described by Young's modulus (E) and Poisson's ratio (ν). Although the soils and rocks are not elastic materials, Young's modulus and Poisson's ratio are used to define the deformation behavior of soils and rocks. However, since the geomaterials are not elastic materials, many types of modulus can be defined from the stress strain curves. Figure 6.1 depicts a typical deviatoric stress versus axial strain graph and the modulus definitions.

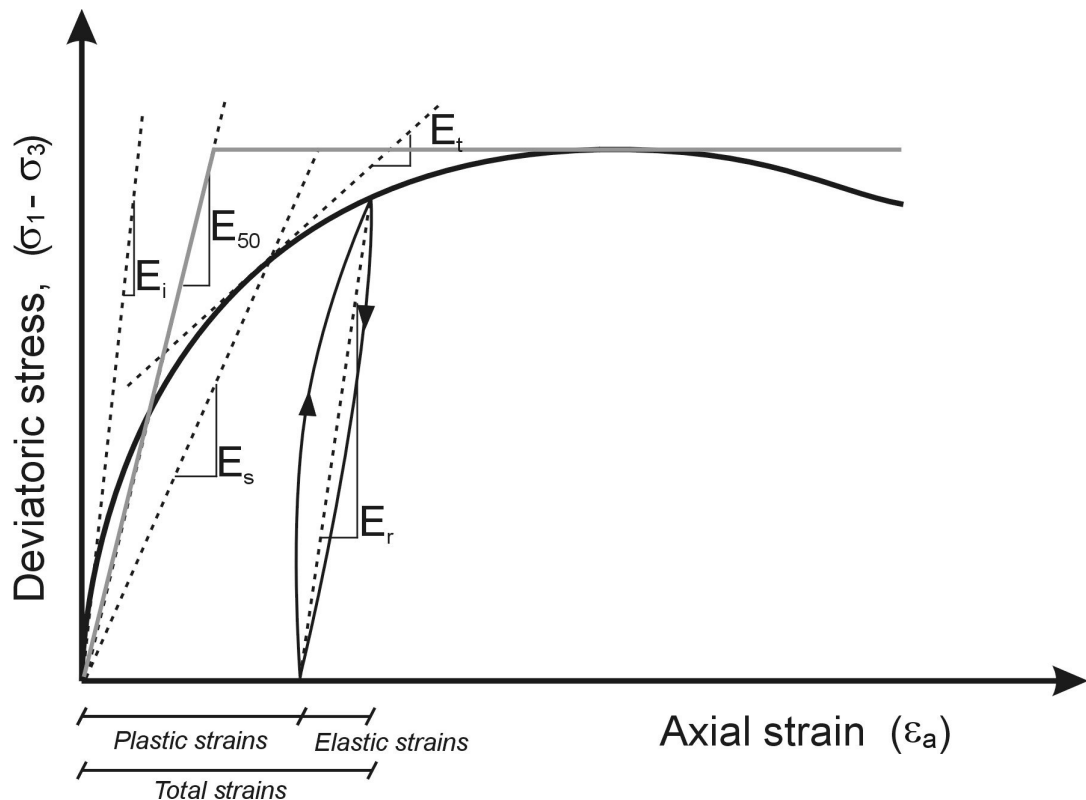


Figure 6.1 A typical deviatoric stress versus axial strain graph and the modulus definitions.

From the stress strain curve, modulus can be defined as initial tangent modulus (E_i), the tangent modulus (E_t) at a specific stress level, secant modulus (E_s), secant at the half of the maximum deviatoric stress (E_{50}) and unloading-reloading modulus (E_r). When the material is unloaded from a point some of the accumulated strains (total strains) will be recovered (elastic strains), and some will remain (plastic strains). Therefore, the unloading-reloading modulus defines the magnitude of elastic strains, also called as modulus of elasticity. The full description of rock – soil deformability should indicate not only the elastic coefficients, but also the permanent deformation associated with any applied stress level. The substitution of the modulus of deformability (or deformation modulus) in

place of modulus of elasticity indicates that the deformability property embraces both recoverable and non-recoverable deformation. In general, whenever the modulus value is directly calculated from the slope of rising portion of a virgin loading curve, the determined property should be reported as a modulus of deformation rather than as a modulus of elasticity (Goodman, 1989). Therefore, the modulus value calculated from the loading portion (pseudo-elastic phase) of the pressuremeter graph corresponds to deformation modulus.

As it was previously explained in Chapter 2, from the slope of the linear part of the pressure expansion curve of the pressuremeter test graph, the shear modulus of the soil is obtained by using the theoretical solution of infinitely long cavity expansion. This shear modulus can be converted to deformation modulus with a suitable Poisson's ratio. Ménard has chosen a Poisson's ratio of 0.33 for the calculation of the deformation modulus, therefore, the calculated modulus is called as Ménard modulus (Baguelin et al., 1978). However, ASTM D4719 (2000) allows the use of a proper Poisson's ratio for the soil or rock tested.

The pressuremeter modulus corresponds to an average modulus for the pressure range " $p_0 - p_f$ " (i.e. where the pseudo-elastic phase is located), while this is acceptable for some calculations (for example, estimating the settlement of small foundations under service loads), this modulus cannot be applied blindly to any problem. In particular, it is clear that in the case of displacements associated with small soil deformations (typically less than 1 %), the pressuremeter modulus cannot be considered to be an indicative of the behavior of the soil.

One of the problems related to borehole deformability tests (i.e. pressuremeter, dilatometer) is that they affect a relatively small volume of rock, and therefore, contain an incomplete sample of the fracture system (Goodman, 1989).

The pressuremeter test only shears the soil or rock. In other words there is theoretically no compression of the soil or rock (Mair and Wood, 1987). However, the stress path followed during the pressuremeter test differs from the laboratory compression tests and the plate load (or foundation loading) tests. Figure 6.2 shows the stress paths followed during the pressuremeter tests, laboratory compression tests and plate loading tests up to the failure.

Shields and Bauer (1975) compared the values of deformation modulus determined from laboratory tests, plate loading tests, and pre-bored pressuremeter in a sensitive clay deposit. They found that the values of deformation modulus determined from the pressuremeter are similar to those values determined from unconsolidated triaxial tests, however, 1/3 to 1/2 smaller than those determined from the plate load tests.

Greenland (1964) compared the values of deformation modulus determined from plate loading tests and from pre-bored pressuremeter tests in a stiff clay deposit, and he found close agreement between both deformation modulus values.

Windle and Wroth (1977a) determined that the initial shear modulus values from the self boring pressuremeter test agree well with the results from the large plate tests in London clay.

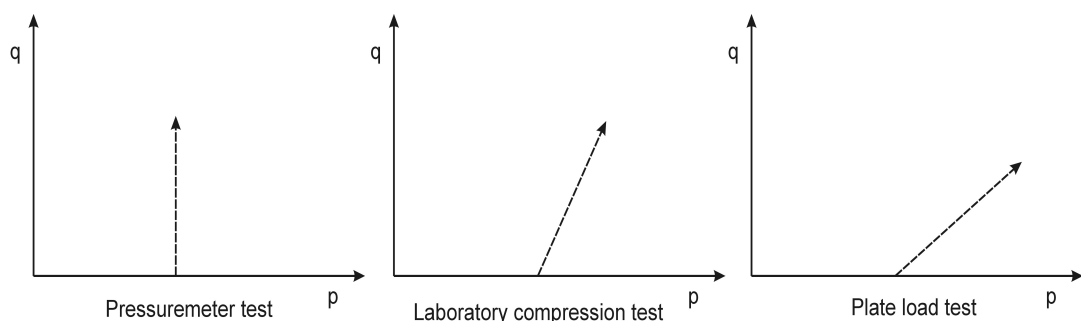


Figure 6.2 Stress paths followed during pressuremeter tests, laboratory compression tests and plate loading tests up to the failure.

Baguelin et al. (1973) performed self boring and Ménard pressuremeter tests in a soft clay for the purpose of comparing the initial modulus value of the self boring probe with the deformation modulus determined from the Ménard probe. They found that the initial modulus determined from the self boring pressuremeter is higher than that determined from the Ménard probe. On the other hand, Amar et al. (1975) reported similar values of deformation modulus on a dense sand. This phenomenon is due to the borehole disturbance.

Robertson and Ferreira (1993) suggested that it is impossible to measure the true maximum shear modulus from the unloading curve, because of the lack of sensitivity of the measuring systems over the small strain range.

Powell (1990) showed that the unloading-reloading modulus values obtained from CSBP, PBP and PIP tests were similar.

Clarke (1993) indicated that the undrained modulus of elasticity determined from back calculation of the observations of settlements of structures are close to the undrained modulus determined from unloading reloading shear modulus. The triaxial stiffness is lower than the undrained modulus of elasticity determined from back-calculation of the observations of settlements of structures.

There are very few alternative in-situ tests feasible in weak rocks (particularly at considerable depths), and pressuremeter testing is a valuable means of obtaining data from which suitable design values of modulus can be assessed (Mair and Wood, 1987). Consideration should be given to the strain level in the pressuremeter test from which a modulus is derived (Mair and Wood, 1987).

Many foundation design problems in weak rocks are dominated by deformation consideration rather than the ultimate capacity, and therefore, the determination of a suitable elastic modulus for design is usually of most

importance. Almost all of the experience of obtaining the deformation modulus has been carried out with the Ménard pressuremeter tests, and this is generally the most suitable type of pressuremeter test for weak rocks (Mair and Wood, 1987).

Wilson and Corke (1990) compared the value of initial loading shear modulus from high pressure dilatometer with the initial loading shear modulus from the plate load test with 865 mm diameter in a sandstone rock mass. They found very similar values of modulus from both tests.

Tan and Kaya (1988) compared the values of deformation modulus from dilatometer and plate load tests. Their results indicate that the values of deformation modulus determined from dilatometer is similar to those determined from plate load tests although there are some different results too which are probably due to the volume of the rock tested by dilatometer is not representative of the rock mass.

Mahmoud et al. (1990) performed 28 pre-bored pressuremeter tests, seven 1000 mm diameter plate load tests, six 300 – 500 mm plate load tests and laboratory compression tests on breccias having carbonate, gypsum, limestone or dolomite matrix. Based on their results, the laboratory compression tests yielded considerably higher values of secant deformation modulus, and the results from eight of the plate load tests were very close to the pressuremeter values. However, the results from 5 of the plate load tests were close to those from the unconfined compression tests.

The pressuremeter test provides a direct measurement of the horizontal modulus of soils. It is commonly assumed that the deformation modulus directly determined from the pressuremeter equals to Young's modulus (Kulhawy and Mayne, 1990).

If the disturbance effects during installation can be ignored, the initial modulus is more likely to be representative for most foundation loading problems in jointed or fissured weak rocks (Mair and Wood, 1987).

6.1.1 Numerical simulation of the pressuremeter tests for determination of deformation modulus

The pressuremeter test was simulated by numerical methods for the purpose of (i) validation of the numerical codes (Flac, Plaxis, Udec), (ii) determination of the effect of pressuremeter geometry, (iii) testing depth on the determined values of deformation modulus, and (iv) determination of the effect of discontinuities on the values of deformation modulus.

6.1.1.1 One-dimensional simulation of the pressuremeter test

Since the equation for the radial expansion of a cylindrical cavity in an infinite elastic medium (Lame, 1852; Ménard, 1961) is used for the determination of the deformation modulus from the pressuremeter curve, the numerical codes used in this study are validated using one-dimensional (i.e. using the same geometry with the theoretical solution) pressuremeter test simulations in linearly elastic materials.

(a) Flac 2D (Fast lagrangian analysis of continua):

Flac is a two-dimensional explicit (time marching method) finite difference code for engineering mechanics computations, which is based on a “Lagrangian” calculation scheme that is well suited for modeling large distortion and material collapse (Flac, 2002). Flac has been tested and verified in a variety of problem settings (Flac, 2002). Dynamic equations of motion are used to find a static solution of the problem. By this way, the stability of the numerical scheme is guaranteed even when the physical system is unstable. The equations of motion are first invoked to derive

velocities and displacements from stresses and forces. Then strain rates are derived from the velocities and new stresses (with constitutive relations) from the strain rates (Flac, 2002).

(b) Plaxis:

PLAXIS v. 7.2 (1998) is a finite element program for plane strain and axisymmetric modelling of soil and rock behaviour. Plaxis has a fully automatic mesh generation, allowing for a virtually infinite number of 6-node and 15-node elements, based on graphical input of soil layers. The models can contain both drained and undrained layers. For undrained layers, excess pore pressures are calculated and elasto-plastic consolidation analysis may be carried out. Large deformations may be analyzed by means of an updated mesh (Lagrangian) calculation. Using this option, the finite element mesh is continuously updated during the calculation. For some situations, a conventional small strain analysis may show a significant change of geometry. In these situations, it is advisable to perform a more accurate Updated Lagrangian calculation (Plaxis, 1998).

(c) UDEC (Universal discrete element code):

UDEC (UDEC, 2000) is a discrete element code which is generally used to model the behavior of discontinuous structures such as rock masses, masonry structures under static and dynamic loading conditions. In this method, discontinuous structure is modeled with discrete blocks which are interacting with each other via joint (discontinuity) properties. UDEC can also model deformability of each block by dividing the block with a finite difference mesh. UDEC uses Lagrangian approach which is appropriate for large deformation calculations and has the option of performing plane strain

and plane stress simulations (UDEC, 2000). The axisymmetrical calculations cannot be performed with UDEC.

Figure 6.3 shows the simplified mesh (grid) for the purpose of presentation and the associated boundary conditions of the one-dimensional model. Actual grid is composed of 40 rectangular finite difference elements. Axisymmetrical and large strain option of the Flac 2D is used. Upper and lower boundary conditions are selected as to simulate expansion of infinitely long cavity, in other words the displacements are only horizontal. Pressure at the right side of the model is incrementally increased and the corresponding displacements of the cavity are calculated.

The values of shear modulus are calculated from the slope of the pressure versus cavity strain graph using the theory of expansion of infinitely long cavities in elastic medium.

The pressure versus cavity strain graphs of one-dimensional pressuremeter simulation in a linearly elastic material for a shear modulus value of 3846.2 kPa is shown in Figure 6.4.

As it is clear from Figure 6.4, the in-situ stress does not have any effect on the determined shear modulus from the pressure versus cavity strain graphs. This is an expected behavior according to the theoretical solution. This one-dimensional simulation was repeated for a range of shear modulus values and the calculated shear modulus values, by using the theory of expansion of infinitely long cavities in elastic medium, were compared with the actual input values. It was determined that the calculated shear modulus values only 0.4 % higher at maximum than the actual input value (i.e. $G_{\text{calc}}/G_{\text{true}} = 1.004$). As it is expected, the calculated values of shear modulus are very close to the actual values. This very small difference is probably due to the grid sizes and numbers. Figure 6.5 shows the one-dimensional pressuremeter simulations using a shear modulus of 3846.2 kPa and two different bulk modulus of 8333.3 and 15000 kPa.

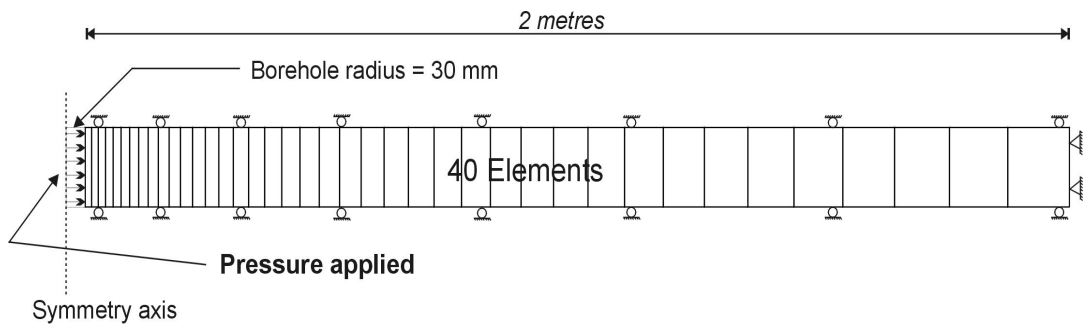


Figure 6.3 Simplified mesh and boundary conditions of the one-dimensional model (y-dimension of the grid is exaggerated for presentation purposes).

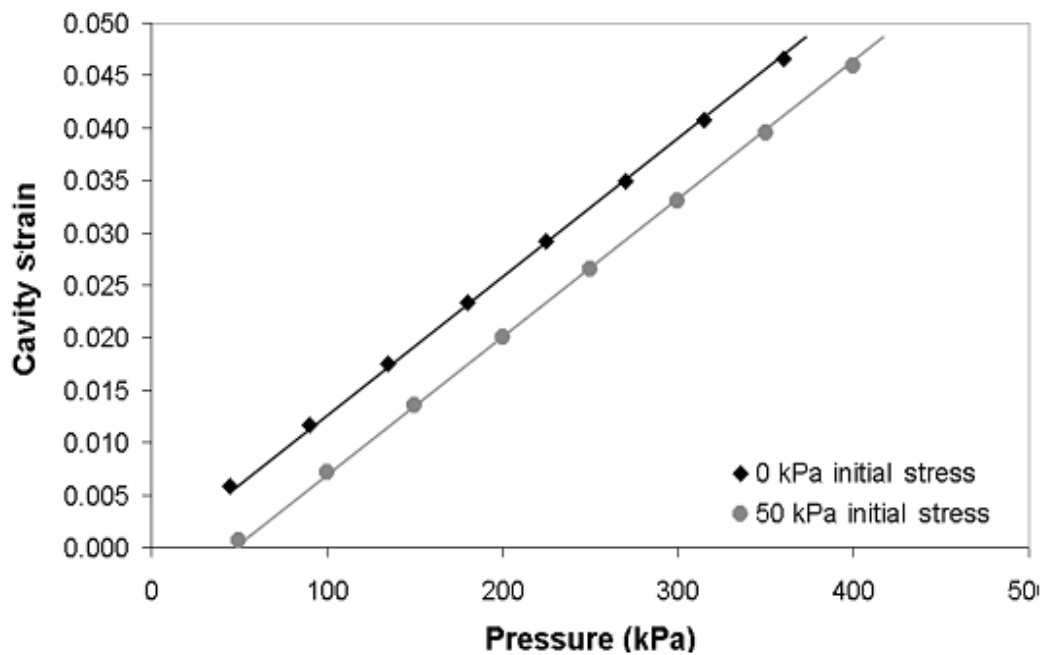


Figure 6.4 Pressure versus cavity strain graphs of one-dimensional pressuremeter simulation in a linearly elastic material for a shear modulus of 3846.2 kPa.

Figure 6.5 suggests that the values of bulk modulus do not have any effect on the calculated pressure versus cavity strain plots. In other words, only the shear modulus controls the slope of the pressure versus cavity strain plots. This result is also expected from the solution of the theory of expansion of infinitely long cavities in elastic medium. Similar one-dimensional simulations were also performed by using Plaxis, and same results with the Flac were obtained.

Since UDEC does not have an axisymmetric option, one-dimensional pressuremeter simulation was performed using plain strain condition with the aid of finite difference grid given in Figure 6.6. Only quarter of the model was used for the simulation due to the symmetry. The model presented in Figure 6.6 is numerically same to that shown in Figure 6.3. The values of shear modulus calculated from the UDEC model in Figure 6.6 are very close to the input values (error is about 2 %). The slightly higher order of error in the calculated shear modulus is probably due to the fact that UDEC approximates the circular section by piecewise linear lines. In other words, the cross section of the pressuremeter is circular; however, UDEC can only approximate this circular cross-section.

Because UDEC is much more suitable for the analyses of discontinuous systems, the model presented in Figure 6.6 is also used for the estimation of the frequency of discontinuities on the determined values of shear modulus. These one-dimensional simulations show the accuracy and the validity of the numerical codes used for the study.

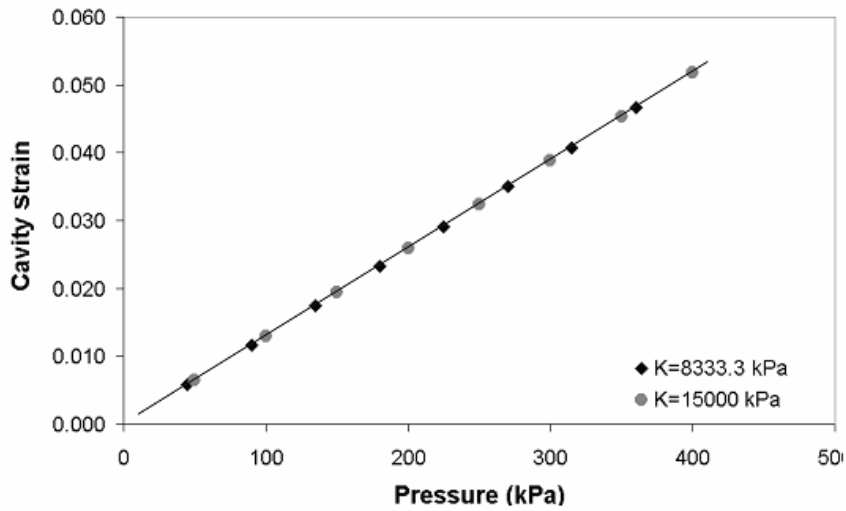


Figure 6.5 One-dimensional pressuremeter simulations using a shear modulus of 3846.2 kPa and two different bulk modulus values, K (8333.3 and 15000 kPa).

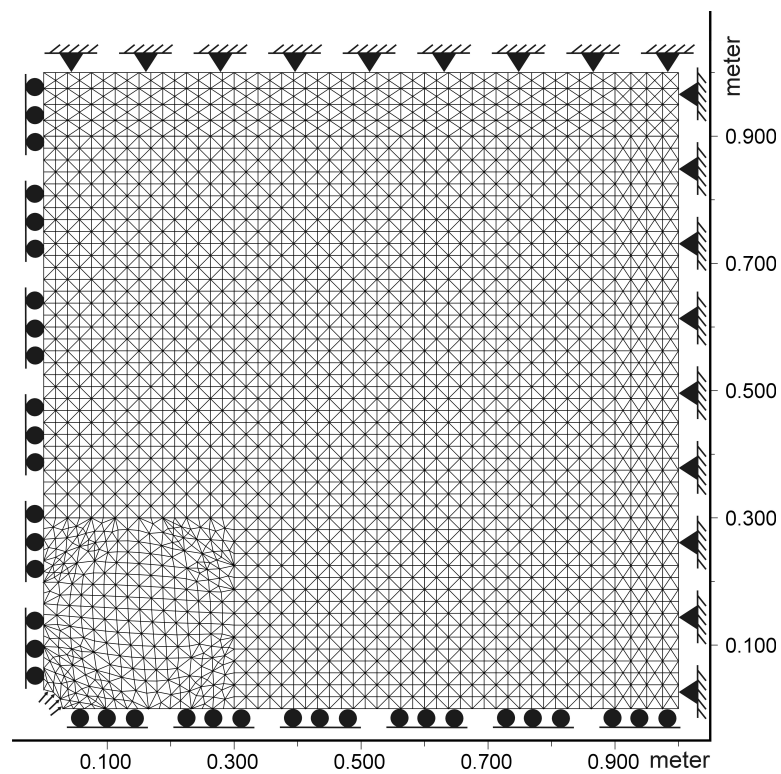


Figure 6.6 The UDEC model for the one-dimensional pressuremeter simulations.

6.1.1.2 Two-dimensional simulation of the pressuremeter test

Two-dimensional numerical simulations of the pressuremeter test in a linearly elastic medium were performed for the determination of testing depth and L/D ratio of the pressuremeter probe on the measured shear or deformation modulus.

For the numerical simulation, finite difference grid was constructed, boundary conditions were applied, in-situ stresses were generated and borehole excavation process was simulated. As a final stage, pressuremeter loading was applied, and corresponding radial displacements and stresses were determined in a stepwise manner. Figure 6.7 shows the mesh (grid) for a pressuremeter simulation at a depth of 3 m. Figure 6.8 shows the boundary conditions at the membrane soil contact.

The grid points at the end of the outer membrane are fixed to any movement to simulate the presence of the steel rings. BX type probe, which is the most widely used one, has a length of 42 cm. The suggested borehole diameters are between 60 and 66 mm, therefore, L/D ratio of the probe ranges between 6.4 and 7 just before it touches the soil. Most of the pressuremeter probes including the self boring pressuremeter has an L/D ratio around 6. In order to understand the effect of pressuremeter geometry on the calculated shear modulus, the pressuremeter simulations were performed with varying L/D ratios such as 5.3, 6.4, 8, 11; simulation depths; and shear modulus. Cavity strain value is calculated from the radial displacement at the middle of the pressuremeter. Based on the analyses results, the values of calculated shear modulus are very close to the real value used in the simulation. Pressuremeter simulations with a constant value of L/D ratio, performed for depths of 1, 3, 5, 7, 10 and 15 m yielded same values of shear modulus. The L/D ratio versus $G_{\text{calc}}/G_{\text{true}}$ relationship, determined from two-dimensional linearly elastic pressuremeter simulations are given in Table 6.1.

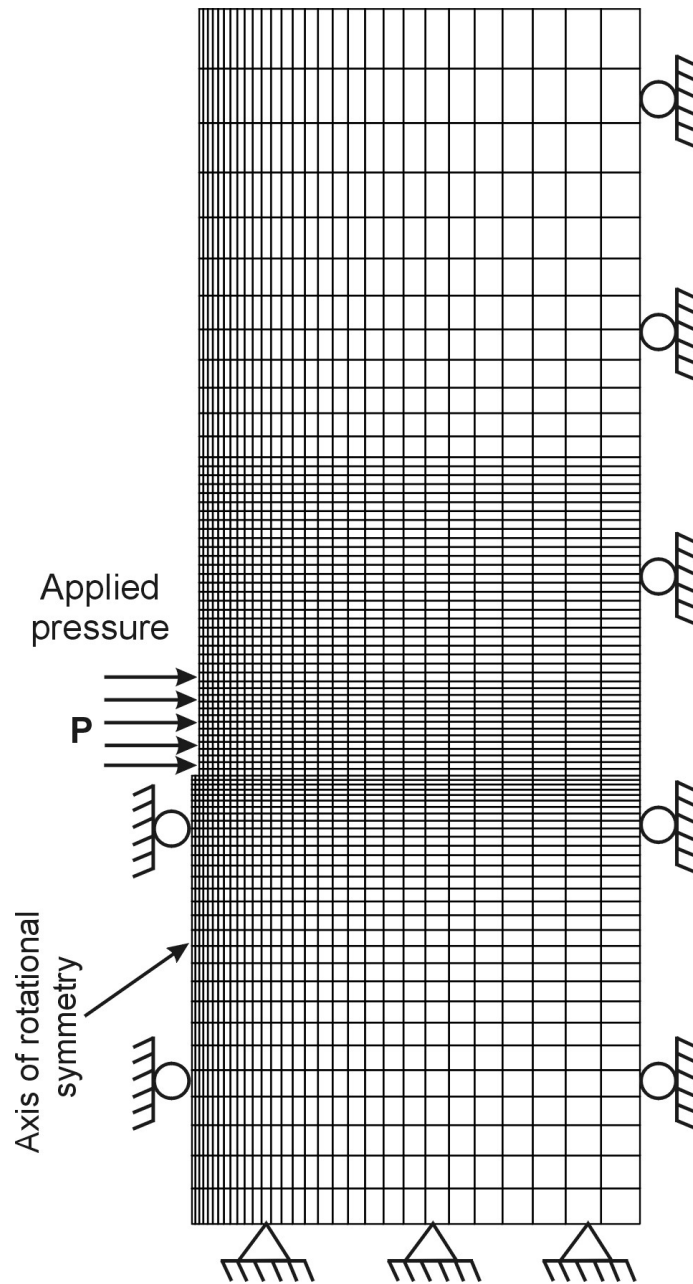


Figure 6.7 Mesh (grid) for a pressuremeter simulation at a depth of 3 m.

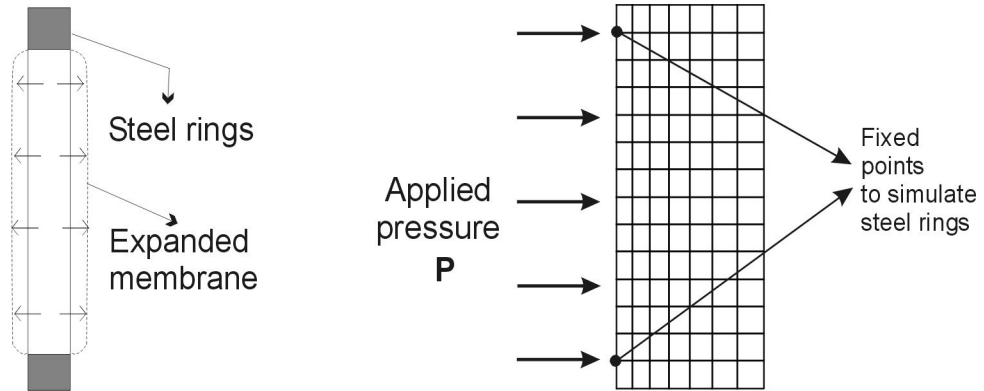


Figure 6.8 The boundary conditions at the membrane soil contact.

Table 6.1 The L/D ratio versus $G_{\text{calc}}/G_{\text{true}}$ relationship, determined from two-dimensional linearly elastic pressuremeter simulations.

L/D	$G_{\text{calc}}/G_{\text{true}}$
11	1.0085
8	1.0115
6.4	1.0155
5.3	1.0225

One-dimensional pressuremeter simulations yielded a value of $G_{\text{calc}}/G_{\text{true}}$ equals to 1.004. However, as the L/D ratio decreases the calculated value of shear modulus slightly increases due to the fact that as the L/D decreases the geometry of the pressuremeter deviates from the idealized infinitely long cavity. But as the difference is minor, it can be concluded that the geometry of the pressuremeter probe has minor effects on the calculated shear modulus. This finding is compatible with those found by Housby and Carter (1993). These investigators also stated that the pressuremeter geometry has no effect on the calculated shear modulus. As a result, it can be suggested that the L/D ratio and testing depth do not have an effect on the calculated shear modulus.

Borehole extension tests load the soil or rock in horizontal direction. Therefore, the deformability and strength parameters obtained from borehole extension test will correspond to horizontal direction. However, since the probes have limited length, there will be some vertical deformations as well as the horizontal deformations particularly at the ends of the probe. In order to understand the effect of anisotropy on the measured value of deformation modulus, two-dimensional finite difference analyses were performed using the transversely isotropic elastic model embodied in Flac. In these analyses, the vertical shear modulus is selected as two times higher than the horizontal shear modulus. The analyses revealed that the pressuremeter mainly senses the horizontal shear modulus, however, there is slight overestimation (about 4 %) of the horizontal shear modulus due to vertical component.

6.1.1.3 Effect of disturbance on shear modulus

Various researchers such as Combarieu and Canépa (2001) indicated that the disturbance during drilling operations causes the shear modulus (or deformation modulus) deduced from the pressuremeter test to become lower than the actual in-situ. Traditionally, the hand augering is known to be the most reliable boring technique for the purpose of the pressuremeter testing (i.e. least disturbing technique). However, the use of hand augering is impossible for most of the soils. Combarieu and Canépa (2001) studied the effects of boring techniques (hand auger, continuous flight auger in dry conditions, rotary percussion drilling or desaggregating tool) on deformation modulus considering various soils. Their results indicate that the more destructive methods, such as rotary percussion drilling, desaggregating tool causes calculated modulus to decrease even up to 1/5 of the modulus determined by testing hand augered borehole. The values of modulus obtained from boreholes opened by hand auger and continuous flight auger under dry conditions are very similar to each others.

In order to investigate the effect of the thickness of the disturbed zone on the calculated shear modulus, one-dimensional and linearly elastic simulations of the pressuremeter test were performed by varying the thickness of the disturbed zone and using the model presented in Figure 6.3. One-dimensional model is appropriate for this analysis as mentioned in Chapter 6.1.1.2. Because shear modulus calculated from the pressuremeter is insensitive to the pressuremeter geometry and testing depth. For the analyses, the value of the shear modulus of the disturbed soil is arbitrarily chosen as the half of the undisturbed soil's shear modulus. Although, in reality, the disturbed zone should not be represented by a single constant value of shear modulus, its average value is assumed to be constant for the analyses. Figure 6.9 indicates the relationship of the ratio of the thickness of the disturbed zone (T_d) to the probe diameter (D_p) with the ratio of the calculated shear modulus to the undisturbed shear modulus.

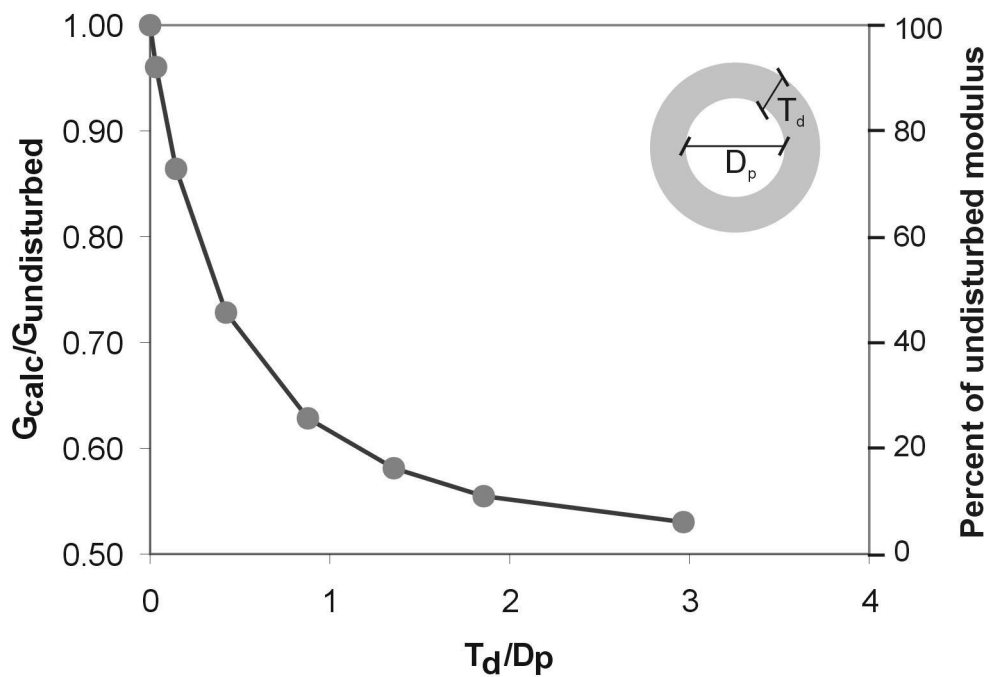


Figure 6.9 The relationship of the ratio of the thickness of the disturbed zone (T_d) to the probe diameter (D_p) with the ratio of the calculated shear modulus to the undisturbed shear modulus.

It is evident from Figure 6.9 that the thickness of the disturbed zone has a very important effect on the measured modulus. For example, if the thickness of the disturbed zone equals to the diameter of the probe, then the pressuremeter can only sense 23 % of the undisturbed zone's shear modulus and rest of the shear modulus includes 77 % of the shear modulus of the disturbed zone.

With all in-situ tests there will be some disturbances of the rock, particularly where blasting must be used to prepare the site, and the test must be designed to evaluate the extent of this disturbance. Furthermore, excavation of the foundation may also involve some disturbance to rock and it is important to make an assessment of the degree of disturbance at the test site compared to that in the actual foundation (Wyllie, 1992).

It should also be noted that the test carried out in galleries, such as plate load test, also suffers from disturbance during the creation of the cavity. The thickness and the level of the disturbance depends on the method of blasting (Palmström and Singh, 2001).

6.1.1.4 Determination of the volume of the material tested by a pressuremeter test

In the application of the dilatometers, pressuremeters and plate load tests in rock masses, it is often regarded as the deformation modulus obtained from such tests represents that of the rock mass. However, it is found that the rock mass volume investigated during borehole extension tests (pressuremeter, dilatometer etc.) frequently may not be regarded as representative for the purposes of the homogeneous rock mass model (Wittke, 1990). Where the discontinuity spacing is small compared to length of the borehole extension test, and the discontinuities are formed in a homogeneous manner, the modulus of deformation determined from the pressuremeter is representative of the rock mass (Wittke, 1990). Dixon (1970) stated that the higher values of deformation modulus determined by pressuremeter are similar to those determined from the laboratory uniaxial compression tests. However, lower pressuremeter test results were considered more indicative of the average in-situ properties in weak sandstones and siltstones.

Mair and Wood (1987) indicated that when the length of the pressuremeter is small compared to the spacing of structural discontinuities in the rock mass, the modulus measured may not be representative of the rock mass.

In order to determine the average volume of the material tested during a typical pressuremeter test and to compare this volume with a typical plate load test (with a 30 cm diameter), two-dimensional axisymmetric numerical

simulations were performed for pressuremeter and plate load tests using a homogenous linearly elastic material by Flac 2D. Although the presence of discontinuities will affect the distribution of stresses by considering homogenous linearly elastic rock mass assumption, it is possible to compare pressuremeter test with plate load test. The stress distributions around the pressuremeter is depicted in Figure 6.10. 10 % and 5 % percent of the stress contours are shown in this figure. Figure 6.11 shows the stress distributions around the plate load test with 10 % and 5 % percent of the stress contours.

Since the 10 % of the applied stress is assumed to be important, 10 % stress contours were selected and digitized, and the integral of the contours are calculated for the determination of the approximate volume of the 10 % stress contours. Volume of the rock mass tested by 30 cm diameter plate is 323600 cm^3 , and the volume of rock mass tested by a standard pressuremeter is 18200 cm^3 . In order to compare these, the volumes, are converted to an equivalent cylindrical samples having $\frac{1}{2}$ diameter to length ratio. Dimensions of the equivalent sample to the plate load test are $59.1 * 118.1 \text{ cm}$ whereas dimensions of the equivalent sample to the pressuremeter test are $22.6 * 45.3 \text{ cm}$. The volumes of the material tested by plate load and pressuremeter tests are compared in Figure 6.12.

As it is clear from the above mentioned analyses, the volume of the rock mass tested by a pressuremeter is very small compared to the volume of the rock mass tested by a 30 cm plate. Therefore, care must be taken during the determination of the modulus of the rock mass. In other words, the volumes tested should include adequate number of discontinuities to represent the rock mass under consideration.

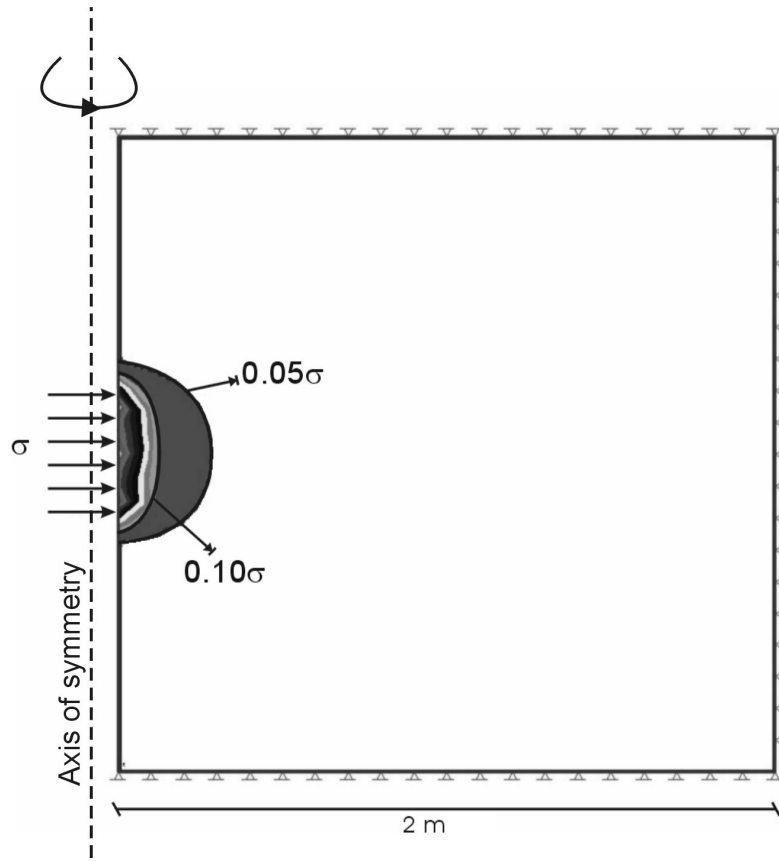


Figure 6.10 Stress distributions around the pressuremeter.

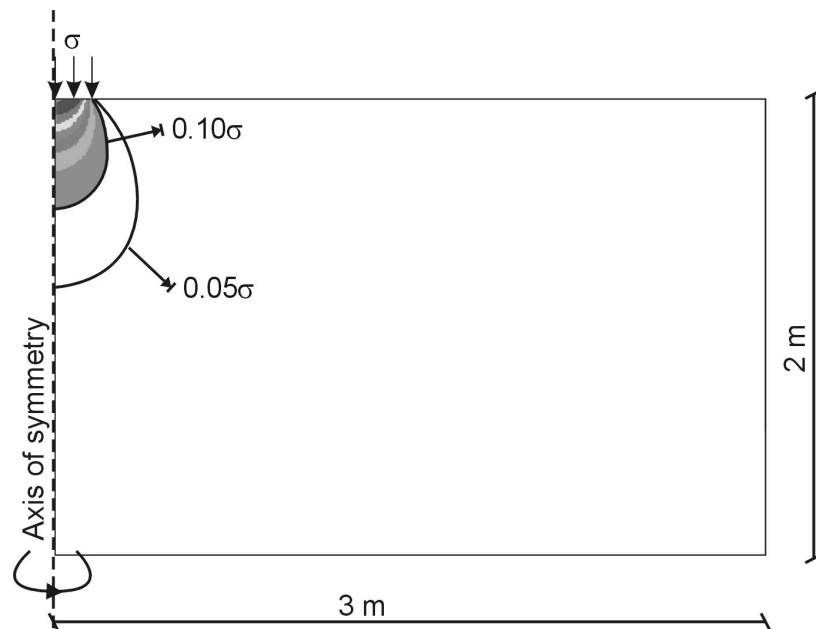


Figure 6.11 Stress distributions around the plate during plate load test.

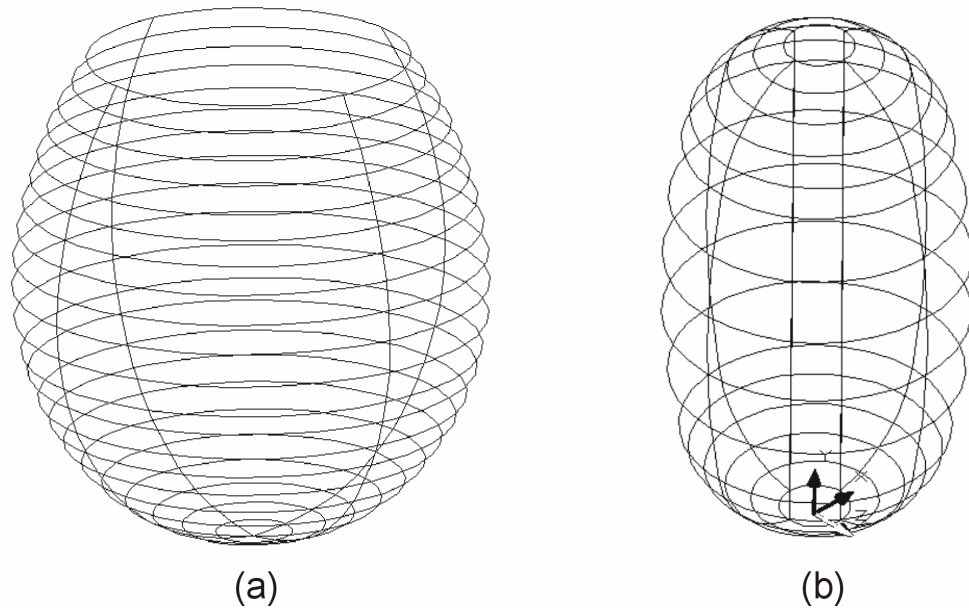


Figure 6.12 Comparison of volumes of the material tested by (a) plate load and (b) pressuremeter tests.

6.1.1.5 Discrete element modeling of pressuremeter test

As discussed in Chapter 2, the equivalent continuum models for a rock mass containing three orthogonal discontinuity sets were developed by several researches such as Goodman and Duncan (1971) and Kulhawy (1978) for the estimation of the deformation modulus of rock mass normal to loading direction. However, the applicability of such models to the borehole extension tests is limited because of the difference in loading conditions.

In this part of the study, two-dimensional distinct element code UDEC was utilized for the assessment of the effect of discontinuity properties on the rock mass deformation modulus determined from the borehole extension tests. Figure 6.13 shows the discontinuity model used in UDEC. In this model, two discontinuity sets orthogonal to each other were used with stiffness values 1/10 of that of the intact rock since discontinuities are much

weaker than the intact rock. The deformation modulus of the rock mass was calculated as 0.53 of the intact rock. Since this model is a plane strain model, the discontinuities run vertically through in plane direction, therefore, they never intersect the borehole. This is clearly not representative of the field conditions. However, the model presented in Figure 6.13 is useful to show how the discontinuities effect the deformation modulus of the rock mass.

The model in Figure 6.13 and equivalent continuum models for a rock mass containing two orthogonal discontinuity sets are gross simplifications of the real situation. Discontinuities also may yield locally in shear in contrast the above models are elastic. For these reasons, an elasto-plastic three-dimensional discrete element simulation of the borehole extension tests are needed to clarify the effects of discontinuity strengths, stiffness, orientation and spacing on the rock mass deformation modulus deduced from the borehole extension tests.

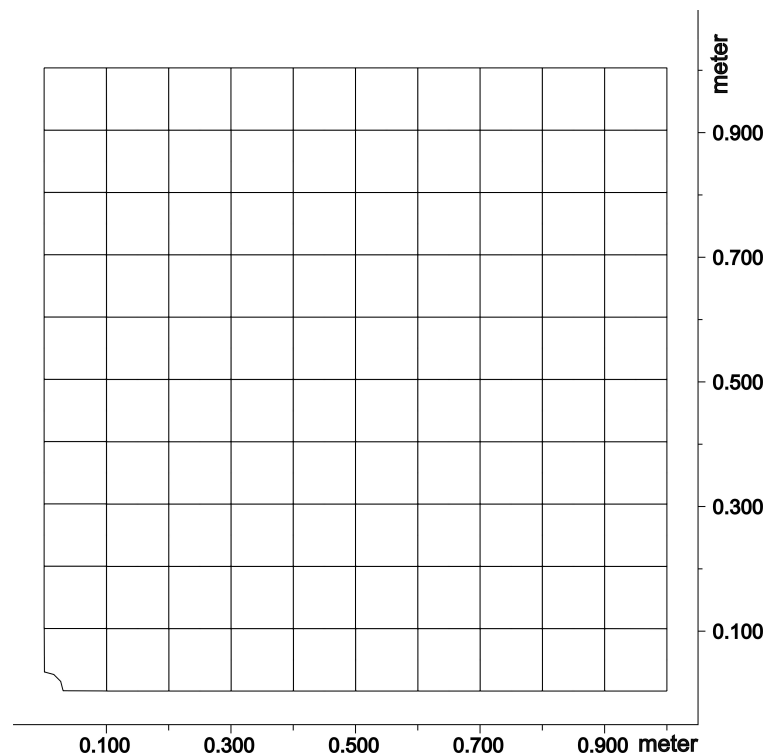


Figure 6.13 The discontinuity model used in UDEC.

6.1.2 Determination of deformation modulus from pressuremeter tests

In this study, pre-bored pressuremeter tests were performed in various geomaterials whose properties are discussed in Chapters 3 through 5. From all of the pressuremeter tests, the values of deformation modulus, and unloading – reloading modulus were obtained. When the ground conditions are appropriate, the values of deformation modulus of the intact rock or soil were also determined from the laboratory compression tests. This section presents a comparison of the deformation modulus obtained from the pressuremeter tests with laboratory tests. The effect of discontinuities on the deformation modulus is also discussed.

6.1.2.1 Eymir Lake clays

The pressuremeter tests, cone penetration tests and field vane tests were performed in the Eymir Lake clays. In addition to the field tests, laboratory unconsolidated – undrained (UU), consolidated – undrained (CU) triaxial tests together with oedometer consolidation tests and one consolidated drained direct shear test were performed in the Eymir Lake clay. The values of the secant modulus at 50 % yield stress, tangent modulus values obtained at 50 % of yield stress and initial tangent modulus obtained from UU tests were compared with the values of deformation modulus obtained from the pressuremeter tests. The results of the CU tests were not used in this comparison, because the samples were consolidated at higher stresses than that present in-situ. From the pressuremeter tests both the values of maximum shear modulus (calculated from the minimum slope of the pseudo – elastic phase) and average shear modulus (calculated from the average slope of the pseudo – elastic phase) were determined. The values of shear modulus were converted to the deformation modulus using a

Poisson's ratio of 0.5 which is appropriate for fully saturated clays under undrained loading conditions (Craig, 1992). The variation of the deformation modulus obtained from the pressuremeter tests and from the UU triaxial tests is shown in Figure 6.14.

Figure 6.14 indicates that the values of deformation modulus obtained from the pressuremeter tests and UU triaxial tests (secant modulus values at 50 % yield stress) are similar to each other except for those at a depth of 3 m. It can be concluded from the slope of the pseudo-elastic phase that pre-bored pressuremeter test yields average deformation modulus as long as the disturbance during drilling operations is kept minimum. Also it is important to note that the values of the initial tangent modulus determined from UU tests are greater than the values of maximum deformation modulus (calculated from the minimum slope of the pseudo – elastic phase). This is probably due to the fact that initial stress – deformation part of the pressuremeter curve corresponds to the contact of probe with the borehole, and the initial tangent modulus could not be obtained from Ménard pressuremeter due to this phenomenon.

At the end of the tests, a small unload-reload loop was performed and the values of unloading – reloading modulus were obtained. The Ménard type pressuremeters (with indirect measurement equipments) are not as suitable as single celled pressuremeters with direct deformation measurement equipments. Because an extreme care should be given for the adjustment of guard cell pressures, their pressure have to be slightly lower than the pressure in measurement cells in order to obtain a true volumetric measurement (ASTM, 2000). These unloading – reloading modulus values are 2.7 to 3.6 times greater than the corresponding average values of deformation modulus.

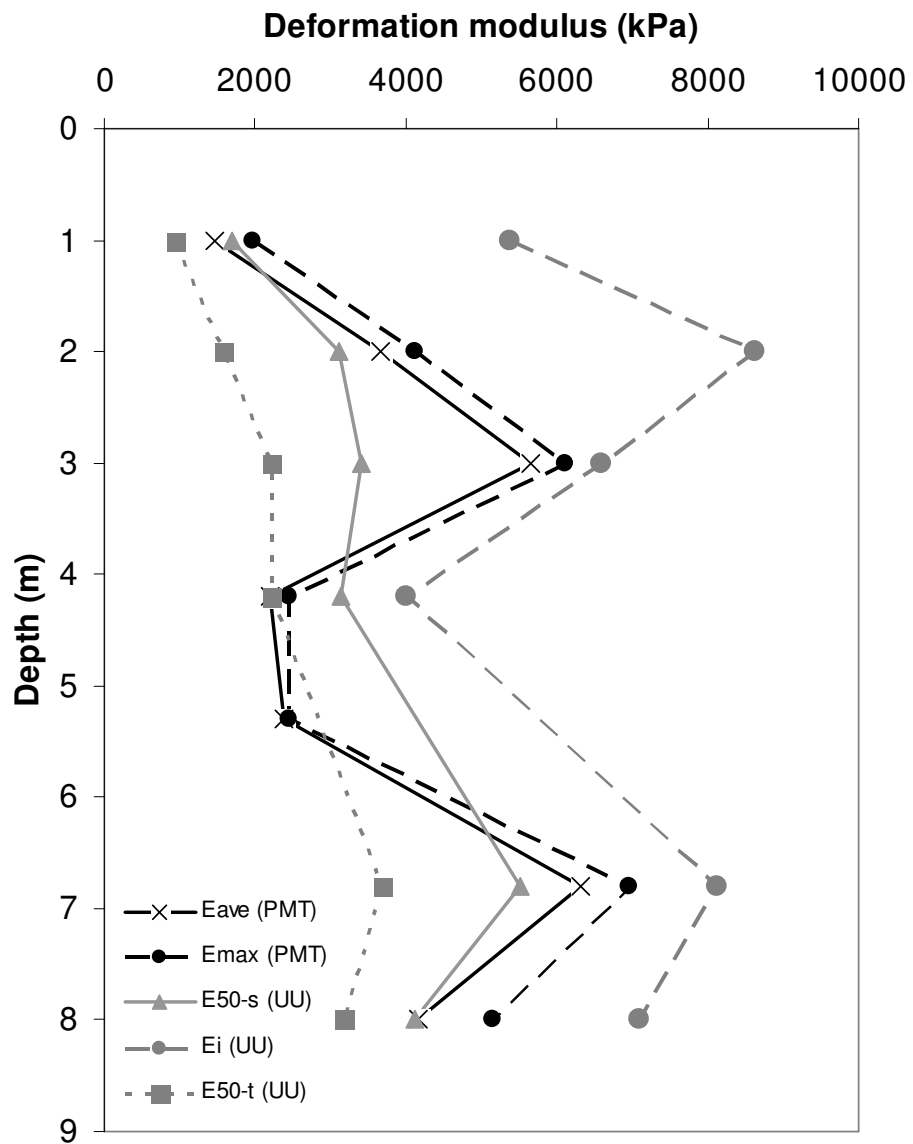


Figure 6.14 The variation of the deformation modulus with depth obtained from pressuremeter tests and from UU triaxial tests.

6.1.2.2 Weathered andesites

Pressuremeter tests were performed in the weathered andesites cropping out in Solfasol, Ovacık and Pursaklar districts together with the uniaxial compression tests on core samples. As explained in Chapter 5, the uniaxial compression tests could not be performed on the samples taken from Solfasol district because of core length inadequacy. However, in the Ovacık and Pursaklar districts the total core recovery is 100 % and the associated RQD values are very high. The results of the unconfined compression tests were utilized for the determination of the secant modulus at 50 % yield stress, tangent modulus values obtained at 50 % of yield stress and initial tangent modulus values. These values are very close to each other due to the fact that the initial part of the axial stress versus axial strain graph is almost linear (Figures 5.5 and 5.6). For this reason, only the secant modulus values at 50 % yield stress are compared to the deformation modulus values obtained from the pressuremeter tests (Figure 6.15). Figure 6.15 suggests that although the deformation modulus determined from the pressuremeter is slightly lower than those from uniaxial compression tests, the values are close to each other. This may be due to the fact that the pressuremeter tests were performed in a rock mass condition which is close to intact rock.

At first, this close relationship may seem to be unrealistic, because the confinement (i.e. σ_3) is zero in the case of an unconfined compression test. However, in the case of a pressuremeter test there is an in-situ stress state. Granular soils are well known to have stress dependency. In other words, as the confinement is increased the deformation modulus also increases. If a similar behavior is observed in the weathered andesites, then the modulus values obtained from the pressuremeter tests are expected to be higher than that obtained from the uniaxial compression tests.

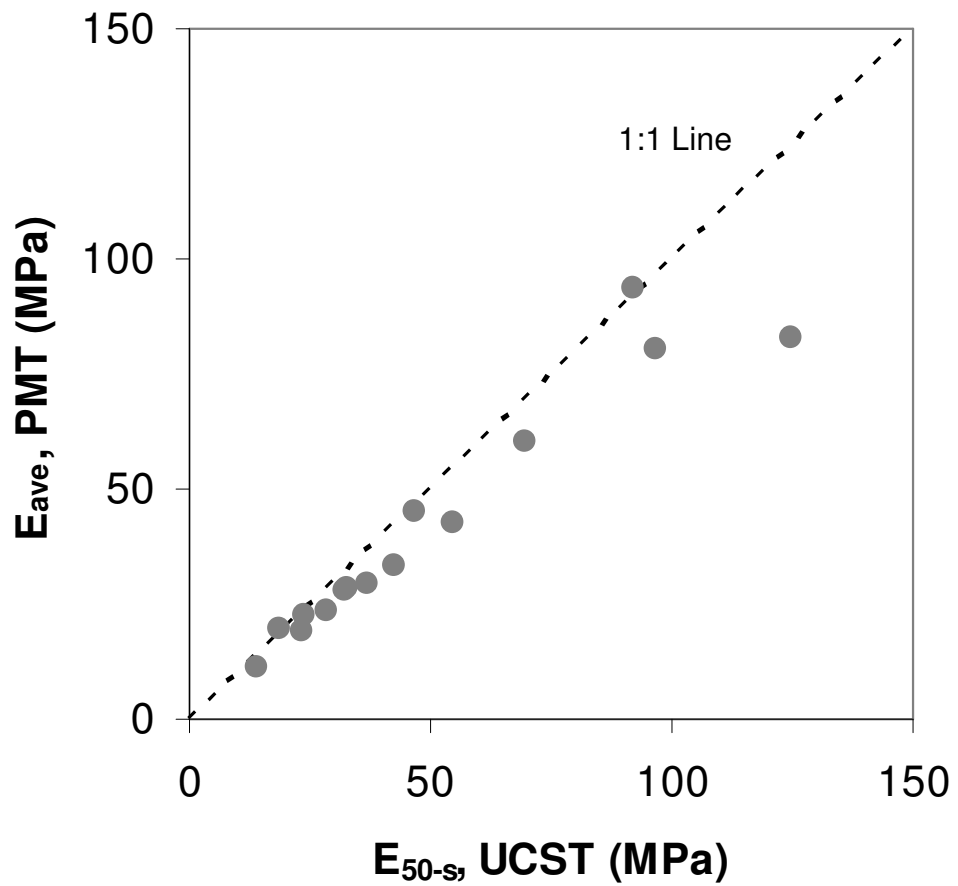


Figure 6.15 The relationship between the values of deformation modulus obtained from the pressuremeter tests (PMT) and uniaxial compression (UCST) tests.

However, the triaxial tests performed on various intact core samples with a wide range of confining stresses show that there is no difference between the values of deformation modulus obtained under different confining stresses (Bieniawski, 1972; Elliott, 1982; Waversik and Fairhurst, 1970). This is probably due to the fact that the consolidation or volumetric hardening is impossible for rocks. However, for granular soils the soil exhibits increasing modulus with increasing confining stresses by the application of confining stress, volume decreases (void ratio decreases) in granular soil. The weathered andesites exposing around Ovacık and Pursaklar districts resemble low porosity rocks, not granular soils (i.e. the grains are still cemented to each other with no evident voids between grains). Kulhawy (1975) stated that the effects of nonlinearity and stress dependency of rock modulus are minor with hard crystalline or homogeneous rock of low porosity, but are significant in porous, clastic or closely jointed rock. Also it is common to measure the intact rock modulus from unconfined compression tests in rock engineering.

A small unloading - reloading loop was performed at the end of the tests for the determination of the values of unloading-reloading modulus, and the ratio of unloading-reloading modulus to deformation modulus value ranging between 1.6 and 3.8 was obtained.

6.1.2.3 Dikmen greywackes

Because the greywacke is highly fractured and sheared, it is not meaningful to compare the laboratory test results with those from the pressuremeter tests. Since greywacke is highly fractured, it can be considered that the values of deformation modulus obtained from the pressuremeter represent the deformation modulus of the in-situ rock mass by considering the length of the pressuremeter probe and the volume of the tested material (see Chapter 6.1.1.3).

A small unloading-reloading loop was performed at the end of the tests, for the determination of the unloading-reloading modulus values. The ratio of unloading-reloading modulus to deformation modulus ranged between 2.4 and 5.2, with higher values corresponding to greywackes exposing in Beytepe campus of Hacettepe University.

In order to control the validity of the assigned GSI values for the Beyaz Ev site, two slope failures described in detail by Çevik (2000) were utilized. These failures occurred in the neighborhood of Beyaz Ev site within highly weathered greywackes. The mean GSI value estimated from the chart by Hoek (1999) is 11, and UCS value ranges between 4.3 and 51 MPa with a mean of 22 MPa. The m_i value is reported as 7.8 (Kumtepe, 1996). Since the slope failures occurred in the relatively weak greywacke rock mass, lower values of UCS (≤ 8 MPa) were used to obtain Hoek – Brown failure envelope (Figure 6.16). This normal stress versus shear strength relationship was used to assess the stability of slope failures by the limit equilibrium method with Morgenstern and Price (1965) methodology. The Hoek – Brown failure parameters are obtained using the methods based on Hoek (1999) and Sönmez and Ulusay (2002). In the analyses a value of 23 kN/m³ unit weight which was determined by the laboratory tests was used. The limit equilibrium analyses were performed using a computer program called Slide v 5.0 (Slide, 2003).

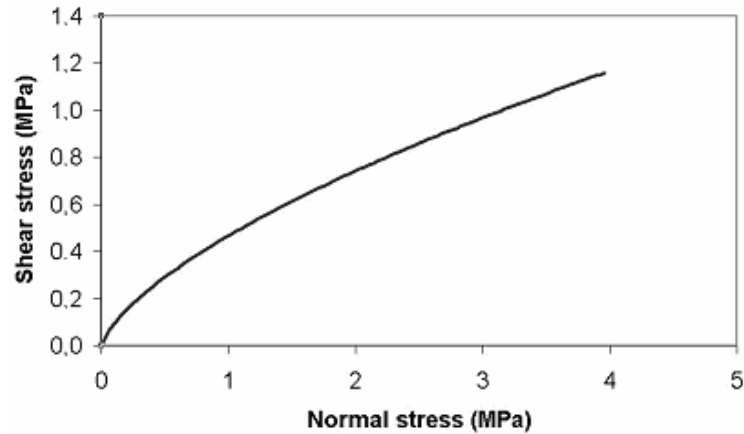


Figure 6.16 Hoek – Brown failure envelope for the greywackes exposed around Beyaz Ev site.

Table 6.2 The Hoek and Brown failure parameters used in the analyses.

	m_b	s	a
Hoek, (1999)	0.325	0.000051	0.580
Sönmez and Ulusay (2002)	0.325	0.000051	0.540

Results of the analyses for slopes 1 and 2 are summarized in Table 6.3. The failure surfaces of slopes 1 and 2 are depicted in Figures 6.17 and 6.18. Results of the limit equilibrium analyses revealed that both slopes are unstable for mean GSI value and lower values of UCS.

Table 6.3 The results of the analyses for slopes 1 and 2

UCS (MPa)	Slope 1		Slope 2	
	Hoek (1999)	Sönmez and Ulusay (2002)	Hoek (1999)	Sönmez and Ulusay (2002)
4.3	0.837	0.961	0.771	0.894
6.0	0.924	1.034	0.857	0.999
8.0	1.002	1.148	0.925	1.090
14.0	1.175	1.352	1.088	1.285
20.0	1.303	1.520	1.203	1.431

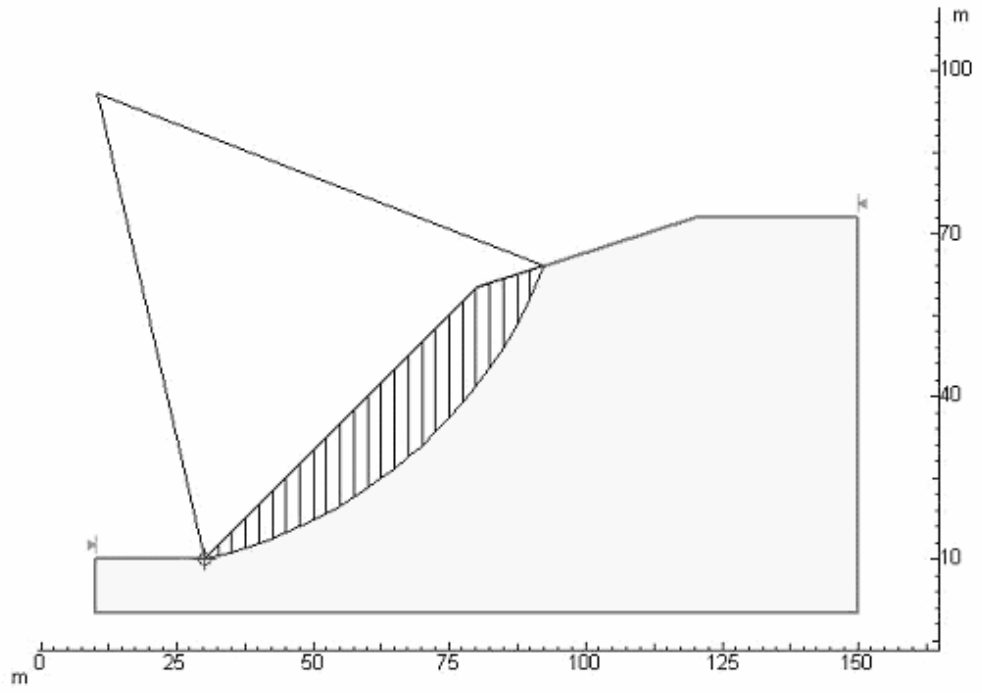


Figure 6.17 The failure surface of slope 1 at Beyaz Ev.

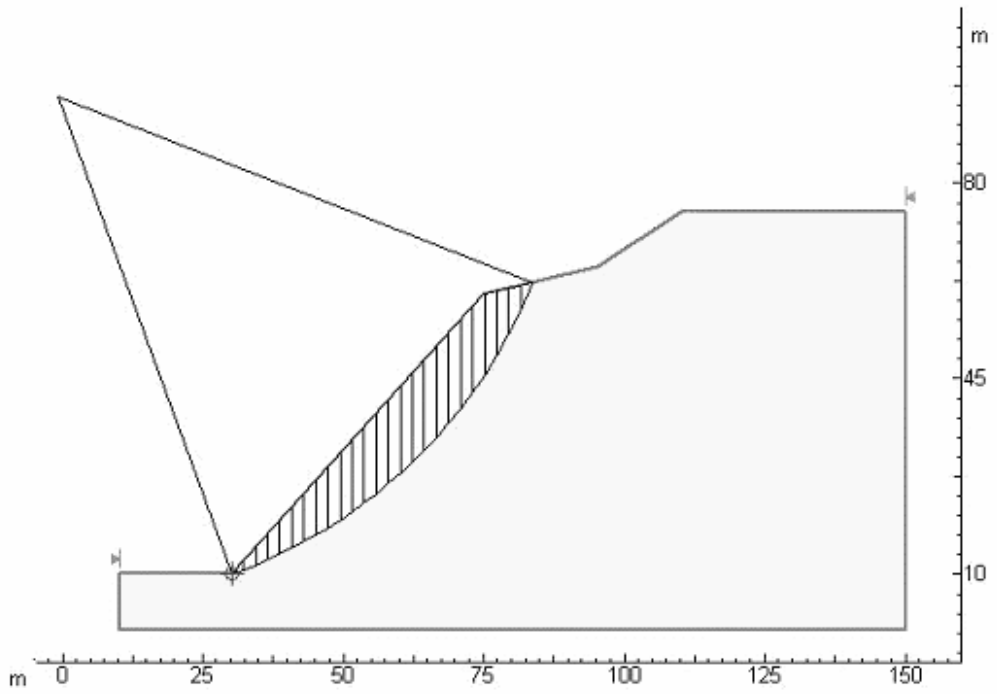


Figure 6.18 The failure surface of slope 2 at Beyaz Ev.

Stability of slope 1 was also assessed by the finite element method. In order to use FEM for the stability assessment, equivalent Mohr – Coulomb failure parameters and modulus of deformability are the necessary inputs. Determination of equivalent Mohr – Coulomb parameters was accomplished by fitting a linear failure envelope to the Hoek – Brown failure envelope (Hoek, 1999) using a value of UCS equal to 8 MPa within the working stress range. The maximum vertical effective stress along the sliding surface determined as approximately 500 kPa. Figure 6.19 shows the Hoek – Brown failure curve and the corresponding Mohr – Coulomb failure envelope within the 0 to 500 kPa normal stress range. The deformation modulus of the rock mass ($E_m = 62.4$ MPa) determined from the pressuremeter tests performed in this vicinity, was employed in the finite element analysis.

Finite element analyses of slopes 1 and 2 were performed using Plaxis v 7.2 with elastic – perfectly plastic constitutive relationship using the Mohr – Coulomb failure criterion. Figure 6.20 shows the finite element mesh and boundary conditions for slope 1. The finite element mesh of slope 1 consists of 746 triangular elements with 16 nodes. Same boundary conditions were also utilized for slope 2. The incremental shear strain contours for slope 1 is depicted in Figure 6.21.

From Figure 6.21 it is seen that the slope is unstable under gravitational loading conditions. For the finite element analysis of slope 2, finite element mesh consisting of 698 triangular elements with 16 nodes was used. Incremental shear strain contours for slope 2 is shown in Figure 6.22.

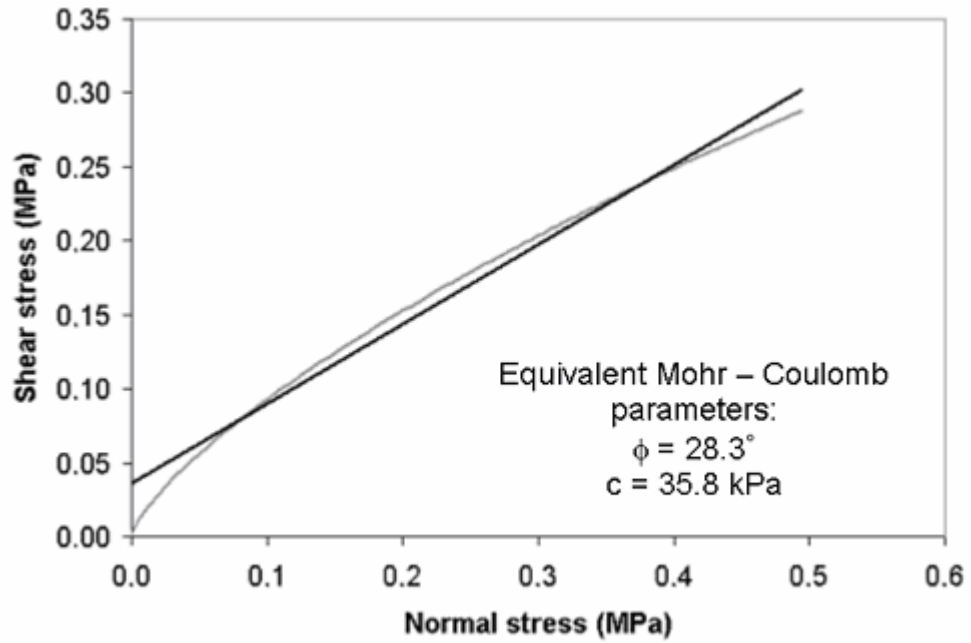


Figure 6.19 The Hoek – Brown failure envelope and the corresponding Mohr – Coulomb failure line within the 0 to 500 kPa normal stress range.

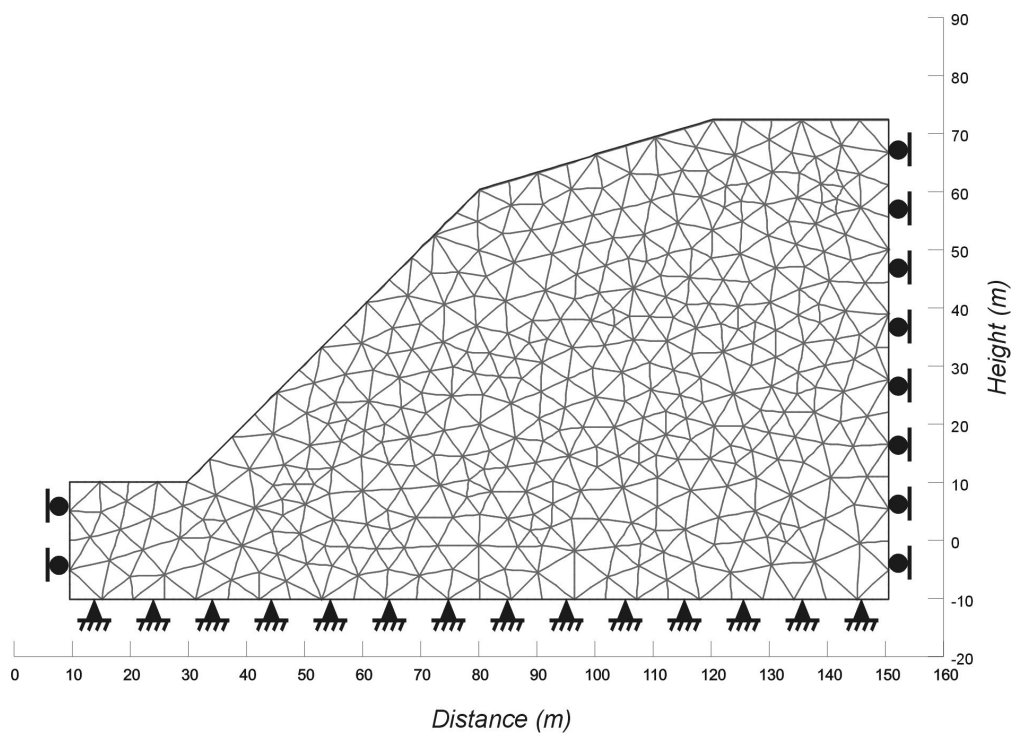


Figure 6.20 The finite element mesh and boundary conditions for slope 1.

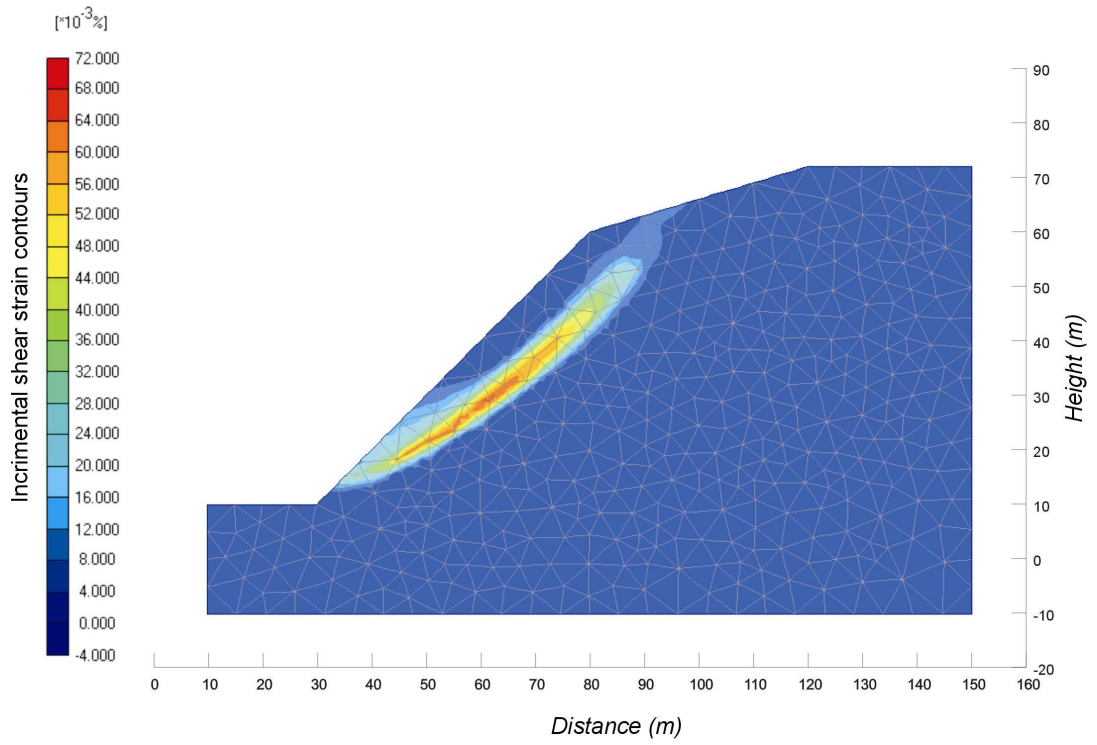


Figure 6.21 The incremental shear strain contours for slope 1.

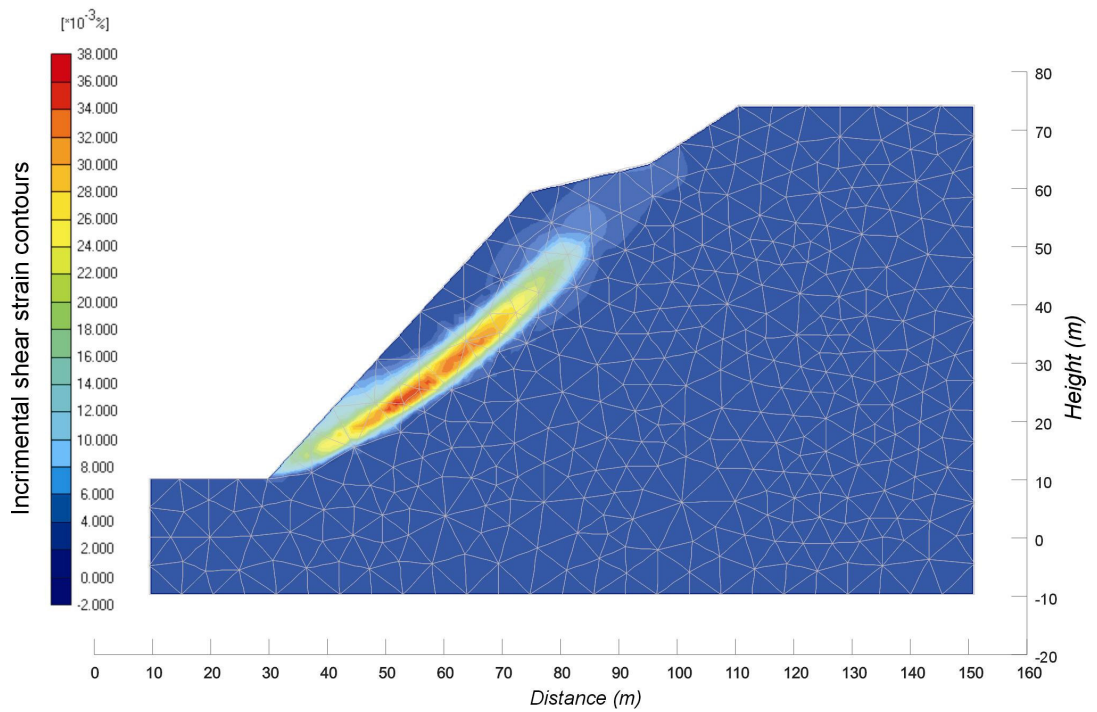


Figure 6.22 The incremental shear strain contours for slope 2.

Based on the rock mass parameters assigned to the greywackes around the Beyaz Ev site, both failed slopes were found as close the limiting equilibrium condition. As a result, it can be concluded that the input parameters of both slopes (i.e. GSI, UCS) are representative of the rock mass exposing around Beyaz Ev site.

The maximum, mean and the minimum values of RMR and GSI are compared with the minimum, mean and maximum values of deformation modulus for each site by assuming that the minimum, mean and maximum values of RMR, GSI and UCS correspond to the minimum, mean and maximum values of the deformation modulus from the pressuremeter tests. Figures 6.23, 6.24 and 6.25 present the relationship of qualitative GSI (Hoek, 1999), quantitative GSI (Sönmez and Ulusay, 2002) and RMR (Bieniawski, 1989) with the rock mass deformation modulus values, respectively. Figure 6.26 shows the UCS (determined from Schmidt hammer tests) with the rock mass deformation modulus values together with the best fitted regression line.

The attempts made to combine the UCS and GSI values for obtaining a better estimation of the rock mass deformation values were unsuccessful, probably due to the uncertainties arising from the UCS values obtained from Schmidt hammer tests.

By examining Figures 6.23 through 6.26, it can be concluded that the GSI is a better index of rock mass classification than the RMR for Dikmen greywackes. Equations from Figures 6.23 through 6.25 (Equations 6.1 to 6.3) can be used to estimate the deformation modulus values of Dikmen greywackes.

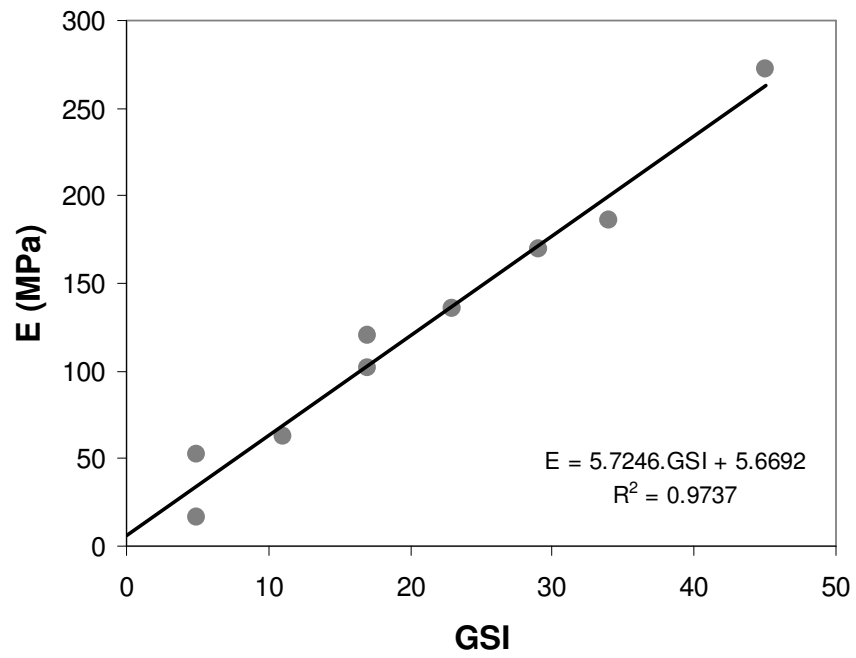


Figure 6.23 Variation of the deformation modulus with GSI estimated from Hoek (1999).

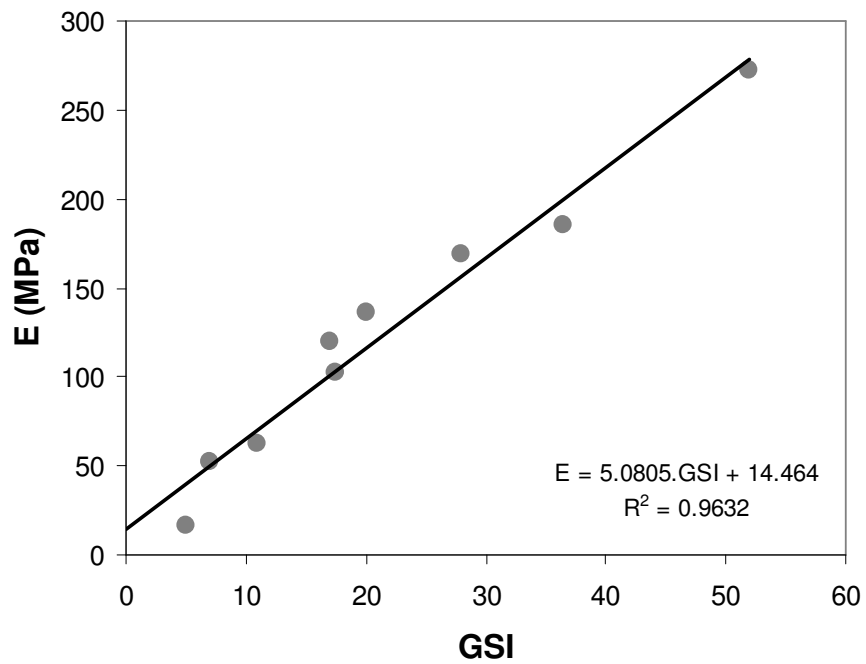


Figure 6.24 Variation of the deformation modulus with GSI estimated from Sönmez and Ulusay (2002).

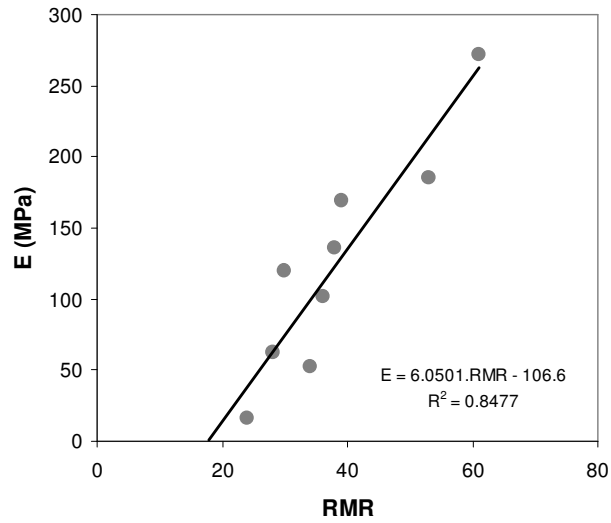


Figure 6.25 Variation of the deformation modulus with RMR estimated from Bieniawski (1989).

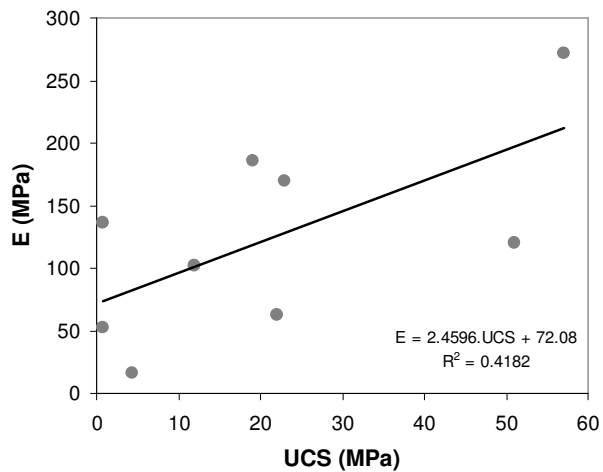


Figure 6.26 Variation of UCS with the rock mass deformation modulus.

$$E = 5.7GSI_H + 5.7 \quad (R^2 = 0.974) \quad (6.1)$$

Where, GSI_H is the GSI value determined according to Hoek (1999).

$$E = 5.1GSI_{SU} + 14.5 \quad (R^2 = 0.963) \quad (6.2)$$

Where, GSI_{SU} is the GSI value determined according to Sönmez and Ulusay (2002).

$$E = 6.05RMR - 106.6 (R^2 = 0.848) \quad (6.3)$$

Because the highly fractured and sheared Dikmen greywackes resemble a rock mass composed of numerous small blocks, some degree of stress dependency may be expected (i.e. dependency of modulus to the confining stresses) as for the case of all blocky rock masses. Although the Hoek and Brown empirical non-linear failure criterion presents the effect of confining stress to shear strength of the rock mass, there is no knowledge of the stress dependency of the rock mass deformation modulus of blocky to heavily fractured rock masses in the literature. For example, Palmström and Singh (2001) indicated that in-situ deformation modulus of the rock mass is not constant but depends on the stress conditions, being generally higher in areas subjected to high stresses than in rock masses under low stresses. As previously discussed, the stress path of the plate load tests (also foundation loading) includes more compression and less shear than those from the pressuremeter test. Therefore, for a geomaterial with confining stress dependent modulus, volumetric hardening will likely to occur during plate load test. This may result in the increased deformation modulus. For this reason, additional research is needed for the determination of the confining stress dependency of the deformation modulus of heavily fractured rock masses and for the comparison of plate load tests with other in-situ tests.

Because direct determination of the deformation modulus of rock masses are expensive and difficult to perform, it is commonly determined by empirical equations. As summarized in Chapter 2, there exist several empirical equations for the purpose. The deformation modulus is estimated using the methods given in Table 6.4. Equations of these empirical methods are given in Chapter 2.1.

Some of the empirical equations listed in Table 6.4 need the intact rock deformation modulus values. Since directly measured UCS values from three core samples and those estimated from BPI tests do not reflect the

overall intact rock conditions of the greywackes, the use of the above mentioned empirical equations yields unacceptably high values of rock mass deformation modulus. In order to overcome this problem, intact rock's deformation modulus of the greywackes should be estimated from the uniaxial compressive strength determined by Schmidt hammer tests. In order to obtain an acceptable predictor of intact rock modulus value, the results of the uniaxial compression tests performed on greywacke core samples were employed. A value of E_i/USC as 197.64 was determined from uniaxial compression tests. Similarly for Berea, Navajo and Tensleep sandstones, Hackensack siltstone and Monticello dam greywacke values of E_i/USC were determined as 261, 183, 264, 214 and 253, respectively (Goodman, 1989). Since these values are close to the one determined from the compression tests on intact greywacke samples a ratio of E_i/USC , which equals to 197.64, was used for the estimation of E_i from the uniaxial compressive strength values based on Schmidt hammer tests. The input parameters used in the empirical equations, for the greywackes are given in Table 6.5. The rock mass deformation modulus values determined by empirical equations for greywackes are summarized in Table 6.6.

Table 6.4 Empirical methods used for the estimation of the deformation modulus.

Method	Parameters considered
Serafim and Pereira (1983)	RMR
Nicholson and Bieniawski (1990)	E_i , RMR
Mitri et al. (1994)	E_i , RMR
Hoek and Brown (1997)	UCS, GSI
Kayabaşı et al. (2003)	E_i , RQD, WD
Gökçeoğlu et al. (2003)	E_i , UCS, RQD, WD
Sönmez et al. (2004)	E_i , s, a
Zhang and Einstein (2004)	E_i , RQD

Table 6.5 The input parameters used in the empirical equations, for the greywackes.

Site	UCS (MPa)	E _i (GPa)	RQD	WD	GSI - Hoek (1999)	GSI -Sönmez and Ulusay (2002)	RMR	s	a
	0.8	0.16	0	3	5	7	34	0.00003	0.625
Workshop	12	2.36	0	3	17	17.5	36	0.00011	0.560
	22.9	4.51	0	3	29	28	39	0.00024	0.525
	4.3	0.85	0	4	5	5	24	0.00003	0.625
Beyaz Ev	22	4.33	0	4	11	11	28	0.00006	0.590
	51	10.05	0	4	17	17	30	0.00011	0.560
	0.8	0.16	27	2	23	20	38	0.00019	0.535
Dikmen	19	3.74	35	2	34	36.5	53	0.00073	0.500
	57.1	11.25	46	2	45	53	61	0.00178	0.500

WD: Degree of weathering; s and a: Hoek – Brown failure envelope constants.

Table 6.6 The rock mass deformation modulus values (MPa) for the greywackes determined by various empirical equations.

Serafim & Pereira (1983)	Nicholson & Bieniawski (1990)	Mitri et al. (1994)	Hoek & Brown (1997)	Kayabaşı et al. (2003)	Gökçeoğlu et al. (2003)	Sönmez et al. (2004)	Zhang and Einstein (2004)			
							Lower Bound	Mean	Upper Bound	PMT
3981	11	41	67	4	664	11	0	2	3	52
4467	189	679	518	102	664	307	6	29	52	102
5309	417	1492	1429	219	664	784	11	56	100	169
2239	36	115	156	22	426	61	2	10	19	16
2818	228	786	497	148	426	431	11	53	96	62
3162	590	2071	1069	401	426	1305	25	124	222	120
5012	14	50	189	9	1806	25	1	6	11	136
11885	639	2048	1735	403	1985	883	41	206	371	185
18836	2642	7530	5667	1623	2242	3170	198	992	1786	272

PMT: Values of deformation modulus from pressuremeter test

It is clear from Table 6.6 that Serrafim and Perraira's (1983) equation yields unacceptably high rock mass deformation values. The measured deformation modulus values are somewhere in between the minimum and average estimations of deformation modulus values estimated from the equations by Nicholson and Bieniawski (1990) and Sönmez et al. (2004). The minimums of the deformation modulus estimated from Mitri et al. (1994), and Hoek and Brown (1997)'s equations are close to the measured values. Although the GSI values are different, Gökçeoğlu et al. (2003) estimate same values of deformation modulus for Hacettepe Beytepe Beyaz Ev and Workshop sites. This is due to the fact that both sites have RQD's equal to zero, constant degree of weathering and greywacke has constant value of E_i/UCS . Also the estimations based on the equations of Gökçeoğlu et al. (2003) are higher than the actual values. According to Table 6.6, the better estimations of the measured deformation modulus values are obtained by the equations of Kayabaşı et al. (2003). The values of deformation modulus measured by pressuremeter lies between the lower and upper bound estimations from the Zhang and Einstein (2004)'s equation.

The difference between the measured and the predicted deformation modulus values can be explained as follows:

- i) Intact rock modulus is estimated from the UCS values determined from the Schmidt hammer rebound values. Uncertainties associated with the Schmidt hammer significantly affect the performance of the empirical equations which already have uncertainties associated with the data and statistical models.
- ii) The greywacke rock mass used for pressuremeter testing is extremely fractured. Fractures are present even in the micro scale. Although apparent higher GSI values were assigned to blocky greywackes exposing in the CAKS site, actual rock mass is weaker than it seems.

iii) Databases used for the development of empirical relationships generally involved stronger rock masses than the greywackes cropping out in Ankara. More commonly results from the plate load tests performed in galleries with higher in-situ stress state are used for the development of empirical relationships. If the rock mass under consideration has a stress dependent stress – strain behavior, the values of deformation modulus expected to be higher.

6.1.2.4 Pressuremeter tests in the mudrocks

A total of 50 pressuremeter tests were performed in the Eocene and Neogene mudrocks cropping out around Sincan region for the determination of deformation modulus. The values of RQD, uniaxial compressive strength and deformation modulus of the intact rock material corresponding to the test section were obtained when available. For highly fractured test sections, the intact rock parameters were determined from the closest representative sample, if present.

Although 50 pressuremeter tests were performed, only 10 data of rock mass deformation modulus, RQD, UCS and E_i values could be obtained because for each of the pressuremeter test, UCS and deformation modulus of the intact rock are not available. By using this database, since RQD is a measure of the degree of fracturing, variation of the ratio of rock mass modulus to intact rock modulus (E_m/E_i) with RQD was obtained (Figure 6.27). Zhang and Einstein (2004) have developed equations for the estimation of the variation of the ratio of E_m/E_i , with RQD. Their results were also indicated in Figure 6.27.

Although RQD is not the sole indicator of the effects of the discontinuities on the deformation modulus (i.e. the stiffness, orientation, persistence, even the shearing strength of discontinuities are needed for full description

of the discontinuities), the equation given in Figure 6.27 may be used for the estimation of rock mass deformation modulus of the mudrocks described above or possibly in similar rocks.

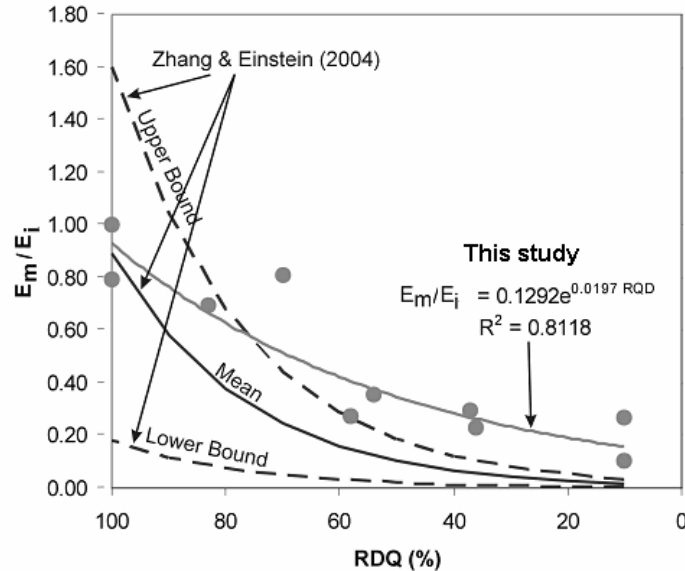


Figure 6.27 Variation of the ratio of rock mass modulus to intact rock modulus (E_m/E_i), with RQD for the mudrocks in Sincan.

6.1.3 Relationship between seismic velocities and shear modulus

Shear wave velocity is related to the value of shear modulus under very low strain levels. In order to figure out the relationship between the shear wave velocity, primary wave velocity and shear modulus, regression analyses were performed (Figure 6.28 and 6.29). The average values of shear modulus and corresponding shear and primary wave velocities were determined for greywackes, weathered andesites and mudrocks exposing around Sincan. Figures 6.28 and 6.29 suggest that there is a very poor relationship between shear wave and primary wave velocities and the deformation modulus. This is probably due to the fact that shear and primary wave velocities generally correspond to the stiffer part of the rock mass (seismic waves propagate within the stronger path of the rock mass).

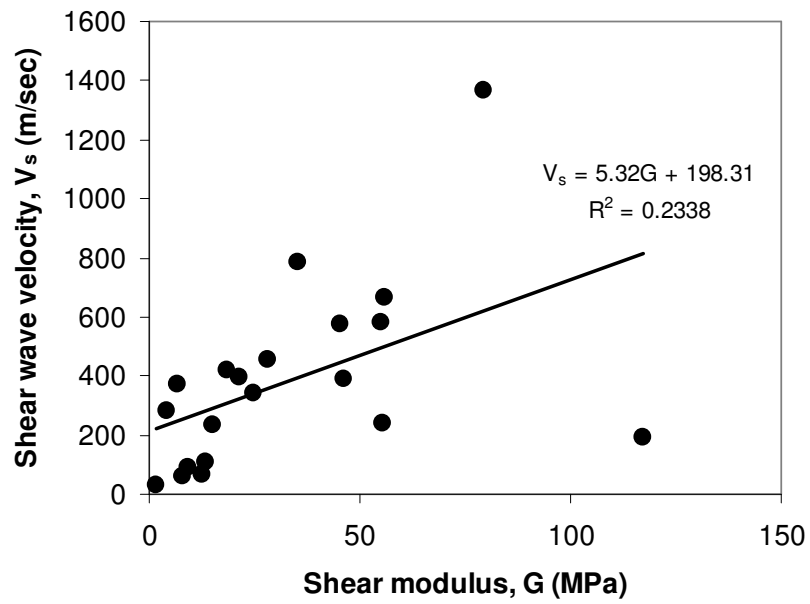


Figure 6.28 Relationship between shear wave velocity and shear modulus.

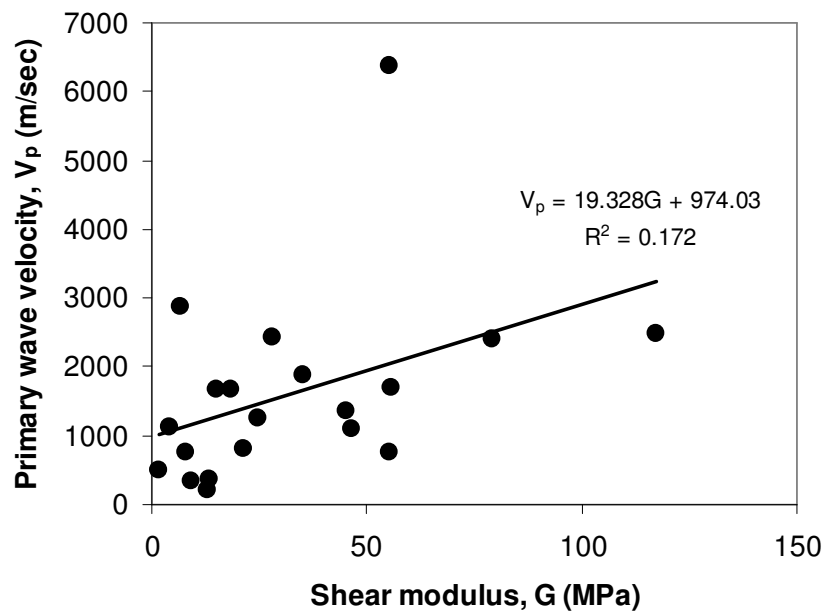


Figure 6.29 Relationship between primary wave velocity and shear modulus.

6.2 Determination of Undrained Shear Strength

The undrained shear strength is half of the maximum deviatoric stress or shear stress during an undrained test. The undrained shear strength is not a unique property of the soil instead it depends on the changes in effective stresses that the soil undergoes. Figure 6.30 shows the total and effective stress paths of an undrained triaxial test in normally consolidated clay.

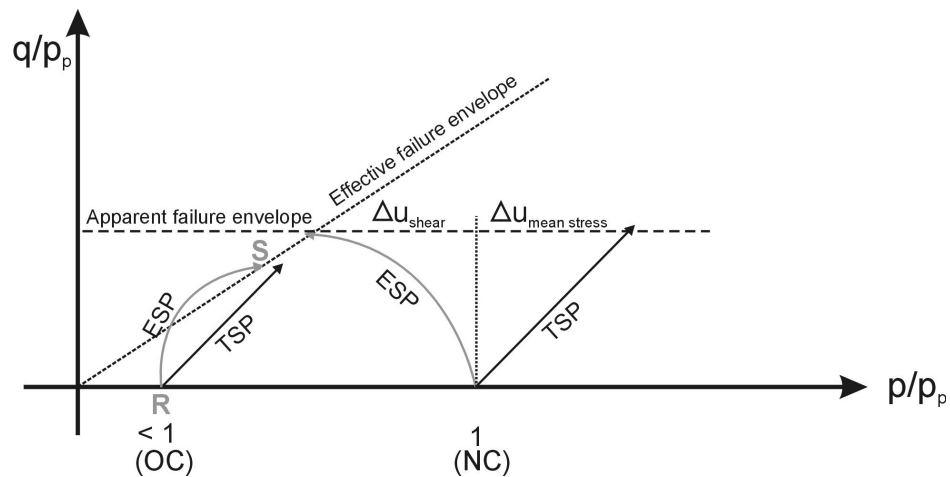


Figure 6.30 Total and effective stress paths of an undrained triaxial test in clay (ESP: effective stress path; TSP: total stress path; OC: overconsolidated; NC: normally consolidated).

The difference between the total and effective stress paths is the excess pore pressure, which is due to an increase in mean total stresses (Δu_{mean}) and shear stresses (Δu_{shear}). Obviously, the total excess pore pressure is not a soil property but it depends on the change in total mean and effective stresses. But the Δu_{shear} is a property of the soil, it depends on the dilative or contractive behavior of the soil during shear (i.e. relative density, overconsolidation ratio).

The shape of the effective stress path of normally consolidated clays is similar to the one displayed in Figure 6.30. However, as the over-consolidation ratio of the clay increases the shape of the effective stress path changes.

In early days of the pressuremeter testing, undrained shear strength of saturated clays was determined by empirical relationships and solutions were based on bearing capacity theory. However, the bearing capacity solutions assume that the limit pressure is independent of the stiffness of the ground, therefore, they are not suitable for pressuremeter test. Figure 6.31 shows the simulated pressuremeter curves in a linearly elastic perfectly plastic soil with same undrained shear strength but different rigidity ($I_r = G/S_u$) values. As it is evident from this figure, increasing shear modulus causes increasing limit pressure although the undrained shear strength is the same. Similarly, early solutions for the determination of the undrained shear strength from cone penetration test were based on bearing capacity theory, however, they were found to be unsatisfactory (Lunne et al., 1997).

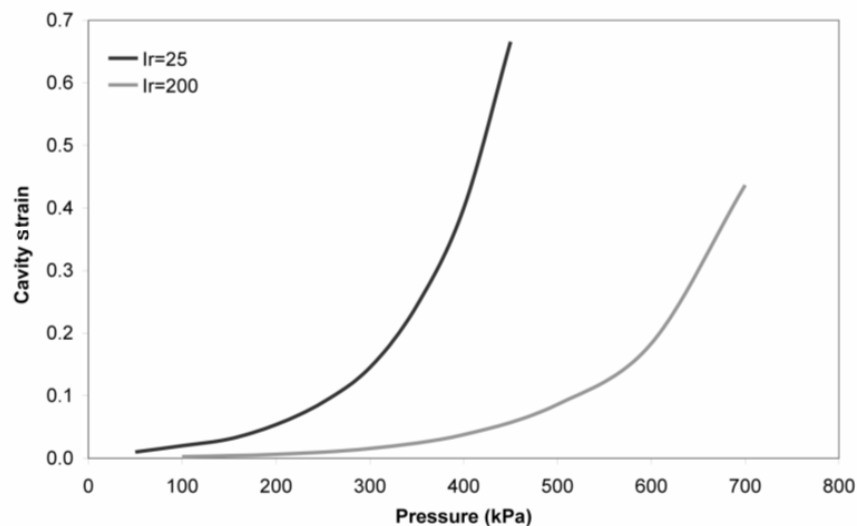


Figure 6.31 Simulated pressuremeter curves in a linearly elastic perfectly plastic soil, having the same undrained shear strength and different rigidity values.

First theoretical solution for the determination of the undrained shear strength from pressuremeter test was presented by Gibson and Anderson (1961). In this solution, the soil is assumed to behave linearly elastic-perfectly plastic. This solution is based on the infinitely long cylindrical cavity expansion in total stresses.

$$P_{lt} - \sigma_h = S_u \left(1 + \ln \frac{G}{S_u} \right) \quad (6.4)$$

Where, P_{lt} is the theoretical limit pressure.

The newer analysis developed by Palmer (1972), Ladanyi (1972) and Baguelin et al. (1972) almost at the same time and independently from each other, does not require an assumption to be made about the stress strain behavior of the soil. These analyses were also based on the assumption of undrained expansion of infinitely long cylindrical cavity. According to Palmer (1972), Ladanyi (1972) and Baguelin et al. (1972), the slope of the pressure versus $\ln(dV/V)$ gives the shear stress, i.e. undrained shear strength. This approach is also valid for large deformations (Baguelin et al., 1978).

The solutions of Gibson and Anderson (1961), Palmer (1972), Ladanyi (1972) and Baguelin et al. (1972) are used for the determination of the undrained shear strength of clays. By using the theoretical limit pressure obtained from pressuremeter test and average shear modulus value (average means the value which represents the overall nonlinear stress - strain behavior of the soil prior to yielding), undrained shear strength can be calculated from the equation proposed by Gibson and Anderson (1961). The slope of the pressure versus $\ln(dV/V)$ yields the undrained shear strength according to Palmer (1972), Ladanyi (1972) and Baguelin et al. (1972), so that a plot of pressure versus $\ln(dV/V)$ can be used for the determination of undrained shear strength. A third technique for the

determination of the undrained shear strength is to use the slope of the pressure versus $\ln(dV/V)$ for each loading step. This procedure allows shear stress versus cavity strain graph to be obtained. However, shear stress vs. cavity strain graphs obtained by this method generally involves irregularities and a post peak plateau probably due to small measurement errors in the field. According to Mair and Wood (1987), this technique is unreliable.

Although exact theoretical solutions are available for the determination of undrained shear strength from pressuremeter test, various researchers stated that the pressuremeter test overestimates the undrained shear strength of clays about 30 – 50 % (Baguelin et al., 1972; Windle and Wroth, 1977 b; Ghionna et al., 1983; Yeung and Carter, 1990; Houlsby and Carter 1993; Bowles, 1996). Overestimations of about 100 %, of prebored pressuremeter test with comparison to field vane test was reported by Roy et al. (1975).

Initially, high values of undrained shear strengths, obtained from pressuremeter test were attributed to the lower disturbance associated with the pressuremeter. However, this cannot explain the differences between the pressuremeter and field vane test results. More recently, this overestimation is attributed to a number of factors:

- i) High strain rate (Wroth, 1984);
- ii) partial drainage during test (Wroth, 1984; Pyrah et al., 1988);
- iii) presence of disturbed annulus around the borehole, (Baguelin et al., 1978, Prevost, 1979, Prapharan et al., 1990);
- iv) uncylindrical expansion (L/D ratio) (Yeung and Carter, 1990; Houlsby and Carter, 1993);
- v) different deformation patterns and stress paths during failure than other tests (Wroth, 1984).

Since the laboratory (triaxial compression, direct simple shear) and in-situ tests (field vane test, pressuremeter test) used for the determination of the undrained shear strength have different total stress paths and shearing modes, the resultant effective stress path of the particular test will be different from each other resulting in different values of undrained shear strength.

Wroth (1984) interpreted the effective stress paths of different laboratory and in-situ tests and presented comparisons of undrained shear strength ratios (S_u/σ'_v) for these tests as a function of the effective friction angle and overconsolidation ratio. Wroth (1984) used the principles of the critical state soil mechanics and Matsuoka and Nakai's (1977) failure criterion which uses all principal stresses in the criterion for relating the results of plain strain tests with triaxial compression tests.

To determine the undrained shear strength at point S on Figure 6.30, the mean effective stress at failure (p_s) has to be known which is related to q_s by the effective strength envelope for isotropically consolidated undrained triaxial loading conditions. Wroth (1984) used the framework of critical state soil mechanics to relate the in-situ mean effective stress (p_R), with the mean effective stress at failure (p_s), therefore, it is possible to relate undrained shear strength ratio of clays (S_{u-tc}/σ'_{v0}) with effective strength failure envelope (M), critical state parameters (r , Λ) and overconsolidation ratio (R) as given in equation 6.5 (where $r \cong 2$, and $\Lambda \cong 0.8$ according to available literature (Wroth, 1984)).

$$\left(\frac{S_{u-tc}}{\sigma'_{v0}} \right) = \frac{M}{2} \left(\frac{R}{r} \right)^\Lambda \quad (6.5)$$

A similar equation was also proposed by Wroth (1984) for K_0 consolidated - undrained triaxial compression tests (equation 6.6) using critical state soil mechanics framework. The result of equation 6.5 is in very good agreement with the laboratory tests (for example Andresen et al., 1979).

$$\left(\frac{S_{u-tc}}{\sigma_{v0}'} \right)_{K_0} = \frac{\sin \phi_{tc}}{2a} \left(\frac{a^2 + 1}{2} \right)^a \quad (6.6)$$

Where, a is equal to:

$$a = \frac{3 - \sin \phi_{tc}}{2(3 - 2 \sin \phi_{tc})} \quad (6.7)$$

In order to determine undrained shear strength ratios (S_u/σ_v') for direct simple shear tests, the effective stress path (Figure 6.32) is approximated by an ellipse. By using the equation of the ellipse, Wroth (1984) obtained the equation for the maximum undrained shear strength ratio (i.e. at point T) which is given by equation 6.8. The elliptical shape of the effective stress path is due to the principal stress rotation during the test.

$$\left(\frac{\tau_{max}}{\sigma_{vc}'} \right) = \left(\frac{1 - \sin \phi_{ps}}{1 + \sin \phi_{ps}} \right) \tan \phi_{ps} \quad (6.8)$$

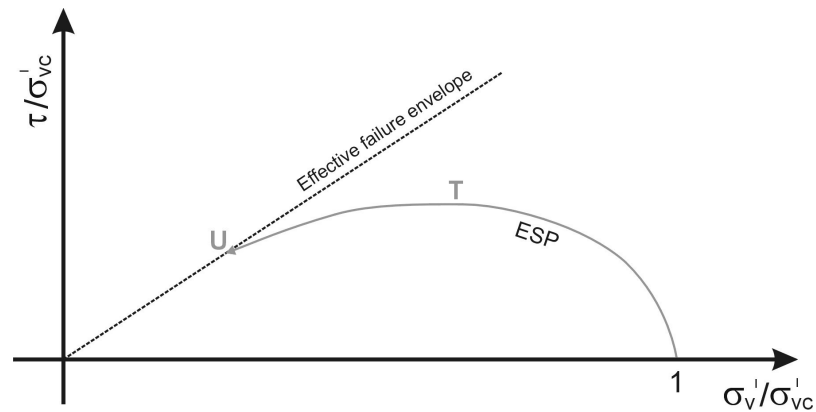


Figure 6.32 The effective stress path of a normally consolidated clay during direct simple shear test.

The field vane test is the most widely used test for the determination of the undrained shear strength of saturated clays. Mair and Wood (1987) stated

that the mode of failure around the vane is similar to direct simple shear test. As the vane rotates the torque, i.e. shear stress around the cylindrical surface of the blade increases, this could only be possible with the increase in the effective tangential stress (σ_{θ}^I) and subsequent decrease in the effective radial stress (σ_r^I). By considering this behavior, Wroth (1984) proposed a simple relationship between the maximum shear stress (i.e. undrained shear strength) and the effective friction angle. Figure 6.33 presents the state of the Mohr circle at the start and at the failure for a vane test. At the start of the test, both radial and tangential stresses are equal to the initial horizontal stress, so the Mohr circle is a point, thereafter, as the vane rotates the shear stress increases by increasing tangential stress (σ_{θ}^I) and decreasing radial stress (σ_r^I).

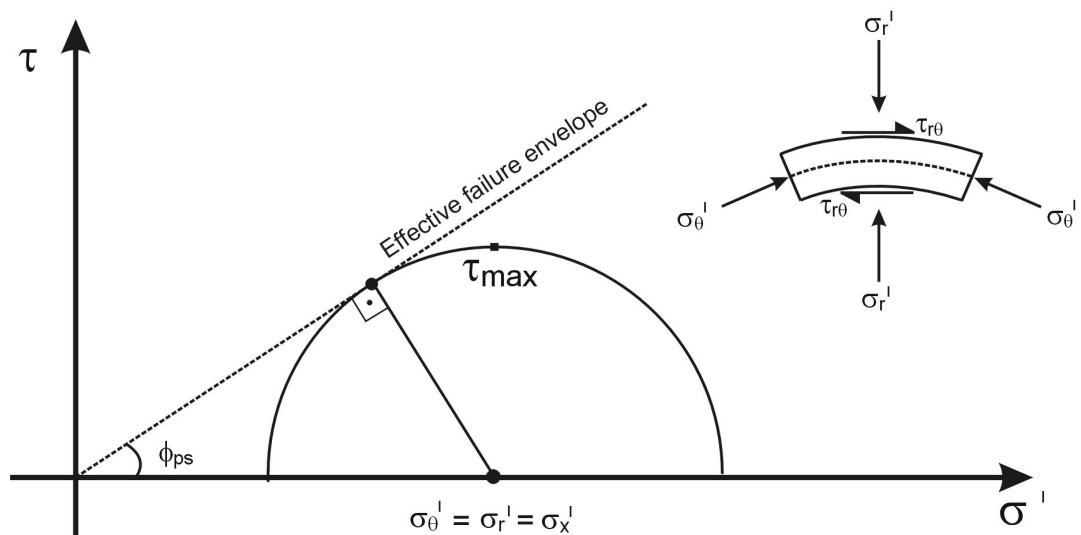


Figure 6.33 The state of the Mohr circle at the start and at the failure for a vane test.

It can easily be shown that the maximum shear stress (τ_{max}) can be given by equation 6.9 (Figure 6.33). Thus the undrained shear strength ratio is expressed by equation 6.10.

$$\tau_{max} = \sigma_h^I \cdot \sin \phi_{ps} \quad (6.9)$$

$$\left(\frac{S_{u-FV}}{\sigma_{v0}'} \right) = \left(\frac{\sigma_h' \sin \phi_{ps}}{\sigma_{v0}'} \right) \approx (1 - \sin \phi_{ps}) \sin \phi_{ps} \quad (6.10)$$

Wroth (1984) stated that the undrained shear strength ratio of the vane test is not well based on experimental data yet, so he recommends the use of it with caution.

It has been well established both theoretically and experimentally that the undrained shear strength ratio of a soil, when normalized by the value for the normally consolidated condition, is proportional to OCR to the power Λ . Wroth (1984) contended that the curve for pressuremeter test will be very similar for plain strain tests on anisotropically consolidated specimens.

Wroth (1984) derived the undrained strength ratio for anisotropically normally consolidated specimens using the modified cam clay model adapted for plain strain conditions (equation 6.11). The equations proposed by Wroth (1984) are presented in Figure 6.34.

$$\left(\frac{S_{u-ps}}{\sigma_{v0}'} \right) \approx \frac{\sin \phi_{ps}}{2c} \left(\frac{c^2 + 1}{2} \right)^\Lambda \quad (6.11)$$

Where:

$$c = \frac{1}{2 - \sin \phi_{ps}} \quad (6.12)$$

Ladd et al. (1980) suggested that the shear strength obtained from a pressuremeter is between the strengths observed from direct simple shear and conventional plain strain compression.

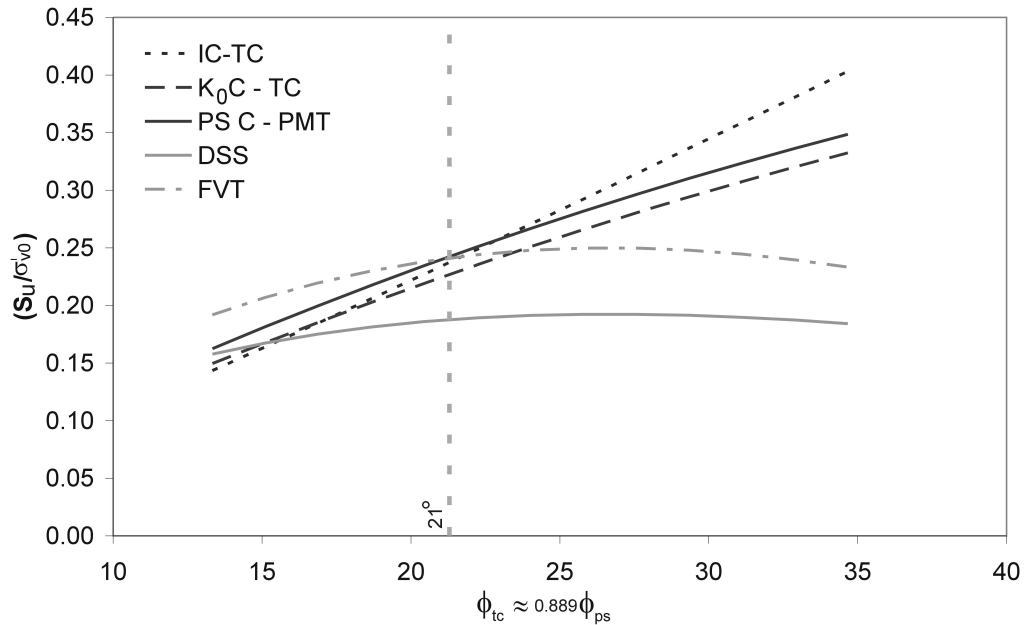


Figure 6.34 Graphical representation of the equations proposed by Wroth (1984).

Consolidated drained direct shear box tests performed on the Eymir Lake clay suggest effective friction angle of 21.9° . This value can be converted to triaxial compression friction angle by using the equation proposed by Kulhawy and Mayne (1990). This conversion yields a triaxial compression friction angle equal to 21.1° . Bowles (1996) reported that the effective friction angle of normally consolidated clays with high plasticity index (PI = 50 – 60) is between 20° and 24° . Laboratory result of the friction angle of the Eymir Lake clay is within this range.

For a friction angle of 21.1° , the pressuremeter-determined undrained shear strengths should not be higher than that of the field vane test and isotropically consolidated triaxial tests (Figure 6.34)

According to ASTM (2000), duration of each loading is 60 sec in the pressuremeter test. A typical pressuremeter test composed of 10 loading steps takes about 15 minutes. The average radial strain rate of the pressuremeter tests performed in the Eymir Lake clays is between 2.78 and 4.92 % per minute, by contrast the strain rate used for the undrained triaxial test is 1 % per minute. However, the strain rate around an expanding pressuremeter varies inversely with the square of the radius (Mair and Wood, 1987). A cavity strain rate of 1 % per minute becomes a radial strain rate of 0.25 % per minute at a radius 2 times the cavity radius. Therefore, the overall strain rate on the soil elements which are affected from pressuremeter loading is much lower than that of the cavity strain.

According to Mair and Wood, (1987), for many soils, undrained shear strength increases by about 10 % for each ten fold increase in strain rate. Penumadu et al. (1998) studied the effect of rate of probe expansion in pressuremeter testing for cohesive soil. In this study, they used a special device (flexible boundary cuboidal shear device) for the simulation of pressuremeter device. According to Penumadu et al. (1998), a ten fold increase in strain rate shows an increase in undrained shear strength of 14 %. Therefore, they concluded that strain rate alone cannot be the cause for the significant discrepancy in the measured undrained shear strength values by considering the strain rates often used for triaxial and self boring pressuremeter testing for clays.

6.2.1 One-dimensional simulation of the pressuremeter test in clays

One-dimensional simulations of pressuremeter test were performed in elastic-perfectly plastic soil possessing only cohesion according to the Mohr – Coulomb failure criterion (i.e. saturated clay behavior). The Mohr – Coulomb failure criterion degenerates to Tresca failure criterion at zero friction (Flac, 2002). Simulations were performed with varying rigidity values ($I_r = G/S_u = 25, 50, 100, 200, 300$ and 400) by using the mesh given in Figure 6.3. But for this purpose, 200 equally spaced finite difference grid was used. For the calculation of the bulk modulus values, Poisson's ratio is selected as 0.49 instead of 0.5 which is valid for the saturated clays. Because a Poisson's ratio of 0.5 means infinite bulk modulus, this can not be used in a numerical simulation. The analyses were performed using the large strain logic. In the large strain mode, the coordinates of the generated grid is updated in every 10 solution steps and the deformed mesh was checked from aspect ratio point of view for the numerical stability (Figure 6.35). This allows a more precise numerical modeling. The results of these analyses were compared with the solution presented by Palmer (1972), Ladanyi (1972) and Baguelin et al. (1972). One-dimensional numerical simulations were performed in stress free, and in-situ stress conditions with various K_0 values, without unloading cases. According to the theoretical solution, the slope of the P versus $\text{LN}(dV/V)$ plot should yield the undrained shear strength independent of the rigidity values. Figure 6.35 depicts the pressure versus $\text{LN}(dV/V)$ plot of the simulation performed for an undrained shear strength value of 100 kPa, and a rigidity value of 100 for in-situ stress free condition. As the displacements increase, the curve becomes concave upwards. This is due to the fact that as the displacements increase aspect ratio of the grids decreases leading to the loss of precision. According to Flac (2002), an aspect ratio close to 1 yields accurate results; however, when the aspect ratio becomes 0.2 the solution becomes potentially

inaccurate. When the distortion is so great, Flac automatically stops the calculation. Therefore the undrained shear strengths are calculated from the linear portion of the LN(dV/V) versus pressure plot. The same methodology is followed for all one and two-dimensional numerical simulations.

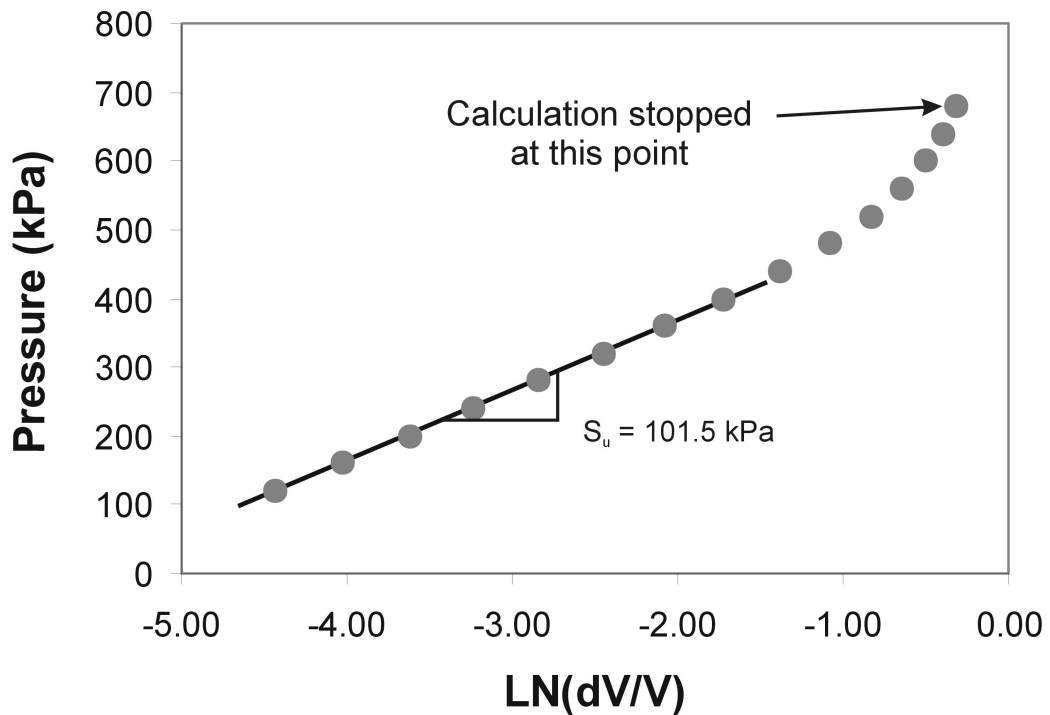


Figure 6.35 The pressure versus LN(dV/V) plot of the one-dimensional pressuremeter simulation for $I_r = 100$.

As it is expected, for all stress conditions (without unloading) and rigidity values, one-dimensional solutions yielded S_u values about 101 - 102 kPa. This means that the error in the one-dimensional solutions is about 2 % at maximum (i.e. $S_{u-m}/S_{u-true} = 1.02$). The one-dimensional simulations displayed the accuracy of finite difference simulations in linearly elastic-perfectly plastic soil. However, the one-dimensional simulations based on the small strain finite element method performed by Houlsby and Carter

(1993) could not yield a value of S_{u-m}/S_{u-true} close to 1, particularly for higher rigidity values.

6.2.1.1 Effect of disturbance on the undrained shear strength derived from pressuremeter

The installation of the pressuremeter, especially pre-bored pressuremeter, disturbs the soil close to the probe which results in the formation of an annular zone of remoulded soil around the probe. This problem was first studied by Baguelin et al. (1978) using the theory of cavity expansion. Prevost (1979), and Prapharan et al. (1990) analyzed same problem using strain path approach. According to Baguelin et al. (1978), Prevost (1979) and Prapharan et al. (1990) analyzing the pressuremeter test as if the soil is homogeneous, gives rise to an initial strength which may be greater than the actual strength of the undisturbed soil. The range of overestimation given by these researchers is between 10 – 100 % depending on the relative strength of the disturbed and undisturbed soils, selected soil behavior model and the thickness of the disturbed zone.

Baguelin et al. (1978) proposed the following equations which are associated with the cavity pressure (P).

$$P = P_0 + \int_0^{g_1} \frac{f(g).dg}{g(1+2g)} + \int_{g_1}^{g_0} \frac{f_1(g).dg}{g(1+2g)} \quad (6.13)$$

$$\frac{g_1}{g_0} = \frac{r_0^2}{r_1^2} = \frac{1}{b} \quad (6.14)$$

Where, P is the pressure in the cavity; P_0 is the in-situ horizontal stress; g_1 is the radial strain at the border of the disturbed and undisturbed zone; g_0 is the cavity strain; r_0 is the initial radius of the cavity; r_1 is the radius of the disturbed zone; $f(g)$ is the shear stress versus strain relationship of the undisturbed ground; $f_1(g)$ is the shear stress versus strain relationship of the disturbed ground.

By integration of equation 6.13, the following equation is obtained.

$$\tau_{ap} = \left(\frac{1+2g_0}{1+2g_1} \right) f(g_1) + \left(f_1(g_0) - \frac{1+2g_0}{1+2g_1} \cdot f_1(g_1) \right) \quad (6.15)$$

Shear stress versus cavity strain plots of undisturbed and completely disturbed soil, and apparent cases for various disturbed zone thicknesses are depicted in Figure 6.36.

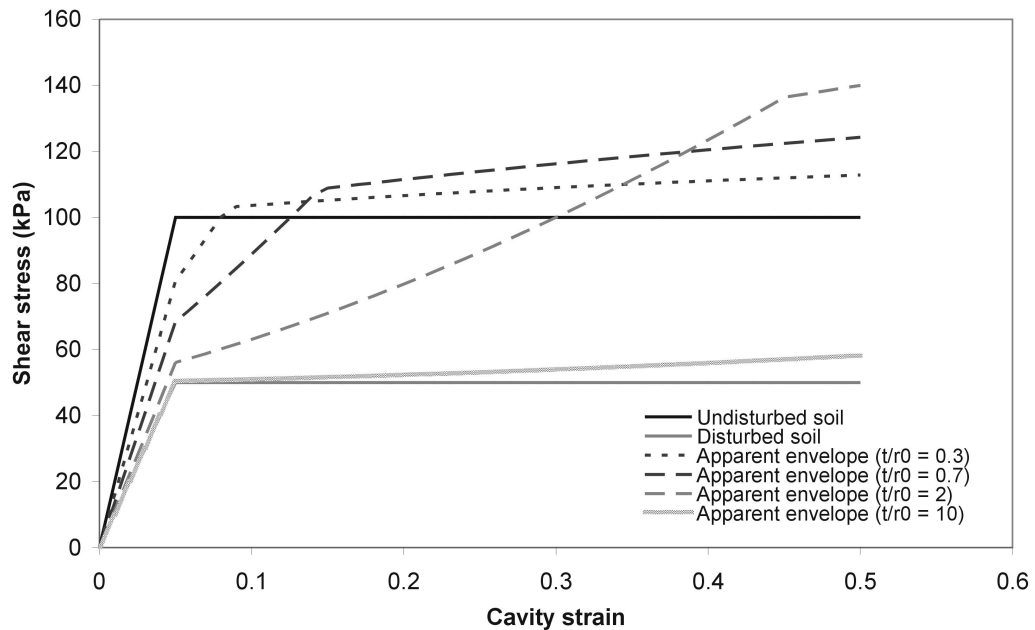


Figure 6.36 Shear stress versus cavity strain plots of undisturbed and completely disturbed soil, and apparent cases for various disturbed zone thicknesses.

Figure 6.36 suggests that the apparent shear stress increases with the cavity strain. Therefore, the apparent undrained shear strength deduced from a pressuremeter tests performed in disturbed ground should depend on the value of cavity strain.

One-dimensional numerical simulations of pressuremeter were performed for three cases with varying thicknesses of the disturbed zone. These cases are:

- a) $S_u = 100$ kPa, $l_r = 50$, disturbed zone properties are half of the undisturbed soil.
- b) $S_u = 100$ kPa, $l_r = 50$, disturbed zone properties are quarter of the undisturbed soil.
- c) $S_u = 100$ kPa, $l_r = 100$, disturbed zone properties are half of the undisturbed soil.

Figure 6.37 depicts shear stress versus cavity strain plots of undisturbed soil, and apparent cases for various disturbed zone thicknesses which are determined with one dimensional Flac (2002) simulations for case “a”.

Increase in the apparent shear strength should be reflected as a concave upward plot in the corresponding pressure versus $\ln(dV/V)$ graph, by considering that the slope of the pressure versus $\ln(dV/V)$ plot equals to the shear stress (Figure 6.38).

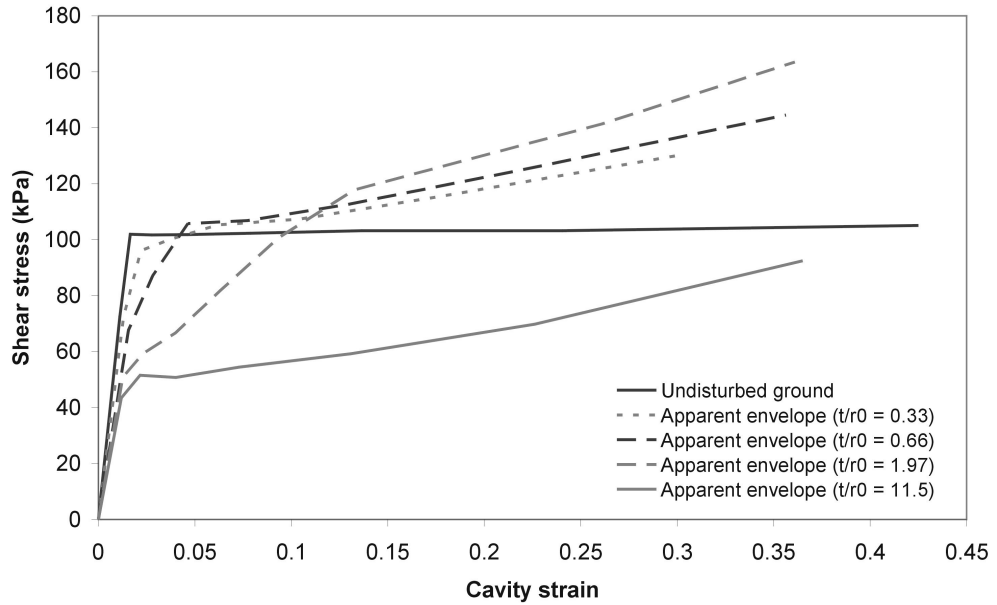


Figure 6.37 Shear stress versus cavity strain, plots of undisturbed soil, and apparent cases for various disturbed zone thicknesses which are determined with one-dimensional Flac (2002) simulations performed for case “a”.

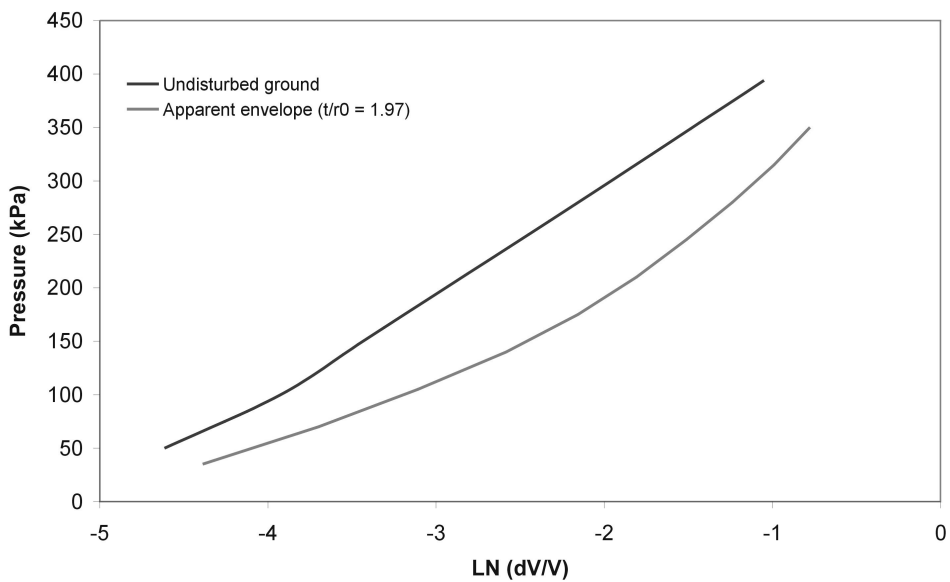


Figure 6.38 The pressure versus LN (dV/V), plots of undisturbed soil and apparent case for t/r_0 equal to 1 determined with one-dimensional Flac (2002) simulations performed for case “a”.

Both Figures 6.37 and 6.38 suggest that a pressuremeter tests performed in an undisturbed ground with significant thickness should yield an increasing shear stress towards the end of the test. The results from the one - dimensional simulation of three cases are shown in Figure 6.39. Calculations of the apparent S_u were carried out using the average value of shear strength between cavity strains of 0.3 – 0.4 since the S_u of the clay commonly determined between these values from field pressuremeter test.

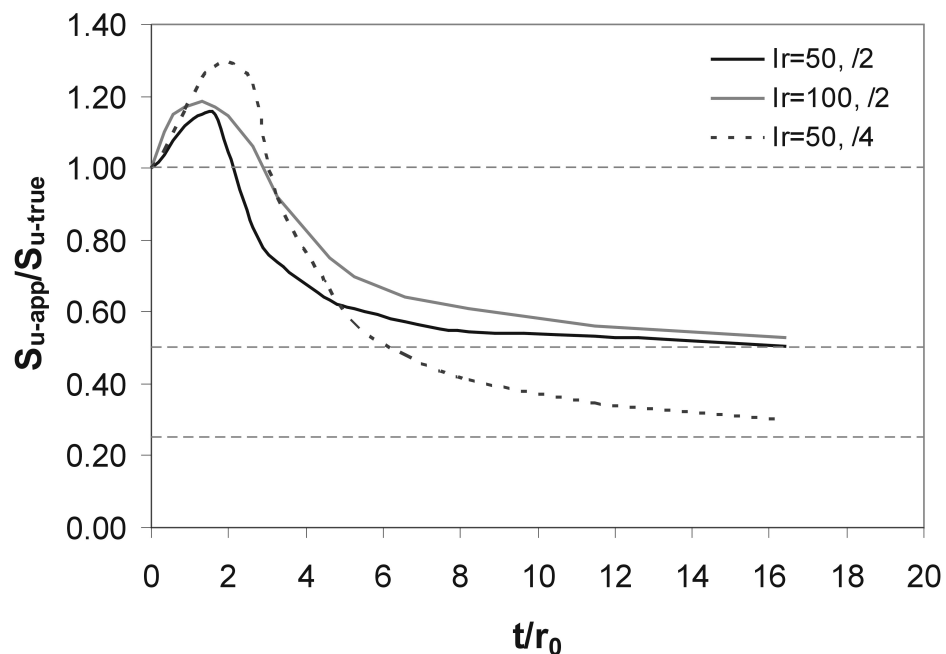


Figure 6.39 The overestimation ratio versus normalized thickness of the disturbed zone.

Increase in l_r does not have a significant effect on the apparent overestimation ratio while the ratio of the undrained strength of undisturbed and disturbed soils have significant effect on the apparent overestimation ratio (Figure 6.39). As the thickness of the disturbed zone increases, the apparent S_u approaches to the undrained strength of the disturbed soil.

6.2.1.2 Effect of unloading on the derived undrained shear strength

Pre-bored pressuremeter tests are performed in the previously drilled boreholes. Borehole opening reduces the in-situ stress states around the borehole. The effect of unloading on the undrained shear strength values deduced from the pressuremeter test was first studied by Prevost (1979), and Prapharan et al. (1990) using the strain path approach. Prapharan et al. (1990) found an overestimation of S_u about 100 % for completely unloaded case assuming unloaded state as the initial state. The experimental studies related to unloading effect were performed by Law and Eden (1982), and Benoit and Clough (1986) using a cutting shoe which was larger than the radius of the self boring probe. Their results indicate overestimation in the S_u as much as 100 %.

Analyses based on the expansion of infinitely long cylindrical cavity such as Palmer (1972), Ladanyi (1972) and Baguelin et al. (1972) assume that the reference datum (or origin) is the initial cavity radius, such that the pressure on the cavity wall at that radius is equal to the total in-situ horizontal stress. Analyzing a pressuremeter test as if it were the expansion of a cavity at the horizontal stress should be clearly identified (Clarke, 1995).

A 100 % overestimation of the S_u , which was determined by various researchers, is true when the unloaded case assumed as if the initial state is considered. Failure of selecting or correcting the reference datum obviously causes high errors in the determination of S_u . However, when the initial state is corrected, the order of the overestimation in S_u is unclear.

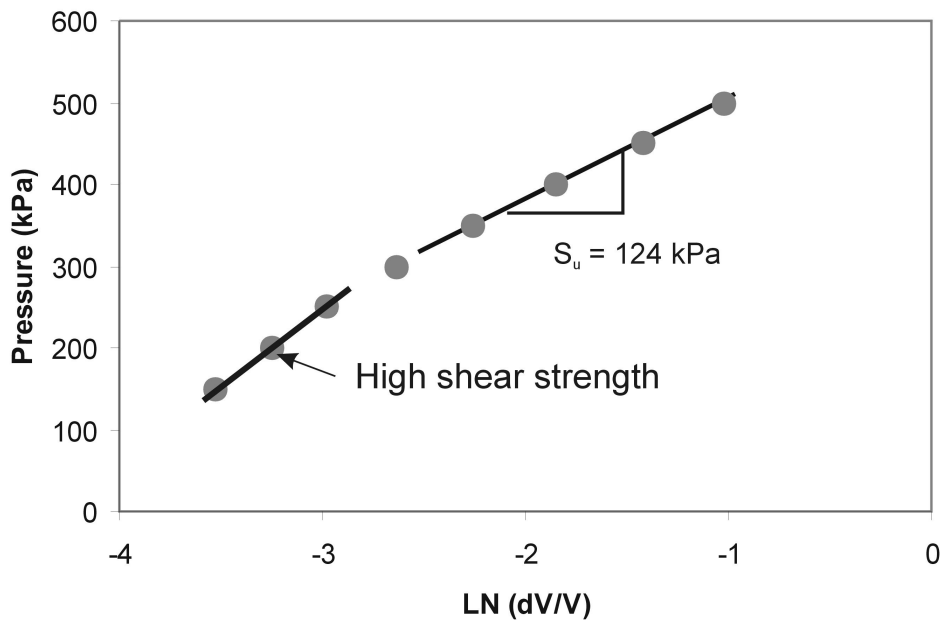
In order to clarify the effect of unloading on S_u , a series of one-dimensional numerical simulations of pressuremeter test were performed. In these simulations, S_u is taken as 100 kPa and l_r values of 50, 100, and 300 were chosen. The results of these simulations are summarized in Table 6.7. The

values given in parentheses are the S_u values determined by correcting the reference datum, while the values outside the parentheses correspond to unloaded case assumed as if the initial state. Unloading and no correction of the reference datum can cause strain softening-like behavior on the plot of $\text{LN}(dV/V)$ versus pressure plot (Figure 6.40, a) although the soil is not strain softening (Figure 6.40 b).

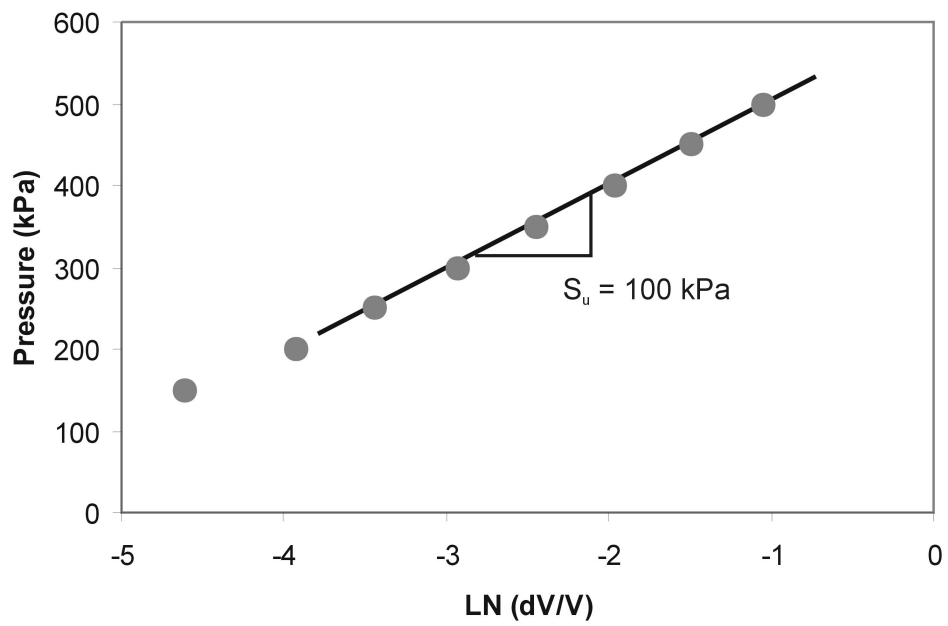
Table 6.7 The results of one-dimensional simulations for the determination of the effect of unloading on S_u .

Ir = 50			
	$\sigma_{vt} = 50 \text{ kPa}$	$\sigma_{vt} = 100 \text{ kPa}$	$\sigma_{vt} = 300 \text{ kPa}$
$K_0 = 0.5$	118.0, (100)	118.4, (100)	130.0, (112)*
$K_0 = 1.0$	119.4, (100)	124.0, (100)	184.4, (147)*
$K_0 = 1.5$	120.4, (100)	127.0, (107)*	265.0, (181.6)*
Ir = 100			
	$\sigma_{vt} = 50 \text{ kPa}$	$\sigma_{vt} = 100 \text{ kPa}$	$\sigma_{vt} = 300 \text{ kPa}$
$K_0 = 0.5$	115.0, (100)	115.6, (100)	127.7, (109)*
$K_0 = 1.0$	116.1, (100)	120, (100)	165.7, (146.7)*
$K_0 = 1.5$	118.4, (100)	126.0, (107)*	230.7, (169)*
Ir = 300			
	$\sigma_{vt} = 50 \text{ kPa}$	$\sigma_{vt} = 100 \text{ kPa}$	$\sigma_{vt} = 300 \text{ kPa}$
$K_0 = 0.5$	114.2, (100)	116.4, (100)	125.7, (107.5)*
$K_0 = 1.0$	115.2, (100)	118.1, (100)	162.0, (133.2)*
$K_0 = 1.5$	116.1, (100)	124.0, (106.4)*	227.3, (163)*

*: Some of the elements yielded during unloading



(a)



(b)

Figure 6.40 (a) Uncorrected LN(dV/V) versus pressure plot of the simulation with $I_r = 100$, $\sigma_{vt} = 100 \text{ kPa}$ and $K_0 = 1.0$ case, (b) after correction.

It is clear from Table 6.7 that no correction on the reference datum causes high errors in the determination of S_u . In addition to this observation, as the total in-situ horizontal stress increases the overestimation in apparent S_u increases, when the total in-situ horizontal stress exceeds the S_u , overestimation becomes even higher than 100 %. If the total horizontal stress exceeds the S_u value, some of the soil around the pressuremeter yields in shear. When the total horizontal stress is lower than S_u value, correction of the reference datum restores the original state, that is S_u is equal to the original value (i.e. soil behaves elastically during loading and unloading). However, if yielding occurs during unloading, correction of the reference datum does not restore the original state. As a result, pre-bored pressuremeter tests may result in significant overestimation of S_u , especially when some of the soil around the borehole yields during unloading which depends on the degree of unloading and this is possible for situations with high total horizontal in-situ stresses and low S_u values.

6.2.1.3 Pore pressure dissipation during pressuremeter test

High gradients of radial stresses are generated around the expanding pressuremeter. Wroth (1984) suggested that partial consolidation may occur within the soil resulting in an overestimation of S_u . In order to determine the amount of pore pressure dissipation in low permeability soils around the pressuremeter, one-dimensional numerical simulations were performed with Plaxis (1998) in which generation of excess pore pressures is allowed by using the undrained logic of this computer code. For the simulation, the model shown in Figure 6.41 was used. The mesh consisted of 1493 number of 15 noded triangular elements. Shear modulus is taken as 10000 kPa. Load is applied to the soil causing plastic zones and excess pore pressures. After the application of the load, a second stage is performed and in this stage the excess pore pressures allowed to dissipate for a 60 second period as in the case of a pressuremeter test. For this

stage, pore pressure dissipation at the selected points was monitored (Figure 6.41). Plaxis uses an automatic time stepping algorithm, in which smallest time step automatically selected depends on permeability, stiffness of the ground, and the smallest mesh size. As the permeability decreases and the stiffness increases the time step also increases. For very low permeabilities, such as 10^{-11} m/sec, the time step is higher than 60 sec. For this case the pore pressure dissipation at 60 sec is determined from the time versus excess pore pressure curve for selected points generated by Plaxis. The excess pore pressures determined by this way may not be precise, but the determination of excess pore pressure is only possible in this way for very low values of permeabilities. Figure 6.42 depicts the relationship between permeability and dissipation of excess pore pressures at the selected points.

Figure 6.42 suggests that for permeabilities lower than 10^{-10} m/sec there is no pore pressure dissipation. For a shear modulus lower than 10000 kPa, the dissipation of pore pressures will even be lower.

Rangeard et al. (2003) presented the results of the one-dimensional undrained simulations of pressuremeter tests for a soil with a shear modulus of 899 kPa, and permeabilities ranging between 10^{-1} to 10^{-9} m/sec using the Cam Clay model. Their results revealed that for permeabilities lower than 10^{-7} m/sec the tests are undrained (i.e pore pressure dissipation is insignificant). For a typical clay soil permeability is around 10^{-9} m/sec, therefore for clay soils, pore pressure dissipations during pressuremeter is not probably a problem. However for silts and silt – clay mixtures, pore pressure dissipations can cause overestimation of undrained shear strength.

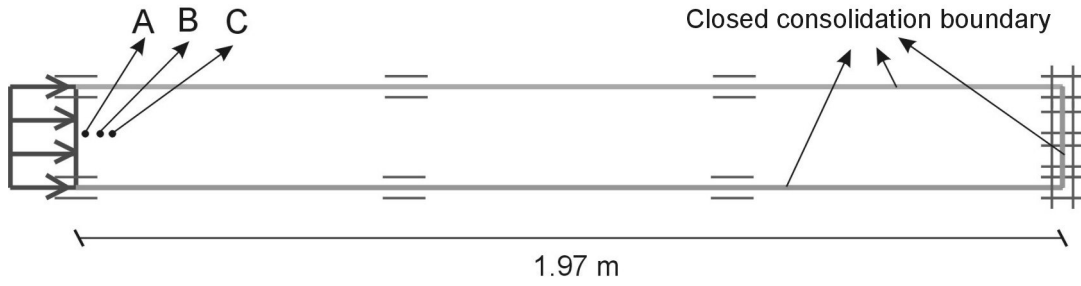


Figure 6.41 One-dimensional model used for the simulation of pore pressure dissipation.

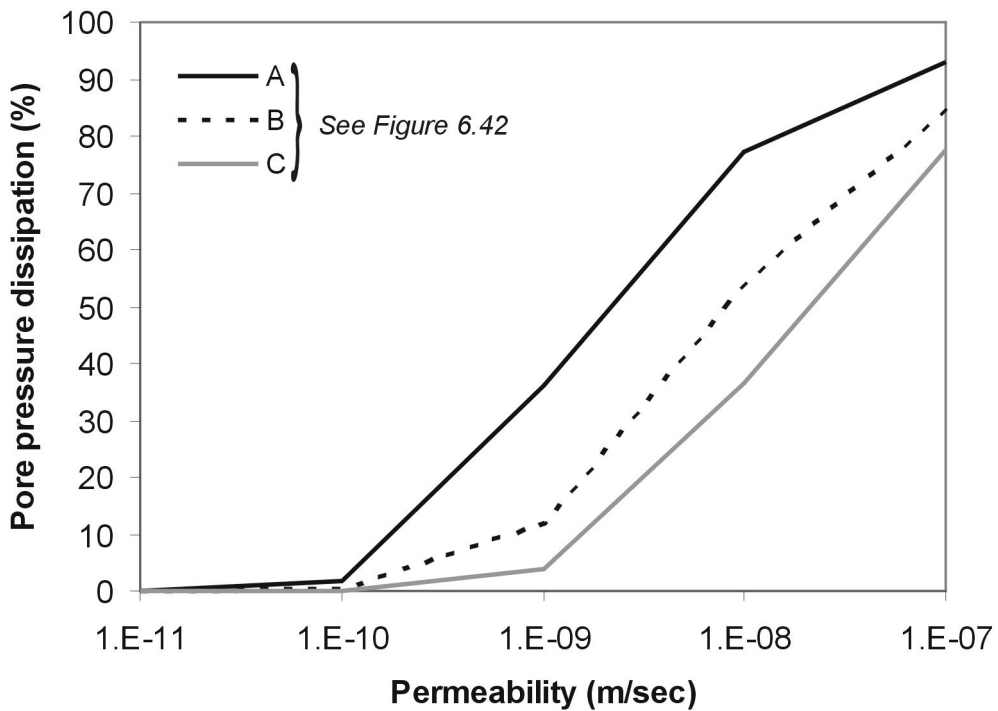


Figure 6.42 Relationship between permeability and dissipation of excess pore pressures at the selected points.

6.2.2 Two-dimensional simulation of the pressuremeter test in clays

Gambin (1995) stated that for an L/D ratio of around 2, the measured limit pressure will be closer to the limit pressure for spherical expansion than for cylindrical expansion, and therefore, higher. The conventional probes have

L/D ratios around 6, so the limit pressures obtained with conventional probes should be higher than that of infinitely long cylindrical cavities. As a result, the strength parameters obtained with conventional probes using the theories which are based on infinitely long cylindrical cavity expansion should be overestimated by some degree.

As discussed in Chapter 2, Yeung and Carter (1990), and Houlsby and Carter (1993) have analyzed this problem by using small strain finite element solutions. Yeung and Carter (1990) suggested increasing correction factors with increasing rigidity values. In contrast, Houlsby and Carter (1993) suggested decreasing correction factors with increasing rigidity values. In addition to this, Yeung and Carter (1990) stated that for tests performed in shallow depths, the overestimation in the undrained shear strength is more pronounced. However, Houlsby and Carter (1993) observed that the depth has a very insignificant effect on the S_u .

In order to clarify the effects of finite pressuremeter length on the S_u , two-dimensional large strain finite difference simulations were performed with Flac (2002). The simulations were performed at a depth of 3 m with varying rigidity (25, 50, 100, 200) and L/D values of 11, 8, 6.3, and 5.3. After this simulations, shallow and deeper simulations (1, 5 and 7 m) were carried out to control the effect of depth on results. The simulations were performed under in-situ stress free case in order to determine only the effect of L/D ratio on the S_u . Because as unloading affects the pressuremeter determined S_u . The grid used for a pressuremeter simulation at a depth of 3 m is given in Figure 6.7.

As explained previously, the slope of the linear portion of the LN(dV/V) versus pressure plot was used to derive the undrained shear strength. Comparison of the undrained shear strength values obtained from L/D ratio of 5.3 and 11 for $I_r = 25$, $S_u = 50$ kPa conditions is depicted in Figure 6.43.

The calculations were performed for various S_u values. But it was determined that the overestimation ratio is independent from the value of

S_u . In addition to this, overestimation is found to be independent of depth. In other words, the simulations performed at 1 m and other depths give almost the same slope in the $\ln(dV/V)$ versus pressure plot even for very low S_u and I_r values at a depth of 1 m. This finding is compatible with the work of Houlsby and Carter (1993). The results of the numerical simulations performed at a depth of 3 m are given in Table 6.8.

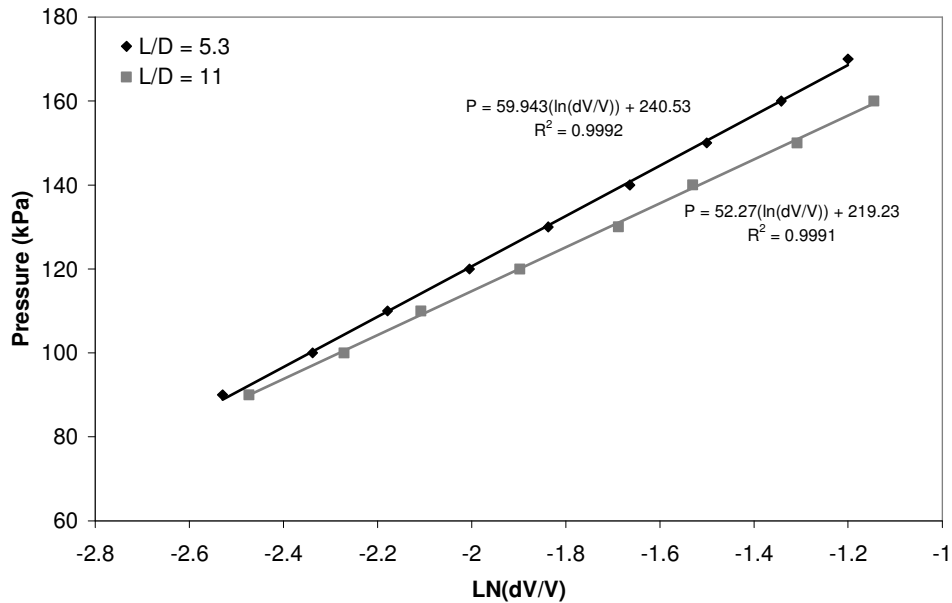


Figure 6.43 Comparison of the undrained shear strength values obtained from L/D ratio of 5.3 and 11 for $I_r = 25$, $S_u = 50$ kPa conditions.

Table 6.8 Results of numerical simulations performed in 3 meter depth.

I _r	L/D			
	5.3	6.4	8.0	11
25	0.833	0.864	0.914	0.956
50	0.820	0.859	0.911	0.960
100	0.833	0.858	0.906	0.960
200	0.820	0.867	0.909	0.960

Based on the two-dimensional simulations, the correction factors for different L/D ratios are given in Table 6.9.

Table 6.9 Correction factors for varying L/D ratios.

L/D	Correction factors for S_u
5.3	0.83
6.4	0.86
8.0	0.91
11	0.96

By using one-dimensional simulations, if the soil behaves elastically during unloading and subsequent loading by pressuremeter, the reference datum correction gives the same results with those from unloaded case. In order to explore the unloading effect on the $\text{LN}(dV/V)$ versus pressure plot, one additional two-dimensional simulation was performed under in-situ stress conditions which are effected to some degree by the borehole opening processes. This simulation consists of three steps.

- (1) Generation of in-situ stresses.
- (2) Borehole opening process.
- (3) Application of pressuremeter loading.

It was observed that after correction of the reference datum, the undrained shear strength determined from the simulation is very similar to that from unloaded case.

6.2.3 Undrained shear strength of the Eymir Lake clays

Undrained shear strength of the Eymir Lake clays determined from laboratory and field tests are compared in this section. For this purpose isotropically-consolidated triaxial compression, field vane, CPT and pressuremeter test results are used.

6.2.3.1 Cone penetration tests in the Eymir Lake clays

The cone penetration test was performed in the Eymir Lake clays with pore pressure measurement. S_u can be determined from the equipment corrected tip resistance by the following equation.

$$S_u = \frac{(q_c - \sigma_v)}{N_k} \quad (6.16)$$

Where, N_k is the cone factor and σ_v is the total in-situ vertical stress.

Methods of interpretation of undrained shear strength from CPT can be classified into two groups; namely empirical correlations and theoretical solutions. The bearing capacity based theoretical solutions yielded cone factors varying between 7 and 9.94. However, the solutions based on the cavity expansion theory yield cone factor as a function of the rigidity index (Figure 6.44).

The results of an extensive review of cone factors for normally consolidated clays by Lunne and Kleven (1981) are shown in Figure 6.45. Figure 6.45 indicates that the cone factor increases with decreasing plasticity index, and they are higher than the cone factors determined from the cavity expansion solutions.

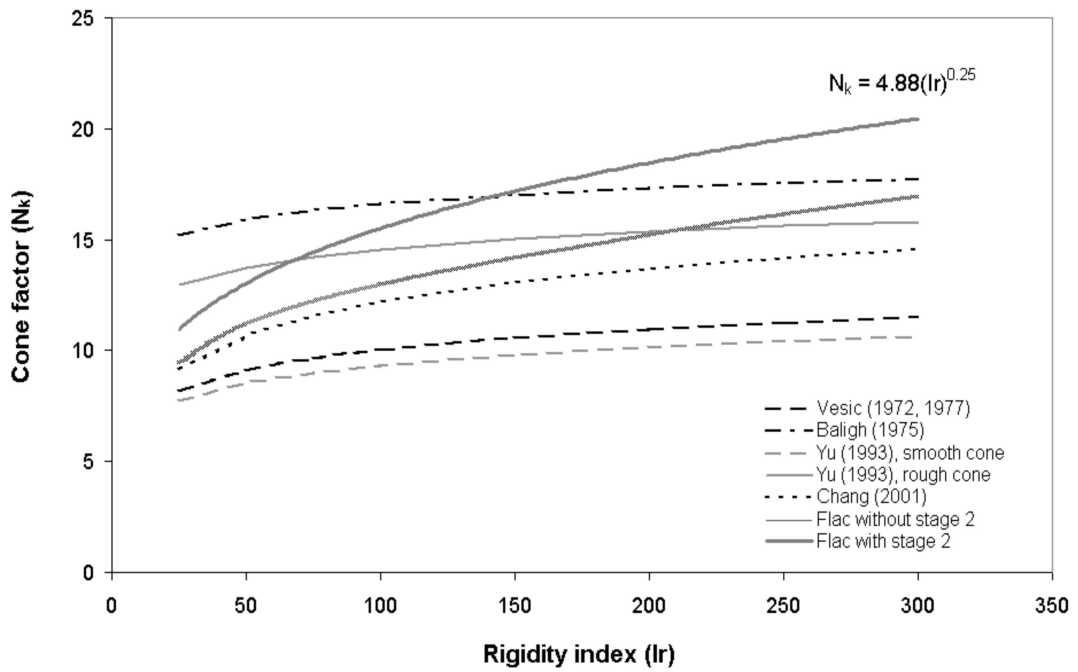


Figure 6.44 Cone factors determined from various solutions.

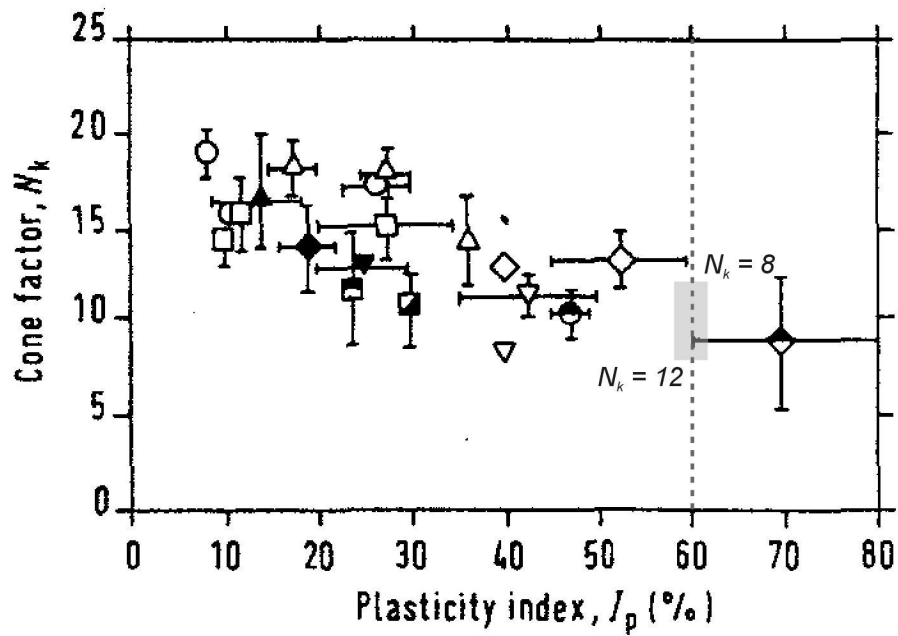


Figure 6.45 Plasticity index versus cone factors (Lunne and Kleven, 1981).

In order to determine the cone factors which are suitable for the Eymir Lake clays, finite difference simulations were performed using total stresses with elastic perfectly plastic model using Flac (2002). The finite difference grid is depicted in Figure 6.46. Cone penetration was simulated in three stages. First stage involves the generation of in-situ stress state before CPT. For this purpose in-situ stresses were applied to the mesh and appropriate K_0 value was assigned to soil by using relationships present in the literature. Second stage involves creation of a cavity in the soil mesh equivalent of the cone dimensions by simply pushing corresponding soil elements horizontally by an amount equal to the radius of the cone from a very small initial cavity radius. In the third stage, the cone was pushed downwards with a constant velocity and the total force on the cone required to maintain constant velocity was recorded with the cone displacements. During the penetration simulations, cone and soil adherence was modeled through interface elements.

It is clear that a small strain analysis could not yield a steady state tip resistance, in other words this type of simulation is not capable of modeling cone penetration (Figure 6.47). Plastic zones during cone penetration for a rigidity index of 50 and 200 are shown in Figures 6.48 and 6.49, respectively.

Plastic zones increase with increasing rigidity during cone penetration (Figures 6.48 and 6.49). In order to assess the effect of horizontal to vertical stress ratio (i.e K_0), simulations were performed with varying K_0 value. Figure 6.50 depicts the tip resistance versus cone displacement for various K_0 values. This figure suggests that the effect of K_0 on the steady state tip resistance is negligible. Therefore, remaining simulations were performed using a value of K_0 equal to 0.5 which is a typical value for the normally-consolidated clays.

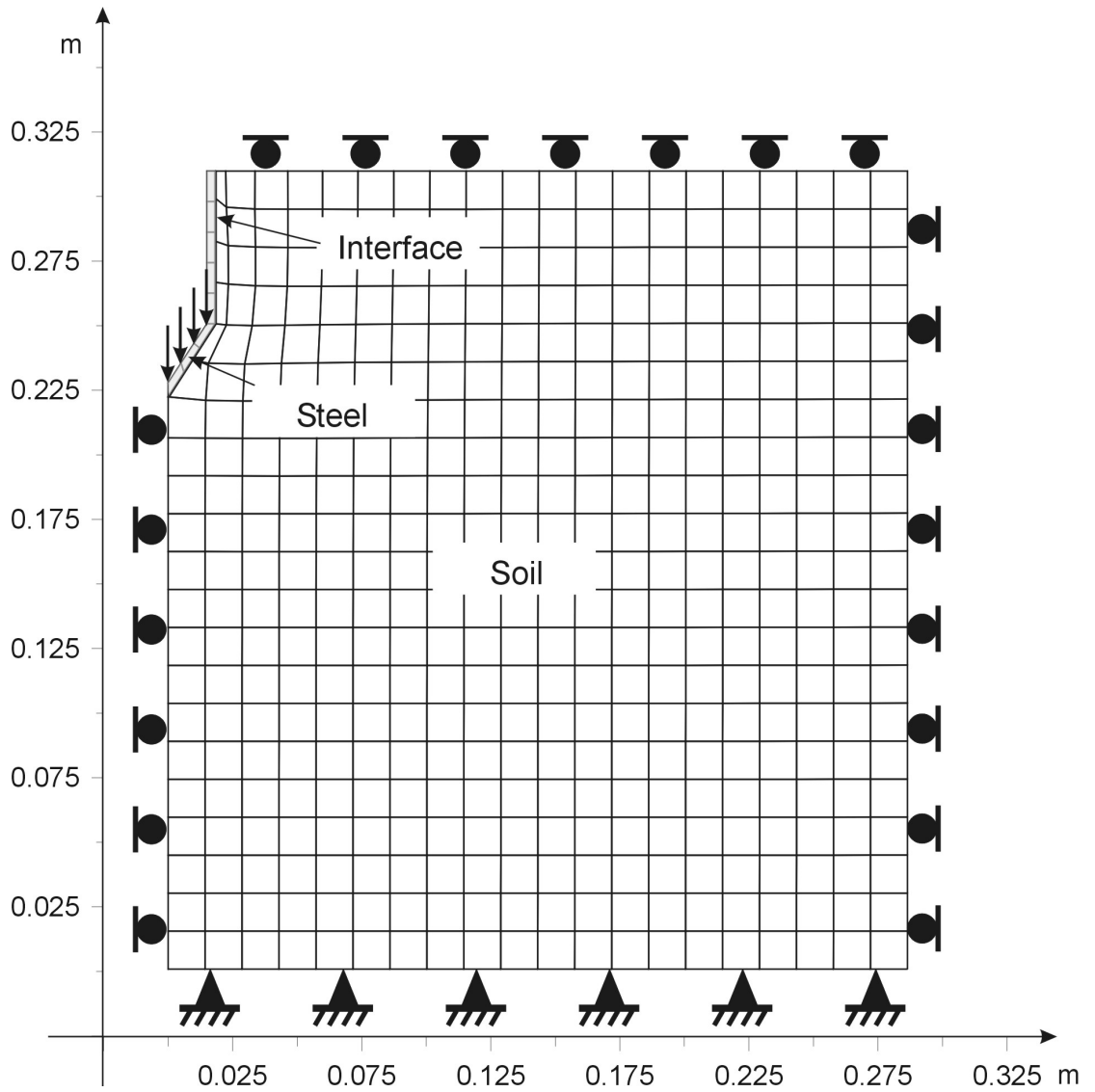


Figure 6.46 The finite difference grid and the boundary conditions used during the study.

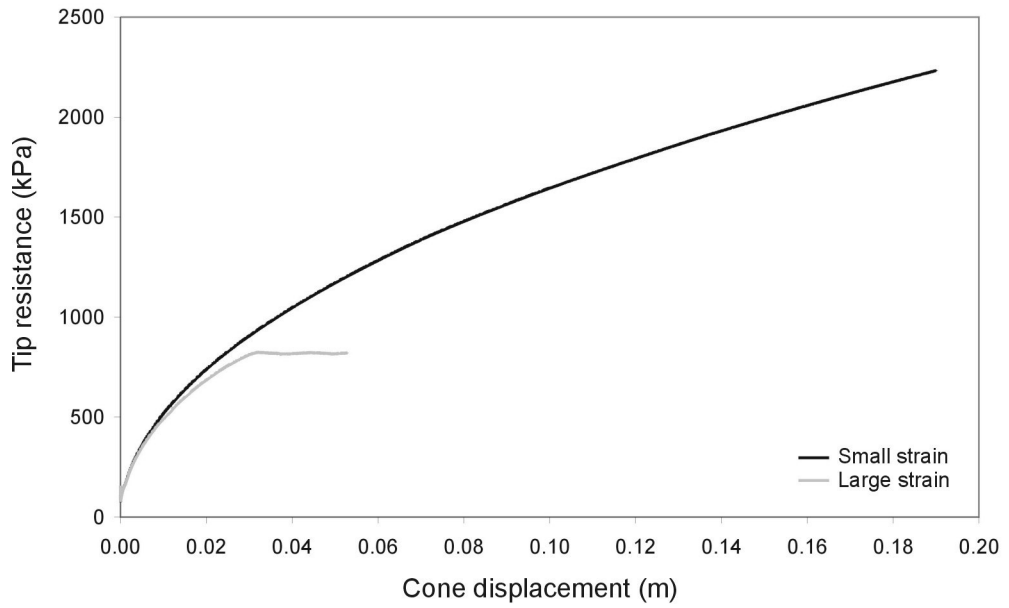


Figure 6.47 Tip resistance versus tip displacement for small and large strain simulations.

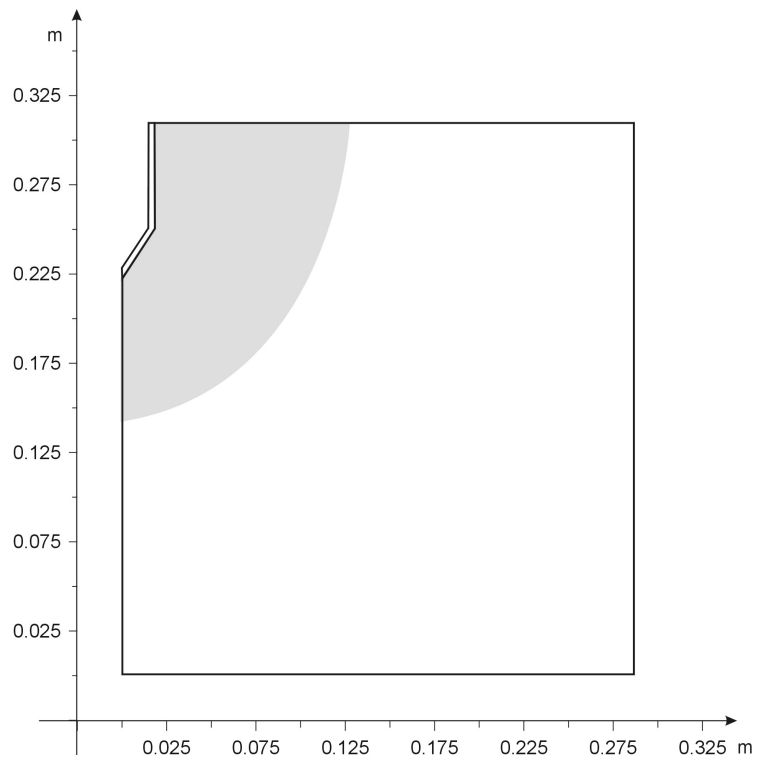


Figure 6.48 Plastic zones during cone penetration for a rigidity index of 50.

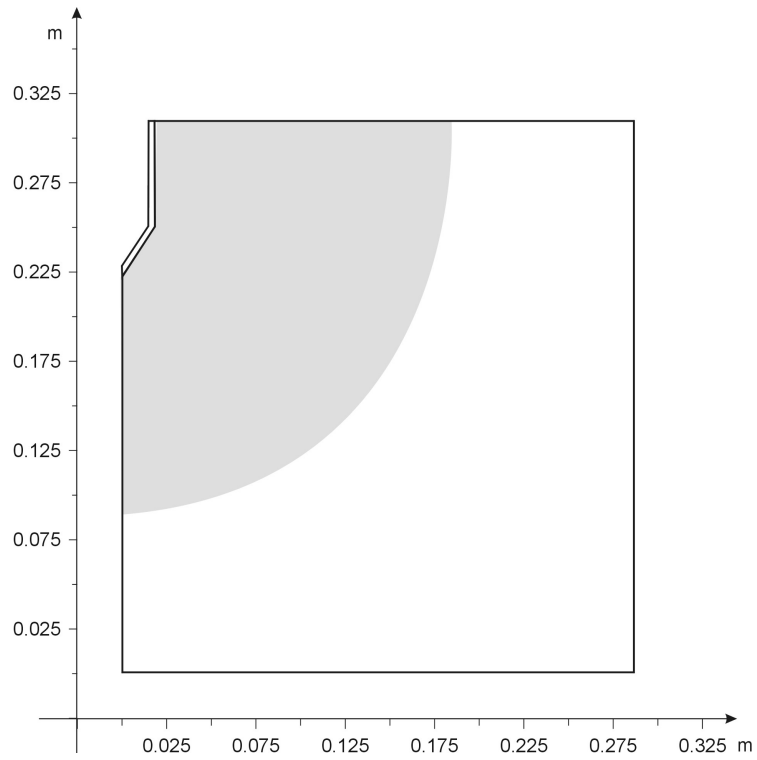


Figure 6.49 Plastic zones during cone penetration for a rigidity index of 200.

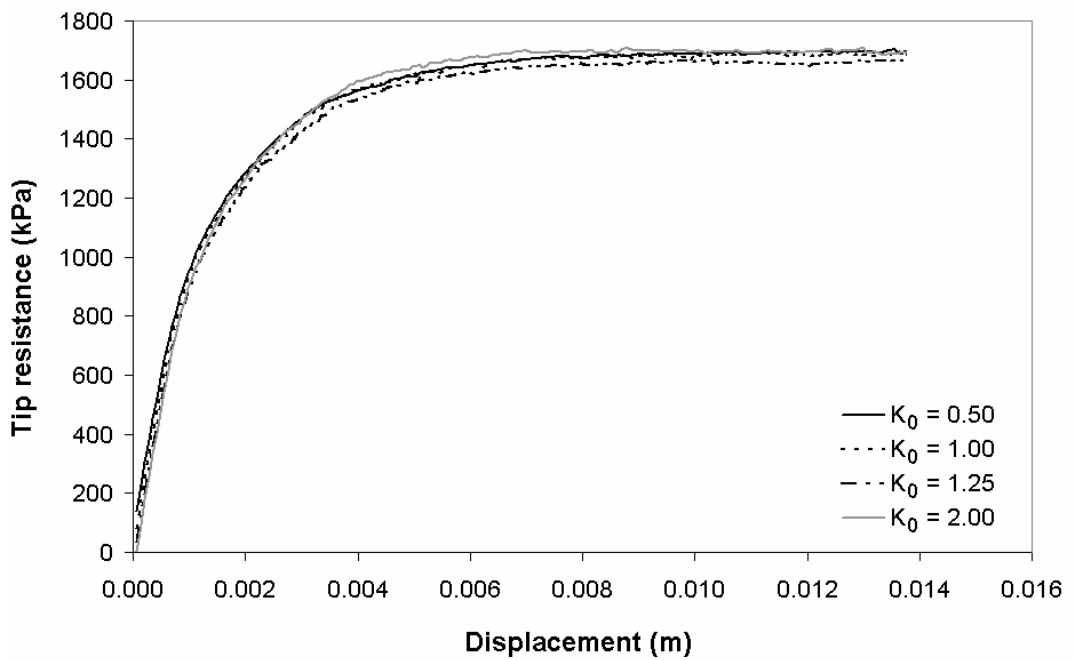


Figure 6.50 Tip resistance versus cone displacement for various K_0 values.

In this study, rigidity index values of 25, 50, 100, 200 and 300 were chosen for the undrained cone penetration simulations, because it is known that the rigidity index affects the cone factor (N_k) according to spherical cavity expansion solutions.

Variation of N_k with I_r , according to large strain finite difference simulations is presented in Figure 6.44. As it is clear from this figure, Flac simulations with stage 2 (i.e soil elements pushed horizontally by an amount equal to the radius of the cone) yielded higher cone factors than cavity expansion solutions. This difference is probably due to the fact that the cavity expansion methods model the cone penetration from the in-situ state of stress, in other words the penetration of the cone above the reference level is neglected. However, the penetration of the cone above the reference level generates higher horizontal and vertical stresses than the in-situ stresses (Figure 6.51). In order to determine the effect of second stage on the calculated cone factors, a second series of analyses were performed without pushing the soil elements horizontally. The variation of the cone factors with rigidity index determined without second stage is also shown in Figure 6.44 which is within the range of cavity expansion solutions.

Since the rigidity values of the Eymir Lake clays are about 25, the cone factor is about 11 based on the numerical simulations. As a result of the finite element simulations and the assessment from the chart of Lunne and Kleven (1983), the cone factor is selected between 8 and 12 for the determination of S_u of Eymir Lake clays from CPT.

S_u of Eymir Lake clays is determined using the theoretical technique of Palmer (1972), Ladanyi (1972) and Baguelin et al. (1972), and empirical methods of Komornik et al. (1969), Amar and Jezequel (1972), and Marshland and Randolph (1977). Datum correction of pressuremeter test results are performed according to the suggestions of Mair and Wood (1987) and Clarke (1995).

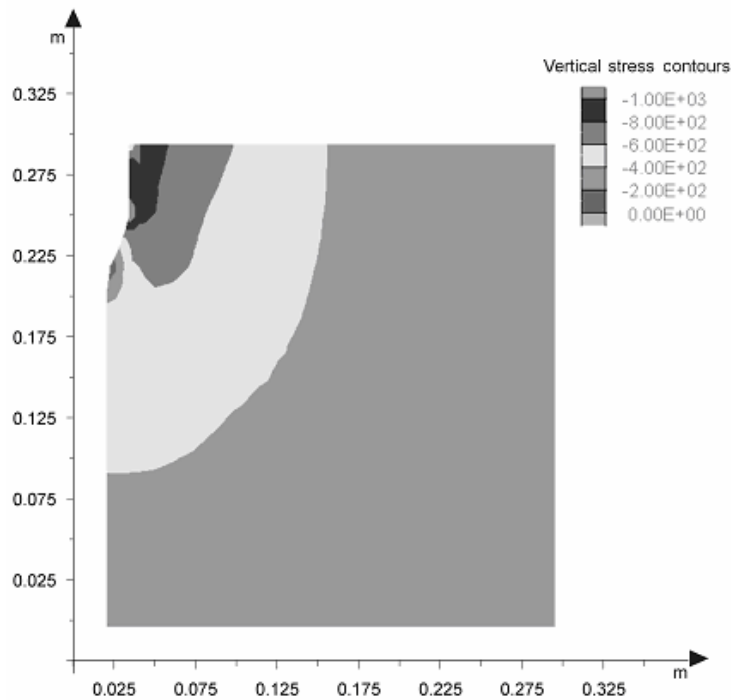
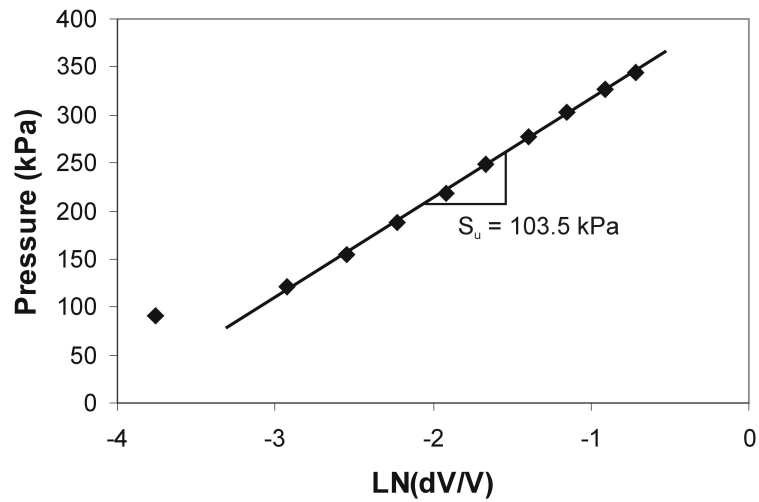


Figure 6.51 Vertical stress distribution due to second stage of the cone penetration simulation.

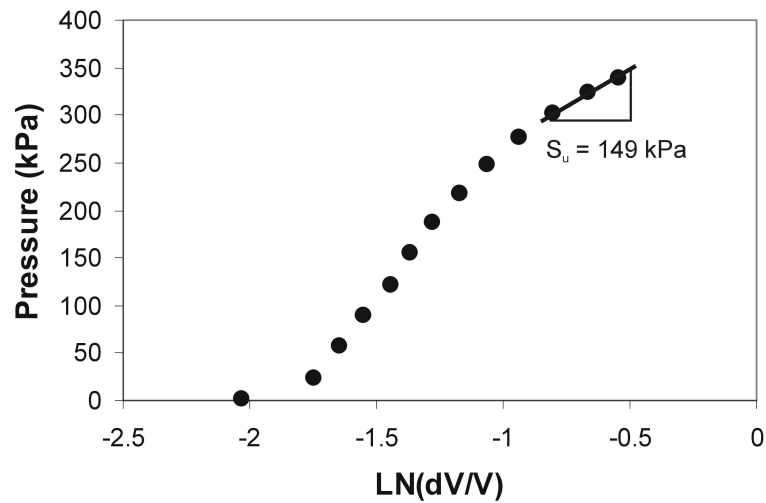
Table 6.10 S_u determined from pressuremeter tests.

Depth (m)	S_u (kPa)
1.0	56.8
2.0	103.5
3.0	106.7
4.2	105.6
5.3	181.0
6.8	165.9
8.0	198.9

Figure 6.52 displays the pressure versus $\ln(dV/V)$ plot for the pressuremeter test performed in 2 meter depth a) for uncorrected and b) datum corrected. The undrained shear strengths of determined from pressuremeter are summarized in Table 6.10. The variation of undrained shear strength of the Eymir Lake clay with depth, determined by various tests is depicted in Figure 6.53.



(a)



(b)

Figure 6.52 The pressure versus LN(dV/V) plot for the pressuremeter test performed at a depth of 2 m (a) for uncorrected, and (b) datum corrected cases.

S_u determined from laboratory vane tests and UU tests are slightly lower than those determined from CU tests, therefore, S_u determined from CU tests are used for comparison. Figure 6.53 suggests that the S_u determined using the theoretical solution of Palmer (1972) is higher than S_u determined from CPT, FVT and CU tests. If the L/D ratio correction applied to the values of S_u determined from Palmer (1972)'s solution, S_u from

pressuremeter approaches to S_u from FVT, however, there is still overestimation. This overestimation is probably due to the differences in mode of failure, presence of disturbed zone around the pressuremeters. S_u determined from pressuremeter by empirical methods are close to those determined from CPT, FVT and CU tests.

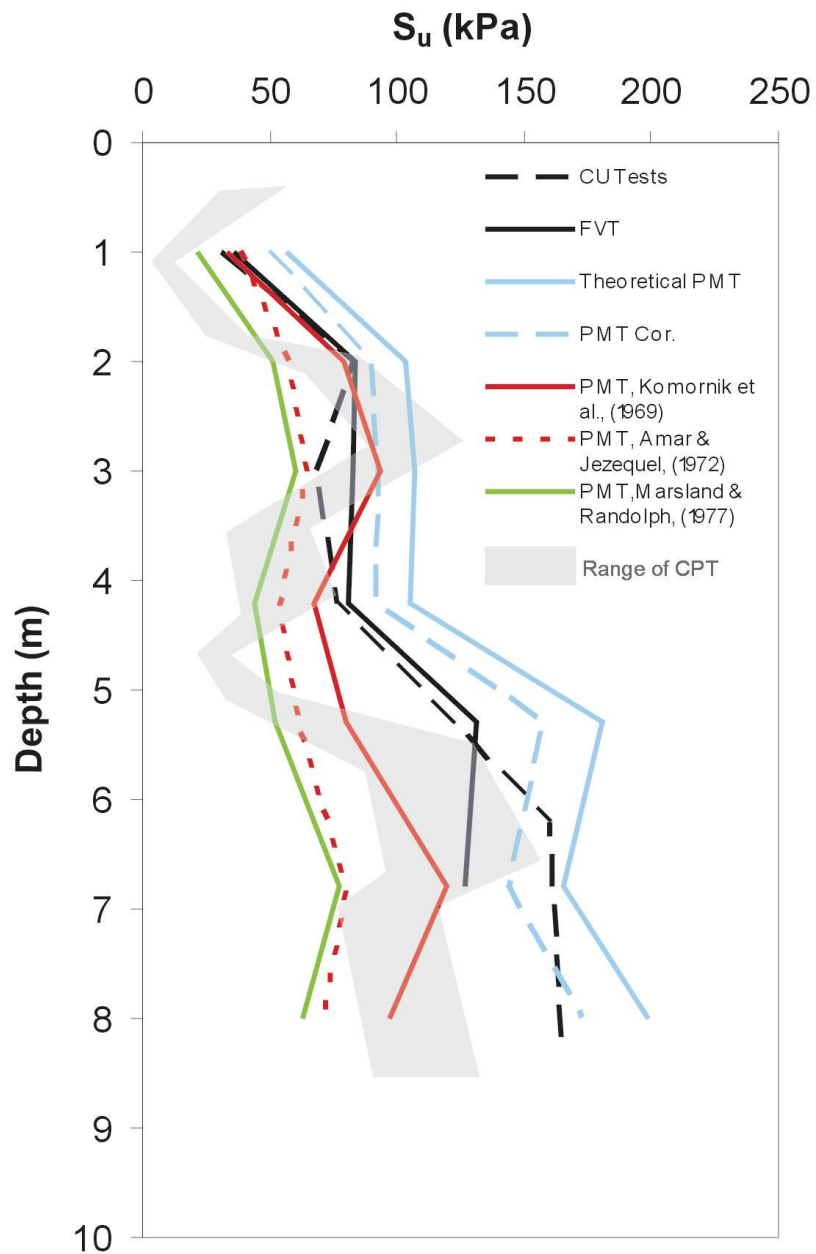


Figure 6.53 Variation of undrained shear strength of the Eymir Lake clay determined by various tests.

6.3 Inverse Analysis Technique

There is no solution for the estimation of the shear strength parameters (both c and ϕ) from the pressuremeter test. However, by using the inverse analysis technique, shear strength parameters of the materials under consideration can be determined. Perfect match between the real test curve and the simulation curve can only be obtained by using only one values of shear modulus, c and ϕ values. Determination of the shear modulus is straightforward from the slope of the elastic portion of the pressuremeter curve. Therefore remaining parameters, c and ϕ have to be determined by trial and error procedure.

For the highly weathered andesites, the inverse analysis technique was applied to the pressuremeter test results performed at a depth of 1.5 m in Solfasol district. The borehole for the purpose of pressuremeter testing was drilled using continuous flight auger without using water in order to achieve minimal disturbance to the ground. The volumetric strain obtained from the pressuremeter test converted to cavity strain and then this cavity strain is converted to radial displacement for the comparison of the experimental curve with the numerical curve. One major problem with the inverse analysis is the determination of the in-situ stress state prior to the pressuremeter test. However, it should be determined because for frictional soils the in-situ stress is an important factor for the shear strength. Vertical effective stress can be estimated considering the unit weight, depth of the layer and the location of the water table. However, the estimation of the lateral effective stress is difficult. Although it is difficult to estimate the in-situ horizontal stress state from pre-bored pressuremeters, the point at which pseudo – elastic phase is close to the active pressure, so the in-situ horizontal stress is higher than the pressure at the start of the pseudo-elastic phase. For the inverse analysis, the horizontal stress is estimated

from pressuremeter test results. Figure 6.54 shows curve matching procedure and obtained geotechnical parameters for the highly weathered andesite from Solfasol district at a depth of 1.5 m.

From a nearby borehole to PMT borehole, an undisturbed sample was obtained from the same depth for direct shear box testing in UU condition. The shear strength parameters obtained from the direct shear box test are $c = 83.3$ kPa and $\phi = 30.1^\circ$. No other undisturbed sample could be obtained from deeper elevations. Shear strength parameters obtained from the inverse analysis are close to those deduced from the direct shear box test.

The same inverse analysis technique was applied to verify the procedure to the highly weathered andesites of Pursaklar district. In this site, two boreholes were drilled next to each other. Figure 6.55 displays curve matching procedure and obtained shear strength parameters for the highly weathered andesite in this district at a depth of 3.2 m.

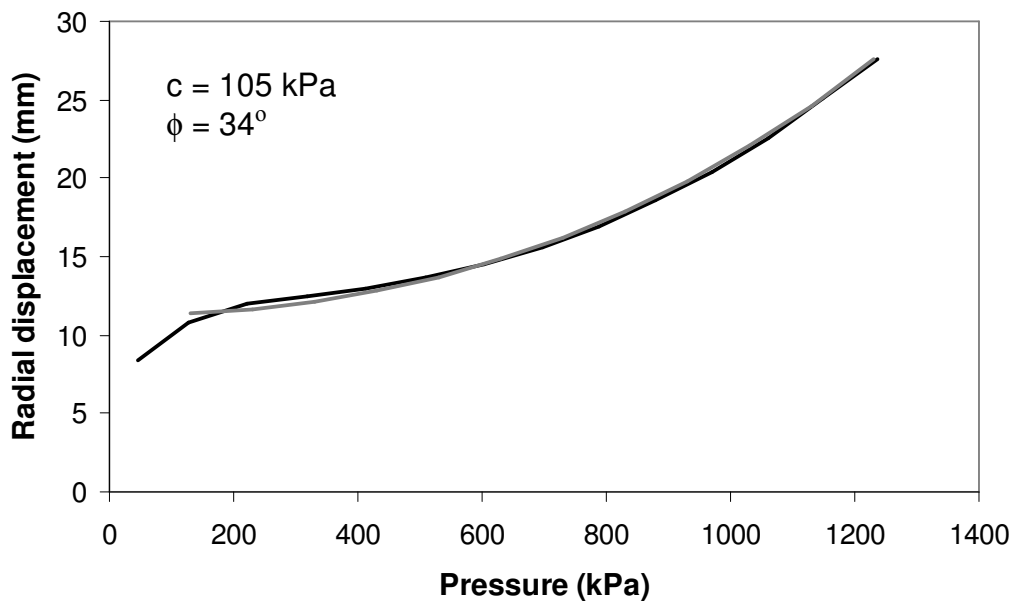


Figure 6.54 Curve matching procedure and obtained geotechnical parameters for the highly weathered andesite from Solfasol district at a depth of 1.5 m.

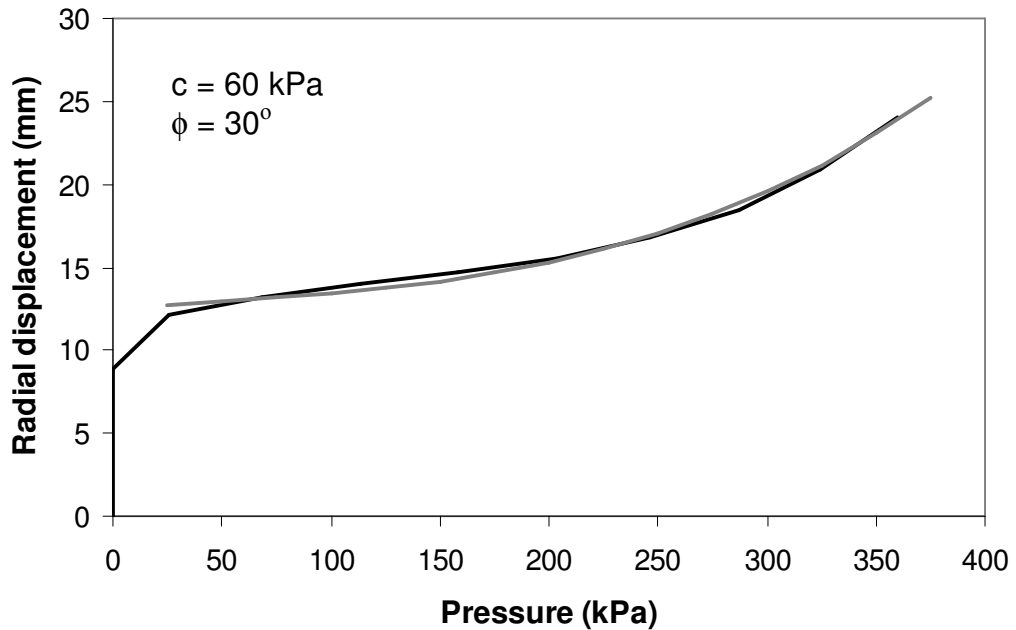


Figure 6.55 Curve matching procedure and obtained shear strength parameters for the highly weathered andesite in Pursaklar district at a depth of 3.2 m.

The shear strength parameters obtained from the direct shear box test are $c = 54.7$ kPa, $\phi = 29.7^\circ$. If the shear strength parameters obtained by inverse analysis technique are compared to those obtained by the direct shear box testing it can be concluded that the inverse analysis technique yields compatible values of shear strength. In order to apply inverse analysis technique, plastic stage of the pressuremeter curve should be available i.e. the pressure capacity of the device should be adequate for the strength of the geomaterial under consideration. For the rock masses with high strength, cylindrical dilatometers can be used instead of pressuremeter to obtain pressure – radial displacement relationship, therefore, the use of inverse analysis technique for higher strength rock masses should be performed with the data obtained from the cylindrical dilatometers.

However, obtaining same parameters with inverse analysis technique and any other shear strength determination test should not be expected identical, because of the differences in disturbance levels and stress - strain paths followed during testing. This procedure can be applied to any kind of geomaterial to obtain shear strength parameters without the necessity of obtaining undisturbed samples. This is especially very important for very weak rocks. In spite of these advantages, two disadvantages may limit the use of this technique. To use the inverse analysis technique, a numerical analysis (finite element, finite difference) software with the ability of axisymmetric 2 dimensional large strain modeling of geomaterials, (especially Mohr – Coulomb failure criterion) should be available. The procedure is somewhat time consuming due to the required trial and error procedure.

CHAPTER 7

CONCLUSIONS AND RECOMMENDATIONS

Two dimensional finite difference simulations revealed that, as the L/D ratio decreases the calculated value of shear modulus slightly increases. But as the difference is minor, it can be suggested that the L/D ratio and testing depth do not have an effect on the calculated shear modulus.

By varying the thickness of the disturbed zone in simulations, it was found out that the thickness of the disturbed zone has a very important underestimation effect on the measured modulus.

According to the two dimensional numerical simulations, it was determined that volume of the rock mass tested by 30 cm diameter plate is 323600 cm³, whereas the volume of the rock mass tested by a standard pressuremeter is 18200 cm³. As it is clear, the volume of the rock mass tested by a pressuremeter is very small compared to the volume of the rock mass tested by a 30 cm plate. Therefore, care must be taken during the determination of the modulus of the rock mass.

Regression analyses suggest that the GSI is a better index of rock mass classification than the RMR for Dikmen greywackes. Equations are suggested for the estimation of the deformation modulus values of Dikmen greywackes using GSI and RMR.

The comparison of the deformation modulus values obtained from pressuremeter test and UCS tests performed on andesites cropping out in

Solfasol, Ovacık and Pursaklar districts, suggests that although the deformation modulus determined from the pressuremeter is slightly lower than those from uniaxial compression tests, the values are close to each other, probably due to pressuremeter tests performed in a rock mass condition which is close to intact rock.

Variation of the ratio of rock mass modulus to intact rock modulus (E_m/E_i) with RQD was obtained for mudrocks cropping out around Sincan.

The values of deformation modulus obtained from the pressuremeter tests and UU triaxial tests (secant modulus values at 50 % yield stress) are similar to each other except for those at a depth of 3 m. It can be concluded that from the slope of the pseudo-elastic phase, pre-bored pressuremeter test yields average deformation modulus as soon as the disturbance during drilling operations kept minimum. The values of initial tangent modulus determined from the UU tests are larger than the values of maximum deformation modulus (calculated from the minimum slope of the pseudo – elastic phase). This is due to the fact that initial stress – deformation part of pressuremeter curve corresponds to the contact of probe with the borehole, and the initial tangent modulus could not be obtained from Ménard pressuremeter due to this phenomenon.

One-dimensional analyses performed for the determination of the effect of disturbance on the undrained shear strength deduced from pressuremeter test, suggest that pressuremeter tests performed in an undisturbed ground with significant thickness should yield an increasing shear stress towards the end of the test. Increase in rigidity index does not have a significant effect on the apparent overestimation ratio, while the ratio of the undrained strength of undisturbed and disturbed soils have significant effect on the apparent overestimation ratio. As the thickness of the disturbed zone increases, the apparent undrained shear strength approaches to the undrained strength of the disturbed soil.

Unloading and not correcting the reference datum can cause strain softening like behavior on the plot of $\ln(dV/V)$ versus pressure plot although the soil is not strain softening and this causes high errors in the determination of S_u . In addition to this observation, it was determined that as the total in-situ horizontal stress increases the overestimation in apparent S_u increases, when the total in-situ horizontal stress exceeds the S_u , overestimation becomes even higher than 100 %. If the total horizontal stress exceeds the S_u value, some of the soil around the pressuremeter yields in shear. When the total horizontal stress is lower than S_u value, correction of the reference datum restores the original state. However, if yielding occurs during unloading, correction of the reference datum does not restore the original state. As a result, pre-bored pressuremeter tests may result in significant overestimation of S_u , especially when some of the soil around the borehole yields during unloading which depends on the degree of unloading.

Numerical pore pressure dissipation analyses revealed that for permeabilities lower than 10^{-10} m/sec there is no pore pressure dissipation. For a shear modulus lower than 10000 kPa, the dissipation of pore pressures will even be lower.

It was determined that the overestimation ratio in undrained shear strength is independent of depth. Based on the two-dimensional simulations, the correction factors for different L/D ratios are suggested.

Comparison of undrained shear strengths of Eymir Lake clays determined from laboratory and field tests suggests that the S_u determined using the theoretical solution of Palmer (1972) is higher than S_u determined from CPT, FVT and CU tests. If the L/D ratio correction applied to the values of S_u determined from Palmer (1972)'s solution, S_u from pressuremeter approaches to S_u from FVT, however, there is still overestimation. This overestimation is probably due to the differences in mode of failure, presence of disturbed zone around the pressuremeters.

The applicability of the inverse analysis was checked using the direct shear box and pressuremeter tests in weathered andesites. It can be concluded that this procedure yields compatible values of shear strength.

For further research, the deformation modulus of the greywackes should be determined from plate load tests and should be compared to those determined from pressuremeter tests. The applicability of the deformation modulus values determined from plate load test and pressuremeter tests should also be checked by using the observations from engineering projects.

In order to fully understand the effect of discontinuities during borehole expansion tests, three-dimensional discrete element simulations of test should be carried out using various discontinuity orientations and properties.

For the estimation of the friction angle of granular soils, numerical simulations can be performed using advanced constitutive models.

For the determination of L/D effect on the undrained shear strength, calibration chamber studies and/or field tests using different probes with various L/D ratios can be performed.

REFERENCES

- Amar, S., and Jézéquel, J. –F., 1972, “Essais en place et en laboratoire sur sols cohérents: comparaisons des résultats”, Bulletin de Liaison des Laboratoires de Ponts et Chaussées, No. 58, pp. 97 – 108.
- Amar, S., Baguelin, F., Jézéquel, J. –F., and Le Méhauté, A., 1975, “In situ shear resistance of clays”, Proceedings of the Conference on In Situ Measurement of Soil Properties, American Society of Civil Engineers, Raleigh, North Carolina, Vol. 1, June, pp. 22 – 44.
- Andresen, A., Berre, T., Kleven, A., and Lunne, T., 1979, “Procedures used to obtain soil parameters for foundation engineering in the North Sea”, Marine Geotechnology, 3, pp. 201 – 266.
- Apageo Segelm, 1997, “Training on the Pressuremeter Test Principle”, France.
- Arıkan, F., 2002, “A weathering classification of acidic volcanic rocks for engineering purposes”, Hacettepe University, Geological Engg. Dept., 245 p.
- ASTM, 1994a, “D 2573, Standard test method for performing electronic friction cone and piezocone penetration testing of soils”, Book of ASTM Standards, Philadelphia.
- ASTM, 1994b, “D 2573, Standard test method for field vane shear test in cohesive soil”, Annual Book of ASTM Standards, Philadelphia.

- ASTM, 1995, "D 4767, Standard test method for consolidated undrained triaxial compression test for cohesive soils", Annual Book of ASTM Standards, Philadelphia.
- ASTM, 1998, "D 3080, Standard test method for direct shear test of soils under consolidated drained conditions", Annual Book of ASTM Standards, Philadelphia.
- ASTM, 1999, "D 2850, Standard test method for unconsolidated-undrained triaxial compression test on cohesive soils", Annual Book of ASTM Standards, Philadelphia.
- ASTM, 2000, "D 4719, Standard test method for pressuremeter testing in soils", Annual Book of ASTM Standards, Philadelphia.
- ASTM, 2001, "D 2435, Test method for one-dimensional consolidation properties of soils", Annual Book of ASTM Standards, Philadelphia.
- Aubeny, C. P., Whittle, A. J., and Ladd, C. C., 2000, "Effects of disturbance on undrained strengths interpreted from pressuremeter tests" ASCE J. Geotech. and Geoenviron. Engineering, 126, 12, pp. 1133 – 1144.
- Baguelin, F., Jézéquel, J. F., Le Mée, and Le Méhauté, A., 1972, "Expansion of cylindrical probes in cohesive soils" J. Soil Mech. Fdn. Div. ASCE, 98, SM 11, pp. 1129 – 1142.
- Baguelin, F., Jézéquel, J. -F., and Le Méhauté, A., 1973, "Etude des pressions interstitielles développées lors de l'essai pressiométrique", Proceedings of the Eighth International Conference on Soil Mechanics and Foundation Engineering, Moscow Vol. 1.1, pp. 19 – 24.

- Baguelin, F., Jézéquel, J. F., and Shields, D. H., 1978, "The Pressuremeter and Foundation Engineering", Trans Tech Publications, Germany, p 617.
- Bakişkan, İ., 1978, "Shear strength of two clays in the Ankara region", MSc Thesis, Middle East Technical University, Ankara, 114 p.
- Baligh, M. M., 1975, "Theory of deep static cone penetration resistance". Report No. R75 – 56, Department of Civil and Environmental Engineering, MIT, USA.
- Barton, N., 2002, "Some new Q value correlations to assist in site characterization and tunnel design", Int. J. Rock Mech. Min. Sci., 39, pp. 185 – 216.
- Barton, N. R., Lien, R., Lunde, I., 1974, "Engineering classification of rock masses for the design of tunnel supports", Rock Mechanics, 6 (4), pp. 189 – 239.
- Benoit, J., and Clough, G. W., 1986, "Self boring pressuremeter tests in soft clay", J. Geotech. Engrg., ASCE, 112 (1), pp. 60 – 78.
- Bieniawski, Z., T., 1972, "Propagation of brittle fracture in rock", Proceedings, 10th Symposium on Rock Mechanics, AIME, pp. 409 – 427.
- Bieniawski, Z. T., 1973, "Engineering classification of jointed rock masses", Trans. South African Inst. Civil Eng., 15, pp. 335 – 344.
- Bieniawski, Z. T., 1978, "Determining rock mass deformability: Experience from case histories", Int. Journal of Rock Mechanics and Mining Sciences, 15, p. 237 – 247.

- Bieniawski, Z. T., 1989, "Engineering Rock Mass Classifications", John Wiley and Sons, 237 pp.
- Bowles, J. E., 1996, "Foundation Analysis and Design", McGraw-Hill, USA, 1175 p.
- Cambou, B., and Lainer, J., 1988, "Induced anisotropy in cohesionless soil: experiments and modeling", Computers and Geotechnics, 6, pp. 291 – 311.
- Cambou, B., Boubanga, A., Bozetto, P., and Haghgou, M., 1990, "Determination of constitutive parameters from pressuremeter tests", Pressuremeters, Proc. of the Symp. on Pressuremeters, British Geotechnical Society, pp. 243 – 252.
- Cambridge In-situ, 2005, "csbp leaflet 2", http://www.cambridge-insitu.com/csbp_leaflet2.html, Last date accessed: 13 May 2005.
- Cao, L. F., Teh, C. I. and Chang, M. F., 2001, "Undrained cavity expansion in modified cam clay I, theoretical analysis." Geotechnique, 51, 4, pp. 323-334.
- Centre D'Etudes Ménard, 1975, "Interpretation and Application of Pressuremeter Test Results to Foundation Design", Sols-Soils No:26, Paris.
- Chang, M. F., Teh, C. I. and Cao, L. F., 2001, "Undrained cavity expansion in modified cam clay II. Application to the interpretation of the piezocone test", Geotechnique, 52(4), 307-311.
- Chaput, E., 1931, "Ankara mıntıkasının 1/135000 mıkyasında jeolojik haritasına dair izahat", İstanbul Darülf. Jeol. Enst. Neşriyatı, 7, 46 p.
- Clarke, B. G., 1993, "The interpretation of pressuremeter tests to produce design parameters", Predictive Soil Mechanics, Proc. Wroth Memorial Symp., Oxford, pp. 75 – 88.

- Clarke, B. G., 1995, "Pressuremeters in Geotechnical Design", Blackie Academic & Professional, Great Britain, 364 p.
- Clayton, C. R. I., Matthews, M. C., and Simons, N. E., 1995, "Site Investigation", Blackwell Science, Great Britain, p. 584.
- Collins, I. F., and Yu, H. S., 1996, "Undrained cavity expansion in critical state soils", International Journal for Numerical and Analytical Methods in Geomechanics, 20, pp. 485 – 516.
- Combarieu, O., and Canépa, Y., 2001, "The unload – reload pressuremeter test", Bulletin Des Laboratoires Des Ponts Et Chaussées, Reference 4381, pp. 37 – 67.
- Craig, R. F., 1992, "Soil Mechanics", ELBS, Great Britain, 427 p.
- Çalgın, R., Pehlivanoğlu, H., Ercan, T, and Şengün, M., 1973, "Ankara civarı jeolojisi", M.T.A. Enst. Jeol. Dairesi, Rapor No: 18, 55 p., (unpublished).
- Çapan, U. Z., and Buket, E., 1975, "Aktepe-Gökdere bölgesinin jeolojisi ve ofiyolitli melanj", Türkiye Jeol. Kur. Bült., 18, S.1, pp. 11 – 16.
- Çevik, S., Y., 2000, "Hoek – Brown Görgül yenilme ölçütü ve jeolojik dayanım indeksinin gelişimi: Ankara grovaklarında (Beytepe Kampüsü) bir uygulama", Hacettepe Üniversitesi Mühendislik Fakültesi Jeoloji Mühendisliği Bölümü, Proje Çalışması (Jeo 462), 83 p.
- Dağar, Z., Öztümer, E., Sirel, E., and Yazlak, Ö., 1963, "Ankara civarında birkaç stratigrafik kesit", Türkiye Jeol. Kur. Bült., 8, S.1-2, pp. 84 – 95.
- Deere, D. U., and Miller, R. P., 1966, "Engineering classification and index properties for intact rock", Technical Report No. AFNL-TR-65-116, Air Force Weapons Laboratory, New Mexico.

- Denby, G. M., 1978, "Self-boring pressuremeter study of San Fransisco Bay Mud, PhD Thesis, University of Stanford.
- Dixon, S. J., 1970, "Pressure meter testing of soft bedrock, determination of the in-situ modulus of deformation of bedrock", ASTM, STP 477, Betlehem.
- D.S.İ., 1976, "Ankara Mürted ovası hidrojeoloji etüd raporu", D.S.İ Genel Müdürlüğü Jeoteknik Hizmetler ve Yeraltısuları Dairesi Başkanlığı Yayını, 49 p.
- Duncan, J. M., and Chang, C. Y., 1970, "Non-linear analysis of stress-strain in soils", Journal of the Soil Mechanics and Foundation Eng. Div., 96, SM5, pp. 1625 – 1653.
- Elliott, G. M., 1982, "An Investigation of a yield criterion for rock, PhD Thesis", University of London.
- Erol, O., 1954, "Ankara ve civarının jeolojisi hakkında rapor", M.T.A. Enst. Bilimsel Dökümantasyon Şubesi, Derleme No. 2491, 238 p.
- Erol, O., 1961, "Ankara bölgesinin tektonik gelişmesi" Türkiye Jeol. Kur. Bül." C. 7, S.2 57 – 85.
- Erol, O., 1968, "Ankara çevresinde Paleozoik arazisinin bölümleri ve Paleozoik – Mesozoik sınırı hakkında", Türkiye Jeol. Kur. Bült, 9, S1-2, pp. 1 – 20.
- Ertürk, E., 1997, "Ankara kenti kuzeyindeki (Solfasol mahallesi) rezidüel toprakların mühendislik özellikleri ve şev duraylılığı sorunları", Master Tezi, Hacettepe Üniversitesi, Ankara, 70 p.

- Ferreira, R. S., and Robertson, P. K., 1992, "Interpretation of undrained self-boring pressuremeter test results incorporating unloading", *Can. Geotech. J.*, 29, pp. 918 – 928.
- Flac., 2002, *Fast Lagrangian Analysis of Continua Users Guide*", Itasca Consulting Group, Inc. Minnesota, 55415, USA.
- Gambin, M., 1995, "Reasons for the success of Ménard pressuremeter", Fourth International Symposium on Pressuremeters, Sherbrooke, Canada.
- Ghionna, V. N., Jamilowski, M., Lacasse, S., Ladd, C. C., Lancelotta, R., and Lunne, T., 1983, "Evaluation of self – boring pressuremeter", *Proc. Int. Symp. Soil and Rock Investigations by In-situ Testing*, Paris, Vol. 2, pp. 294 – 301.
- Gibson, R. E., and Anderson, W. F., 1961, "In-situ measurement of soil properties with the pressuremeter" *Civ. Engng. Pub. Wks. Rev.* 56, No. 658, pp. 615 – 618.
- Goodman, R. E., and Duncan, J. M., 1971, "The role of structure and solid mechanics in the design of surface and underground excavations in rock, *Proc. Conf. on Structure*", *Solid Mechanics and Engineering Design*, Part 2, Paper 105, Wiley, New York, p. 1379.
- Goodman, R. E., 1989, "Introduction to Rock Mechanics", John Wiley and Sons, New York.
- Gökçeoğlu, C., 1997, "Killi, yoğun süreksizlik içeren ve zayıf kaya kütlelerinin mühendislik sınıflamalarında karşılaşılan güçlüklerin giderilmesine yönelik yaklaşımlar.", PhD Thesis, H.Ü. Fen Bil. Enst., 214 p (unpublished).

- Gökçeoğlu, C., Sönmez, H., and Kayabaşı, A., 2003, "Predicting the deformation moduli of rock masses", *International Journal of Rock Mechanics & Mining Sciences*, 40, p. 701 – 710.
- Gökçeoğlu, C., and Zorlu, K., 2004, "A fuzzy model to predict the uniaxial compressive strength and the modulus of elasticity of a problematic rock", *Artificial Intelligence*, 17, pp. 61 – 72.
- Gökçeoğlu, C, Yeşilnacar, E., Sönmez, H., Kayabaşı, A., 2004, "A neuro – fuzzy model for modulus of deformation of jointed rock masses", *Computers and Geotechnics*, 31, pp. 375 – 383.
- Göncüoğlu, C., 2005, "Personal communication", METU Geological Engineering Department, Ankara.
- Greenland, 1964, "Economic loading tests with the Ménard pressuremeter", *Proceedings of the Symposium on the Economic use of Soil Testing*, Birmingham.
- Hagedoorn, J. G., 1959, "The plus-minus method of interpreting seismic refraction sections", *Geophys. Prosp.*, 7, pp. 158 – 182.
- Head, K. H., 1986, "Manual of Laboratory Testing: Volume 2 Permeability, Shear Strength and Compressibility Tests", Pantech Press, London, 747 p.
- Henderson, G., Smith, P. D. K., and St John, H. D., 1979, "The development of the push-in pressuremeter for offshore soil investigation", *Proc. Conf. Offshore Site Invest.*, Society for Underwater Technology, London, pp. 159 – 167.
- Hoek, E., and Brown, E. T., 1997, "Practical estimates of rock mass strength", *International Journal of Rock Mechanics & Mining Sciences*, 34(8), p. 1165 – 1186.

- Hoek, E., 1999, "Putting numbers to geology – an engineer's view point", *Quarterly Journal of Engineering Geology*, 32, pp 1 – 19.
- Houlsby, G. T., and Witters, N. J., 1988, "Analysis of the cone pressuremeter test in clay", *Geotechnique*, 38, 4, pp. 575 – 587.
- Houlsby, G. T., and Yu, H. S., 1990, "Finite element analysis of the cone pressuremeter test, Pressuremeters, Proc. of the Symp. on Pressuremeters, British Geotechnical Society, pp. 221 – 230.
- Houlsby, G. T., and Carter, J. P., 1993, "The effects of pressuremeter geometry of the results of tests in clay", *Géotechnique*, 43, 4, pp. 567 – 576.
- Houlsby, G. T., and Carter, J. P., 1995, "Discussion on the effects of pressuremeter geometry of the results of tests in clay", *Géotechnique*, 45, 4, pp. 741 – 748.
- Hughes, J. M. O., Wroth, C. P., and Windle, D., 1977, "Pressuremeter tests in sands", *Géotechnique*, 27, 4, pp. 455 – 477.
- ISO, 1999, "13320-1, Particle size analysis – laser diffraction method, Part 1 General Principles", Geneva, Switzerland.
- ISRM, 1981, "ISRM suggested methods: rock characterization, testing and monitoring". E. T. Brown (ed.), Pergamon Press, London, 211 pp.
- Jefferies, M. G., 1988, "Determination of horizontal geostatic stress in clay with self-bored pressuremeter", *Can. Geotech. J.*, 25, 3, pp. 559 – 573.
- Karacan, E., 1984, "Ankara andezitlerindeki kırık ve çatlakların jeomekanik çözümlenmesi", *Yük. Müh. Tezi*, Hacettepe Üniversitesi, Ankara, 123 p.

- Karpuz, C., 1982, "Rock mechanics characteristics of Ankara andesites in relation to their degree of weathering", PhD Thesis, Middle East Technical University, Ankara.
- Kasapođlu, K. E., 1980, "Ankara kenti zeminlerinin jeo-mühendislik özellikleri", Doçentlik Tezi, H: Ü. Jeoloji Müh. Bölümü, Beytepe, Ankara, 206 p.
- Kayabaşı, A., Gökçeođlu, C., and Ercanođlu, M., 2003, "Estimating the deformation modulus of rock masses: a comparative study", International Journal of Rock Mechanics & Mining Sciences, 40, p. 55 – 63.
- Komornik, A., and Frydman, S., 1969, "A study of in-situ testing with pressuremeter", Proc. of the Conf. organized by the British Geotechnical Society in London, pp. 145 – 154.
- Kulhawy, F. H., 1975, "Stress deformation properties of rock and rock discontinuities", Engineering Geology, 9, 4, pp. 327 – 350.
- Kulhawy, F. H., 1978, "Geomechanical model for rock foundation settlement", Journal of Geotechnical Engineering, ASCE, 104, pp. 211 – 227.
- Kulhawy, F. H., and Mayne, P. W., 1990, "Manual on Estimating Soil Properties for Foundations Design", Report EL – 9800 to Electric Power Research Institute, Cornell University, Ithaca, New York.
- Kumtepe, P., 1996, "Ankara yöresi grovaklarının kütle dayanımının ve elastisite moduölünün ampirik ilişkilerle belirlenmesi ve anizotropi özelliklerinin araştırılması", Hacettepe Üniversitesi Fen Bilimleri Enstitüsü, MSc thesis, 68 p.

- Lacasse, S., D'orazio, T. B., and Bandis, C., 1990, "Interpretation of self-boring and push-in pressuremeter tests", Pressuremeters, Proc. of the Symp. on Pressuremeters, British Geotechnical Society, pp. 273 – 308.
- Ladanyi, B., 1972, "In-situ determination of undrained stress – strain behaviour Sensitive clays with the pressuremeter" Can. Geotech. J. 9, pp. 313 – 319.
- Ladd, C. C., Germaine, J. T., Baligh, M. M., and Lacasse, S. M., 1980, "Evaluation of self boring pressuremeter tests in Boston blue clay", Report FWHA/RD-80/052., Washington DC: Federal Highway Authority.
- Lade, P. V., and Oner, M., 1984, "Elasto-plastic stress-strain model, parameter evaluation, and predictions for dense sand", Constitutive Relations for Soils, Balkema, pp. 154 – 174.
- Lamé, G., 1852, "Leçons sur la théorie mathématique de l'élasticité des corps solides, Bachelier, Paris.
- Law, K, and Eden, W. J., 1982, "Effects of disturbance on pressuremeter tests, Proc. ASCE Conf. On Updating Subsurface Samplings of Soils and Rocks and Their In Situ Testing", Santa Barbara, California, pp. 292 – 303.
- Leuchs, K., 1944, "İç Anadolu Tersiyer arazisinin taksimi hakkında (Trans. Şevket Birand)", Ankara Yüksek Ziraat Enst. Dergisi, 1, 2, pp. 614 – 643.
- Lunne, T. and Kleven, A., 1981, "Role of CPT in North Sea foundation engineering (in Cone penetration testing and experience", Edited by G. M. Norris and R. D. Holtz). Proc. Session sponsored by Geotechnical Engineering Division at Am. Soc. Civ. Engrs. National Convention, St. Louis (Missouri), pp. 76 – 107.

- Lunne, T., Robertson, P. K., and Powell J. J.M., 1997, "Cone Penetration Testing in Geotechnical Practice", Blackie Academic & Professional, London.
- Mahmoud, M., Evans R. J., and Trenter N. A., 1990, "The use of pressuremeter test in weak rocks at the port of Jebel Ali", Pressuremeters Proc. of the Third Int. Symp. On Pressuremeters, organized by British Geotechnical Soc., Thomas Telford, London, pp. 341 – 350.
- Mair, R. J., and Wood, D. M., 1987, "Pressuremeter Testing", Ciria Butterworths, London.
- Marshland, A., and Randolph, M. F., 1977, "Comparisons of the results from pressuremeter tests and large in-situ plate tests in London Clay", *Géotechnique*, 27, 2, pp. 217 – 243.
- Matsuoka, H., and Nakai, T., 1977, "Stress – strain relationship of soil based on the spatially mobilized plane", Proc. 9th Int. Conf. Soil Mech., Tokyo, Special Session 9, pp. 153 – 162.
- Ménard, L., 1956, "An apparatus for measuring the strength of soils in place" M. Sc. Thesis, University of Illinois, Urbana, IL.
- Ménard, L., 1961, "Influence de l'amplitude et de l'histoire d'un champ de contraintes sur le tassement d'un sol de foundation", C. R. 5 e Congrès International MSTF, tome 1, Paris.
- Mitri, H. S., Edrissi, R., and Henning J., 1994, "Finite element modeling of the cable – bolted stopes in hard rock ground mines", Presented at the SME annual meeting, New Mexico, Albuquerque, p. 94 – 116.
- Morgenstern, N. R., and Price V. E., 1965, "The analysis of the stability of general slip surfaces", *Geotechnique*, Vol. 15, No. 1, pp. 77 – 93.

- Nadai, A., 1950, "Theory of Flow and Fracture of Solids", Vol. 1, McGraw – Hill Book Company Inc., NewYork.
- Nathaneil, I., 1972, "Laboratory determination of some static and mechanical properties of Ankara andesite", Ms. Thesis, Middle East Technical University, Ankara, 162 p.
- Nicholson, G. A., and Bieniawski, Z. T., 1990, "A nonlinear deformation modulus based on rock mass classification" International Journal of Min. Geol. Eng., 8, p. 181 – 202.
- Norman, T., 1972, "Ankara Yahşihan bölgesinde Üst Kretase-Alt tersiyer istifinin stratigrafisi", Türkiye Jeol. Kur. Bült., 15, 2, pp. 180 – 276.
- Norman, T., 1973, "Ankara melanjinin yapısı hakkında", Cumhuriyetin 50. Yılı, Yerbilimleri Kongresi Tebliğleri, M.T.A. Enst. Yayını, pp. 77 – 94.
- Nurlu, Y. E., 1996, "Ankara grovaklarının bozunma derecelerinin saptanması – sınıflandırılması ve haritalandırılması", Yüksek Lisans Tezi, Hacettepe Üniversitesi Fen Bilimleri Enstitüsü.
- Oyo Corporation, 2005, "elastmeter-2", <http://www.oyo.co.jp/english/busi/productinfo/elastmeter-2.html>, Last date accessed:13 May 2005.
- Özdoğan, N., 1973, "Laboratory determination of dynamic elastic constants of Ankara andesite by resonant frequency techniques", Ms. Thesis, Middle East Technical University, Ankara, p. 111.
- Özilcan, S., 2004, "Ankara Batısı (Bilkent – Beytepe – Beysukent – Ümitköy) zeminlerinin jeo-mühendislik özellikleri", Yüksek Lisans Tezi, Hacettepe Üniversitesi Fen Bilimleri Enstitüsü.
- Palmer, A. C., 1972, "Undrained plain strain expansion of a cylindrical cavity in clay: a simple interpretation of the pressuremeter test", Géotechnique, 22, pp. 451 – 457.

- Palmstörn, A., and Singh, R., 2001, "The deformation modulus of rock masses – comparisons between in situ tests and indirect estimates", *Tunneling and Underground Space Technology*, 16, pp. 115 – 131.
- Penumadu, D., Skandarajah, A., and Chameau, J. L., 1998, "Strain – rate effects in pressuremeter testing using a cuboidal shear device: experiments and modelling", *Can. Geotech. J.*, 35, pp. 27 – 42.
- Plaxis, 1998. "Finite element code for soil and rock analyses" Balkema, Netherlands.
- Powell, J. J. M., 1990, "A comparison of four different pressuremeters and their methods of interpretation in a stiff heavily overconsolidated clay", *Pressuremeters, Proc. of the Symp. on Pressuremeters*, British Geotechnical Society, pp. 287 – 298.
- Prapcharan, S., Chameau, L., Altschaeffl, A. G., and Holtz, R. D., 1990, "Effect of disturbance on pressuremeter results in clays", *Journal of Geotechnical Engineering, ASCE*, 116, 1, pp. 35 – 53.
- Prevost, H., 1979, "Undrained shear tests on clay" *J. Geotech. Engrg.Div.ASCE*, 105 (1), pp. 49 – 64.
- Pyrah, I. C., Anderson, W. F. and Pang, L. S., 1988, "Effects of test procedure on constant rate of strain pressuremeter tests in clay", *Proc. 6 th Conf. Numerical Methods in Geomechanics*, Innsbruck, pp. 647 – 652.
- Rangear, D., Hicher, P. Y., and Zentar, R., 2003, "Determining soil permeability from pressuremeter tests", *Int. Jour. for Num. An. Methods in Geomechanics.*, 27, 1, pp. 1 – 24.
- Rimrock Geophysics, 1992, "User's Guide to SIP programs".

- Robertson, P. K., and Hughes, J. M. O., 1986, "Determination of properties of sand from self-boring pressuremeter tests, Proc. 2nd Int. Symp. Pressuremeter Marine Appl., Texam, USA, ASTM STP 950, pp. 283 – 302.
- Robertson, P. K., and Ferreira, R. S., 1993, "Seismic and pressuremeter testing to determine soil modulus", Predictive Soil Mechanics, Proc. Wroth Memorial Symp. Oxford, pp. 434 – 448.
- Roy, M., Juneau, R., La Rochelle, P., and Tavenas, F., 1975, "In-situ measurement of the properties of sensitive clays by pressuremeter tests", Proceedings of the Specialty Conference on In-situ Measurement of Soil Properties, ASCE, Raleigh, North Carolina, Vol. 1, pp. 350 – 372.
- Salgado, F. M., and Bryne, P. M., 1990, "Finite element analysis of pressuremeter chamber tests in sand", Pressuremeters, Proc. of the Symp. on Pressuremeters, British Geotechnical Society, pp. 209 – 218.
- Serafim, J. L., and Perreira, J. P., 1983, "Considerations on the geomechanical classification of Bieniawski" In: Proceedings of the Symposium on Engineering Geology and Underground Openings. Portugal, Lisboa. P. 1133 – 1144.
- Shields, D., and Bauer, G., 1975, "Determination of the modulus of deformation of a sensitive clay using laboratory and In situ tests", Proceedings of the Specialty Conference on In Situ Measurement of Soil Properties, American Society of Civil Engineers, Raleigh, North Carolina, Vol. 1, pp. 395 – 421.
- Silvestri, V., 1998, "On the determination of the stress – stain curve of the clay from the undrained plain – strain expansion of hollow cylinders: a long forgotten method", Canadian Geotechnical Journal, 35, pp. 360 – 363.

- Slide, 2003, "2D Limit Equilibrium Slope Stability for Soil and Rock Slopes Users Guide", Rocscience, Toronto.
- Sönmez, H., and Ulusay, R., 1999, "Modifications to the geological strength index (GSI) and their applicability to stability of slopes", International Journal of Rock Mechanics and Mining Sciences, 36, 6, pp. 219 – 233.
- Sönmez, H., and Ulusay, R., 2002, "A discussion on the Hoek – Brown failure criterion and suggested modifications to the criterion verified by slope stability case studies", Yerbilimleri, 26, p. 77 – 99.
- Sönmez, H., Gökçeoğlu, C., and Ulusay, R., 2004, "Indirect determination of the modulus of deformation of rock mass based on the GSI system", International Journal of Rock Mechanics Mining Sciences, 41, pp. 849 – 857.
- Sülükçü, S., and Ulusay, R., 2001, "Evaluation of the block punch index test with prime consideration on size effect, failure mechanism and its effectiveness in predicting rock strength", Int. J. Rock Mech. Min. Sci., 38(8), pp. 1091 – 1111.
- Tan, Y., and Kaya, A., 1988, "Aşağı Çorum Havzası Deriner Barajı Elastmeter 200 Deney Sonuç raporu", Elektrik İşleri Etüd İdaresi Genel Müdürlüğü Yayını, 88, 25.
- UDEC, 2000, "UDEC Universal Distinct Element Code User's Guide", Itasca Consulting Group, Inc. Minnesota , USA.
- Ulusay, R., 1975, "Ankara kenti kuzey – orta bölgesinin jeo-mühendislik özellikleri", Yüksek Lisans Tezi, Hacettepe Üniversitesi, Jeoloji Mühendisliği Bölümü, Ankara, 81 p.

- Ulusay, R., 1991, "Geotechnical evaluations and deterministic design considerations for pitwall slopes at Eskişehir (Yatağan – Muğla) strip coal mine", PhD Thesis, Middle East Technical University, Geological Engineering Dept., Ankara, Turkey, 340 p.
- Ulusay, R., and Gökçeoğlu, C., 1997, "The modified block punch index test", *Can. Geotech. J.*, 34, pp. 991 – 1001.
- Ulusay, R., and Gökçeoğlu, C., 1998, "An experimental study on the size effect in block punch index test", *Int. J. Rock Mech. Min. Sci.*, 35 (4-5), pp. 628 – 629 (In: NARMS'98 ISRM International Symposium, Cancun, Mexico, Paper No. 008).
- Ulusay, R., Gökçeoğlu, C., and Sülükçü, S., 2001, "Draft ISRM suggested method for determining block punch strength index (BPI)", *International Journal of Rock Mechanics and Mining Sciences*, 38, pp. 1113 – 1119.
- Vesic, A. S., 1972, "Expansion of cavities in infinite soil mass", *Journal of the Soil Mechanics and Foundations Division, ASCE*, 98, pp. 265 – 290.
- Vesic, A. S., 1977, "Design of pile foundations, national Cooperative Highway Research Program", *Syntesis of Highway Practice 42*, Transportation Research Board, National Research Council, Washington, D. C.
- Wawersik, W. R., and Fairhurst, C., 1970, "A study of brittle rock fracture in laboratory compression experiments", *International Journal of Rock Mechanics Mining Sciences & Geomechanical Abstracts*, 7, pp. 561 – 575.
- Wesley, L. D., 1988., "Engineering classification of residual soils". *Proc. Second Int. Conf. On Geomechanics in Tropical Soil, Singapore 1*: 77 – 84.

- Wilson, W., and Corke, D. J., 1990, "A comparison of modulus values of sandstone derived from high pressure dilatometer, plate loading, geophysical and laboratory testing", *Pressuremeters, Proc. of the Symp. on Pressuremeters, British Geotechnical Society*, pp. 351 – 360.
- Windle, D. and Wroth, C. P., 1977a "In situ measurement of the properties of stiff clays" *Proc. 9th Int. Conf. on Soil Mechanics and Foundation Engineering, Tokyo, Vol. 1*, pp. 347 – 352.
- Windle, D., and Wroth, C. P., 1977b, "The use of a self – boring pressuremeter to determine the undrained properties of clays", *Ground Engineering*, 10, 6, pp. 37 – 46.
- Wittke, W., 1990, "Rock Mechanics (Theory and Applications with Case Histories)", Springer – Verlag, Berlin.
- Wroth, C. P., and Hughes, J. M. O., 1973, "An instrument for the in-situ measurement of the properties of soft clays", *Proc. 8th Int. Conf. SMFE, Moscow, 12*, pp. 487 – 494.
- Wroth, C. P., 1984, "The interpretation of in-situ soil tests", *Géotechnique*, 34, 4, pp. 449 – 489.
- Wyllie, D. C., 1992, "Foundations on Rock", E & FN Spon, England, p. 333.
- Yeung, S. K., and Carter, J. P., 1990, "Interpretation of the pressuremeter test in clay allowing for membrane end effects and material non – homogeneity", *Pressuremeters, Proc. of the Symp. on Pressuremeters, British Geotechnical Society.*, pp. 199 – 208.
- Yu, H. S., 1993, "Discussion on: singular plastic fields in steady penetration of a rigid cone", *Journal of Applied Mechanics, ASME*, 60, pp. 1061 – 1062.

- Yu, H. S., Schnaid, F., and Collins, I. F., 1996, "Analysis of cone pressuremeter tests in sands", *Journal of Geotechnical Engineering*, 122, 8, pp. 623 – 632.
- Zentar, R., Hicher, P. Y., and Moulin, G., 2001, "Identification of soil parameters by inverse analysis", *Computers and Geotechnics*, 28, 2, pp. 129 – 144.
- Zhang, L., and Einstein, H., 2004, "Using RQD to estimate the deformation modulus of rock masses", *International Journal of Rock Mechanics & Mining Sciences*, 41, p. 337 – 341.

VITA

PERSONAL INFORMATION

Surname, Name: Işık, Nihat Sinan
Nationality: Turkish (TC)
Date and Place of Birth: 16 December 1973 , Diyarbakır
Marital Status: Married
Phone: +90 312 212 68 20/1613
email: nihatsinan@gazi.edu.tr

EDUCATION

Degree	Institution	Year of Graduation
MS	METU Geological Engineering	1999
BS	METU Geological Engineering	1996
High School	Deneme High School, Ankara	1991

WORK EXPERIENCE

Year	Place	Enrollment
1998- Present	Gazi University Tech. Edu. Fac. Construction Dep.	Research Assistant

FOREIGN LANGUAGES

Advanced English

SELECTED PUBLICATIONS

1. Işık N., S., Doyuran, V., and Ulusay, R., 2004, "Assessment of a coastal landslide subjected to building loads at Sinop, Black Sea region, Turkey, and stabilization measures", Engineering Geology, 75, pp. 69 – 88.
2. Teoman, M. B., Topal, T., and Işık, N. S., 2004, "Assessment of slope stability in Ankara clay: a case study along E90 highway", Environmental Geology, 45, pp. 963 – 977.
3. Çetin, K. Ö., Işık, N. S., Batmaz, A., and Karabiber, S., 2005, "A comparative study on the actual and estimated seismic response of Kıralkızı Dam in Turkey", Journal of Earthquake Engineering, 9, 4, pp. 445 – 459.

4.Çetin, K. Ö., Işık, N., and Unutmaz, B., 2004, “Seismically induced landslide at Değirmendere Nose, İzmit Bay during Kocaeli (İzmit) – Turkey earthquake”, Soil Dynamics and Earthquake Engineering, 24, pp. 189 – 197.

HOBBIES

Computer Technologies, Aquarium, Pen collection